CONTRIBUTORS TO THIS VOLUME

J. R. COLLINS
D. P. CRAIG
A. DEDIEU
INGA FISCHER-HJALMARS
G. A. GALLUP
ANITA HENRIKSSON-ENFLO
J. M. NORBECK
A. A. OVCHINNIKOV
M. YA. OVCHINNIKOVA
M.-M. ROHMER
T. THIRUNAMACHANDRAN
R. L. VANCE
A. VEILLARD

ADVANCES IN
QUANTUM CHEMISTRY

EDITED BY
PER-OLOV LÖWDIN

DEPARTMENT OF QUANTUM CHEMISTRY
UPPSALA UNIVERSITY
UPPSALA, SWEDEN
AND
QUANTUM THEORY PROJECT
UNIVERSITY OF FLORIDA
GAINESVILLE, FLORIDA

VOLUME 16–1982

ACADEMIC PRESS
A Subsidiary of Harcourt Brace Jovanovich, Publishers
New York • London
Paris • San Diego • San Francisco • São Paulo • Sydney • Tokyo • Toronto

ACADEMIC PRESS, INC.
111 Fifth Avenue, New York, New York 10003

United Kingdom Edition published by
ACADEMIC PRESS, INC. (LONDON) LTD.
24/28 Oval Road, London NW1 7DX

LIBRARY OF CONGRESS CATALOG CARD NUMBER: 64-8029

ISBN 0-12-034816-0

PRINTED IN THE UNITED STATES OF AMERICA

82 83 84 85 9 8 7 6 5 4 3 2 1

CONTRIBUTORS

Numbers in parentheses indicate the pages on which the authors' contributions begin.

J. R. COLLINS (229), Department of Chemistry, University of Nebraska, Lincoln, Nebraska 68588

D. P. CRAIG (97), Research School of Chemistry, The Australian National University, Canberra, A.C.T. 2600, Australia

A. DEDIEU (43), Institut Le Bel, Université Louis Pasteur, 67000 Strasbourg, France

INGA FISCHER-HJALMARS (1), Institute of Theoretical Physics, University of Stockholm, Stockholm, Sweden

G. A. GALLUP (229), Department of Chemistry, University of Nebraska, Lincoln, Nebraska 68588

ANITA HENRIKSSON-ENFLO (1), Institute of Theoretical Physics, University of Stockholm, Stockholm, Sweden

J. M. NORBECK* (229), Department of Chemistry, University of Nebraska, Lincoln, Nebraska 68588

A. A. OVCHINNIKOV (161), L. Ya. Karpov Physico-Chemical Research Institute, Moscow, USSR

M. YA. OVCHINNIKOVA (161), Institute of Chemical Physics of the Academy of Sciences of the USSR, Moscow, USSR

M.-M. ROHMER (43), Institut Le Bel, Université Louis Pasteur, 67000 Strasbourg, France

T. THIRUNAMACHANDRAN (97), Department of Chemistry, University College London, London WC1H 0AJ, England

*Present address: Ford Motor Research Laboratory, Dearborn, Michigan 48121.

R. L. VANCE* (229), Department of Chemistry, University of Nebraska, Lincoln, Nebraska 68588

A. VEILLARD (43), Institut Le Bel, Université Louis Pasteur, 67000 Strasbourg, France

*Present address: Dow Chemical Co., Midland, Michigan 48640.

PREFACE

In investigating the highly different phenomena in nature, scientists have always tried to find some fundamental principles that can explain the variety from a basic unity. Today they have not only shown that all the various kinds of matter are built up from a rather limited number of atoms, but also that these atoms are constituted of a few basic elements of building blocks. It seems possible to understand the innermost structure of matter and its behavior in terms of a few elementary particles: electrons, protons, neutrons, photons, etc., and their interactions. Since these particles obey not the laws of classical physics but the rules of modern quantum theory of wave mechanics established in 1925, there has developed a new field of "quantum science" which deals with the explanation of nature on this ground.

Quantum chemistry deals particularly with the electronic structure of atoms, molecules, and crystalline matter and describes it in terms of electronic wave patterns. It uses physical and chemical insight, sophisticated mathematics, and high-speed computers to solve the wave equations and achieve its results. Its goals are great, but perhaps the new field can better boast of its conceptual framework than of its numerical accomplishments. It provides a unification of the natural sciences that was previously inconceivable, and the modern development of cellular biology shows that the life sciences are now, in turn, using the same basis. "Quantum biology" is a new field which describes the life processes and the functioning of the cell on a molecular and submolecular level.

Quantum chemistry is hence a rapidly developing field which falls between the historically established areas of mathematics, physics, chemistry, and biology. As a result there is a wide diversity of backgrounds among those interested in quantum chemistry. Since the results of the research are reported in periodicals of many different types, it has become increasingly difficult for both the expert and the nonexpert to follow the rapid development in this new borderline area.

The purpose of this serial publication is to try to present a survey of the current development of quantum chemistry as it is seen by a number of the internationally leading research workers in various countries. The authors have been invited to give their personal points of view of the subject freely and without severe space limitations. No attempts have been made

to avoid overlap—on the contrary, it has seemed desirable to have certain important research areas reviewed from different points of view. The response from the authors has been so encouraging that a seventeenth volume is now being prepared.

The Editor would like to thank the authors for their contributions which give an interesting picture of the current status of selected parts of quantum chemistry. The topics in this volume range from studies of the role of metals in biology in general, *ab initio* calculations of the properties of metalloporphyrins, interactions between radiation and molecules, the problems of nonlinear radiationless processes in chemistry, to practical valence-bond calculations.

It is our hope that the collection of surveys of various parts of quantum chemistry and its advances presented here will prove to be valuable and stimulating, not only to the active research workers but also to the scientists in neighboring fields of physics, chemistry, and biology who are turning to the elementary particles and their behavior to explain the details and innermost structure of their experimental phenomena.

PER-OLOV LÖWDIN

Metals in Biology: An Attempt at Classification

INGA FISCHER-HJALMARS and ANITA HENRIKSSON-ENFLO
Institute of Theoretical Physics
University of Stockholm
Stockholm, Sweden

I. Introduction

Many chemical and physical properties of the elements can be fairly well described by their position in the periodic table; in biology, however, this is not the case. This is especially true for the transition metals, many of which occur in small amounts in the body and are essential for the normal functions of life (Williams, 1976a).

The essential metals occur often in very specific enzymes, and a substitution of one metal for another, even though chemically very similar, will alter the biological activity. Thus, in human hemoglobin, for example, the iron atom is necessary; in frog hemoglobin, it is the copper atom; and in alcohol dehydrogenase and in carbonic anhydrase, the Zn atom is necessary. There have been attempts to substitute other atoms for Zn in these enzymes that resulted in appreciable changes in activity (Lindskog and Malmstrõm, 1962; Hay, 1976).

ADVANCES IN QUANTUM CHEMISTRY, VOLUME 16

ISBN 0-12-034816-0

The reaction of the enzymes is supposed to take place at the metal atom. The metal is said to be the reaction center, and the role of the surrounding part is thought to be to modify the reactivity of the metal and to help the reacting parts to join.

Metals can also perform other functions in the body such as stabilizing conformations, as is done by Ca, Mg, and Zn, for example. There are also many essential metals for which the biological functions are not yet known. This is especially the case for metals that occur in the body in very small amounts—the ultratrace elements. These elements, which have only lately been discovered to be essential (because of experimental difficulties), are of course very difficult to isolate in sufficiently large amounts for detailed studies. One example is chromium, which is found to be essential from nutrition experiments. It is known that this metal can be found in the glucose tolerance factor, but neither the structure of this agent nor the function of the chromium are known yet (Vokal *et al.*, 1975).

There are other elements that have not yet been found to serve any positive function in life processes. There are also many elements that have definite negative or toxic effects, such as the very toxic metals mercury, cadmium, and lead. It should also be pointed out that many essential metals become toxic when occurring in large amounts or when present in a different form. Thus, iron, though very important, can be toxic when it occurs in too large amounts or in the ferric state. Copper, although essential, is also found to be toxic in rather small amounts: the problem with copper pipes used for supplying drinking water is well known. There has been no explanation of the specificity of the metals, especially the transition elements, in biology, although the problem has been intensively studied for a long time (Ahrland *et al.*, 1958; Österberg, 1976; Williams, 1976b).

An attempt to classify the metals according to their binding properties to certain ligands has been made (Ahrland *et al.*, 1958; Pearson, 1963). This classification into hard and soft acids and bases has been useful for many cases, but does not give the complete answer.

The goal of our project was originally to explain why certain metals cause contact allergies, whereas other chemically very similar metals are nearly harmless. It is well known that among metals there are three that are strongly allergenic: chromium, cobalt, and nickel. Because the development of an allergy depends both on the reactivity and the frequency of occurrence, there could be many other metals also causing an allergy to the same extent if their occurrence were comparable. On the other hand, there are also certain metals, occurring with the same, or even greater, frequency that do not seem to cause allergy. To these belong the chemically related metals iron and copper.

When comparing the three well-known allergenic metals with the classification of the metals into hard, soft, and intermediate, it is found that they belong to different classes: Cr^{3+} is hard and Ni^{2+} and Co^{2+} are intermediate; but the harmless Zn^{2+} also belongs to the intermediate class. It should also be pointed out that different oxidation states of a certain metal can place the same metal into different classes. The zero oxidation state is classified as soft for all metals.

In this situation it would seem to be worthwhile to study the binding between metal and ligand in more detail. Here, a quantum chemical investigation could be of great help, e.g., to obtain indices that are difficult to measure experimentally, such as net, gross, and overlap populations in each orbital and orbital energies.

A quantum chemical study can be made in many different ways. The first problem is to choose the system to be studied. It is well known that all metals do not react with the same molecule in the body. How do we find a system that is appropriate to study for whole series of metals?

The most common ligands in biological systems are oxygen, nitrogen, and sulfur. However, there are a large number of different molecules that contain these atoms, each of which has its special properties. To find a single system simulating all these is impossible. The problem is therefore to find a system including as many reactions as possible.

Our general problem is to find a system of classification of metals that cause allergies. An understanding of the mechanisms behind such reactions is therefore of great importance. It is known that the immune system is involved; however, the detailed mechanism is not known. In the case of chromium, it is known that Cr(VI) ions in an alkaline medium cause allergies (e.g., the well-known cement exzema among cement workers). Whether chromium in other oxidation states can also cause allergy is under debate. What concerns us about the two other metals, cobalt and nickel, is that we know that pure metals can cause allergies. Even in this case the mechanism is not known, nor is the oxidation state causing the reaction. It may be that small amounts of metal ions (probably in this case in the +2 oxidation state) are dissolved from the metal by the body fluids, and that the metal ion is the real allergen.

It is therefore not known what happens when the substance comes into contact with the body. We have been especially interested in the case of contact exzema, which is the most common form of metal allergy. In this case, the contact occurs through the skin. In order to discuss possible reactions, a knowledge of the structure and composition of the skin is needed.

A special feature of the skin is the large quantity of free amino acids, in particular, sulfur-containing amino acids. For this reason and because of the central role of amino acids in other biological systems, we have chosen

to study complexes between amino acids and metals, their structure and reactivity. As already pointed out our tool of investigation has been quantum chemical calculations. These calculations can be performed on different levels of sophistication. In the present project it is not known which index may be important. We thus need an overall picture of the system as accurate as possible in order to find a pattern for classification and clarification. Therefore, we found it necessary to use an *ab initio* method and, accordingly, were limited to studies of rather small systems.

II. Choice of Model System

A. The Main Model

Our aim is to compare the effect on the skin produced by a series of different metals. Since we expect the first step of the reaction to be a complex formation between the metal and an amino acid, it seems natural to choose a complex of this kind as the object of a quantum chemical study. Such a choice is also facilitated by the fact that structures of some of these complexes are known from X-ray analysis (Freeman, 1967). Amino acids can react with metals in many different ways. Very often a chelate formation takes place. In most cases the coordination numbers are 4 or 6, which means that 2 or 3 bidentate ligands bind to the metal (see Fig. 1). It is of course not necessary that all ligands be the same; very often the fifth and sixth ligands may be some loosely bound water molecules. Even if these complexes appear small and nice from a chemical point of view, they are far too big for quantum chemical calculations on an *ab initio* level,

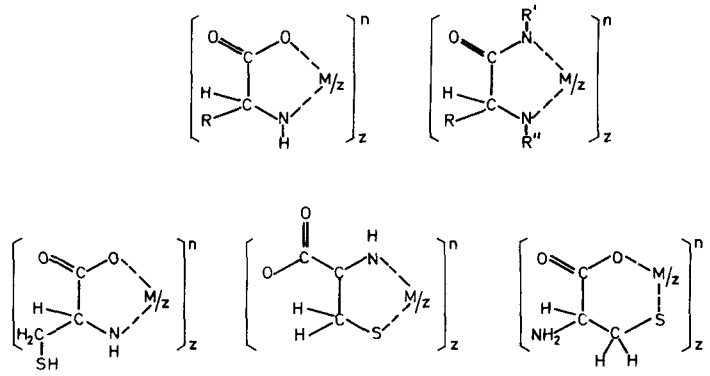

Fig. 1. Complexes of amino acids with metals, in general, four-coordinated ($z = 2$) or six-coordinated ($z = 3$). The overall charge n can equal the charge of the free metal ion or have a lower value.

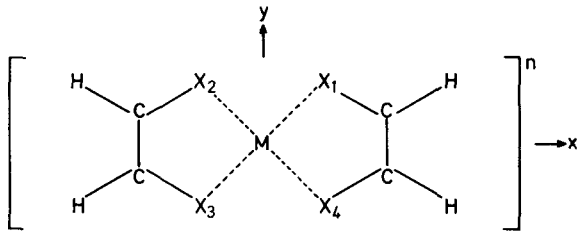

Fig. 2. Model system: X_i = NH, O, or S; n is the overall charge of the complex.

at least in terms of the computing resources available at present and the long series of systems to be studied. It is therefore necessary to reduce the size of the model system even more.

One way of reducing the size of the model is to choose a system where the metal is bound to only one ligand. Such studies have been made in many cases and valuable information obtained from such models (Pappas, 1978b).

On the other hand, it is well known that in a condensed phase the metal ion will always be surrounded by at least four ligands. Another way of reducing the system is therefore to keep the full coordination but reduce the size of the ligand. The smallest possible ligands are X and XH, where X is one of the heteroatoms most common in biology, i.e., nitrogen, oxygen, or sulfur, known to bind to metal ions (Fig. 1). This kind of model has been used, e.g., by Bair and Goddard (1978) for studies of both ground state and several excited states.

One may ask whether all properties are well described by XH as a model of a bioligand. It is well known that metals in biology often form chelates with five-membered rings, not only with amino acids but also with peptides, catechol structures, etc. In most cases these ligands are unsaturated. We have therefore chosen a model system with an unsaturated chelate structure (Fig. 2). The ligating atoms X_i chosen are those most commonly occurring in biology, namely nitrogen, oxygen, and sulfur. It is assumed that the two carbon atoms of the five ring will simulate the organic skeleton of bidentate ligands.

The bulk of our study has been devoted to systems where all four ligating atoms are equal, i.e., complexes with high symmetry D_{2h}. This choice has several advantages: It is important to start with a system as simple as possible. For such systems it is easier to find a systematization since one can afford to change one parameter at a time. It is possible to vary the overall charge n and to include complexes of a series of different metal ions. Further, there are several biosystems where this structure can

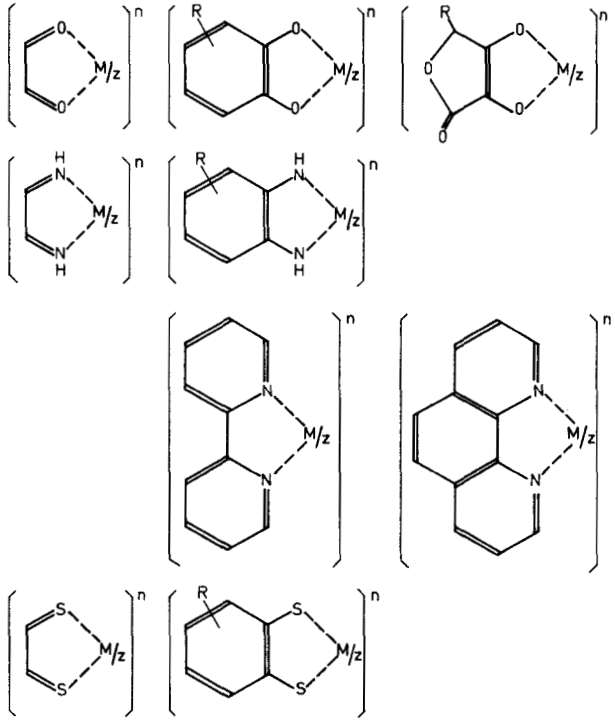

Fig. 3. Larger molecules containing the present model system.

be important, for example, metals interacting with such ligands as methylglyoxal, ascorbic acid, catecholic structures (epinephrine, etc), peptides, dimethylglyoxime, and bispyridyl (Fig. 3). Results from a theoretical analysis of the highly symmetric compounds can also be used to predict properties of compounds of lower symmetry which more closely simulate complexes between metals and amino acids.

A further advantage is that the highly symmetric metal complexes have been studied experimentally rather extensively, especially where X_j is sulfur (Gray, 1965; Schrauzer, 1968; McCleverty, 1968; Hoyer *et al.*, 1971; Burns and McAuliffe, 1979). Experiments have shown that the most stable overall charge is $n = -1$, but reversible oxidation and reduction to other charged states can easily take place. These easily occurring electron transfer reactions imply interesting properties as, for example, semiconductors and catalysts. Compounds of this type have also been used experimentally as model compounds for iron–sulfur proteins, especially ferredoxin and rubredoxin, molybdenum–sulfur proteins, as xanthine

oxidase and nitrogenase, as well as copper proteins (Siiman and Carey, 1980).

Our series of investigation includes compounds with different metal ions. Magnesium has been studied since it is an essential and, according to the present knowledge, not a harmful metal. Nickel has been chosen since it can cause contact allergy, and zinc since it has a healing effect on the skin. Copper has been studied since its participation in important biological reactions is well known, particularly in oxidation–reduction processes. Partly for computational reasons we found it important to include some lighter metals in our series which would allow more extensive variation of the various parameters of the model, for example, geometry and symmetry. Beryllium, which in many respects simulates transition metals (Schaefer, 1977), was therefore studied as well as the lightest metal, lithium. Beryllium is known to be a very toxic metal; whether or not it can cause exzemas is under discussion. Lithium is also of considerable biological interest, e.g., as a drug.

Some complexes of transition metals from the beginning of the series have been studied by a pseudopotential method: Sc, Ti, and Cr (Pettersson, 1981). Chromium is known to be the strongest allergenic metal. Whether Sc and Ti cause any biological reactions is not well known, but a systematic study of the present kind may help in predicting biological properties of these and other metals.

The overall charge n of the compounds has been varied. In the case of divalent metals and closed shells we have studied $n = +2, 0, -2$. In the case of Li we included $n = +1, 0, -1$; for Cu, $n = +2, +1, 0, -1, -2, -3$, and for Sc, Ti, and Cr, we included $n = +2, +1, 0, -1, -2$.

Our choice of model system subsequently received support by the results of others. The importance of choosing a model where the metal ion is fully coordinated is underlined by the investigation of Rode (1974). Choosing formamide as an amino acid model he showed that the bonding pattern of $[Li(HCONH_2)_2]^+$ with a four-coordinated Li^+ ion is strikingly different from that of the two-coordinated complex $[Li(HCONH_2)]^+$. More recently, Pullman and Demoulin (1979) have made a very careful study of the effect of the number of ligands of zinc complexes $[ZnL_m]^n$, where L = H_2O, OH^-, NH_3, ImH (imidazol), Im^-, $m = 1, 2, 4, 6$, and $n = +1$ and $+2$. They studied complexes of both high and low symmetry, but the general conclusions were applicable to all types of compounds. They found that the charge and the binding energy of a given ligand depends much more strongly on the number of ligands than on the nature of the other ligands. The total binding energy (BE) was found to increase with m, and for a given value of m, the BE was found to be appreciably higher for $n = +1$ than for $n = +2$.

In our laboratory the two-coordinated complexes $[Be(XCHCHY)]^n$ are currently compared to the corresponding four-coordinated compounds (Davstad, 1981). In agreement with the results of Pullman and Demoulin (1979), we have found the four-coordinated compounds to be the more stable ones. As discussed in more detail below in Section IV,E,4, the charge distribution within the two-coordinated complexes gives an exaggerated picture of the features typical for the four-coordinated species. As an example, the charge transfer between S and Be is almost twice as large in the two-coordinated case. Moreover, the two ligating atoms O and S are not changed in the same way by incomplete coordination.

B. Comparison between Different Models

We have also studied model systems with the simple ligands XH^-, $[Zn(XH)_4]^{2-}$ and systems with saturated ligands $[Zn(C_2H_4X_2)_2]^{2-}$ in order to compare them to $[Zn(C_2H_2X_2)_2]^{2-}$ (Henriksson-Enflo *et al.*, 1981). It was found that many properties were different for the different model systems. Thus, for example, the highest occupied orbitals were always mainly ligand orbitals but of different types for different models. The ordering of the orbitals was different also for the lower lying orbitals.

It is shown in Section IV,A that Koopmans' theorem is valid for the highest occupied and lowest empty orbitals. As these orbitals are of great importance for the chemical reactivity of the molecule, a difference in their nature and symmetry can lead to quite different reactivity of the different complexes. The differently charged complexes also have different electronic structures and thus different reactivities.

Other properties also, such as binding energies and charges on different atoms, are affected by the nature of the ligand. The stabilizing effect of chelate formation is already clearly seen in the energy differences, and is not just due to the entropy effect; this has also been stressed by Rode (1974).

It has also been found that the saturated complex is nearer the small complex than the unsaturated. Another important finding is that an unsaturated chelate can occur with different overall charges more easily than the saturated chelates. Because electron transport is a common mechanism in biology, it is obvious that in such reactions an unsaturated chelate should be more favorable.

Finally, it should be pointed out that the larger the ligand is, the more dominating are the properties of the ligand compared to those of the metal. Certain reactions are supposed to take place at the ligand part, and in such cases the only role of the metal is to perturb the ligand orbitals, i.e., some catalytic effect. This is especially the case with unsaturated

ligands. It is thus important to choose carefully the model system. We conclude that for studies of metal–amino acid complexes and metal–peptide complexes, the unsaturated, four-coordinated compound shown in Fig. 2. is the proper choice.

III. Method and Details of Calculation

A. Computational Method

As already mentioned, we have carried out quantum chemical calculations on the *ab initio* level. Most of the calculations were performed within the single determinant MO–LCAO–SCF framework. At the initial stage only closed-shell configurations were treated, later open shells were also included. Most cases include all electrons. In some cases a pseudopotential method was employed, treating only valence electrons explicitly. The calculations were performed partly on a CDC 6400 and partly on a VAX 11/780 computer. Integral and SCF calculations were done using the program system MOLECULE (Almlöf, 1974) and more recently the joint MOLECULE–ALCHEMY system (Bagus, 1972; Wahlgren, 1977). Mulliken population analysis was carried out with a computer program POPUL (Johansen, 1974).

Basis sets of Gaussian type were used: for hydrogen the 4s basis of Huzinaga (1965) scaled by 1.25; for first-row atoms the 7s3p basis; for second-row atoms the 10s6p basis of Roos and Siegbahn (1970); and for the metals a modification of the basis of Roos *et al.* (1971). The three outermost s functions on Ni, Cu, and Zn were deleted, because they can be described as well by the totally symmetric combination of d functions. Since our aim is to describe the bonding, two additional diffuse p functions and one d function were added, and the innermost s function was deleted. The final primitive bases were thus for Li and Be, 7s1p; for Mg, 10s6p; for Ni, Cu, and Zn, (8 + 4)s7p4d. Contractions were mainly to double-zeta basis, except for transition metal K and L shells and sulfur K shell where minimal basis was used. The numbers of contracted basis functions were thus: [H/2s], [Li, Be/4s, 1p], [C, N, O/4s, 2p], [S, Mg/5s, 4p] and [Ni, Cu, Zn/(3 + 3)s, 5p, 3d]. Full details of the basis sets are given elsewhere (Henriksson-Enflo *et al.*, 1981).

In the main part of the investigation d-functions on sulfur were excluded. This was necessary since it would have been impossible for us to carry out the project outlined above with d functions on five centers. Since the role of sulfur d functions is so much debated, we have studied their influence in a specific case which is presented later in Section IV,G.

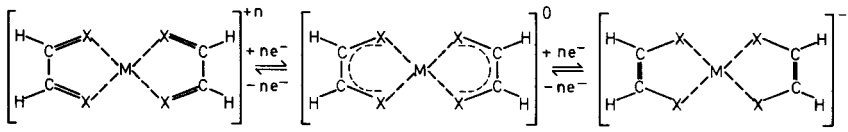

Fig. 4. Structure formulas for different values of the overall charge n: formula A as built up from a positively charged metal ion and two neutral ligands with clear double-bond character of the C=X bonds; formula C, again as built up from a positively charged metal ion and two ligands with two negative charges each, the C=C bond having clear double-bond character; for formula B no definite valence-bond structure can be written.

B. Choice of Geometry

In quantum chemical *ab initio* calculations it is preferable that the geometry of the compound be optimized in each case. In the present study such an approach would be very costly and beyond the limits of our resources. Since our main goal is to find general trends within groups of similar compounds, it seems acceptable to choose a standard geometry for each group. Accordingly, we have fixed the geometry for each choice of ligand, assuming it to be independent of the overall charge n. Moreover, since the ionic radii of most of the metals studied are very similar, we have assumed the MX distance to be the same for all different M with the exception of Be with an ionic radius of 0.31 Å. There is also experimental evidence that there are only small changes in geometry when the charge n or the metal M is changed (Sartani and Truter, 1967).

The geometry of free *trans*-glyoxal has been determined by electron diffraction (Kuchitsu *et al.*, 1969). Free *cis*-glyoxal has been studied by microwave spectroscopy (Durig *et al.*, 1972). The geometries of free glyoxal diimine and thioglyoxal are not known. The unsaturated character of the system implies different structures for different charges (Fig. 4.)

For our model compounds we employ planar geometries that should represent the most likely average of assumed geometries of differently charged metal complexes. Since the oxygen complexes were expected to occur mainly as positive or neutral compounds, a geometry close to that of free glyoxal was chosen. The main modification is a lengthening of the CO bond from 1.21 to 1.26 Å, expected because of the oxygen–metal interaction.

The nitrogen complexes were also expected to occur mainly as positive and neutral compounds. Since the free glyoxal diimine does not exist, the geometry must be chosen with reference to standard values of bond lengths and angles. The CC distance is expected to be close to that of glyoxal. In conjugated molecules a typical C=N distance is 1.27 Å. A

TABLE I

GEOMETRY OF COMPLEXES $[M(C_2H_2X_2)_2]^n$

Distance or angle[a]	X = NH	X = O	X = S	Distance or angle[a]	X = NH	X = O	X = S
CX	1.31	1.26	1.73	XX	2.81	2.76	3.10
CC	1.50	1.50	1.37	XX′	3.01	2.95	2.92
CH	1.09	1.09	1.09	MX	2.06	2.02	2.13
NH	1.02	—	—	<CCX	120°	120°	120°

[a] X and X′ belong to different monomers; distances in angstroms.

slightly larger distance, 1.31 Å, was chosen for the same reasons as in the CO case.

Metal dithioglyoxal complexes are found to be neutral or negatively charged in most cases. As indicated by Fig. 4C, one would therefore expect the CC bond to be close to a double bond and the CS bond to be more like a single bond. This is also supported by many X-ray studies. The geometry chosen in this case is a mean value of different experiments (Kennard *et al.*, 1972). Atomic distances and bond angles according to our chosen standard geometry are collected in Table I. The geometry of the Be complexes is given elsewhere (Blomberg *et al.*, 1980).

A partial geometry optimization was carried out for the Be complexes (Blomberg *et al.*, 1980). It was found that our choice of standard geometries was quite reasonable. Even more essential is that the various properties, discussed below, were found to be rather insensitive to the detailed geometry. Therefore, the general trends of these properties do not change if the geometry is optimized for each compound separately.

IV. Results

A. Binding Energies

There is some uncertainty as to how the complexes are formed and how the binding energy should be defined. We have thus used different definitions in different papers. Here we shall adopt the definition of Fischer-Hjalmars and Henriksson-Enflo (1980). We define the vertical binding energy of a complex $[M(C_2H_2X_2)_2]^n$ as the difference between the total energy of that complex and the sum of the energies of the constituents, calculated with the same basis set. The constituents are two neutral ligand monomers $C_2H_2X_2$, a metal ion M^{2+} (or M^+), and the number of free electrons necessary to obtain the overall charge n of the complex. It

should be stressed that we do not expect to obtain absolute values of binding energies, but only to compare similar compounds. It has been shown that basis set effects work in the same direction for all the different systems studied. We therefore believe that energy differences of 1 eV or more are indeed significant.

During the initial stage of the present project we had access only to the MOLECULE SCF program, which treats only closed-shell configurations. It was therefore possible only to calculate energies for divalent metal complexes with $n = \pm 2$ and 0. Subsequently, the MOLECULE–ALCHEMY system was installed at our laboratory, allowing treatment of open-shell systems so that energies for all the values $n = \pm 2, \pm 1$, and 0 could be obtained. It was then found that Koopmans' theorem worked rather well both for ionization potentials (energy of highest occupied molecular orbital, HOMO) and for electron affinities (energy of lowest unoccupied molecular orbital, LUMO; cf. Table II). Since the deficiency of Koopmans' theorem is very similar in all cases, we expect to obtain comparable energy values this way. In Table III we have therefore listed binding energies for $n = \pm 2$ and 0, obtained from SCF calculations together with energies for $n = \pm 1$, obtained from Koopmans' theorem.

Table III includes complexes of Be, Mg, Ni, Cu, and Zn. For comparison, values are also given for the dimer with the two ligands in the same position as in the complexes but without any metal ion, and for an artificial system where the metal ion is replaced by a point charge +2 without any orbitals around it.

The neutral dimers are slightly unstable. This is to be expected since the polar groups of the two ligands are repelling each other. This repulsion

TABLE II

BINDING ENERGIES WITH REFERENCE TO FREE NEUTRAL LIGAND AND FREE M^{2+} OBTAINED FROM KOOPMANS' THEOREM, COMPARED TO THOSE FROM SCF CALCULATIONS

Complex	Overall charge n	Binding energies (eV)		
			Koopmans	
		SCF	HOMO	LUMO
$[Cr(C_2H_2O_2)_2]^n$	+1	20.2	19.6	20.0
	−1	26.4	26.1	25.7
$[Be(OC_2H_2S)_2]^n$	+1	25.1	24.4	24.5
	−1	33.6	32.6	32.5

TABLE III

BINDING ENERGIES[a] OF COMPLEXES $[M(C_2H_2X_2)_2]^n$ WITH REFERENCE TO FREE $C_2H_2X_2$ AND M^{2+}

Ligand	Metal	Overall charge n				
		+2	+1[d]	0	−1[d]	−2
Nitrogen	None[b]	−0.6	−3.9	−11.6	−22.9	−38.2
	+2[c]	15.9	23.0	25.6	24.6	19.2
	Be	17.6	25.6	28.9	27.6	21.8
	Mg	13.8	21.5	24.6	23.5	18.1
	Ni	13.7	21.4	24.5	23.5	18.1
	Zn	15.2	22.9	26.0	24.9	19.5
Oxygen	None[b]	−0.2	−1.8	−8.3	−18.2	−32.6
	+2[c]	9.4	18.7	23.0	23.9	19.9
	Be	14.0	24.1	29.1	30.0	25.9
	Mg	9.7	19.4	24.2	25.2	21.4
	Ni	8.9	18.7	23.6	24.9	21.2
	Cu	14.9	—	29.6	—	27.0
	Zn	10.9	20.7	25.5	26.5	22.7
Sulfur	None[b]	−0.9	0.5	−2.5	−9.8	−21.5
	+2[c]	10.3	22.1	29.5	32.7	31.4
	Be	11.5	23.4	30.9	33.6	31.8
	Mg	3.6	15.5	23.0	26.0	24.4
	Ni	6.9	18.5	25.9	28.4	26.5
	Cu	11.7	—	30.8	—	31.6
	Zn	6.9	18.7	26.2	28.9	27.0

[a] In electron volts.
[b] No metal; n is reduced by two units.
[c] Point charge without basis functions.
[d] From Koopmans' theorem.

increases considerably when electrons are added to the system with one exception. The dimer $(C_2H_2S_2)_2^-$ is seen to be slightly stable. This is a consequence of the positive electron affinity of $(C_2H_2S_2)_2$ (Section IV,B). For more negative values of n all dimers are unstable. Table III shows that the instability decreases in the order NH > O > S. This is remarkable in view of the fact that the SS′ distance according to experimental data is 2.92 Å, considerably shorter than the distance expected from van der Waals' radii, 3.6 Å.

The stabilities of the complexes show some interesting features. It is seen that for $n = +2$ the stability is in the order NH > O > S for all the metals and for $n = -2$ the order is reversed, S > O > NH. For $n = 0$

there is no clear trend. All NH complexes are most stable for $n = 0$. The O complexes have almost the same energy for $n = 0$ and $n = -1$, the latter being slightly more stable according to Table III. Sulfur complexes have almost the same energy for $n = -1$ and $n = -2$, although $n = -1$ is somewhat more stable according to Table III. If correlation energy could be considered, this order might change both for O complexes ($n = 0$ or -1) and for S complexes ($n = -1$ or -2). These different stability orders means that in different surroundings, for example, different pHs, different types of complexes may arise. In fact, it has been verified by experiments that different types of metal–amino acid complexes are formed at different pHs (Carlson and Brown, 1966). It is worth pointing out again that there are also other molecules of different kinds that can be involved in the reaction with metal ions.

When comparing the different metals it is seen that the Be complexes are more stable than the others. This extreme stability may be connected

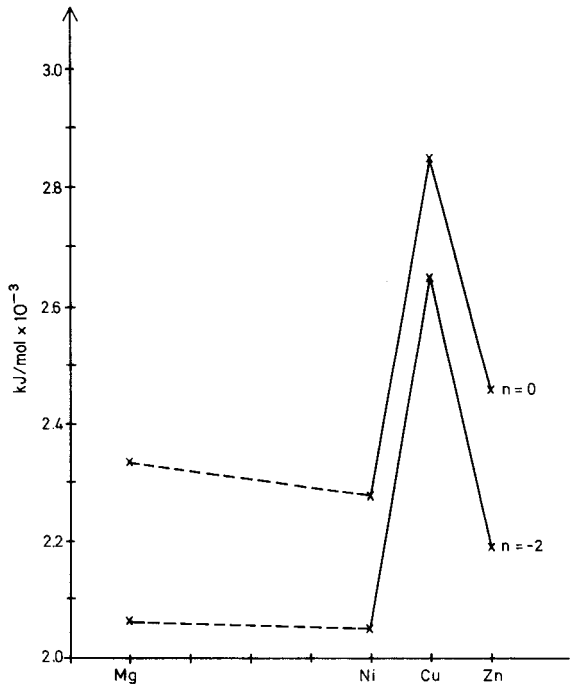

Fig. 5. Binding energies of complexes $[M(C_2H_2O_2)_2]^n$ for M = Mg, Ni, Cu, Zn and $n = 0$ and -2.

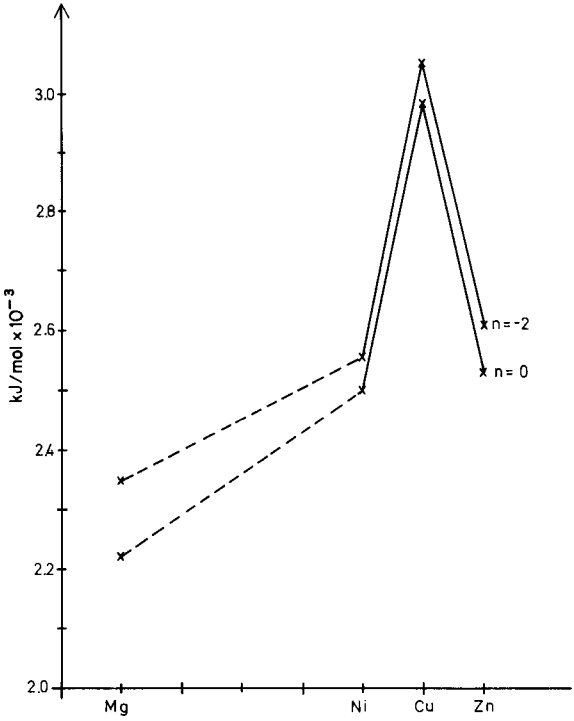

Fig. 6. Binding energies of complexes $[M(C_2H_2S_2)_2]^n$ for M = Mg, Ni, Cu, Zn and $n = 0$ and -2.

with the high toxicity of this metal. A comparison within the series Mg, Ni, Cu, Zn is outlined in Figs. 5 and 6. It is interesting that the trends are the same as in Irving–Williams diagrams (Irving and Williams, 1953).

B. Electron Affinities

As already mentioned, Koopmans' theorem seems to be reasonably valid as far as electron affinities (EAs) are concerned. A comparison between EAs obtained by different methods is given in Table IV.

Electron affinities of a series of complexes are shown in Table V. It is interesting that for a given ligand X and a given n, the EA values of the different metal complexes are almost constant. On the other hand, Table V shows that the free-ligand monomers as well as the dimers all have negative EA values (with one exception) very different from those of the

TABLE IV

COMPARISON OF ELECTRON AFFINITIES[a] OBTAINED FROM KOOPMANS' THEOREM WITH THOSE FROM ΔSCF CALCULATIONS

Overall charge n	$[Cr(C_2H_2O_2)_2]^n$		$[Be(OC_2H_2S)_2]^n$	
	ΔSCF	Koopmans	ΔSCF	Koopmans
+2	10.2	9.9	12.1	11.4
+1	4.6	5.0	5.5	6.2
0	1.6	1.1	3.0	2.0
−1	−4.1	−3.6	−4.8	−3.7

[a] In electron volts.

TABLE V

ELECTRON AFFINITIES[a] OF COMPLEXES $[M(C_2H_2X_2)_2]^n$ FROM KOOPMANS' THEOREM

Ligand	Metal	Overall charge n			
		+2	+1	0	−1
Nitrogen	Monomer[b]	−1.9	−9.6	—	—
	Dimer[c]	−3.3	−7.6	−11.3	−15.3
	+2[d]	7.2	2.5	−1.0	−5.4
	Be	8.0	3.3	−1.3	−5.8
	Mg	7.7	3.1	−1.1	−5.4
	Ni	7.7	3.1	−1.0	−5.4
	Zn	7.7	3.1	−1.1	−5.4
Oxygen	Monomer[b]	−0.3	−8.8	—	—
	Dimer[c]	−1.6	−6.4	−9.9	−14.4
	+2[d]	9.4	4.2	0.9	−4.0
	Be	11.1	5.0	0.9	−4.1
	Mg	9.7	4.8	1.0	−3.8
	Ni	9.8	4.9	1.3	−3.7
	Zn	9.8	4.8	1.0	−3.8
Sulfur	Monomer[b]	1.8	−5.1	—	—
	Dimer[c]	1.4	−3.0	−7.3	−11.7
	+2[d]	11.8	7.4	3.2	−1.3
	Be	11.9	7.5	2.7	−1.8
	Mg	11.9	7.5	3.0	−1.6
	Ni	11.8	7.4	2.5	−1.9
	Zn	11.8	7.5	2.7	−1.9

[a] In electron volts.
[b] From the ΔSCF method; n is reduced by two units.
[c] No metal; n is reduced by two units.
[d] Point charge without basis functions.

complexes. But the dimers in the field of a positive point charge do have the same affinities as the complexes. Thus it can be concluded that the *electron affinity of the complex can be classified as the property of the ligand dimer in the field of any positive metal ion.*

Table V shows that for all values of n the EA value increases in the order N < O < S. It is generally accepted that O is more electronegative than N, but not that S compounds should be more electronegative than O compounds. However, according to *ab initio* calculations by Hotop and Lineberger (1975), it was found that the EA values of the O and S atoms were 1.46 and 2.08 eV, respectively. As is discussed in more detail in Section IV,F, the electronegativity concept seems to be most subtle and strongly dependent upon the surrounding of the atom in question (see also Pappas, 1978a).

C. Orbital Energies

The pattern of orbital energies is found to be rather similar for complexes $[M(C_2H_2X_2)_2]^n$ for given X and n. As an example, Table VI summarizes calculated valence orbital energies of the following species: the free-ligand $C_2H_2S_2$, the dimer $(C_2H_2S_2)_2$, and complexes $[(C_2H_2S_2)_2M]^0$ with M = Be, Ni, Cu, and Zn. Metal orbitals and ligand orbitals, although mixed together, can be distinguished from each other in most cases. Obviously, the metal orbitals must have different energies for different metals. The ligand orbital energies are, however, rather constant. As an example, the deepest $p\pi$ (b_{1u}) orbital has an energy varying between −13.1 and −14.0 eV. Even with a considerable mixing of a metal orbital into a ligand orbital the energy is kept almost constant; see, e.g., the a_g, C orbital −18.1 to −19.1 eV. Similar results are found for other complexes; see, e.g., Fischer-Hjalmars and Henriksson-Enflo (1981) where orbital energies of $[(C_2H_2O_2)_2M]^0$ are presented.

The orbital pattern shown in Table VI agrees with measurements of ionization potentials. Furlani and Cauletti (1978) have reviewed ionization measurements on different series of transition metal complexes with ligands not very different from our model compound. From their tables it is seen that, e.g., the ionization potential of the uppermost ligand π orbital in acetyl acetonate complexes is found between the limits of 8.06 and 8.49 eV in a series with nine different metals as central atom. They have found similar results for other ligand orbitals and other complexes.

The only orbitals where the constancy of the energy is noticeably perturbed are the outermost σ lone pairs on sulfur: a_g, b_{3u} at −10.9, −9.8 eV, and b_{2u}, b_{1g} at −9.5, −8.2 eV. In particular, the b_{1g} orbitals of the Ni and Cu complexes with a vacancy in the b_{1g} metal d orbital are stabilized by almost 4 eV compared to the Be and Zn complexes.

TABLE VI

CALCULATED ORBITAL ENERGIES[a] FOR $[M(C_2H_2S_2)_2]^0$

Symmetry	Orbital type	Monomer[b]	Dimer[c]	Metal			
				Be	Ni	Cu	Zn
a_g	C,S	−31.7	−31.3	−31.6	−31.5	−31.6	−31.6
b_{3u}	C,S		−31.3	−31.5	−31.4	−31.4	−31.4
b_{2u}	S,C	−27.1	−26.9	−27.6	−27.5	−27.5	−27.5
b_{1g}	S,C		−26.7	−27.2	−27.3	−27.3	−27.4(0.2)
a_g	S,C	−24.2	−24.1	−25.1	−25.1	−25.2	−25.4(0.2)
b_{3u}	S,C		−23.7	−24.2	−24.2	−24.2	−24.3
b_{1g}	M				—	−16.0(0.8)	−23.0(1.5)
b_{3g}	M				−16.1(1.9)	−18.8(2.0)	−21.8(2.0)
a_g	M				−14.5(1.4)	−20.1(1.7)	−21.8(1.9)
b_{2g}	M				−15.7(1.6)	−18.6(1.9)	−21.7(2.0)
a_g	M				−16.7(1.0)	−18.3(1.1)	−21.6(1.8)
b_{2u}	C,S	−19.9	−19.9	−20.7	−20.5	−20.6	−20.6
b_{1g}	C,S		−19.3	−19.5	−19.9(0.1)	−20.0(0.1)	−19.0(0.3)
b_{3u}	C	−19.1	−18.8	−18.8	−18.7	−18.7	−18.7
a_g	C		−18.8	−18.8	−18.1(0.9)	−18.8(0.7)	−18.7
a_g	S,C	−14.8	−15.5	−17.1	−19.1(0.5)	−16.3(0.5)	−16.9(0.1)
b_{3u}	S,C		−13.5	−14.2	−14.2	−14.3	−14.3
b_{2u}	C,S	−13.5	−13.9	−14.8	−14.6	−14.6	−14.7
b_{1g}	C,S		−12.5	−12.7	−13.2(0.2)	−13.6(0.3)	−12.7
b_{1u}	C,S	−13.3	−13.1	−14.0	−13.9	−13.9	−14.0
b_{2g}	C,S		−12.9	−13.5	−13.0(0.3)	−13.3(0.1)	−13.4
a_g	S	−10.7	−10.9	−12.8	−12.1(0.2)	−12.4(0.1)	−12.6
b_{3u}	S		−9.8	−11.8	−11.4	−11.6	−11.7
b_{3g}	S	−9.6	−9.6	−10.9	−10.4(0.1)	−10.6(0.1)	−10.7
a_u	S		−9.1	−9.8	−9.9	−9.9	−9.9
b_{2u}	S	−9.3	−9.5	−11.3	−10.8	−11.0(0.1)	−11.1
b_{1g}	S		−8.2	−9.2	−11.7(0.4)	−12.1(0.2)	−8.6(0.2)
b_{1u}	C,S			−7.4	−7.4	−7.4	−7.5

[a] In electron volts. M = Be, Ni, Cu, Zn. Most of the orbitals are ligand orbitals, with clear ligand character and very stable from molecule to molecule. The five d orbitals are clumped together in a special group, even if the orbital energies vary considerably. Values in parenthesis are d-orbital population of the orbital (populations less than 0.1 are not given).

[b] Glyoxal monomer in its cis structure with the same geometry as in the complex.

[c] No metal.

As discussed in Section IV,B we have found that the EA of a complex depends mainly on the ligands. To obtain insight into the mechanism of the binding we may therefore assume that a neutral complex is formed from a metal ion M^{2+} and a negatively charged ligand dimer L_2^{2-}, although we know that this method of formation is not identical to the real process.

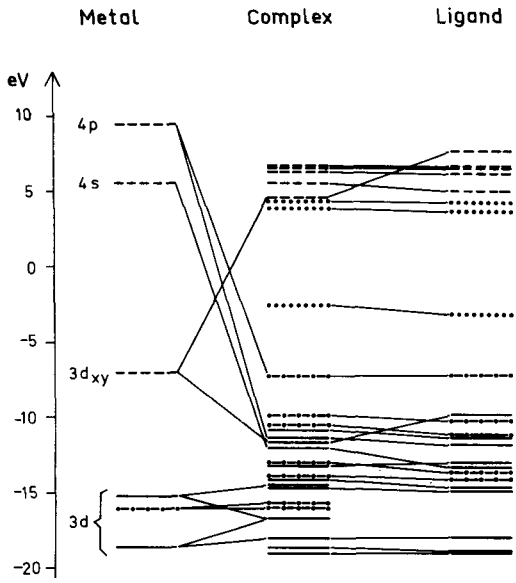

Fig. 7. Orbital diagram for formation of $[Ni(C_2H_2S_2)_2]^0$ from metal ion Ni^{2+} and ligand $(C_2H_2S_2)_2^{2-}$: (—) filled σ orbitals, (– · –) filled π orbitals, (---) empty σ orbitals, (· · ·) empty π orbitals.

In Fig. 7 we have depicted the pattern of orbital levels of the complex $[Ni(C_2H_2S_2)_2]^0$ and correlated these levels to those of its constituents Ni^{2+} and $(C_2H_2S_2)_2^{2-}$. To remove the pure electrostatic effect on the levels, the ligand orbitals are taken from the dimer with a point charge of +2 at the central position and the metal levels from a calculation where the hole in the d shell is fixed to be the d(xy) orbital. The metal levels are shifted by 20 eV due to the −2 charge of the ligands. With this model the 3d level of the free Ni^{2+} ion is split as indicated in Fig. 7. The π levels d(xz) and d(yz) at −16 eV are unperturbed, and the σ level of d(z^2) at −15 eV is only slightly perturbed by complex formation. The σ level d($x^2 - y^2$) at −18 eV mixes formally with the SC antibonding ligand level at −16 eV, but the overlap between metal and ligand orbitals is negligible. Bonding interaction is mainly found between sulfur σ lone-pair orbitals, −11 to −12 eV, and vacant metal orbitals 3d(xy), 4s, and 4p. There is also some bonding interaction between 3d(xy) and deeper ligand orbitals. The overall effect is that the ligand donates 2.1 electron units to the metal ion, and the total overlap is found to be 1.9 e.u. The distribution between σ and π, s, p, and d orbitals is shown in Table VII. It is interesting that only one-third of the donated electrons goes to the vacant d orbital and that the overlap with 4p is larger than that with 3d.

TABLE VII

POPULATIONS[a] ON THE METAL IN DIFFERENT TYPES OF ORBITALS IN $[Ni(C_2H_2S_2)_2]^0$ REFERRED TO Ni^{2+} ($3d^8$)

	Extra gross			Extra net			Overlap		
Orbital	σ	π	Total	σ	π	Total	σ	π	Total
s	0.60	—	0.60	0.32	—	0.32	0.54	—	0.54
p	0.51	0.22	0.73	0.23	0.08	0.31	0.56	0.28	0.84
d	0.79	−0.04	0.75	0.54	−0.06	0.48	0.50	0.04	0.54

[a] In electron units.

D. Metal Bridge Effect on Energy Gap

A detailed discussion of the orbital energy diagrams including both filled and vacant orbitals has been given before (Blomberg *et al.*, 1980; Fischer-Hjalmars and Henriksson-Enflo, 1980). It was shown that for $n = +2$ the HOMO is of σ type and the almost degenerate LUMO of π type. When electrons are added to the complex, they will go to these π orbitals. After addition of four electrons, the two π orbitals are filled and the LUMO is of σ type for $n = -2$. When less than four electrons are added, $n = \pm 1, 0$, both HOMO and LUMO are π-type orbitals.

It was also found that the energy gap $\Delta\epsilon$ between HOMO and LUMO

$$\Delta\epsilon = \epsilon(\text{LUMO}) - \epsilon(\text{HOMO})$$

is rather large, around 10 eV, when the two almost degenerate π orbitals are either empty or completely filled. When these orbitals are only partially filled, the energy gap decreases drastically, to 3–5 eV. These features of the HOMO and LUMO energies are typical not only for the metal complexes, but also for the ligand dimers $[(C_2H_2X_2)_2]^n$ without any metal at all. Table VIII lists the energy gap for $n = \pm 2$ and 0 for M = Be, Mg, Ni and Zn. The dimer as well as the point-charge system are also included. It is seen that the energy gap is almost constant for a given ligand X and a given value of n. The artificial systems of dimer with point charge or no metal do not deviate from the metal complexes. The variation of the energy gap with the overall charge n is thus a ligand property, more precisely a property of the ligand dimer. The monomer alone cannot give rise to a reduced energy gap. When electrons are added to a monomer, the values of ϵ(HOMO) and ϵ(LUMO) are both shifted upward, but the value of $\Delta\epsilon$ is almost constant, 10–13 eV. *The reduced energy gap is a property of*

TABLE VIII

ORBITAL ENERGY GAP $\Delta\epsilon^a$ OF COMPLEXES $[M(C_2H_2X_2)_2]^n$

	Overall charge n								
	Nitrogen ligand			Oxygen ligand			Sulfur ligand		
Metal	+2	0	−2	+2	0	−2	+2	0	−2
None[b]	13.0	3.7	7.4	12.9	3.5	9.6	6.8	4.3	9.7
+2[c]	13.2	3.5	9.3	13.2	3.3	11.8	7.7	4.1	11.4
Be	12.7	4.6	8.6	13.1	4.1	9.9	6.9	4.7	11.1
Mg	12.8	4.1	6.4	12.9	3.8	7.6	7.5	4.6	9.3
Ni	12.8	4.1	9.1	13.0	3.6	11.6	7.7	4.9	11.0
Zn	12.7	4.2	9.1	13.0	3.7	11.6	6.4	4.8	11.1

[a] In electron volts.
[b] For no metal, n is reduced by two units.
[c] Point charge without basis functions.

the ligand dimer. What then is the role of the metal? The positive ion has two important functions: (1) it is essential for the formation of the dimer; (2) it is necessary in order to increase the electronegativity of the system. Binding energies for formation of dimers are included in Table III; it is seen that they are all negative. To obtain a reduced energy gap, electrons should be added to these unstable dimers. Table V shows that all dimers have negative electron affinities. In order to remove these instabilities, *a positive charge must be brought into the system forming a bridge between the two monomers.* The effect of such a bridge is shown by the artificial point charge +2 included in Tables III and V. It is seen that this charge stabilizes the dimer and increases the EA sufficiently for formation of the ions with reduced energy gap. In fact, even a charge of +1 is sufficient for this purpose (Fischer-Hjalmars and Henriksson-Enflo, 1980). Any positive metal ion seems to have the required stabilizing effect. It has therefore been called *the metal bridge effect.*

These findings about the metal bridge effect on the energy gap have interesting consequences for various physical properties. One is the electronic excitation energy. A reduction of $\Delta\epsilon$ means a shift to longer wavelengths of the first N–V transition. In fact, for some compounds, $[M(C_2H_2S_2)_2]^n$, the electronic spectra have been measured (Schrauzer and Mayweg, 1965), and it has been found that when $n = 0$ or -1, the first intense absorption band lies in the visible or near-IR part of the spectrum, but when $n = -2$ this absorption is shifted to the UV region. Our energy-

gap calculations are thus in accord with these measurements.[1] Other interesting properties such as electrical resistivity and redox potentials are also in conformity with our calculations (Rosa and Schrauzer, 1969).

E. Charge Distribution

1. *Definitions*

The electronic charge distribution in the molecule can be presented in the form of graphs, for example, as isodensity maps. These maps give a very good overall picture of the distribution but may be difficult to quantify. The most common way to describe the charge distribution is with the aid of Mulliken population analysis (Mulliken, 1955), including gross atomic, net atomic, and overlap populations. As is well known the Mulliken scheme is not completely perfect. For example, the definition of gross population gives too much population to the less electronegative atom of a strongly polar bond. Nevertheless, the scheme is very useful for a study of trends in shifts of density in series of similar molecules. It can be an indicator of situations where possible reactivity indices deserve a closer analysis.

The *gross charge* on an atom is in our terminology the sum of the positive nuclear charge and the negative gross atomic population. In the same way we introduce the *net charge* as the sum of nuclear charge and negative net atomic population. We also define the *extra net population* as the difference between the net atomic population of the atom in the molecule and the number of electrons of the neutral atom, H, C, N, O, S, and metal. Both overlap and net populations can be further partitioned into their σ and π parts.

2. *Charge on Metals*

Charges on the metals, derived from gross populations, are displayed in Fig. 8 for complexes of the ligands, $C_2H_2X_2$, X = NH, O, S, with a series of metals. There are three columns for each metal giving the gross charges on the metal ions for overall charge $n = +2, 0, -2$. The upper row shows metal charges in NH complexes; the middle row, O complexes; and the bottom row, S complexes. The metal charge in NH complexes is seen to be close to +1 for all the metals studied. The metal charge does not change much with the overall charge n, but it does de-

[1] After the submission of the present article, extensive INDO calculations on electronic spectra of $[Ni(C_2H_2S_2)_2]^n$ (I) and $[Ni(C_3H_3S_2)_2]^n$ (II) were published by Herman *et al.* (1982). These authors calculated $\Delta\epsilon$ values of 3.8 and 6.8 eV for compounds I and II, respectively. The corresponding excitation energies were found to be 1.4 eV (11.6 kK) and 2.5 eV (19.8 kK), demonstrating the connection between $\Delta\epsilon$ values and N–V transitions.

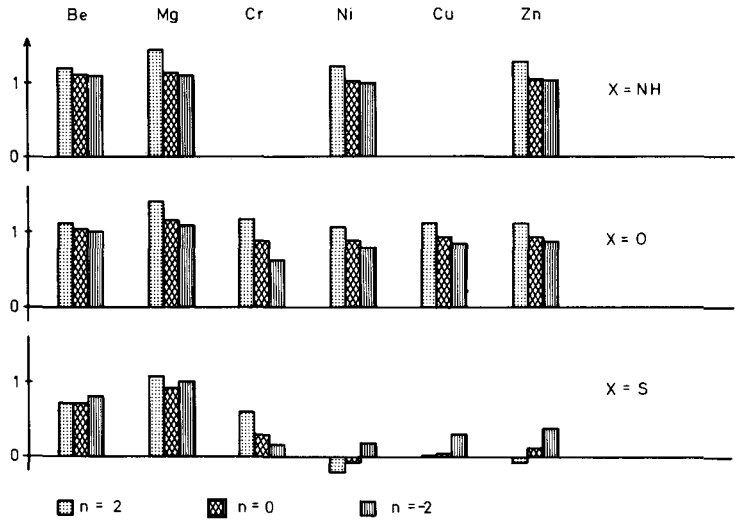

Fig. 8. Gross charges on the metals of complexes $[M(C_2H_2X_2)_2]^n$, $n = 2, 0, -2$.

crease slightly when n decreases from +2 to −2. In the O complexes there is a larger difference between the different metals. The charges on Be and Mg are almost the same in NH and O complexes for all n values. Charges on transition metals are somewhat lower in O complexes than in NH complexes, particularly for $n = -2$. Inspection of S complexes shows that charges on Be and Mg complexes are somewhat lower than in NH and O complexes, particularly for $n = +2$. For $n = -2$, the Mg ion in the S complex has almost the same charge as in NH and O complexes. The decrease of metal charge when n is lowered, found for NH and O complexes, is not a general feature of S complexes. For Be and Mg the charge is almost the same for all three values of n. Considering S complexes of transition metals, Fig. 8 shows a drastic lowering of the metal charge compared to NH and O complexes. All charges are close to zero, even negative in some cases. A low value of the charge on the metal is in harmony with experiments, Larsson *et al.* (1978–1979), Grim *et al.* (1974), and with CNDO calculations by Ciullo and Sgamellotti (1976). In Cr complexes the metal charge decreases with decreasing n, but for Ni, Cu, and Zn, the metal charge increases. Obviously, the *interaction between transition metals and sulfur has special properties* not found for their interaction with nitrogen or oxygen, nor for the interaction of Mg with sulfur. For the S complex of Be there is some decrease of the metal charge though less pronounced than for the transition metals.

TABLE IX

MX Overlap of Complexes $[M(C_2H_2X_2)_2]^n$

	X								
	NH			O			S		
M	σ	π	Total	σ	π	Total	σ	π	Total
Be									
+2	0.32	0.01	0.33	0.30	0.01	0.31	0.40	0.01	0.41
0	0.32	0.04	0.36	0.30	0.04	0.34	0.39	0.04	0.43
−2	0.34	0.03	0.37	0.32	0.03	0.35	0.39	0.03	0.43
Mg									
+2	0.25	0.01	0.26	0.24	0.02	0.26	0.31	0.02	0.33
0	0.27	0.10	0.37	0.27	0.07	0.34	0.30	0.10	0.40
−2	0.34	0.08	0.42	0.31	0.06	0.37	0.30	0.08	0.38
Ni									
+2	0.28	0.01	0.29	0.32	0.02	0.34	0.54	0.02	0.56
0	0.28	0.09	0.37	0.34	0.07	0.41	0.52	0.09	0.61
−2	0.32	0.07	0.40	0.37	0.07	0.45	0.48	0.05	0.53
Cu									
+2				0.31	0.03	0.33	0.54	0.03	0.57
0				0.32	0.07	0.39	0.51	0.10	0.61
−2				0.35	0.08	0.43	0.48	0.04	0.53
Zn									
+2	0.26	0.02	0.28	0.30	0.02	0.32	0.53	0.03	0.56
0	0.26	0.09	0.34	0.30	0.07	0.37	0.48	0.10	0.58
−2	0.29	0.08	0.39	0.33	0.08	0.41	0.45	0.08	0.53

For an analysis of the origin of the different charge distributions in the case of different ligating atoms X, we shall restrict the details to the case of $n = 0$. Table IX shows MX overlap populations partitioned into σ and π parts. The σ part is obviously dominating in all cases; BeX and MgX overlaps do not change much for different ligands X. The change of transition metal overlap is more pronounced. Since there are four bonds from each metal it turns out that change of MX overlap is responsible for one-third to one-half of the change of gross charge. However, it must be remembered that the gross charge on M is composed of net charge on M, MX bonding overlap, and nonbonding negative overlap between the metal and the hydrocarbon part of the ligand.

To clarify the specific interaction of the transition metals with the ligands, one should look for the role of the d orbitals. To this end, the net charge (cf. Section IV,E,1), partitioned into s, p, and d contributions, is

TABLE X

NET CHARGES ON THE METALS IN COMPLEXES $[M(C_2H_2X_2)_2]^0$ PARTITIONED INTO s, p, AND d CONTRIBUTIONS

Ligand	Orbital	Metal				
		Be	Mg	Ni	Cu	Zn
Oxygen	s	1.81	1.87	1.81	1.79	1.78
	p	−0.22	−0.30	−0.26	−0.28	−0.30
	d	—	—	−0.08	−0.04	−0.03
	Sum	1.59	1.57	1.47	1.47	1.45
Sulfur	s	1.81	1.86	1.66	1.63	1.60
	p	−0.29	−0.33	−0.31	−0.35	−0.40
	d	—	—	−0.48	−0.27	−0.11
	Sum	1.52	1.52	0.87	1.01	1.09

listed in Table X. In Table XI, overlap on the metal (half of the total overlap between metal and ligand) is partitioned into s, p, and d parts. For comparison Table XI also lists values of nonbonding overlap.

Table X shows that net charges on Mg and Be are almost identical in O and S complexes. The charges on transition metals including Zn are different in the two kinds of complexes. With S ligands the net charge on Zn decreases in all three parts, s, p, and d, but mostly in s. On metals with incompletely filled d shells, Ni and Cu, the largest decrease of net charge is found in the d part. Table XI shows that the nonbonding overlap is very similar in O and S complexes of all the metals. The bonding overlap on Be and Mg is somewhat larger for X = S than for X = O, mainly due to increased p overlap. As for Ni, Cu, Zn, the increase in bonding overlap is distributed over all three orbitals, s, p, and d, and the total MX overlap is the same for these three metals.

The conclusion to be drawn from Tables X and XI is that *vacancies in the* d *shell are unimportant for the total overlap and are only reflected in the net atomic populations*. Similar conclusions have been drawn by other authors, e.g., Pappas (1978b) where references to earlier work are given. However, as is discussed in Section IV,H, we want to stress that our conclusion *refers to the later part of the series* of transition metals and not necessarily to the first part where there are fewer particles than holes.

3. *Ligands and Complexes of High Symmetry*

The Mulliken population analysis of complexes with different metal ions shows that the hydrocarbon part of the ligands has very similar

TABLE XI

OVERLAP POPULATIONS[a] ON THE METALS IN COMPLEXES $[M(C_2H_2X_2)_2]^0$ PARTITIONED INTO s, p, AND d CONTRIBUTIONS

Ligand	Overlap	Metal				
		Be	Mg	Ni	Cu	Zn
Oxygen	Bonding	0.68	0.67	0.81	0.78	0.76
	s	0.27	0.22	0.22	0.24	0.25
	p	0.41	0.45	0.42	0.43	0.45
	d	—	—	0.17	0.11	0.06
	Nonbonding	−0.13	−0.27	−0.28	−0.26	−0.27
	s	−0.07	−0.06	−0.07	−0.07	−0.08
	p	−0.06	−0.21	−0.17	−0.16	−0.17
	d	—	—	−0.04	−0.02	−0.02
Sulfur	Bonding	0.87	0.80	1.21	1.21	1.18
	s	0.30	0.24	0.35	0.38	0.40
	p	0.57	0.56	0.55	0.63	0.70
	d	—	—	0.31	0.20	0.08
	Nonbonding	−0.09	−0.20	−0.25	−0.22	−0.21
	s	−0.05	−0.05	−0.08	−0.09	−0.10
	p	−0.04	−0.15	−0.13	−0.13	−0.13
	d	—	—	−0.04	−0.00	0.02

[a] In electron units.

populations for all metals considered (cf. Table XI; Fischer-Hjalmars and Henriksson-Enflo, 1981). In what follows we shall only discuss the charge distribution of the ligands for some typical cases. Further details are given elsewhere (Fischer-Hjalmars and Henriksson-Enflo, 1981; Blomberg *et al.*, 1979).

Table XII shows extra net populations and Table XIII bond overlap populations of free-ligand monoanions L^- and metal complexes $[BeL_2]^0$ and $[NiL_2]^0$ for L equal to $C_2H_2O_2$ and $C_2H_2S_2$. The unsymmetrical ligand L equal to OCH—C′H′S, also included in the Tables XII and XIII, is discussed below in Section IV,E,4. Since EA is essentially due to the ligand (see Section IV,B), it seems correct to consider the complex $[ML_2]^n$ as composed of M^{2+} and two $L^{(n-2)/2}$. As typical examples we have chosen to describe the effect of the metal as the difference between populations of L^- and the complexes $[BeL_2]^0$ and $[NiL_2]^0$.

Some comments on the populations of the free ligands should first be given. It is seen from Table XII that O of $(C_2H_2O_2)^-$ has an extra net population of 0.34 e.u., but S of $(C_2'H_2'S_2)^-$ has only 0.05 extra net population. When looking at the π part it is found that O and S have equal

populations, 0.37 and 0.41, respectively. It is the σ distribution that is different, -0.03 on O and -0.37 on S. This difference of σ distribution on the two ligating atoms is also mirrored in the populations on C and H. The π parts on C and C′ are equal (-0.17 and -0.20), but the σ parts are as different as -0.87 and 0.01. The net populations on H and H′ are also somewhat different, -0.26 and -0.47, respectively. Table XIII shows that the CO bond has a much larger overlap, 0.87, than the CS bond with an overlap of 0.57. Again, the difference is in the σ part. Table XIII also reveals that not only the CX bonds but also the CC bonds are different. In particular, the very small σ overlap of the C′C′ bond, 0.07, is remarkable. As discussed in detail by Fischer-Hjalmars and Henriksson-Enflo (1981),

TABLE XII

EXTRA NET ATOMIC POPULATIONS[a] OF FREE-LIGAND MONOANIONS L^- AND COMPLEXES $[BeL_2]^0$, $[NiL_2]^0$, AND $[BeL]^+$

	L = $C_2H_2X_2$			L = OCH–C′H′S		
	L^-	$[BeL_2]^0$	$[NiL_2]^0$	L^-	$[BeL_2]^0$	$[BeL]^+$
			Oxygen ligands			
O:σ	−0.03	−0.20	−0.24	−0.06	−0.16	−0.26
π	0.37	0.44	0.41	0.32	0.41	0.47
Total	0.34	0.23	0.17	0.26	0.25	0.21
C:σ	−0.87	−0.84	−0.83	−0.88	−0.88	−0.77
π	−0.17	−0.27	−0.27	−0.39	−0.41	−0.53
Total	−1.04	−1.11	−1.10	−1.27	−1.29	−1.30
H:σ	−0.26	−0.52	−0.53	−0.32	−0.52	−0.62
M:σ		−1.67	−1.55		−1.62	−1.54
π		0.08	0.11		0.06	0.03
Total		−1.60	−1.44		−1.56	−1.52
			Sulfur ligands			
H′:σ	−0.47	−0.61	−0.61	−0.45	−0.60	−0.60
C′:σ	0.01	0.02	−0.13	0.01	0.09	0.09
π	−0.20	−0.27	−0.25	0.09	−0.08	−0.16
Total	−0.20	−0.25	−0.38	0.10	0.01	−0.07
S:σ	−0.37	−0.60	−1.02	−0.32	−0.73	−1.13
π	0.41	0.39	0.34	0.43	0.41	0.66
Total	0.05	−0.21	−0.68	0.12	−0.31	−0.47
M:σ		−1.58	−0.91			
π		0.07	0.03			
Total		−1.52	−0.89			

[a] In electron units.

TABLE XIII

OVERLAP POPULATIONS[a] OF FREE LIGANDS L^- AND COMPLEXES $[BeL_2]^0$, $[NiL_2]^0$, AND $[BeL]^+$

Bond	L = $C_2H_2X_2$			L = OCH–C'H'S		
	L^-	$[BeL_2]^0$	$[NiL_2]^0$	L^-	$[BeL_2]^0$	$[BeL]^+$
			Oxygen ligands			
OM : σ		0.30	0.34		0.21	0.27
π		0.04	0.07		0.02	0.01
Total		0.34	0.41		0.22	0.28
CO : σ	0.65	0.48	0.47	0.67	0.54	0.52
π	0.21	0.19	0.19	0.31	0.25	0.26
Total	0.87	0.67	0.66	0.97	0.78	0.77
CH : σ	0.67	0.75	0.76	0.76	0.79	0.77
CC or CC' : σ	0.44	0.57	0.61	0.24	0.35	0.31
π	0.21	0.23	0.23	0.19	0.24	0.19
Total	0.65	0.80	0.84	0.42	0.59	0.50
			Sulfur ligands			
C'C' : σ	0.07	0.18	0.34			
π	0.30	0.33	0.33			
Total	0.36	0.51	0.67			
C'H' : σ	0.78	0.76	0.75	0.75	0.73	0.71
C'S : σ	0.37	0.25	0.42	0.30	0.17	0.29
π	0.20	0.18	0.09	0.11	0.14	0.08
Total	0.57	0.43	0.60	0.40	0.31	0.37
SM : σ		0.39	0.52		0.44	0.59
π		0.04	0.09		0.05	0.04
Total		0.43	0.60		0.49	0.63

[a] In electron units.

CC bonding in $(C_2H_2S_2)^n$ is mainly due to π electrons. The free ligand is therefore only stable when $n = -1$ or -2. In fact, Hoyer *et al.* (1971) remark that, as far as they are aware, the neutral $C_2H_2S_2$ does not exist, but the dianion is well known.

The covalent part of the MX bonds is essentially of σ type (cf. Table XIII; Fischer-Hjalmars and Henriksson-Enflo, 1981). The metal ion gains some extra net atomic population, also mainly of σ type (see Table XII). The total gross population accepted by the metal ion of the $[Be(C_2H_2O_2)_2]^n$ complexes (cf. Fig. 8) is 1.0 e.u. and only 0.1 of π type. The σ population is donated by the O atoms, 0.68 e.u.; CO bonds, also 0.68 e.u.; and by the H atoms, 1.04 e.u. Thus the remote H atoms donate a large part to the

metal ion. It is also interesting that the loss of σ population at the O atoms is partly recompensated by a gain of π population. This is not true for the CO bonds where the π overlap is unchanged. The σ and π rearrangements also include the C atoms and the CC and CH bonds. Both bonds gain some σ overlap and the C atoms lose some π population.

The redistribution of charge described for the $[Be(C_2H_2O)_2]^0$ complex is very similar to that of other metal–oxygen complexes. As an example, the details of the charge distribution within the Ni–O complex are included in Tables XII and XIII.

We summarize as follows: (1) *redistribution of charge is not localized* to the MX_4 region but the *whole ligand is involved;* (2) C atoms lose a little, O atoms somewhat more, and H atoms lose most net population; (3) CC and CH overlaps increase and CO overlap decreases. These calculated shifts can be compared with the reactivity of the methine (CH) hydrogen of amino acids (Phipps, 1979). Experimentally, it is found that this H atom is very stable in the free amino acids, but in the presence of a metal ion, Cu^{2+} or Co^{3+}, it easily undergoes substitution reactions: for example, addition of acetaldehyde, CH_3CHO, to glycine, NH_2CH_2COOH, in the presence of Cu^{2+} yields threonine, $CH_3CH(OH)CH(NH_2)COOH$. This effect is in agreement with our finding that H loses population in the metal complex, i.e., its positive charge is increasing. This shift obviously makes it easier for a H^+ ion to leave the molecule.

In case of the $[Be(C_2H_2S_2)_2]^0$ complex the charge redistribution is similar to that already described for $[Be(C_2H_2O_2)_2]^0$, but there are some differences. The gross population accepted by Be is somewhat larger, 1.3 e.u., but the π part is as small as in the O complex. The loss from the H atoms is smaller, but their final positive net charge, 0.6, is larger than in the O complex, 0.5, since H atoms of $[C_2H_2S_2]^n$ are more positive than those of $[C_2H_2O_2]^n$. At the S atoms of the complex the loss in σ is not counterbalanced by any gain in π. In total, S atoms lose 1.0 e.u. and H atoms 0.6 e.u. The four C'S bonds together lose 0.5 e.u. of σ overlap. In the free ligand the σ overlap of one C'C' bond is only 0.1, but in the Be complex it increases to 0.2. The total C'C' overlap increases from 0.4 to 0.5, becoming larger than the total C'S overlap of 0.4.

The charge distribution of the Mg–S complex is similar to the Be–S complex. But the transition metals change the ligands differently. Since the gross population transferred to the metal is much larger, 2.1 e.u. in case of Ni, some differences must be found. As could be foreseen, the S atoms lose considerably more σ population. In total, they lose 0.65 e.u. each, or 2.6 together. But the C'S bond does not lose overlap as in the Be complex. Rather, it gains a little and the C'C' overlap increases even more than in the Be complex. So the whole ligand seems to be stabilized by the Ni atom.

4. *Ligands and Complexes of Lower Symmetry*

As discussed in Section II there are many reasons to choose a model system of high symmetry. Therefore the main part of our project has been devoted to such complexes. But we know that nature in several cases has chosen metal complexes without symmetry (cf. Fig. 1). It is therefore important to study complexes of asymmetrical ligands. For computational reasons we have chosen the ligand OCH–C'H'S (OS ligand) as our first example of lowering the symmetry. Details of these calculations will be reported by Davstad (1981).

Tables XII and XIII include populations of L^- equal to the OS-ligand monoanion as well as the four-coordinated complex $[BeL_2]^0$ and the two-coordinated complex $[BeL]^+$. Our first comments deal with a comparison of the free OS ligand with the symmetrical ligands $C_2H_2X_2$.

Table XIII shows that the CO and CH overlap populations, 0.97 and 0.67 e.u., respectively, are larger, and the C'S overlap, 0.40, is smaller in the OS ligand than in the symmetrical ligands. The overlap of the CC' bond, 0.42, is close to that of the CC bond in $C_2H_2S_2$, 0.36. With overlap as a measure, the CC' and C'S bonds of the OS ligand are similar and both are much weaker than the CO bond. The net atomic populations of Table XII show that in the OS ligand, O, C, and H have lost and C' and S gained population compared to $C_2H_2X_2$. This increases the difference between the two carbon atoms of the ligand, C bound to O and C' bound to S. In fact, gross atomic populations show that *electronic charge has been transferred from the* CHO *half to the* C'H'S *half* of the ligand. The extra gross population of the CHO group is 0.2 and that of the CHS group is 0.8 in L^-. The corresponding values of L are -0.1 for CHO and 0.1 for CHS. In L^{2-} the extra gross populations of CHO is 0.6 and of CHS 1.4 e.u. This result of population analysis conforms to the monomer EAs of Table V, Section IV,B, showing that $C_2H_2O_2$ has a negative and $C_2H_2S_2$ a positive EA value. It is also in agreement with experimental pK_a values: 16 for ROH and 11 for RSH.

In the four-coordinated, low-symmetry complex $[BeL_2]^0$, the BeS overlap is almost the same as for symmetrical ligands $C_2H_2X_2$ but the BeO overlap is reduced. The net charge on Be, 1.56, is in between those of the symmetrical O and S complexes, 1.60 and 1.52, respectively. The gross population, transferred to Be, 1.1, is only slightly larger than that transferred to Be in $[Be(C_2H_2O_2)_2]$, 1.0. The main donors are the S, H, and H' atoms. At the O atoms the loss in σ is completely balanced by the gain in π. As in the free OS ligand the extra gross population of the C'H'S part, 0.4, is larger than that of the CHO part, 0.1, but the difference between the two parts is reduced.

A comparison of the four-coordinated complex $[BeL_2]^0$ and the two-

TABLE XIV

TOTAL CHARGE Q ON METAL AND LIGAND L DERIVED FROM GROSS POPULATIONS ON FOUR-COORDINATED COMPLEXES $[BeL_2]^n$ AND TWO-COORDINATED COMPLEXES $[BeL]^n$ WITH L = OC_2H_2S

	$[BeL_2]^n$			$[BeL]^n$		
	$n = 2$	1	0	$n = 2$	1	0
Q(Be)	0.97	0.95	0.94	1.26	1.11	0.94
Q(L)	0.51	0.02	−0.47	0.74	−0.11	−0.94

coordinated $[BeL]^+$ shows that the net population of the metal and the overlap of the BeO bond are slightly larger in $[BeL]^+$. The BeS overlap has increased even more. Since there are only two bonds to Be its gross population is reduced by 0.2. The total charge on Be, derived from gross populations, is found to be 0.94 in the case of $[BeL_2]^0$ and 1.11 for $[BeL]^+$. It has been shown before (Demoulin *et al.*, 1977; Fischer-Hjalmars and Henriksson-Enflo, 1981) that the total charge on the metal undergoes only minor changes when the overall charge n of the complex is changed. In Table XIV total charges Q on the Be ion are shown for the two complexes $[BeL_2]^n$ and $[BeL]^n$ for some values of n. Table XIV also includes the total charge on each ligand L. It is remarkable that Q(Be) is so insensitive to both the coordination number and the overall charge n.

An obvious consequence of the invariability of Q(Be) is the dependence of Q(L) on both n and the coordination number. Similar results were found by Pullman and Demoulin (1979). The two OS complexes of Tables XII and XIII, $[BeL_2]^0$ and $[BeL]^+$, are seen to have Q(L) values as different as −0.47 and −0.11. The detailed charge distribution within the ligands is also rather different. In $[BeL]^+$ the O atom has lost more in σ and gained more in π than in $[BeL_2]^0$; for the C atom it is just the opposite. In $[BeL]^+$, H has lost in σ and C′ in π; the CC′ overlap is reduced. The most remarkable change is in the population at the S atom where compared to $[BeL_2]^0$, there is a large loss of σ population, 0.40 e.u. This loss in σ is only partly balanced by a gain of 0.25 e.u. in π population. In spite of this loss at the S atom the gross population of the C′H′S group is larger than that of the CHO group: 0.16 and 0.05 e.u., respectively.

In conclusion, the comparison between $[BeL_2]^0$ and $[BeL]^+$ amplifies the importance of choosing a model system where the coordination is representative of the metal in question, at least when ligand properties are of interest.

TABLE XV

BOND POLARITY OF LIGANDS L = $C_2H_2X_2$ AND OCH–C'H'S AND COMPLEXES $[ML_2]^0$ AND $[ML]^+$, M = Be AND Ni

	L = $C_2H_2X_2$			L = OCH–C'H'S		
Bond	L^-	$[BeL_2]^0$	$[NiL_2]^0$	L^-	$[BeL_2]^0$	$[BeL]^+$
			Oxygen ligands			
OM : σ		1.47	1.31		1.46	1.28
π		0.36	0.30		0.35	0.44
Total		1.83	1.61		1.81	1.73
OC : σ	0.84	0.64	0.59	0.82	0.72	0.51
π	0.54	0.71	0.68	0.71	0.82	1.00
Total	1.38	1.34	1.27	1.53	1.54	1.51
CH : σ	−0.61	−0.32	−0.30	−0.56	−0.36	−0.15
C'C : σ				0.89	0.97	0.86
π				0.48	0.33	0.40
Total				1.37	1.30	1.23
			Sulfur ligands			
C'H' : σ	0.48	0.63	0.48	0.46	0.69	0.69
C'S : σ	0.38	0.62	0.89	0.33	0.82	1.22
π	−0.61	−0.66	−0.59	−0.35	−0.50	−0.82
Total	−0.25	−0.04	0.30	−0.02	0.32	0.40
SM : σ		0.98	−0.11		0.89	0.41
π		0.32	0.31		0.35	0.63
Total		1.31	0.21		1.25	1.05

F. Bond Polarity

As is well known a polar bond is characterized by an unsymmetrical charge distribution between the bonded atoms. However, the measure of polarity is not always defined. Frequently charges derived from gross populations have been used. To make the polarity measure less dependent on the surroundings we prefer to *define the polarity of the bond* between atoms X and Y *as the difference between the extra net populations of the two atoms* (Fischer-Hjalmars and Henriksson-Enflo, 1981). Since populations are partitioned into σ and π parts we can define σ and π polarities in this way. For the sign we shall use the convention that the polarity of the XY bond is positive when X has a larger extra net population than Y, i.e., X^-Y^+.

Table XV shows the polarity of bonds in some ligands and complexes with both high and low symmetry. The CO bond of all ligands and com-

plexes has the expected polarity both in σ and π. The polarity of the CH bond is different in different surroundings and it is sensitive to the overall charge n. The polarity of the CS bond is also most variable. In fact, σ and π polarities have different signs. According to σ polarity, C is more negative than S, but according to π polarity, S is the more negative atom. When the compound is neutral or has a positive charge the σ polarity dominates; when π electrons are added, the π polarity increases and may dominate.

In the metal complexes of $C_2H_2O_2$ the OC polarity is reduced in the σ part and increased in the π part. The total effect is rather small. The negative polarity of the CH bond is reduced but remains C^+H^-. In metal complexes of $C_2H_2S_2$ the polarity C^-H^+ remains (Ni) or is increased (Be). Since the positive charge at H′ is increased in both complexes (see Table XII), charge and polarity cooperate to facilitate the leaving of a H^+ ion from the complex. The σ part of the C′S polarity is substantially changed by the metal. It increases from 0.38 in the free ligand to 0.62 in the Be complex and further to 0.89 in the Ni complex. Since the π polarity is unchanged the C^+S^- bond of the free ligand becomes nonpolar in the Be complex and C^-S^+ in the Ni complex.

The unsymmetrical OS ligand has some interesting features compared to $C_2H_2X_2$. In the present context the main difference is that *the* CC′ *bond of the* OS *ligand is polar;* σ and π polarities have the same sign and the total CC′ polarity, 1.37, is *almost as large as the* CO *polarity* of 1.53. The C′S polarity is almost zero. The polarities of the two CH bonds are as different as -0.56 in the CHO group and 0.46 in the C′H′S group. In the CHO group the C^+H^- polarity is reduced by the Be^{2+} ion in the same way as in $[Be(C_2H_2O_2)_2]^n$. The C^-H^+ polarity of the CHS group is increased by the metal as in the symmetrical S complex. It is therefore expected that electrophilic substituents replace the hydrogen of CHS rather than CHO. The C′S polarity is strongly perturbed by the metal and becomes C^-S^+.

Comparison between the two complexes $[BeL_2]^0$ and $[BeL]^+$ shows that all polarity changes are in the same direction but are exaggerated in the two-coordinated complex. For example, the σ polarity of the C′S bond is as large as 1.22 in $[BeL]^+$, compared to 0.82 in $[BeL_2]^0$. It is even larger than in $[Ni(C_2H_2S_2)_2]^0$, where the value is 0.89.

G. Effect of d Orbitals on Sulfur

As shown in Section IV,E, complexes between metal ions and ligands with sulfur as ligating atoms seem to be of particular importance. It is a common opinion in chemistry that when metals bind to sulfur-containing compounds, the low-lying empty d orbitals on sulfur play an important role in the binding. In quantum chemical calculations, d orbitals, espe-

cially when situated on different centers, cause computational problems that concern time and size requirements for the integral calculations. In order to perform calculations on such large systems as in the present case, it was impossible for us also to include d orbitals on sulfur. Moreover, quantum chemical calculations on organic sulfur compounds were made earlier, and it was found that in most of these cases the d orbitals on sulfur play a minor role and then only as polarization functions that extend the basis set (Roos and Siegbahn, 1971; Gelius *et al.*, 1972). In order to study this problem in more detail we made quantum chemical studies of a metal–sulfur complex having the same symmetry as our previously studied complexes, but also included d orbitals on sulfur (Henriksson-Enflo and Holmgren, 1981). The smallest possible complex for this study is the $[M(SH)_4]^n$ complex. For metal M we have chosen Zn and Ni. These two metals with d^{10} and d^8 configurations, respectively, represent two cases of interaction: one with a closed d shell and the other with an empty d orbital on the metal.

It was found that the d orbitals on sulfur play a minor role in the binding. The d-orbital population on sulfur was only 0.01–0.1 in all cases. The effect on other orbitals was larger, however. This is an effect of extending the basis set and not a d orbital effect. The effect on the central metal was also shown to be rather large because of the fact that there are four sulfur atoms present, each contributing the same amount.

Each effect, small or not as small, varied in a very systematic way. Thus, for example, in all cases the charge on the metal grew more positive as the total charge on the complex grew more negative. This effect was even exaggerated by the inclusion of d orbitals on sulfur. We can thus conclude that contrary to popular chemical opinion, *d orbitals on sulfur do not play any important role in the binding between metal and sulfur.*

H. Effect of d Orbitals on Transition Metals

The specific properties of transition metal compounds are generally attributed to the incompletely filled d shell of the metal. In Section IV,E,2, we have shown that the interaction between transition metals and sulfur is different from the interaction between magnesium and sulfur. However, Fig. 8 shows that properties not only of Ni and Cu but also of Zn deviate from those of Mg. In fact, complexes of the three metals Ni, Cu, and Zn are strikingly similar in many respects (see also Tables IX–XI). It is also interesting that biological properties of Zn are not very different from those of such transition metals as Co. It is well known that Zn^{2+} of carbonic anhydrase can be replaced by Co^{2+}, giving an enzyme that in several respects has properties very similar to those of the Zn enzyme (Lindskog and Malmström, 1962). Tables X and XI show that not only 3d but also 4s and 4p contribute to the specific properties of the MS interaction.

Figure 7 demonstrates that metal orbitals mix mainly with the lone pairs of the ligands. The deeper lying metal orbitals are almost unperturbed by complex formation. Table VI shows that the Zn d orbitals are remote from the lone-pair orbitals with energies between −9 and −11 eV. The mixing of d orbitals into the lone pairs is also negligible. In case of Ni and Cu the situation is very similar with the exception of b_{1g} orbitals where the vacant d(xy) orbital plays a certain role. Can we make any prediction about the role of d orbitals in complexes of other transition metals?

Studies of complexes of the transition metals Sc, Ti, and Cr have been initiated in our laboratory (Pettersson, 1981). These studies show that the d orbitals of such complexes belong to the outer orbitals. In fact, in complexes $[M(C_2H_2O_2)_2]^{2+}$, M = Sc or Ti, the highest occupied orbital is mainly a metal d orbital. It is also found that these d orbitals are very unstable when the overall charge is lowered and mix in an irregular manner with ligand orbitals; the Cr complexes behave similarly.

These findings can be related to orbital energies obtained from calculations on free metal ions. Calculations on Sc^{2+}, Ti^{2+}, and Zn^{2+}, with the basis set described in Section III,A, give the following d-orbital energies −24.6, −27.9, and −42.0 eV (Davstad, 1981). Corresponding experimental ionization potentials (Moore, 1949) are 24.8, 28.1, and 39.7 eV, respectively. The agreement is seen to be very satisfactory. Now we are interested in d-orbital levels in D_{2h} symmetry, close to D_{4h}. In this symmetry the d level is split into lowest lying, almost degenerate levels d(xz), d(yz), (b_{2g}, b_{3g}) which are π levels in our complex. Next come two a_{1g} levels, d(z^2) and $d(x^2 - y^2)$, and highest d(xy) in b_{1g} symmetry. This splitting has been obtained by atomic calculations on M^{2+} ions with D_{4h} configuration without spherical averaging (Davstad, 1981). Energies of d orbitals from such calculations are afterward shifted upward by 20 eV to simulate the field of negative ligands in complexes $[ML_2]^0$. Orbital energies obtained by this method for the entire series Sc^{2+} to Zn^{2+} are displayed in Fig. 9, which also shows the levels of oxygen lone pairs, 12–14 eV, and sulfur lone pairs, 9–13 eV. It is seen that d levels of Sc and Ti are indeed above the lone-pair levels and Cu and Zn well below. The d levels of Ni and Co approach the lone pair levels. The d-levels of Cr and Mn are just in the lone pair range and the Fe level is very close. Therefore we *predict* that bonding orbitals of complexes of transition metals Cr, Mn, and Fe will show considerable mixing between ligand lone-pair orbitals and metal d orbitals.

Admittedly the calculations behind Fig. 9 are rather crude, but the prediction about strong interaction between the Cr d level and lone pairs of the ligands is confirmed by full calculations on complexes $[Cr(C_2H_2X_2)_2]^n$, X = O and S (Pettersson, 1981).

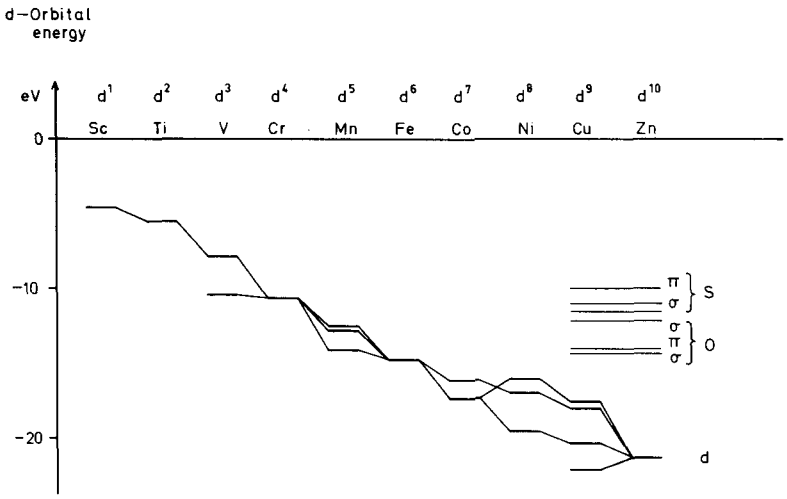

Fig. 9. Energy levels of d orbitals of divalent transition-metal ions in D_{4h} symmetry and of ligand lone pairs in complexes $[M(C_2H_2X_2)_2]^0$, X = O and S.

V. Summary and Conclusions

As is well known (cf. Section I), different metals play very different roles in biology. Some are needed in large amounts, others are essential but traces are sufficient, still others are toxic. In particular, transition metals, though chemically similar, have very different biological activities. The main purpose of our study has been to search for some classification of the metals with respect to their biological behavior.

To obtain some insight into the binding of metals in biology we have made quantum chemical *ab initio* calculations on a model system (shown in Fig. 2, Section II,A). The main reason for choosing this system was to model complexes between metal ions and amino acids or peptides. The advantage of the model is discussed in Section II. The system can also serve as a model of complexes of metals with other important bioligands such as glyoxal, ascorbic acid, catechols, and glyoxime (cf. Fig. 3, Section II,A). The ligating atoms X were chosen as X = NH, O, or S. The metals studied were Li, Be, Mg, Sc, Ti, Cr, Ni, Cu, and Zn. The overall charge of the complex n has been varied for each complex and includes some or all of the values $n = \pm 2, \pm 1$, and 0. A series of results from our investigations is presented in Section IV. Comparison with relevant experiments have been made as extensively as possible.

To calculate accurate values of binding energies is not an easy matter. It is not to be expected that the present level of *ab initio* method is sufficient for this purpose. Nevertheless, a comparison within series of similar systems is expected to give some useful information. As shown by Table III of Section IV,A, the connection between binding energy and overall charge n is different for different ligands X. When $n = +2$ the most stable complexes are formed with nitrogen ligands. When $n = -2$ the complexes with sulfur ligands are the most stable. For intermediate values of n the picture is less clear. These different stability orders mean that in different surroundings, for example, different pHs, different types of complexes may arise. It has been verified by experiments that different types of metal–amino acid complexes are formed at different pHs.

When comparing the different metals it is seen that the Be complexes are more stable than the others. This extreme stability may be connected with the high toxicity of this metal. Binding energies of the series Mg, Ni, Cu, Zn are compared in Figs. 5 and 6. It is gratifying that the trends are the same as in Irving–Williams diagrams.

The EAs of the various complexes are shown in Table V and discussed in Section IV,B. It is shown that this affinity is almost independent of the metal involved and can be classified as a property of the ligand in the field of any positive ion. Electron affinities are found to be positive when the overall charge n is positive. For sulfur ligands the affinity is larger than for other ligands and clearly positive even when $n = 0$.

Most of the filled molecular orbitals of the complexes can be classified as either ligand orbitals or metal orbitals (see Table VI, Section IV,C). The ligand orbital energies are shifted by the Coulomb field of the ion but are otherwise independent of the metal. This result agrees with measurements of ionization potentials.

The highest of the occupied orbitals (HOMO) and the lowest of the unoccupied orbitals (LUMO) are known to give useful reactivity indices. It has been found that they are ligand orbitals for all complexes studied here. In the four-coordinated compounds the HOMO–LUMO energy gap is large when $n = \pm 2$ but is considerably reduced when $n = \pm 1$ or 0 (see Section IV,D and Table VIII). The reduction of the energy gap has important physical consequences. It means a shift to longer wavelengths of the first N–V transition. Such shifts have been found experimentally. Electrical resistivity and redox potentials are also changed.

The reduction of the energy gap is a property of the ligand dimer. But this property can only be manifest in the presence of a positive metal ion, forming a bridge between the two monomers. It can therefore be called a metal bridge effect.

As pointed out, most of the orbitals of the free-ligand dimer can be

easily recognized in the metal complex; however, there are some exceptions. The ligand lone-pair orbitals are clearly perturbed by the metal. They are found to interact with vacant metal orbitals and are responsible for the covalent part of the bonding. This bonding varies with both metal and ligand. As an example, Table VII shows the electron population on Ni in the complex $[Ni(C_2H_2S_2)_2]^0$. It is seen that the overlap population is largest in 4 p and equal in 4s and 3d. The complete orbital diagram of this complex is shown in Fig. 7.

A useful tool for the study of covalent bonding is the distribution of electronic charge. This distribution can be quantified by the use of Mulliken population analysis as discussed in Section IV,E. The gross charges on the metals are displayed in Fig. 8. It is seen that there is a considerable transfer of charge from the ligands to the metal ions. In the case of nitrogen ligands all the metals have similar charges, close to +1. With oxygen ligands some details are different but the overall picture is the same as with nitrogen. As for sulfur ligands there is a clear distinction between Be and Mg on the one hand and transition metals on the other. The charge transfer is almost 2 e.u. in the latter case. Obviously, the interaction between transition metals and sulfur has special properties. A comparison between oxygen and sulfur complexes of transition metals shows that both net charges on the metals and overlap populations are different (see Tables IX–XI). It is interesting that vacancies in the d shell are unimportant for the total overlap, that is, for the covalency of the bond (see Table XI).

The effect of some metals on different ligands is analyzed in Tables XII and XIII. It is found that the redistribution of charge is not localized to the MX_4 region but includes the entire ligand. In particular, the H atoms are found to lose electrons when the metal complexes are formed. As a consequence, the reactivity of the H atoms increases considerably, as is also found experimentally. As for the sulfur ligand, it is remarkable that the CC bond is rather weak in the free ligand but strengthened considerably in metal complexes.

Metal complexes in biological systems often have lower symmetry than D_{2h} (see Fig. 1). A study of unsymmetrical ligands has therefore been initiated (see Section IV,E,4 and Tables XII and XIII). It was found that the unsymmetrical ligand OCH—C′H′S has a rather weak CC′ bond that is strengthened by complex formation. The net charges on C and C′ are very different, 1.3 and −0.1 e.u., respectively. The H′ atom is somewhat more positive than H in both the free ligand and the complex.

For the unsymmetrical ligand a comparison has been made between a four-coordinated and a two-coordinated complex. Table XIV shows that the gross charge on the metal is close to +1 for both kinds of complexes but the total ligand charge is very different. The details of charge distribu-

tion within the ligands show the same trends for two- and four-coordinated complexes but are grossly exaggerated in the former case. As an example, the σ net population on S is -1.13 and -0.73 e.u., respectively. This underlines the necessity to study fully coordinated complexes, at least when ligand properties are of interest.

The concept of bond polarity is discussed in Section IV,F. It is suggested that extra net populations should be used as a measure of polarity. Table XV shows the polarity of bonds in some ligands and complexes. The polarity of the CH bond is seen to be very different in different surroundings, e.g., 0.6 C^+H^- in the CHO group and 0.5 C^-H^+ in the CHS group. For the CS bond, σ polarity is C^-S^+ and π polarity is C^+S^-. Thus, the total polarity can easily change sign, e.g., by the presence of a metal ion. In the unsymmetrical ligand the polarity of the CC′ bond is almost as large as the CO polarity. The OM polarity is very similar in Be and Ni complexes, but the SM polarity is completely different for these two metals.

Since it was found that the interaction between metal and sulfur does distinguish the transition metals from other metals, it is important to analyze the details of this interaction. It is popular opinion in chemistry that the d orbitals on sulfur may play an important role in the binding. For technical reasons it was impossible to include sulfur d orbitals generally, but some test cases were studied, as described in Section IV,G. Our result was that d orbitals on sulfur are not important for the binding.

Generally, the specific properties of transition metals are attributed to the incompletely filled d shell of the metal; however, our analysis has shown that overlap and polarity of the MS bond are very similar for the three metals Ni, Cu, and Zn, so an open d shell can not be crucial. On the other hand, it was also found that the main bonding interaction takes place between ligand pairs of σ type and vacant metal orbitals (see Fig. 7 and Section IV,C). As shown in Tables VI and VII, vacant d orbitals participate but do not dominate this interaction.

A prediction about the role of d orbitals in complexes of other transition metals has been made in Section IV,H. For this purpose calculations on free M^{2+} ions but in D_{4h} symmetry have been compared to calculations on complexes of Sc, Ti, Cr, Ni, Cu, and Zn. It is found that d orbital energies of the complexes are well reproduced by the free-ion calculations when the d orbitals are either below or above the ligand lone-pair orbitals. When d-orbital energies are close to lone-pair orbitals as in Cr complexes an appreciable and irregular mixing occurs. Figure 9 shows energy levels of free-ion d orbitals of the entire series of transition metals as well as lone-pair energy levels. According to this diagram, we can predict that bonding between metal and ligand in complexes of the transition metals Cr, Mn, and Fe must have particularly interesting properties.

To sum up, our model system has shown many interesting and also unexpected properties of the metal complexes. The similarities between our model and several biological metal systems have revealed new aspects to the intricate problem of metals in biology. We hope that this will stimulate future research in the field.

Acknowledgments

The late Marianne Sundbom initiated several research projects on the role of metals in biology. We want to express our deep appreciation of her inspiring and continuous interest in this work. We are also greatly indebted to all members of the quantum chemistry group at the University of Stockholm for valuable discussions about the subject of this article. We are particularly grateful to Margareta Blomberg, Kjell Davstad, Daniel Demoulin, Hans Holmgren, Indira Murthy, Jan Pappas, Lars Pettersson, and Ulf Wahlgren for fruitful cooperation within this project.

This work has been partly supported by grants from the Swedish Work Environment Fund and from the Swedish Natural Science Research Council, which is gratefully acknowledged.

References

Ahrland, S., Chatt, J., and Davies, N. R. (1958). *Q. Rev. Chem. Soc.* **12,** 265.

Almlöf, J. (1974). USIP-Report 74-29, University of Stockholm Institute of Physics.

Bagus, P. S. (1972). Documentation for Alchemy—Energy Expressions for Open Shell Systems. IBM Research Report RJ1077.

Bair, R. A., and Goddard, W. A., III. (1978). *J. Am. Chem. Soc.* **100,** 5669.

Blomberg, M. R. A., Fischer-Hjalmars, I., and Henriksson-Enflo, A. (1979). USIP-Report 79-11, University of Stockholm, Institute of Physics.

Blomberg, M. R. A., Fischer-Hjalmars, I., and Henriksson-Enflo, A. (1980). *Isr. J. Chem.* **19,** 143.

Burns, R. P., and McAuliffe, C. A. (1979). *Adv. Inorg. Chem. Radiochem.* **22,** 303.

Carlson, R. H., and Brown, T. L. (1966). *Inorg. Chem.* **5,** 268.

Ciullo, G., and Sgamellotti, A. (1976). *Z. Phys. Chem. Neue Folge* **100,** 67.

Demoulin, D., Fischer-Hjalmars, I., Henriksson-Enflo, A., Pappas, J. A., and Sundbom, M. (1977). *Int. J. Quantum Chem.* **12** (Suppl. 1), 351.

Durig, J. R., Tong, C. C., and Li, Y. S. (1972). *J. Chem. Phys.* **57,** 4425.

Fischer-Hjalmars, I., and Henriksson-Enflo, A. (1980). *Int. J. Quantum Chem.* **18,** 409.

Fischer-Hjalmars, I., and Henriksson-Enflo, A. (1981). *Ann. N.Y. Acad. Sci.* **373,** 37.

Freeman, H. C. (1967). *In* "Advances in Protein Chemistry" (C. B. Anfinsen, ed.), p. 258. Academic Press, New York.

Furlani, C., and Cauletti, C. (1978). *Struct. Bond.* **35,** 119.

Gelius, U., Roos, B., and Siegbahn, P. (1972). *Theor. Chim. Acta* **27,** 171.

Gray, H. B. (1965). *Transit. Metal Chem.* **1,** 240.

Grim, S. O., Matienzo, L. J., and Swartz, Jr., W. E. (1974). *Inorg. Chem.* **13,** 447.

Hay, R. W. (1976). *In* "An Introduction to Bio-Inorganic Chemistry" (D. R. Williams, ed.), p. 51. Thomas, Springfield, Illinois.

Henriksson-Enflo, A., and Holmgren, H. (1981). Preliminary Report, University of Stockholm.
Henriksson-Enflo, A., Demoulin, D., and Holmgren, H. (1981). Preliminary Report, University of Stockholm.
Herman, Z. S., Kirchner, R. F., Loew, G. H., Mueller-Westerhoff, U. T., Nazzal, A., and Zerner, M. C. (1982). *Inorg. Chem.* **21,** 46.
Hotop, H., and Lineberger, W. C. (1975). *J. Phys. Chem. Ref. Data* **4,** 539.
Hoyer, E., Dietzsch, W., and Schroth, W. (1971). *Z. Chem.* **11,** 41.
Huzinaga, S. (1965). *J. Chem. Phys.* **42,** 1293.
Irving, H., and Williams, R. J. P. (1953). *J. Chem. Soc. (London)* 3192.
Johansen, H. (1974). Program POPUL. DTH. Lyngby, Denmark.
Kennard, O., Watson, D. G., Allen, F. H., Isaacs, N. W., Motherwell, W. D. S., Pettersen, R. C., and Town, W. G. (1972). "Molecular Structures and Dimensions," Vol. A1 (Int. Union of Crystallograph). Unwin, London.
Kuchitsu, K., Fukuyama, T., and Morino, Y. (1969). *J. Mol. Struct.* **4,** 41.
Larsson, R., Folkesson, B., and Lykvist, R. (1978–1979). *Chemica Scripta* **13,** 178.
Lindskog, S., and Malmström, B. G. (1962). *J. Biol. Chem.* **237,** 1129.
McCleverty, J. A. (1968). *Prog. Inorg. Chem.* **10,** 49.
Moore, C. E. (1949). "Atomic Energy Levels." Circular No. 497. National Bureau of Standards, Washington, D.C.
Mulliken, R. S. (1955). *J. Chem. Phys.* **23,** 1833.
Österberg, R. (1976). *In* "An Introduction to Bio-Inorganic Chemistry" (D. R. Williams, ed.), p. 13. Thomas, Springfield, Illinois.
Pappas, J. A. (1978a). *Acta Chem. Scand.* **B32,** 389.
Pappas, J. A. (1978b). Ph. D. Thesis, Institute of Physics, University of Oslo.
Pearson, R. (1963). *J. Am. Chem. Soc.* **85,** 3533.
Phipps, D. A. (1979). *J. Mol. Catal.* **5,** 81.
Pullman, A., and Demoulin, D. (1979). *Int. J. Quantum Chem.* **16,** 641.
Rode, B. M. (1974). *Chem. Phys. Lett.* **26,** 350.
Roos, B., and Siegbahn, P. (1970). *Theor. Chim. Acta* **17,** 209.
Roos, B., and Siegbahn, P. (1971). *Theor. Chim. Acta* **21,** 368.
Roos, B., Veillard, A., and Vinot, G. (1971). *Theor. Chim. Acta* **20,** 1.
Rosa, E. J., and Schrauzer, G. N. (1969). *J. Phys. Chem.* **73,** 3432.
Sartani, D., and Truter, M. R. (1967). *J. Chem. Soc. (London)* **A,** 1264.
Schaefer, H. F., III. (1977). *Acc. Chem. Res.* **10,** 287.
Schrauzer, G. N. (1968). *Transit. Metal Chem.* **4,** 299.
Schrauzer, G. N., and Mayweg, V. P. (1965). *J. Am. Chem. Soc.* **87,** 3585.
Siiman, O., and Carey, R. R. (1980). *J. Inorg. Biochem.* **12,** 353.
Vokal, H., Hellsten, E., Henriksson-Enflo, A., and Sundbom, M. (1975). USIP-Report 75-21, University of Stockholm, Institute of Physics.
Williams, D. R. (ed.) (1976a). "An Introduction to Bio-Inorganic Chemistry." Thomas, Springfield, Illinois.
Williams, D. R. (1976b). *In* "An Introduction to Bio-Inorganic Chemistry" (D. R. Williams, ed.), p. 190. Thomas, Springfield, Illinois.

Ab Initio Calculations of Metalloporphyrins

A. DEDIEU, M.-M. ROHMER, and A. VEILLARD
Institut Le Bel
Université Louis Pasteur
Strasbourg, France

I. Introduction

The metalloporphyrins (Fig. 1a) are fascinating molecules to both the coordination chemist and the biologist. They appeal to the coordination chemist for several reasons: their ability to incorporate a wide variety of metals, their rich stereochemistry, their variety of oxidation states, and their ability to bind and to activate small ligands. To the biologist, the metalloporphyrins are notable by their presence in many proteins and enzymes which are responsible for the storage and transport of electrons and molecular oxygen, the decomposition of hydrogen peroxide, and the activation of oxygen. For these reasons, the last 20 years have witnessed an explosion of experimental studies on the metalloporphyrins. Despite this, there are yet many unknowns regarding the electronic structure and the stereochemistry of the metalloporphyrins, either in the biological molecules or in their synthetic models. The reasons for this are various: In some cases the experimental conditions preclude the use of most experimental tools; for instance, some biological hemes are not accessible to

ADVANCES IN QUANTUM CHEMISTRY, VOLUME 16

ISBN 0-12-034816-0

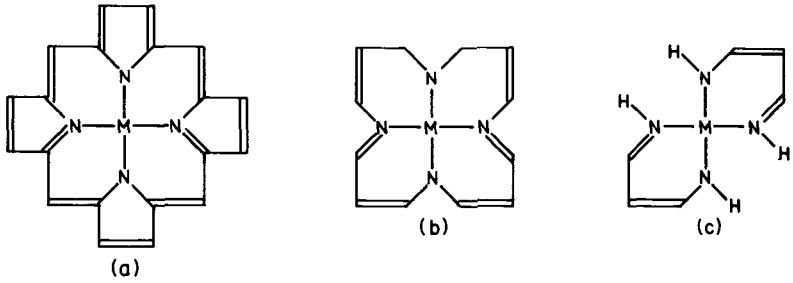

Fig. 1. (a) The unsubstituted metalloporphyrin; (b) the same with the β carbons of the pyrrole rings deleted; (c) Model II (see text).

X-ray or neutron diffraction studies. The dioxygen compounds of several metalloporphyrins are so unstable that their study is possible only at low temperatures and in solution. Many experimental techniques suffer from inherent uncertainties due to the assumptions made in the interpretation, and their conclusions may be regarded as reliable only after cross-checking. For instance, the electron-density maps obtained from X-ray and neutron diffraction data depend on the assumptions made regarding the thermal motion. To give just another example, the iron dioxygen unit in the oxyheme models has been formulated as Fe(III)—O_2^-, based on the fact that the corresponding ν (O_2) frequency at 1159 cm^{-1} in the IR spectrum is extremely close to the value of 1145 cm^{-1} for the free superoxide ion (Collman *et al.*, 1976). However, this is at variance with the short O—O separations of 1.16 and 1.23 Å compared to the bond length of 1.34 Å for the superoxide anion. The interpretation of data obtained from many spectroscopic techniques, such as EPR and Mössbauer spectroscopy, requires some knowledge of the electronic state of the system and of the corresponding wave function, which are usually not available. The requirement is even more severe for photoelectron spectroscopy, which takes for granted a detailed knowledge of the electronic states of the ion.

Basically, quantum mechanical studies appear ideally suited to answer some of the questions yet unsolved regarding the structure and electronic properties of the metalloporphyrins:

(1) Whenever there is a choice between different structures, the calculations should indicate which structure is the most stable. This type of problem has been encountered for the catalase compound I, for which two different structures have been proposed, one with an oxo ligand occupying an axial site and the other with the oxygen atom inserted into a Fe—N bond of the heme (Fig. 2) (Chevrier *et al.*, 1981).

(2) The assignment of the ground state and a knowledge of the electronic wave function should facilitate interpretation of EPR and

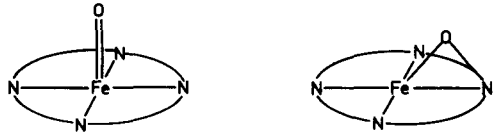

Fig. 2. Two different structures proposed for the catalase compound I (only the MN_4 unit of the metalloporphyrins is represented).

Mössbauer spectra (for instance, quadrupole splitting of Mössbauer spectra is related to the electric field gradient at the nucleus, which itself depends on the electronic configuration of the metal). A knowledge of the energy levels of the molecule or, better, of the electronic states of the parent ion will facilitate assignment of the photoelectron spectra.

(3) From the electronic wave function, it is possible to construct electron-density maps (or differential density maps) which are directly comparable to the experimental maps derived from X-ray and neutron diffraction data.

For more than a decade, theoretical study of the metalloporphyrins has been restricted to the semiempirical methods of quantum chemistry (for a review, see Gouterman, 1978). It is only recently that improvements in the methodology of *ab initio* calculations, together with the rapid development of electronic computers, have made it possible to treat these large molecules at the *ab initio* level (Dedieu *et al.*, 1976c, 1977). We present here a review of the *ab initio* calculations on the metalloporphyrins which have been carried out in our group over the last seven years (furthermore, it should be emphasized that this work is still in progress). *Ab initio* calculations have also been reported by Olafson and Goddard (1977) on models of the heme. The work of two other groups is worth special mention since it represents a series of calculations with an organized effort to understand many properties of the metalloporphyrins. Magnesium porphine and systems related to the chlorophyll have been investigated by Christoffersen and his group (Spangler *et al.*, 1977) through self-consistent field (SCF) and configuration interaction (CI) calculations with a basis of floating spherical Gaussian orbitals. Ohno and his group have studied the electronic structure of several metalloporphyrins through SCF and limited CI calculations and this work has been reviewed by Ohno (1979).

II. General Features of the Calculations

A. The Model Systems

In the natural hemes, a number of substituent groups (methyl, vinyl, etc.) are found at the periphery of the porphyrin ring. Substituent groups

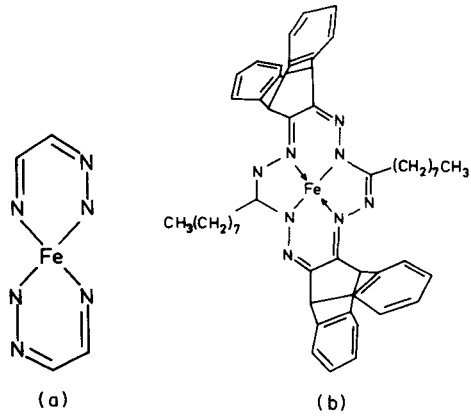

Fig. 3. (a) A model used to study oxygen binding to the iron(II) porphyrin; (b) the synthetic oxygen carrier of Baldwin and Huff.

are also found in the synthetic porphyrins such as etioporphyrin, octaethylporphyrin[1] and $\alpha,\beta,\gamma,\delta$-tetraphenylporphyrin. However, for the sake of economy, these *ab initio* calculations of transition metal porphyrins have been carried out for the unsubstituted porphyrin represented in Fig. 1. This may be justified on the basis that many electronic properties of the transition metal porphyrins are probably rather insensitive to the nature of these peripherical substituents. In spite of this simplification, the porphyrin with a molecular formula $MN_4C_{20}H_{12}$ (M is the transition metal) still represents a formidable problem in terms of computation (notwithstanding the axial ligands). For this reason, one may wonder whether one could find a simpler system, more amenable to the calculation and still able to mimic the essential properties of the metalloporphyrins. For instance, since several structural features (such as the out-of-plane displacement of the metal or the doming of the porphyrin) are associated with the central unit MN_4, one may seek to simplify the porphin ligand to some degree. An extrema along this line corresponds to the model system $M(NH_2)_4$, introduced by Olafson and Goddard (1977), with the porphyrin ligand represented as four NH_2 groups in a plane (called later Model I). [In fact, to ensure the overall charge neutrality of this system, the ligand should be a dianion $(NH_2)_4^{2-}$]. More realistic models represent some simplification of the porphin ligand and bear some relationship to the synthetic models of the heme developed by coordination chemists. For instance, the model of Fig. 3a has been used by Dedieu *et al.* (1976b) to

[1] We have used the following abreviations throughout this article: P, porphin; OEP, octaethylporphyrin; TPP, tetraphenylporphyrin; TpivPP, tetrapivalamidophenylporphyrin; and Im, imidazole.

study oxygen binding to the iron(II) porphyrin and corresponds to the inner part of the synthetic oxygen carrier shown in Fig. 3b (Baldwin and Huff, 1973). A related model, shown in Fig. 1c and called Model II, has been used independently by Hall (1980) and Dedieu *et al.* (1979b) and is derived from the porphin ligand, first by deleting the β carbons of the pyrroles as in Fig. 1b and then by retaining only two out of the four C—C—C bridges.

Some care has to be exercised, however, in the use of these models since they suffer from a number of drawbacks. For instance, the ground state of the manganoporphyrin MnP corresponds to the high-spin electronic configuration $(xy)^1(xz)^1(yz)^1(z^2)^1(x^2-y^2)^1$ for the Mn atom. Yet the SCF calculation for the model system $Mn(NH_2)_4$ yields a ground-state electronic configuration $(x^2-y^2)^0(4\pi)^1$ (4π denotes the highest π orbital of the ligand), rather than $(x^2-y^2)^1(4\pi)^0$. This is a consequence of the lack of delocalization in the model system, with the 4π orbital too low in energy and lower than the $3d_{x^2-y^2}$ orbital. Furthermore, Olafson and Goddard (1977) emphasize that this model lacks the geometric stabilization due to the bridging methene groups, thus leading to optimized geometries with the hole radius artificially smaller than in the corresponding porphyrin system (the calculated Fe—N distances being underestimated by about 0.03 Å). This model seems to describe the out-of-plane displacement of the metal reasonably well. The same is probably true of Model II, which should be used rather safely for any structural or electronic property associated with the coordination sphere of the metal. It is rather obvious that this model will not reproduce satisfactorily the electronic properties of the porphyrins which reflect the electronic delocalization (such as the orbital energies considered as an approximation to the ionization potentials or the electronic excitation energies). To give just an example, the optical properties of the transition metal porphyrins have been analyzed mainly in terms of a four-orbital model (see for instance Gouterman, 1978), the two top filled orbitals of symmetry a_{2u} and a_{1u} and the lowest empty orbital of symmetry e_g. The *ab initio* calculation for the system MnP yields two π levels of symmetry a_{1u} at -0.242 a.u. and a_{2u} at -0.241, while the calculation for the system $MnN_4C_6H_{10}$ (Model II) gives two high-lying π levels at -0.285 a.u. (b_{1u} symmetry) and -0.276 a.u. (b_{3g} symmetry) (Dedieu *et al.*, 1979b). These four levels are sketched in Fig. 4. While the b_{1u} level of the model shows the same nodal properties as the a_{2u} level of the porphyrin system, clearly, the electronic distribution of the b_{3g} level of the model and the a_{1u} level of the porphyrin are completely different.

With these three models [Model I, $M(NH_2)_4$; Model II, $MN_4C_6H_{10}$; and the porphyrin MP or $MN_4C_{20}H_{12}$], we have studied the following systems:

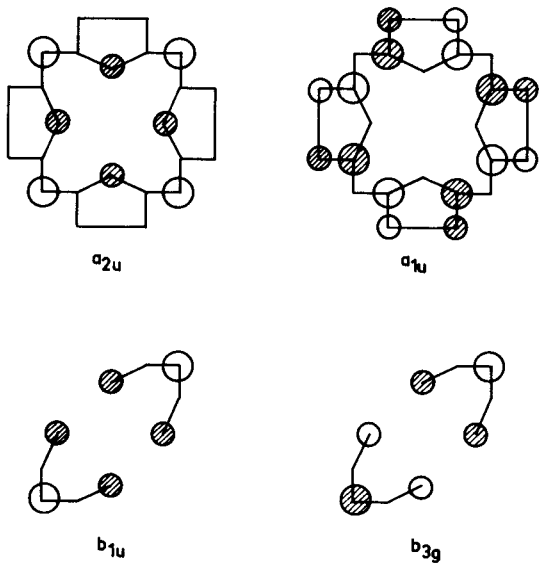

Fig. 4. The high-lying molecular orbitals $a_{2u}(\pi)$ and $a_{1u}(\pi)$ of the porphin dianion and $b_{1u}(\pi)$ and $b_{3g}(\pi)$ of the ligand $N_4C_6H_{10}$ of Model II.

(1) $Mn(NH_2)_4$, $MnN_4C_6H_{10}$, $Fe(NH_2)_4$, MnP, FeP, and CoP, which represent the four-coordinate porphyrins

(2) $Fe(NH_2)_4NH_3$, $Fe(NH_2)_4SH$, and $FePNH_3$ (Fig. 5), which represent a number of five-coordinate porphyrins, mainly the deoxyheme models

(3) MPO_2NH_3 (M = Fe and Co) (Fig. 6), $FePO_2Im$, and MPO_2 (M = Ti and Mn) (Fig. 7), which correspond to the dioxygen complexes of the metalloporphyrins and most notably to the oxyheme models

(4) $FeN_4C_6H_{10}O$ as a model of the active oxygen complex of catalase.

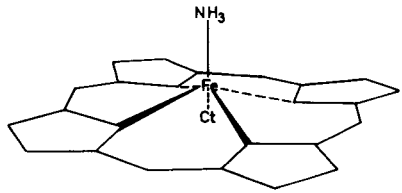

Fig. 5. The $FePNH_3$ model.

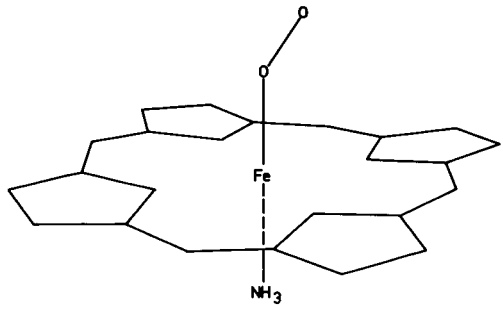

Fig. 6. The $FePO_2NH_3$ model with the bent structure for the iron–dioxygen unit.

B. The SCF Calculations

1. *The Choice of Geometry*

Choosing the geometry to be used in the calculations is not very easy, but it is important in many respects. For instance, the calculated out-of-plane displacement of the metal is probably quite sensitive to the porphyrin hole radius. The cost of the calculations practically excludes any extensive geometry optimization, except for a small number of specific parameters (for instance, the O—O bond length in the dioxygen complexes). For this reason, we have incorporated in the calculations as much data from the experimental structures as possible (whenever the structures are available for the system under study or for a related system). When the calculation is intended to elucidate a structural problem, such as the mode of coordination of the dioxygen ligand or the out-of-plane displacement of the metal atom, only one structural parameter is allowed to vary; all the other parameters (bond distances and bond angles) are kept fixed. Two simplifying assumptions have been used throughout these calculations:

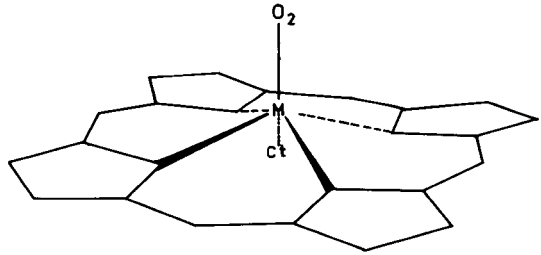

Fig. 7. The MPO_2 model (M = Ti and Mn).

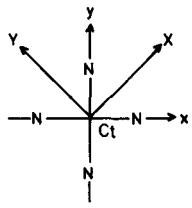

Fig. 8. The choice of axis.

(1) The porphine ligand has been generally assumed to be planar. Although both the experimental and theoretical (cf. Section IV,A,1) evidence point to the porphyrin ligand as highly flexible, in many of the transition metal porphyrins the porphin ligand shows only mild distortion from planarity (Hoard, 1975). However, whenever the experimental structure pointed to a strong deviation from planarity [as is the case for the $S = 1$ iron(II) porphyrin], we adopted a *nonplanar geometry*.

(2) Somewhat idealized geometries with a fourfold symmetry (see Fig. 8 for our choice of axis) have been used since most of the experimental structures of the transition metal porphyrins show only small deviations from the fourfold symmetry (Hoard, 1975). There are, of course, a few exceptions; for instance, systems such as that shown in Fig. 2 with the fifth ligand bonded not only to the iron atom but to a pyrrole nitrogen as well (Chevrier *et al.*, 1981), and clearly, for such a case, the experimental geometry, somewhat idealized to C_s symmetry, is used in the calculations. We also note that Model II retains the fourfold symmetry only at the level of the MN_4 core.

With these simplifications, most important are the geometrical parameters of the porphyrin ligand. The geometry of the porphyrin is known to be rather sensitive to the spin state of the metal. For this reason, we have used different geometries for the systems FeP, $FePNH_3$, and $FePO_2NH_3$. $FePNH_3$ is a model for the deoxyheme which is high-spin ($S = 2$), and the geometry corresponds to a set of regularized coordinates (Eaton *et al.*, 1978) with a distance $Ct \cdots N_{pyrrole}$ of 2.01 Å (this is near the values of 2.03–2.04 Å reported for a number of high-spin five-coordinate iron(II) porphyrins (Hoard, 1975). For FeP and $FePO_2NH_3$, which are model systems, respectively, for the compound FeTPP ($S = 1$) and for the oxyheme ($S = 0$), the geometry of the porphyrin core was taken as the experimental geometry (somewhat idealized) of FeTPP (Collman *et al.*, 1975a) with a $Fe—N_{pyrrole}$ distance of 1.97 Å. For $TiPO_2$ we have used the hole radius porphyrin ring in $TiOEPO_2$ (Guilard *et al.*, 1976). Details of the geometries (including the bond lengths and bond angles for the axial

ligands) may be found in the original publications by Dedieu *et al.*, 1977, 1979a, 1981).

While for most of the hexacoordinated metalloporphyrins the metal atom sits in or near the coordination plane (defined by the four pyrrole nitrogens), the out-of-plane displacement of the metal is a ubiquitous feature of the five-coordinate porphyrins. For $TiPO_2$ the metal atom was located 0.62 Å off the equatorial plane [namely, the experimental displacement in $TiOEPO_2$ (Guilard *et al.*, 1976)]. For $MnPO_2$ we have considered two different values, 0.25 and 0.62 Å, for the displacement of the manganese atom. For the deoxyheme model $FePNH_3$, the out-of-plane displacement was optimized by repeating the calculations for the values of 0, 0.25, 0.50, and 0.75 Å. Finally, the calculation of the out-of-plane displacement for the four-coordinate metalloporphyrins may shed some light on the origin of the displacement observed for the five-coordinate porphyrins (Olafson and Goddard, 1977; Veillard *et al.*, 1980). For this reason, the out-of-plane displacement has been also optimized for the two high-spin systems FeP ($S = 2$) and MnP ($S = 5/2$). In the intermediate and low-spin systems FeP ($S = 1$) and CoP ($S = 1/2$), the metal is either known or is assumed to be in the coordination plane.

One initial goal of this work was to study the mode of coordination of the dioxygen ligand to the heme. At the time this work was started, no experimental structure had been reported for the heme in oxyhemoglobin or oxymyoglobin. To find which was the most stable structure, we have carried out calculations for the systems MPO_2 and MPO_2NH_3, with the bent structure, or with the perpendicular structure, or with the kinked structure. Given the interest in the mode of coordination of the dioxygen ligand in the oxyheme, limited geometry optimization has been carried out for the FeO_2 unit in $FePO_2NH_3$ by varying the O—O bond length and the FeOO angle. An outline of the systems studied, with the basis set used and the reference to the original publication, is given in Table I.

2. *The Basis Sets*

Ab initio calculations of metalloporphyrins have now been carried out in our group for a period of seven years. During this period, the increased efficiency of the SCF programs has led to a marked reduction of computation time. Calculations which seven years ago were carried out at the minimal basis set level are now feasible with a double-zeta basis set. Also, the calculations need not be carried out at the same level of accuracy for the different systems under study. In the case of the oxyheme model $FePO_2NH_3$, the search on the potential energy surface of the iron–dioxygen unit required a relatively large number of calculations and this could be achieved only with a minimal basis set (however, we also per-

TABLE I

OUTLINE OF THE SYSTEMS STUDIED AND THE CORRESPONDING BASIS SET[a]

System	Basis set	Reference
Porphin dianion P^{2-}	BSI	Dedieu *et al.* (1977)
	BSII	Dedieu *et al.* (1979b)
	BSIII	Dedieu *et al.* (1979b)
FeP ($S = 0$)	BSI	Dedieu *et al.* (1977)
$FePO_2$	BSI	Dedieu *et al.* (1977)
$FePO_2(NH_3)$	BSI	Dedieu *et al.* (1977)
	BSII	Dedieu *et al.* (1979a)
$FePO_2Im$	BSI	Dedieu *et al.* (1977)
FePCO	BSI	Dedieu *et al.* (1977)
$MnPO_2$	BSI	Dedieu *et al.* (1979a)
	BSII	Dedieu *et al.* (1979a)
$TiPO_2$	BSI	Dedieu *et al.* (1979a)
$CoPO_2NH_3$	BSI	Dedieu *et al.* (1979a)
$FePNH_3$ ($S = 2$ and $S = 0$)	BSII	Dedieu *et al.* (1981)
FeP ($S = 1$)	BSII	Dedieu *et al.* (1981)
	BSIII	Dedieu *et al.* (1981)
($S = 2$)	BSII	Dedieu *et al.* (1981)
CoP ($S = 1/2$)	BSIII	Bénard (1982)
MnP ($S = 5/2$)	BSII	Dedieu *et al.* (1979b)
$Fe(NH_2)_4(NH_3)$	BSII	Dedieu *et al.* (1979b)
$Fe(NH_2)_4(SH)$	BSII	Dedieu *et al.* (1979b)
$Mn(NH_2)_4$	BSII	Dedieu *et al.* (1979b)
$MnN_4C_6H_{10}$	BSIV	Dedieu *et al.* (1979b)
	BSIV + f functions	Dedieu *et al.* (1979b)
$Fe(N_4C_6H_{10})O(NH_3)$ (model for $FePONH_3$)	BSIV	Strich and Veillard (1981)
FePO	BSII	Veillard and Strich (1981)

[a] See Table II for definition of basis sets.

formed one calculation with a split valence basis set in order to check the results of the minimal basis set calculations). For the deoxyheme model, the calculation was intended to yield a rather accurate value of the out-of-plane displacement of the iron atom, and we felt that this would require the use of a basis set of double-zeta quality at the level of the valence shells (but minimal for the inner shells). Finally, the calculations on the four-coordinate system FeP (intermediate spin $S = 1$) was intended to test the quality of the wave function by comparing the calculated quad-

TABLE II

BASIS SETS USED

Basis set	Gaussian basis set	Contracted basis set	Reference
BSI	10, 6, 4/7, 3/3	4, 3, 2/2, 1/1	Roos *et al.* (1971) Roos and Siegbahn (1970) Huzinaga (1965)
BSII	11, 7, 5/8, 4/4	5, 4, 2/3, 2/2	Roos *et al.* (1971) Whitman and Hornback (1969) Huzinaga (1965)
BSIII	13, 8, 5/9, 5/4	8, 5, 3/4, 2/2	Hyla-Kryspin *et al.* (1981) Huzinaga (1971)
BSIV	13, 8, 6/9, 5/4	8, 5, 3/4, 2/2	Hyla-Kryspin *et al.* (1981) Huzinaga (1971)

rupole splitting to the experimental value derived from the Mössbauer spectra. This was done with a basis set which was of full double-zeta quality. For these reasons, we have been led to use different basis sets (BS) and they are summarized in Table II: BSI is a minimal basis set except for the 3d functions which are split; BSII is minimal for the inner shells and the shells 4s and 4p of the metal; double zeta for the valence shells of the light atoms and the shells 3s, 3p, and 3d of the metal; BSIII and BSIV are double-zeta basis sets except for the 4p shell of the metal which is minimal and the 3d shell which is of triple-zeta quality; BSIII and BSIV differ only by one additional diffuse function of 3d symmetry in BSIV (of exponent 0.09 for Mn and Fe). More details about the basis sets used, the values of the exponents and the choice of the contraction may be found in the original publications.

Except for one case (Demuynck *et al.*, 1979) no previous calculations of transition metal complexes and organometallics have included polarizations functions of the f type on the metal atom. One set of f functions was used in the calculation of the model system $MnN_4C_6H_{10}$, their exponent was varied between 0.1 and 0.3.

3. *The Calculations*

Calculations for the metalloporphyrins require basis sets including up to 700 Gaussian functions and more than 300 contracted functions, with a total number of electrons exceeding 200 (Table III). The calculations for the model systems still demand up to 400 Gaussians and nearly 200 contracted functions. Even with a moderately fast computer (all the calcula-

TABLE III

SIZE OF BASIS SETS AND NUMBER OF ELECTRONS

System	Basis set	Number of Gaussian functions	Number of contracted functions	Number of electrons
FeP	BSIII	691	305	186
$FePNH_3$	BSII	622	284	196
$FePO_2NH_3$	BSII	662	302	212
$MnN_4C_6H_{10}$	BSIV +f functions	363	171	99
$Fe(N_4C_6H_{10})O(NH_3)$	BSIV	413	187	118

tions were run on a Univac 1110 monoprocessor), this requires an extremely efficient program if the computation times are to be kept reasonable. The calculations were run with the system of programs that Asterix developed in our laboratory (Bénard *et al.*, 1981) for relatively large systems with transition metals. High efficiency has been achieved due to the following features:

(1) Evaluation of the two-electron integrals over s, p, d, and f Gaussian functions, based on the block techniques (Bénard, 1976; Bénard and Barry, 1979).

(2) Use of original recursion formulas based on the formalism of Taketa *et al.* (1966) for the effective computation of the repulsion integrals (Bénard, 1976; Bénard and Barry, 1979).

(3) Full exploitation of the symmetry operations pertaining to nondegenerate point groups in order to avoid redundant computation and storage of blocks of integrals which are equivalent by symmetry, according to the algorithm proposed by Pitzer (1973).

(4) A high degree of optimization of the SCF programs. In the earlier version of these programs, the Fock matrix was built from the two-electron repulsion integrals. In the latest version, this is done from the P supermatrix (Veillard, 1975). A convergence guarantee is obtained through the use of the level-shift procedure proposed by Saunders and Hillier (1973) for the closed-shell cases and by Guest and Saunders (1974) for the open-shell cases (with a restricted Hartree–Fock formalism).

All one- and two-electron integrals were computed with single-word accuracy (word of 36 bits). The SCF calculations for the closed-shell systems with less than 229 basis functions were carried out with double-word accuracy. The other SCF calculations have been performed with

single-word accuracy and the total energy was calculated with double-word accuracy after the wave function had converged (this ensures that the numerical accuracy of the integrals is retained in the calculation of the energy as the sum of a very large number of small terms, and hence that small energy differences, calculated as the difference of two energy values, are numerically significant).

III. Ground-State Assignments and Electronic Configurations

A. Ground-State Assignments

1. *The Deoxy Systems*

a. The Biological importance of the deoxy porphyrins. In normal deoxyhemoglobin A, the iron(II) atom of the heme is five-coordinate, high spin ($S = 2$), and is axially bound to the imidazole ring of the proximal histidine residue. Furthermore, it is displaced out of the plane of the porphyrin ring and this out-of-plane displacement has been estimated to 0.60 Å (±0.1 Å) from the refinement of a 2.5-Å resolution X-ray diffraction study with the porphyrin assumed planar (Fermi, 1975). In a number of model five-coordinate compounds, the out-of-plane displacement of the iron atom appears to be somewhat smaller, with a value of 0.42 Å from the mean plane of the pyrrole nitrogens in Fe(TPP) (2-MeIm) (Hoard and Scheidt, 1973) and a value of 0.399 Å from the mean plane of the pyrrole nitrogens in Fe(TpivPP) (2-MeIm) (Jameson *et al.*, 1978c, 1980). As a matter of fact, the steric hinderance of the 2-MeIm ligand in these two molecules may induce an increased out-of-plane displacement of the iron from its intrinsic, unstressed value (Collman, 1977) since the presence of the methyl substituent may result in short contacts with the porphinato atoms.

The out-of-plane displacement of iron in deoxyhemoglobin plays a key role in the theories constructed in order to explain a number of properties of hemoglobin, such as cooperativity (Perutz, 1976). When oxygen binds to deoxyhemoglobin, the iron moves into the plane of the porphyrin ring and becomes low spin. The proximal histidine residue moves with the iron. Perutz (1970, 1972) has proposed a sequential process by which the concerted movement of the iron and F8 histidine residue toward the heme plane triggers a series of changes in the positions of key aminoacids and in the interactions within and among the four heme subunits. He has shown how these changes can account for the cooperativity of dioxygen bonding. Perutz has suggested that the low-oxygen affinity of the deoxyhemoglobin may be related to the increased tension at the heme in each subunit which constrains the iron atom to be further away from the porphyrin plane than

its equilibrium position and thus opposes its movement into the ring upon reaction with oxygen.

Thus knowledge of the *intrinsic* equilibrium position of the iron in a high-spin, five-coordinate ferroporphyrin is essential. For instance, a number of arguments in support of a lack of strain on the heme group in the deoxy quaternary structure have been given (Huynh *et al.*, 1974a,b; Eisenberger *et al.*, 1976; Spiro *et al.*, 1976; Gelin and Karplus, 1977), and a recent EXAFS study of deoxyhemoglobin has yielded an out-of-plane displacement in the range 0.2–0.3 Å (Eisenberger *et al.*, 1978).

The low-spin Co(II) analog of deoxyHb still exhibits cooperativity (Hoard and Scheidt, 1973). In the deoxy form, the Co(II) atom is approximately 0.25–0.36 Å out of the heme plane and moves in the plane upon oxygenation.

More accessible to theoretical studies and subject to a wealth of experimental studies are the unligated metalloporphyrins. The four-coordinate $\alpha,\beta,\gamma,\delta$-tetraphenylporphinatoiron(II) FeTPP has been intensively studied (Collman *et al.*, 1975a). The iron atom with an intermediate spin ($S = 1$) is at the center of the molecule.

The ground-state configuration of iron(II) porphyrins has been discussed by many authors. The analysis of the proton NMR spectra of FeTPP indicates large π contact shifts, thus requiring unpaired spins in d_{xz} and d_{yz} and suggests that the orbital ground state is nondegenerate, which leaves the state $^3A_{2g}$ as the only candidate for the ground-state configuration (Goff *et al.*, 1977). The same ground state has been proposed by Collman *et al.* (1975a) on the basis that it could fit both the magnetic data and the data obtained from Mössbauer spectroscopy. Yet, the Mössbauer spectra of Fe(TPP) (Lang *et al.*, 1978) and the proton NMR spectra of a number of four-coordinate ($S = 1$) ferrous porphyrins (Mispelter *et al.*, 1980) could as well be accounted for by assuming that in these complexes the ground state results from a spin–orbit mixing of the two states $^3A_{2g}$ and ^3E_g. On the other hand, the resonance Raman spectra of ferrous octaethylporphyrin (FeOEP) has been intepreted in terms of a ^3E_g ground state (Kitagawa and Teraoka, 1979).

Our theoretical study of the four- and five-coordinate porphyrins was aimed at the following points:

(1) Calculation of the out-of-plane displacement of the iron atom for a five-coordinate iron(II) porphyrin, considered as a model of the heme and free of the influence of the globin molecule

(2) Elucidation of the origin of the out-of-plane displacement

(3) Calculation of the electric field gradient at the iron nucleus in order to investigate the relationship between the quadrupole splitting value and the electronic configuration of the ground state of the heme.

Related studies include the *ab initio* GVB–CI calculations on the model systems $Fe(NH_2)_4$ and $Fe(NH_2)_4NH_3$ of Olafson and Goddard (1977) and the *ab initio* SCF calculations of FeP and CoP (Kashiwagi *et al.*, 1978; Kashiwagi and Obara, 1981).

b. The four-coordinate systems: MnP, FeP, *and* CoP. Since we deal with open-shell systems with the 3d orbitals incompletely filled, several electronic states corresponding to different electronic configurations are expected to have close energy values for a system with a given multiplicity. In the four-coordinate square planar systems MP (M = Mn, Fe, Co), the orbitals d_{xy}, d_{xz}, d_{yz}, and d_{z^2} are expected to be close in energy, while the orbital $d_{x^2-y^2}$ is destabilized through the antibonding interactions with the lone pairs of the pyrrole nitrogens. For the ground state of FeTPP (Kobayashi and Yanagawa, 1972; Brault and Rougee, 1974; Collman *et al.*, 1975a; Goff *et al.*, 1977), three electronic configurations are compatible with the spin value:

$$(xy)^1(xz)^2(yz)^2(z^2)^1 \qquad {}^3B_{1g}$$

$$(xy)^2(xz)^1(yz)^1(z^2)^2 \qquad {}^3A_{2g}$$

$$(xy)^2(xz)^{1.5}(yz)^{1.5}(z^2)^1 \qquad {}^3E_g$$

(these states are labeled according to D_{4h} symmetry, with the orbitals $3d_{xz}$ and $3d_{yz}$ degenerate, although the FeTPP molecule shows only S_4 symmetry due to extensive ruffling of the porphinato core). For the high-spin ($S = 5/2$) four-coordinate MnTPP (Kirner *et al.*, 1977), there is only one possible electronic configuration for the ground state:

$$(xy)^1(xz)^1(yz)^1(z^2)^1(x^2 - y^2)^1 \qquad {}^6A_{1g}$$

Similarly, for the low-spin ($S = 1/2$) CoTPP (Madura and Scheidt, 1976), the ground-state configuration is known to be $(xy)^2(xz)^2(yz)^2(z^2)^1$ ${}^2A_{1g}$ (Griffith, 1958; Lin, 1976).

In Table IV we have reported the total SCF energies computed for the corresponding model systems with different geometries and basis sets, the metal atom being in the plane of the four nitrogen atoms. According to the SCF energy values of Table IV for FeP, the state ${}^3A_{2g}$ is lower in energy than the state ${}^3B_{1g}$ for both the planar and ruffled structures of the porphyrin ring. Furthermore, the calculated value for the quadrupole splitting of the ${}^3B_{1g}$ state (see discussion below) rules out this state as the ground state. Unfortunately, our SCF open-shell program is presently limited to the half-closed-shell case, so no selection of the ground state between the states ${}^3A_{2g}$ and ${}^3E_g$ could be made thus far on energy criteria.

c. The five-coordinate deoxy systems: $FePNH_3$ *and* FePSH. In the five-coordinate systems the orbital d_{z^2} is somewhat destabilized

TABLE IV

TOTAL SCF ENERGIES FOR THE FOUR-COORDINATE SYSTEMS

System	Electronic configuration	Electronic state	Structure of the porphyrin ring	Total energy (a.u.) BSI	BSII	BSIII
MnP	$(xy)^1(xz)^1(yz)^1(z^2)^1(x^2-y^2)^1$	$^6A_{1g}$	Planar	−2124.065	−2129.7671	
FeP	$(xy)^1(xz)^2(yz)^2(z^2)^1$	$^3B_{1g}$	Planar		−2241.0690	
			Ruffled			−2243.90
	$(xy)^2(xz)^1(yz)^1(z^2)^2$	$^3A_{2g}$	Planar		−2241.0951	
			Ruffled		−2241.0755	−2243.93
	$(xy)^2(xz)^1(yz)^1(z^2)^1(x^2-y^2)^1$	$^5B_{2g}$	Planar		−2241.1400	
CoP	$(xy)^2(xz)^2(yz)^2(z^2)^1$	$^2A_{1g}$	Ruffled			−2362.84

through the interaction with the axial ligand. Since the iron atom of the deoxyheme is high-spin ($S = 2$), each of the three possible configurations for the ground state of the model $FePNH_3$ corresponds respectively to one of the orbitals d_{xy}, d_{xz}, and d_{yz} being doubly occupied (Fig. 9).

According to the energy values of Table V, the ground state of the system $FePNH_3$ corresponds to the configurations $^5A''$ $(xy)^1(xz)^1(yz)^2(z^2)^1(x^2-y^2)^1$ and $^5A'$ $(xy)^1(xz)^2(yz)^1(z^2)^1(x^2-y^2)^1$ which are practically degenerate. They are also the ground-state configurations in the extended Hückel calculations (Loew and Kirchner, 1978) and in the GVB–CI model calculations (Olafson and Goddard, 1977). Our ground-state assignment is at variance with the assignment of Goff and La Mar (1977) of a ground-state configuration $(xy)^2(xz)^1(yz)^1(z^2)^1(x^2-y^2)^1$. Extended Hückel calculations for a system $FePH_2O$, together with the fitting of the temperature

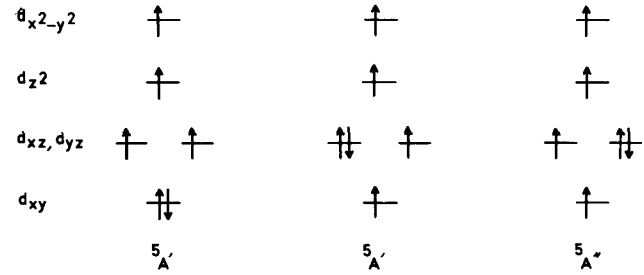

Fig. 9. The electronic configurations of lowest energy for the deoxyheme model $FePNH_3$.

TABLE V

TOTAL SCF ENERGIES FOR $FePNH_3$ ($S = 2$) WITH BSII AS A FUNCTION OF THE OUT-OF-PLANE DISPLACEMENT

Electronic configuration	Electronic state	Z (Å)	Total SCF energy (a.u.)
$(xy)^1(xz)^1(yz)^2(z^2)^1(x^2-y^2)^1$	$^5A''$	0	−2297.2574
		0.25	−2297.2673
		0.50	−2297.2645
		0.75	−2297.2494
$(xy)^2(xz)^1(yz)^1(z^2)^1(x^2-y^2)^1$	$^5A'$	0	−2297.2551
		0.25	−2297.263
		0.50	−2297.262
$(xy)^1(xz)^2(yz)^1(z^2)^1(x^2-y^2)^1$	$^5A'$	0	−2297.2573

dependence of the quadrupole splitting resulted in a ground-state configuration $(xy)^1(xz)^2(yz)^1(z^2)^1(x^2-y^2)^1$ (Trautwein *et al.*, 1975).

Caron *et al.* (1979) have described a model of the active site of the reduced cytochrome P_{450}, with a mercaptide ligand as the fifth ligand of a high-spin iron(II). This system is devoid of the steric interaction due to the methyl group in the 2-MeIm ligand. We have used the model system $[Fe(NH_2)_4SH]^-$ to compare some structural and electronic properties of this compound with those of the deoxyheme. The calculated ground-state configuration for our model system also corresponds to the degenerate configurations $^5A''$ and $^5A'$.

2. *The Oxy Systems*

a. Situation of the problem. The detailed nature of the metal oxygen bond in dioxygen complexes of metalloporphyrins has been pending for a long time. Many experimental efforts have been devoted to the characterization of the metal dioxygen unit in MPO_2 and MPO_2L systems [with M a metal(II) and L a neutral ligand such as imidazole] through either a metal(II)–O_2 neutral dioxygen formulation, a metal(III)–O_2^- superoxide formulation, or a metal(IV)–O_2^{2-} peroxide formulation. The corresponding data may be summarized as follows:

(1) For the peroxotitaniumoctaethylporphyrin the diamagnetism of the system and a O—O bond length of 1.445 Å (as indicated by the X-ray crystal structure) are unambiguously indicative of a peroxo type of bonding (Guilard *et al.*, 1976, 1978).

(2) No X-ray crystal structure is available for the $Cr(O_2)(TPP)(py)$(py, pyridine). A magnetic moment of 2.7 μ_B is indicative of two unpaired

electrons and the IR band at 1142 cm^{-1} (which is assigned to ν_{O-O}) has been taken as evidence (Cheung *et al.*, 1976) for a superoxo-type ligand by analogy with the dioxygen adducts of cobalt–Schiff-base complexes (see for instance Basolo *et al.*, 1975).

(3) The dioxygen adduct of the manganese tetraphenylporphyrin and of other Mn(II)–porphyrins has been characterized at low temperature (Weschler *et al.*, 1975; Hoffman *et al.*, 1976, 1978). A spin state $S = 3/2$ was assigned on the basis of the EPR spectra. The absence of spin transfer to dioxygen found in the experiments with 50% ^{17}O enriched O_2 was used to rule out a Mn(III)–O_2^- formulation. On the basis of the EPR spectra (which are quite atypical, however) the system has been repeatedly formulated as Mn(IV)(O_2^{2-}) with the Mn(IV) in the $(t_2)^3$ configuration.

(4) For the iron system, the O—O bond length of the coordinated dioxygen is rather short [1.16 Å—probably grossly underestimated—in Fe(TpivPP)(1-MeIm)O_2 and 1.23 Å in Fe(TpivPP)(2-MeIm)O_2]. This clearly supports a Fe(II)O_2 formulation. Nevertheless, the superoxide formalism Fe(III)(O_2^-) has been assigned to these systems, on the basis of the ν_{O-O} stretching frequency (1159 cm^{-1}) (Collman *et al.*, 1976), again close to the values for the free superoxide ion (1145 cm^{-1}) and for a number of Co(II)–Schiff-base dioxygen adducts. The dioxygen complex of the picket-fence porphyrin has been found to be diamagnetic (Collman, 1977), in agreement with the early results of Pauling and Coryell (1936) on the oxyhemoglobin. Recent experimental data (Koster, 1975; Cerdonio *et al.*, 1977, 1978) are indicative, however, of a thermal equilibrium between a ground singlet state and an excited triplet state (although their interpretation has been questioned by Pauling, 1977).

(5) A spin state $S = 1/2$ has been assigned to the dioxygen adducts of cobalt(II) porphyrins which have been formulated as Co(III)–O_2^- complexes. This was based on the analysis of the corresponding EPR spectra (Walker, 1970; Hoffman and Petering, 1970; Yonetani *et al.*, 1974; Wayland *et al.*, 1974; Collman *et al.*, 1978), which are similar to those reported for the low-spin $S = 1/2$ dioxygen adducts or Co(II)–Schiff-base complexes (Basolo *et al.*, 1975).

It should be pointed out, however, that the characterization of the electronic structure of the metal dioxygen unit M–O_2 as either M(II)–O_2, M(III)–O_2^-, or M(IV)–O_2^{2-} is rather formal (see, for instance, Drago, 1979). A better way of characterizing the metal dioxygen unit is possible if the ground-state electronic configuration is known: if we adopt the notation scheme introduced by Enemark and Feltham (1974) and if we denote the MO_2 fragment by $\{MO_2\}^n$, where n is the number of electrons associated with the metal d orbitals and the π^* orbitals of dioxygen ($1\pi_g$ for molecular oxygen), then a ground-state electronic configuration of the

type $d^{n-2}\pi^2$ will be referred to as a M(II)–O_2-type configuration, a $d^{n-3}\pi^3$ configuration as a M(III)–O_2^- superoxo-type configuration, and a $d^{n-4}\pi^4$ configuration as a M(IV)–O_2^{2-} peroxo-type configuration. Again, one should keep in mind that one never has pure π dioxygen and d metal orbitals: these orbitals mix with each other and with the other ligand orbitals. However, there should be some correlation between the oxidation state representation and the extent of the charge transfer from the metal to the dioxygen ligand.

It is important to know the extent of this charge transfer in order to understand the reactivity of the oxyporphyrins. Elucidation of the rules which govern the trend of the experimental data when one proceeds from Ti to Co along the transition series is also desirable: the formal oxidation states seem to be distributed at random, some of the experimental data are puzzling (especially for Mn and Fe). These questions should be answered once the ground-state electronic configuration has been assigned.

As dioxygen complexes of the metalloporphyrins we considered the model systems $TiPO_2$, $MnPO_2$, $FePO_2NH_3$, and $CoPO_2NH_3$, i.e., corresponding to the known coordination number of the metal atom: Ti(OEP)O_2 (Guilard *et al.*, 1976, 1978) and Mn(TPP)O_2 (Weschler *et al.*, 1975; Hoffman *et al.*, 1976) have been reported to be five coordinate. [A six-coordinate adduct $TiPO_2$(L) has also been observed (Latour *et al.*, 1979).] On the other hand, the dioxygen complexes of the picket-fence porphyrin Fe(TpivPP) are six coordinate with an imidazole ligand to complete the coordination sphere of the iron atom (Collman *et al.*, 1974; Jameson *et al.*, 1978a, 1980). One also finds a sixth imidazole ligand in the oxymyoglobin (Phillips, 1978) and in the oxyerythrocruorin (Weber *et al.*, 1978). This is also true for the dioxygen adduct of the cobaltomyoglobin (Petsko *et al.*, 1981). For each of these systems the experimental value of the spin state was generally assumed. This reduced the number of electronic configurations which had to be considered. Moreover, due to the correlation error, it would have been difficult to compare at the Hartree–Fock level the relative stabilities of electronic states with different numbers of unpaired electrons.

b. The $TiPO_2$ *system.* For the $TiPO_2$ system we have considered only closed-shell electronic configurations. This is a safe assumption since the $OEPTiO_2$ complex has been found to be diamagnetic (Guilard *et al.*, 1978). For both structures, perpendicular and bent,[2] the electronic configuration of the ground state is $d^0(\pi_g^a)^2(\pi_g^b)^2$.[3] The computed total SCF ener-

[2] To characterize the M–O_2 geometrical structures, we shall use the terms perpendicular, or Griffith structures, and bent, or Pauling structures, interchangeably.

[3] In the following, π_g^a and π_g^b denote the two π_g antibonding orbitals of the dioxygen ligand which are, respectively, symmetrical and antisymmetrical with respect to the plane containing the MO_2 unit.

gies of the possible closed-shell electronic configurations may be found in the original publications by Rohmer *et al.* (1977) and Dedieu *et al.* (1979a). According to what has been said previously it would be defined as a $Ti(IV)O_2^{2-}$ peroxo-type configuration (in fact, neither the π_g^a nor the π_g^b orbital are pure orbitals of the dioxygen ligand since they mix with d orbitals, e.g., with d_{xz} and d_{xy}, respectively, in the perpendicular structure). This result is in good agreement with the formulation of the bonding in the molecule $OEPTiO_2$ in terms of a peroxotitanium unit which was based on the O—O distance of 1.44 Å and the ν(O—O) IR absorption at 898 cm^{-1} (Guilard *et al.*, 1976, 1978).

c. The $MnPO_2$ *system.* The nature of the ground-state electronic configuration of the $MnPO_2$ system has been the subject of a continuing controversy (see, for instance, Dedieu *et al.*, 1979a and Hoffman *et al.*, 1978). For a spin state of $S = 3/2$ (experimental value deduced from the EPR spectra) there are 14 possible configurations for the ground state (we have assumed that the $3d_{x^2-y^2}$ orbital is always empty, which is likely to be the case). According to the Enemark and Feltham notation, three of them can be characterized as being of the $d^3\pi^4$ type [or $Mn(IV)O_2^{2-}$], five of the $d^4\pi^3$ type [or $Mn(III)O_2^-$] and six of the $d^5\pi^2$ type [or $Mn(II)O_2$]. Using first the minimal basis set (BS I) we found that for a 0.25 Å out-of-plane displacement of the Mn atom and an eclipsed[4] conformation of the O_2 unit, no stationary value of the energy could be obtained for the three configurations of the $d^3\pi^4$ type: starting with a trial wave function in which the three open shells were predominantly of d type led invariably to a solution where one of these open shells and a closed shell of the same symmetry—either π_g^a or π_g^b—had switched, thus leading to a configuration of the $d^4\pi^3$ type. This result was traced to the fact that the π_g orbitals of dioxygen do not appear to lie below the 3d orbitals of the Mn atom (see Ref. 57 of Dedieu *et al.*, 1979a). The experimental assignment ($d^3\pi^4$) based on EPR spectra seemed therefore to be ruled out by our calculations. The lowest energy configuration, although different for the bent and perpendicular structures, was in both cases of the $d^4\pi^3$ type with a Mn(III) atom of intermediate spin (d^4, $S = 1$). We refer the reader to the original publications by Dedieu and Rohmer (1977) and Dedieu *et al.* (1979a) where a complete list of the energies of the 14 configurations in both geometries can be found. Since the same result was obtained with a larger basis set (the valence split basis set II) the lack of a peroxo-tyype ground-state configuration could not be traced to our initial choice of a minimal basis set.

[4] The term eclipsed refers to the oxygen atoms being eclipsed with respect to the pyrrole nitrogens; the term staggered refers to the oxygen atoms being staggered with respect to the pyrrole nitrogens.

TABLE VI

TOTAL SCF ENERGIES FOR SOME REPRESENTATIVE CONFIGURATIONS[a] AND STRUCTURES OF $Mn(P)O_2$ ($S = 3/2$)

Electronic configuration	Ct · · · Mn = 0.25 Å		Ct · · · Mn = 0.62 Å	
	Bent, eclipsed (a.u.)	Perpendicular, eclipsed (a.u.)	Perpendicular, eclipsed (a.u.)	Perpendicular, staggered (a.u.)
(1) $(\pi_g^a)^2(\pi_g^b)^2(xy)^1(xz)^1(yz)^1$	*b*	*b*	*b*, *e*	*b*, *e*
(3) $(\pi_g^a)^2(\pi_g^b)^2(xy)^1(yz)^1(z^2)^1$	*b*	*b*	—	−2273.04[c] −2272.082[d]
(4) $(\pi_g^a)^2(\pi_g^b)^1(xy)^2(yz)^1(xz)^1$	−2273.129[c]	−2273.041[c]	−2273.041[c]	—
(6) $(\pi_g^a)^2(\pi_g^b)^1(xy)^2(yz)^1(z^2)^1$		−2273.077[c]	−2273.094[c]	−2273.085[c] −2273.121[d]

[a] We use our original numbering here [see Dedieu *et al.* (1979a)].

[b] No stationary value of the energy was found corresponding to this configuration.

[c] O—O separation of 1.25 Å.

[d] O—O separation of 1.46 Å.

[e] There is an important mixing between π_g^a and xz. As a result, the open shell has a greater component on π_g^a than on xz, and the configuration is best described as being $(\pi_g^a)^1(\pi_g^b)^2(xy)^1(xz)^2(yz)^1$.

The influence of the Ct · · · Mn distance and of the conformation of the dioxygen unit (eclipsed or staggered) has been now investigated more carefully for the perpendicular structure. The corresponding results are summarized in Table VI. For the eclipsed conformation the lengthening of the Ct · · · Mn distance does not lead to a stabilization of the $d^3\pi^4$-type configurations. On the other hand, for the staggered conformation we now obtained a stationary value of the energy for one $d^3\pi^4$ configuration, namely, configuration (3) which can be abbreviated as[5] $(\pi_g^a)^2(\pi_g^b)^2(xy)^1(Yz)^1(z^2)^1$ (or perhaps more precisely $(\pi_g^a + Xz)^2(\pi_g^b)^2(xy)^1(Yz)^1(z^2)^1$. This result has been previously rationalized (see Ref. 50 of Dedieu *et al.*, 1979a) in terms of symmetry arguments. Note that this configuration was found to be consistent with the data of the EPR spectra (Hoffman *et al.*, 1978), especially with the lack of spin density on O_2. A lower energy value has been found, however, for a $d^4\pi^3$-type configuration (see Table VI). The increase of the O—O bond length to 1.46 Å (i.e., typical of a peroxo unit) does not change these results, all computed energies being lowered.

[5] In our choice of axes, X is the axis in the dioxygen plane and Y is the axis perpendicular to the dioxygen plane.

There is still some disagreement between these results and the experimental results [which would favor configuration (3)]. It is less severe than previously, however, since we now find a $d^3\pi^4$-type configuration (which belongs to the set of those experimentally postulated), although it is about 1 eV higher in energy than our lowest $d^4\pi^3$ configuration. Moreover, our description of the ground state by a single determinantal wave function is perhaps less appropriate for $MnPO_2$ than for other metalloporphyrins (*vide infra*). Each state may be a mixture of several electronic configurations (some of them being also of the $d^5\pi^2$ type; see Dedieu *et al.*, 1979a). The situation is even more intricate when one goes from the C_{2v} symmetry (perpendicular geometry) to the C_s symmetry (bent geometry). A more appropriate description of the ground state would probably be obtained through CI calculations; thus far we cannot give a definite conclusion at the SCF level.

Calculated ^{55}Mn and ^{17}O hyperfine splitting obtained from an iterative extended Hückel wave function were used to assess the ground-state electronic configuration of the $MnPO_2$ system (Hanson and Hoffman, 1980). The results which are said to agree with the experimental results do not reconcile theory and experiment, however, since in order to get the agreement the authors have to assume an open-shell orbital of lower energy than a closed-shell orbital. Such a treatment is inappropriate for a one-electron Hamiltonian, since one obtains a lower total energy by placing the three open-shell orbitals above the closed-shell orbitals. When this is done the ground-state energy configuration turns out to be (in our notation) $(\pi_g^a + Xz)^2(\pi_g^b)^1(xy)^2(Yz)^1(z^2)^1$, i.e., configuration (6), which we have found to be the lowest in an SCF treatment and which is of $d^4\pi^3$ type. If the ground-state configuration of the $MnPO_2$ system were a $d^3\pi^4$-type configuration, then one should explain why the energy-based treatment fails to yield the correct result. Our feeling is that the dioxygen adduct of the manganese porphyrin represents an intermediate case, when going from titanium porphyrins to cobalt porphyrins, for the characterization of the ground state (and of the geometry as we shall show later). We note that the ground-state dioxygen adducts of the manganese phtalocyanine (Lever *et al.*, 1979, 1981) and of a manganese phtalocyanine derivative (Moxon *et al.*, 1981) have been characterized as being of the $d^4\pi^3$ superoxo type in agreement with our conclusion for $MnPO_2$. Another possibility would be that the change in the equatorial ligand has switched the ground-state configuration from $d^3\pi^4$ to $d^4\pi^3$. This would be indicative that both configurations are close in energy and should contribute to the ground-state description.

d. The $FePO_2NH_3$ *system.* For the Pauling geometry of the $Fe(P)O_2NH_3$ system, a number of singlet and triplet electronic states were considered. The singlet states were either of the closed-shell type (config-

uration of the $d^6\pi^2$ type where d^6 stands for $d_{xy}^2 d_{xz}^2 d_{yz}^2$) or of the open-shell type (configurations of the $d^5\pi^3$ type). The triplet states corresponded to $d^5\pi^3$ configurations. The lowest energy of the system was indeed found for a triplet state $^3A'$ with the configuration $d_{xy}^2 d_{xz}^2 d_{yz}^1 (\pi_g^a)^2 (\pi_g^b)^1$ (see Dedieu *et al.*, 1977, 1979a). We emphasized, however, that the correlation error should bias the energy results in favor of the open-shell calculation and assigned therefore the ground state to the closed-shell configuration $(d_{xy})^2(d_{xz})^2(d_{yz})^2(\pi_g^a)^2$, which lies only slightly higher in energy. (The correlation energy between the closed-shell and the open-shell configurations would be of the order of a pair correlation energy, about 0.03 a.u., and probably larger due to the near degeneracy of the two orbitals of the dioxygen π_g^a and π_g^b; see Ref. 63 of Dedieu *et al.*, 1979a.) This totally spin-paired ground-state electronic configuration has been found to provide a satisfactory basis for the interpretation of the observed transition energies and polarization in the electronic absorption spectra of oxymyoglobin and oxyhemoglobin (Eaton *et al.*, 1978; Churg and Makinen, 1978). That a triplet state lies in the vicinity of the singlet ground state is also in agreement with the experimental results of Cerdonio *et al.* (1977, 1978) and Koster (1975).

Other calculations on oxyheme systems also yield the diamagnetic singlet state as the ground state: the CI–Pariser–Parr–Pople (PPP) calculation of Case *et al.* (1979) led to a singlet ground state which was dominated by the closed-shell SCF $d^6(\pi_g^a)^2$ configuration. The singlet diamagnetic ground state was obtained in an INDO–SCF–CI calculation (Herman and Loew, 1979) and a triplet state (having the same composition as that of our lowest) was found very near in energy (at 0.6×10^{-3} a.u.).

Using the oxidation-state formalism, the ground state of the $Fe(P)O_2NH_3$ system would therefore correspond to an iron(II) dioxygen complex. Indeed, the net charge of the O_2 ligand as obtained from a Mulliken population analysis is +0.02, i.e., indicative of no charge transfer to the dioxygen ligand. This conclusion does not change when using a basis set of better quality: with the valence split basis set the net charge of the dioxygen ligand was computed to be +0.08. A neutral dioxygen ligand also results from the PPP calculations of Case *et al.* (1979) and of the GVB–CI calculations of Goddard and Olafson (1977). The INDO calculation of Herman and Loew (1980), as well as the earlier iterative extended Hückel calculations of Kirchner and Loew (1977), point to a $Fe(II)O_2$-type configuration but end with a net negative charge for the O_2 unit which is traced to a nonnegligible back-bonding from iron to dioxygen.

The $Fe(II)O_2$ formalism is at variance with the superoxide formulation $Fe(III)O_2^-$, which has been deduced mainly from the interpretation of the value found for the dioxygen IR stretching frequency (see Collman *et al.*,

1976, 1977). We have shown, however, (see Dedieu *et al.*, 1976b) that the experimental shift of the O—O frequency from O_2 (1556 cm^{-1}) to the dioxygen complex of the picket-fence porphyrin (1159 cm^{-1}) is well reproduced by the minimal basis set calculation [although the calculated stretching frequencies are too large: 1741 cm^{-1} for O_2 and 1326 cm^{-1} for $Fe(P)O_2NH_3$]. The correlation between the O—O stretching frequency and the charge of the dioxygen unit which is often advocated seems therefore to be a rather loose one. This view is also shared by Case *et al.* (1979) and by Drago (1979) and is gaining wide acceptance because experimental data (see Jones *et al.*, 1979) indicate that the O—O IR stretching frequency for end-on bonded dioxygen complexes is quite insensitive to ligand and metal variation, and is thus insensitive to the amount of electron transfer.

e. The $CoPO_2NH_3$ *system.* There are four possible electronic configurations for the low-spin $S = 1/2$ ground state of $Co(P)O_2NH_3$ (Dedieu *et al.*, 1976a). Two of them are of $d^7\pi^2$ type and the other two of the $d^6\pi^3$ type. According to our calculations (see Dedieu *et al.*, 1979a), the ground-state configuration for the bent structure (the most stable one) is $(d_{xy})^2(d_{xz})^2(d_{yz})^2(\pi_g^a)^2(\pi_g^b)^1$, i.e., a $d^6\pi^3$ $Co(III)O_2^-$ superoxo-type configuration. This is in agreement with the known experimental data.

f. Rationalization of the results. The next step in our analysis was to rationalize the changes in the configuration of the dioxygen ligand as a function of the transition metal of the metalloporphyrin: along the sequence of metals Ti, Mn, Fe, and Co, the dioxygen ligand is successively described as peroxo, superoxo (or possibly with a great admixture of peroxo character), neutral dioxygen, and, again, superoxo. Although this classification is rather formal, it is indeed reflected in the charge given by

TABLE VII

THE CHARGE OF THE DIOXYGEN LIGAND FROM THE POPULATION ANALYSIS VERSUS THE FORMAL CHARGE

System	Ground-state configuration	$Q(O_2)$
$TiPO_2$	$d^0(\pi_g^a)^2(\pi_g^b)^2$	16.66
$MnPO_2$	$(d_{xy})^2(d_{yz})^1(d_{xz})^1(\pi_g^a)^2(\pi_g^b)^1$[a]	16.45
	$(d_{xy})^2(d_{yz})^1(d_{z^2})^1(\pi_g^a)^2(\pi_g^b)^1$[b]	16.33
$FePO_2NH_3$	$d_{xy}^2\, d_{xz}^2\, d_{yz}^2(\pi_g^a)^2$	15.98
$CoPO_2NH_3$	$(d_{xy})^2(d_{xz})^2(d_{yz})^2(\pi_g^a)^2(\pi_g^b)^1$	16.45

[a] Lowest energy configuration for the bent structure.

[b] Lowest energy configuration for the perpendicular structure.

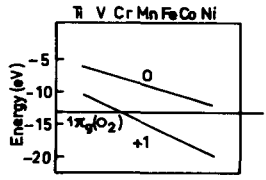

Fig. 10. The energies of the orbital $1\pi_g$ of O_2 and of the 3d orbitals in the first-transition series. (Reprinted with permission from Hoffman *et al.*, 1977. Copyright 1977, American Chemical Society.)

the population analysis (see Table VII). The rationale behind these changes lies in the relative electronegativities of the metal d orbitals and of the dioxygen π^* antibonding orbitals. This is illustrated in Fig. 10 where the relative energies of the $1\pi_g$ orbitals and of the 3d orbitals of the transition metal (the latter depending, of course, on the charge of the metal) are shown. One notices immediately that the energy of the 3d orbitals decreases along the transition series. Assuming a positive charge of the order of the unity on the metal (as usually is found in a population analysis), the 3d orbital energy is probably greater than the energy of the $1\pi_g$ O_2 orbital at the beginning of the series, while in the middle the two energies are probably similar. Since the molecular orbitals of the MO_2 unit are built from the interaction of the metal d and O_2 π^* orbitals (see our original papers and also Hoffmann *et al.*, 1977), these molecular orbitals are mostly dioxygen orbitals when M is an early transition metal. This results in a charge transfer from the metal to the dioxygen ligand, as found for $TiPO_2$: the two π_g orbitals are lower than the d_{xz} orbital and are filled with four electrons, hence the peroxo-type $Ti(IV)O_2^{2-}$ configuration. Proceeding along the transition series, the electronegativity of the d orbitals increases and progressively matches the corresponding value for the π^* orbitals of O_2. The charge transfer from the metal to the ligand decreases from $Ti(IV)(O_2^{2-})$ to $Fe(II)O_2$ in $FePO_2NH_3$ where we do not find any significant charge transfer: the metal d orbitals of pseudo-t_{2g} symmetry[6] which are lower in energy than the π^* orbitals of O_2 are filled, together with the dioxygen π_g^a orbital. In the $CoPO_2NH_3$ system the additional electron has the choice between one of the e_g orbital[7] (namely, $3d_{z^2}$) and the other π^* orbital (π_g^b). Since this e_g orbital is at a much higher energy, it turns out to be energetically more favorable to put this electron in the π_g^b orbital, hence the charge transfer configuration $Co(III)-O_2^-$.

One would have noticed that the V, Cr, and Mn atoms lie in a borderline region where the metal d and dioxygen π^* orbitals are similar in energy. As a consequence, many electronic configurations are close in energy.

[6] We refer here to the pseudo-O_h symmetry-point group of the $FePO_2NH_3$ system.

TABLE VIII

^{57}Fe MÖSSBAUER PARAMETERS FOR FOUR- AND FIVE-COORDINATE Fe(II) PORPHYRINS AND DEOXYHEME

System	Spin value	ΔE_Q (mm/sec)	V_{zz}	Reference
FeTPP	1	1.51	>0	Collman *et al.* (1975)
(2-MeIm)FeTPP	2	2.28	<0	Collman *et al.* (1975) Kent *et al.* (1979)
DeoxyMb	2	2.29	>0	Gonser *et al.* (1974)
		2.22	<0	Kent *et al.* (1976, 1979)
DeoxyHb	2	2.38		Huynh *et al.* (1974)
		2.40	<0	Kent *et al.* (1979)

This is best exemplified by our work on $MnPO_2$: obviously, a multiconfigurational wave function is necessary in order to get a good representation of the Mn–O_2 unit. On the other hand, as pointed out previously, the ground state of the $FePO_2NH_3$ system has been found by Case *et al.* (1979) to be dominated by the closed-shell SCF configuration in their PPP–CI calculation. This is again consistent with the greater energy separation between the 3d metal orbital and the O_2 π^* orbitals.

B. Calculation of the Quadrupole Splitting

The Mössbauer spectroscopy of the ^{57}Fe atom provides a unique way to probe the electronic structure of the iron atom in the iron(II) porphyrins, since the quadrupole splitting ΔE_Q is related to the electric field gradient at the iron nucleus and hence at the electronic distribution in the 3d orbitals (see, for instance, Lang, 1970). Many studies, both experimental and theoretical, have been devoted to the Mössbauer spectra of the four-coordinate iron(II) porphyrins (S = 1) (Collman *et al.*, 1975a; Dolphin *et al.*, 1976; Lang *et al.*, 1978); the five-coordinate iron(II) porphyrins (S = 2) (Kent *et al.*, 1979); and deoxymyoglobin and deoxyhemoglobin (Huynh *et al.*, 1974a,b; Gonser *et al.*, 1974; Eicher *et al.*, 1976; Maeda *et al.*, 1976; Kent *et al.*, 1977). Experimental values of ΔE_Q together with the sign of V_{zz} are summarized in Table VIII. For FeTPP, the value of the quadrupole splitting has been used to assign the ground-state configuration. The configuration $(d_{xy})^1(d_{xz})^2(d_{yz})^2(d_{z^2})^1$ (state $^3B_{1g}$) was rejected on the basis that it would give a strongly negative quadrupole interaction and the configuration $(d_{xy})^2(d_{xz})^{1.5}(d_{yz})^{1.5}(d_{z^2})^1$ (state ^3E_g) was also rejected on the basis that it does not exhibit the required magnetic properties. The configuration $(d_{xy})^2(d_{xz})^1(d_{yz})^1(d_{z^2})^2$ (state $^3A_{2g}$) was retained as the ground-state

configuration, although the value of ΔE_Q could be explained only by postulating an extremely large electronic transfer from the porphinato nitrogen atoms to the $d_{x^2-y^2}$ orbital (Collman *et al.*, 1975; Lang *et al.*, 1978).

For the five-coordinate high-spin molecule (2-MeIm)Fe(TPP) the experimental value of 2.28 mm/sec is extremely close to the corresponding values for the deoxyheme molecules (Kent *et al.*, 1979). A great many theoretical studies have been devoted to the analysis of the Mössbauer spectra of the deoxyheme molecules, but the conclusions have been rather conflicting. A first group of studies finds V_{zz} positive, parallel to the heme plane (Gonser *et al.*, 1974; Huynh *et al.*, 1974; Eicher *et al.*, 1976; Maeda *et al.*, 1976). However, a more recent analysis of the spectra of the three molecules (2-MeIm)Fe(TPP), deoxyMb, and deoxyHb yields V_{zz} negative (Kent *et al.*, 1979).

We have calculated the electric field gradient (EFG) tensor with an ammended version of the one-electron properties package of the POLYATOM program (Neumann *et al.*) and the calculated values of the quadrupole splitting are reported in Tables IX and X for FeP and $FePNH_3$, respectively. Before discussing these results, we should emphasize their limitations. These theoretical values are based on single-determinantal wave functions, and in some cases they are to some extent sensitive to the basis set used. Finally, for the five-coordinate system, the electric field gradient at the iron nucleus may also depend on the nature of

TABLE IX

CALCULATED QUADRUPOLE SPLITTING[a] FOR FeP AS A FUNCTION OF THE ELECTRONIC CONFIGURATION

Electronic configuration ($S = 1$)	Electronic state	ΔE_Q (mm/sec) FeP planar BSII	ΔE_Q (mm/sec) FeP ruffled BSIII
$(xy)^1(xz)^2(yz)^2(z^2)^1$	$^3B_{1g}$	−4.84	−5.38
$(xy)^2(xz)^1(yz)^1(z^2)^2$	$^3A_{2g}$	−0.28[b]	+0.21
$(xy)^2(xz)^{1.5}(yz)^{1.5}(z^2)^1$	^3E_g	+1.37[c]	+1.97[c]

[a] The quadrupole splitting is related to the EFG tensor through $\Delta E_Q = \frac{1}{2}QV_{zz}(1 + \eta^2/3)^{1/2}$ with the convention $|V_{zz}| \geq |V_{yy}| \geq |V_{xx}|$ and $\eta = (V_{xx} - V_{yy})/V_{zz}$; sign of ΔE_Q is sign of largest magnitude V_{ii}; $Q = 0.20$ barn.

[b] $\Delta E_Q = -0.19$ mm/sec for the ruffled porphyrin ring.

[c] Using the SCF wave function for the $^3A_{2g}$ state.

TABLE X

CALCULATED QUADRUPOLE SPLITTING FOR $FePNH_3$ ($S = 2$) WITH BSII AS A FUNCTION OF THE ELECTRONIC CONFIGURATION AND OF THE OUT-OF-PLANE DISPLACEMENT OF IRON

Electronic configuration	Electronic state	Z (Å)	ΔE_Q (mm/sec)
$(xy)^1(xz)^1(yz)^2(z^2)^1(x^2-y^2)^1$	$^5A''$	0.1	−3.7
		0.25	+3.7
		0.50	+4.0
$(xy)^2(xz)^1(yz)^1(z^2)^1(x^2-y^2)^1$	$^5A'$	0	+6.5
		0.25	+6.1
		0.50	+5.3
$(xy)^1(xz)^2(yz)^1(z^2)^1(x^2-y^2)^1$	$^5A'$	0	−3.7

the fifth ligand: the calculations have been carried out for an ammonia ligand, whereas the Mössbauer experiments refer to an imidazole ligand.

For FeP the calculated values of ΔE_Q (Table IX) for the configuration $(xy)^2(xz)^{1.5}(yz)^{1.5}(z^2)^1$ (state ^3E_g) is positive and sufficiently close to the experimental value of +1.51 mm/sec. This would tend to support the assignment of this configuration as the ground-state configuration. However, we also obtain a positive value of ΔE_Q for the state $^3A_{2g}$, so that one cannot definitely rule out the possibility of an $^3A_{2g}$ ground state. In the Hartree–Fock approximation, the wave function is represented by a single determinant and one easily finds that there is one other $3d^6$ configuration of ^3E_g symmetry and two other $3d^6$ configurations of $^3A_{2g}$ symmetry which can mix with the above configurations in the ground-state wave function. A large admixing of these configurations in one of the two ground-state wave functions may alter the calculated value of the quadrupole splitting.

For $FePNH_3$ (Table X) the configuration $(xy)^2(xz)^1(yz)^1(z^2)^1(x^2-y^2)^1$ ($^5A'$) gives a large positive quadrupole interaction (5–6 mm/sec), whereas the experimental measurements correspond to a much smaller value of 2.3 mm/sec. This substantiates our conclusion based on the energy values of Table V that this configuration is not the ground-state configuration. [It was assigned as the ground-state configuration in the ligand–field calculations (Trautwein *et al.*, 1975) and in the crystal field model with a tetragonal symmetry (Huynh *et al.*, 1974)]. For the two other configurations which are nearly degenerate, they yield identical values of ΔE_Q. One notices that the sign of ΔE_Q changes with the out-of-plane displacement between $Z = 0$ and $Z = 0.25$ Å, while the absolute value of ΔE_Q remains practically constant. Thus the measured values of ΔE_Q should be rather

insensitive to the displacement of the iron as long as the system remains in a high-spin state.

C. Energy Levels and Ionization Potentials

Studies on the oxidation–reduction properties of metalloporphyrins have long been a problem to biochemists and chemists alike because of the importance of these systems as biological electron-transfer agents. The interpretation of the properties of oxidized porphyrins requires a knowledge of their energy levels (Dolphin and Felton, 1974). Furthermore, there has been an upsurge of photoelectron spectroscopic studies of metalloporphyrins (Khandelwal and Roebber, 1975; Muralidharan and Hayes, 1978; Kitagawa *et al.*, 1979; Dupuis *et al.*, 1980; see also Nakato *et al.*, 1976). In this section we consider first the energy levels and next the calculation of ionization potentials.

The energy levels of metalloporphyrins have been discussed by many authors (see, for instance, Gouterman, 1959; Maggiora, 1973; Dedieu *et al.*, 1977). For the sake of simplicity, we consider first the energy levels of the porphine dianion (Table XI). One finds as the highest occupied orbitals a set of two π orbitals, nearly degenerate, of symmetry a_{1u} and a_{2u}. Somewhat below are a number of π orbitals intermixed with the orbitals

TABLE XI

THE ENERGY LEVELS AND ORBITAL ENERGIES[a] OF THE PORPHIN DIANION WITH DIFFERENT BASIS SETS AND GEOMETRIES

Orbital[b]	Planar, BSI	Ruffled		
		BSI	BSII	BSIII
$3a_{2u}(\pi)$	+0.014	+0.013	+0.054	+0.051
$1a_{1u}(\pi)$	−0.045	−0.043	+0.023	+0.023
$9b_{1g}(n)$	−0.106	−0.105	−0.071	−0.070
$3e_g(\pi)$	−0.115	−0.114	−0.060	−0.059
$2b_{2u}(\pi)$	−0.121	−0.121	−0.065	−0.063
$17e_u(n)$	−0.143	−0.143	−0.114	−0.111
$2a_{2u}(\pi)$	−0.167	−0.164	−0.100	−0.099
$11a_{1g}(n)$	−0.187	−0.188	−0.166	−0.162
$2e_g(\pi)$	−0.201	−0.193	−0.126	−0.125
$1b_{1u}(\pi)$	−0.258	−0.243	−0.179	−0.178

[a] In atomic units.

[b] The notations π and n denote, respectively, the porphin π and σ MOs composed mainly of the nitrogen lone pairs.

TABLE XII

THE ENERGY LEVELS AND ORBITAL ENERGIES OF THE LOW-SPIN ($S = 0$) IRON(II) PORPHYRIN (PLANAR GEOMETRY)

Orbital	BSI (a.u.)	BSII (a.u.)	Orbital	BSI (a.u.)	BSII (a.u.)
$1a_{1u}(\pi)$	−0.317	−0.238	$9b_{2g}(d_{xy})$	−0.518	−0.468
$5a_{2u}(\pi)$	−0.316	−0.253	$19e_u(n)$	−0.525	−0.471
$4e_g(\pi)$	−0.413	−0.348	$1b_{1u}(\pi)$	−0.536	−0.459
$2b_{2u}(\pi)$	−0.424	−0.357	$9b_{1g}(n)$	−0.537	−0.473
$4a_{2u}(\pi)$	−0.442	−0.374	$2e_g(d_{xz}, d_{yz})$	−0.554	−0.500
$3e_g(\pi)$	−0.469	−0.390	$14a_{1g}(n)$	−0.588	−0.541

made essentially from the nitrogen lone pairs. The other σ orbitals are found at lower energies (Dedieu *et al.*, 1977). From the results of Table XI, one notices the following:

(1) The orbital energy values are practically the same for the two geometries considered—planar or ruffled

(2) The orbital energies of these high-lying levels are raised when the basis set improves from minimal to double zeta

(3) The orbital energies are practically the same for the two basis sets BSII and BSIII, which differ only at the level of the inner shells (one being minimal and the other double zeta for the inner shells).

In Table XII we have reported the energy levels of the low-spin ($S = 0$) iron(II) porphyrin FeP. We have considered this closed-shell low-spin system rather than the intermediate-spin ($S = 1$) open-shell system, which is known experimentally, in order to make a significant comparison with the porphin dianion, since orbital energies from closed-shell and open-shell SCF theories are not necessarily comparable. The π a_{2u} and a_{1u} orbitals are practically degenerate and are separated from the next occupied orbital by a gap of about 0.1 a.u. or 3 eV. The sequence of energy levels is rather similar to that found for the porphine dianion, the main differences being the following:

(1) A net stabilization of the orbitals of the iron(II) porphyrin, which is due to the charge cancellation

(2) A preferential stabilization of the $a_{2u}(\pi)$ orbital in the iron(II) porphyrin as a consequence of mixing with the iron $4p_z$ orbital

(3) A preferential stabilization of the molecular orbitals (MOs) b_{1g}, e_u, and a_{1g} made mainly from the lone pairs of the nitrogen atoms, this stabili-

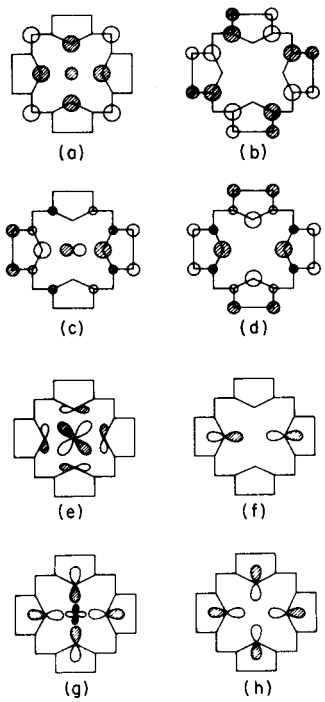

Fig. 11. The high-lying MOs of iron(II) porphyrin. The size of the lobes is approximately proportional to the basis functions coefficients. The view is looking down the positive z axis at the upper lobe of the $p\pi$ and $d\pi$ basis functions for the π MOs: (a) $5a_{2u}(\pi)$; (b) $1a_{1u}(\pi)$; (c) $4e_g(\pi)$; (d) $2b_{2u}(\pi)$; (e) $9b_{2g}(d_{xy})$; (f) $19e_u(n)$; (g) $9b_{1g}(n)$; (h) $14a_{1g}(n)$.

zation being larger for the MO $b_{1g}(n)$ as a consequence of the bonding interaction with the $3d_{x^2-y^2}$ orbital of iron.

These high-lying MOs are sketched in Fig. 11. Essentially the same features are found in the sequence of energy levels for MnP ($S = 5/2$), FeP ($S = 1$), and CoP ($S = 1/2$) (Table XIII; with the restriction that the energy of an open-shell orbital is not comparable to that of a closed-shell orbital). One notes again, from the values reported for FeP ($S = 1$), that the orbital energies are practically the same for the two geometries, planar and ruffled, and for the basis sets BSII and BSIII. Furthermore, the orbital energies for the π levels are nearly identical for FeP ($S = 1$) and CoP ($S = 1/2$). The only exception corresponds to an inversion of the levels e_g and b_{2u}, a consequence of the fact that the $e_g(\pi)$ orbital of FeP is stabilized through a bonding interaction with the orbitals d_{xz} and d_{yz} of iron.

The above description of the energy levels has some relationship to a

TABLE XIII

THE ENERGY LEVELS AND ORBITAL ENERGIES OF THE MANGANESE(II) PORPHYRIN ($S = 5/2$), THE IRON(II) PORPHYRIN ($S = 1$), AND THE COBALT(II) PORPHYRIN ($S = 1/2$)

MnP($^6A_{1g}$), BSII[a]		FeP($^3A_{2g}$)				CoP($^2A_{1g}$), BSIII[c]	
			Energy level (a.u.)				
Orbital (a.u.)	Energy level (a.u.)	Orbital (a.u.)	BSII[a]	BSII[c]	BSIII[c]	Orbital (a.u.)	Energy level (a.u.)
$b_{1g}(d_{x^2-y^2})$	+0.011*[b]	$e_g(d_{xz}, d_{yz})$	−0.076*	−0.076*	−0.071*	$a_{1g}(d_{z^2})$	−0.088*
$b_{2g}(d_{xy})$	−0.058*	$a_{1u}(\pi)$	−0.239	−0.237	−0.234	$a_{1u}(\pi)$	−0.230
$e_g(d_{xz}, d_{yz})$	−0.067*	$a_{2u}(\pi)$	−0.254	−0.251	−0.248	$a_{2u}(\pi)$	−0.251
$a_{1g}(d_{z^2})$	−0.070*	$b_{2u}(\pi)$	−0.357	−0.357	−0.353	$e_g(\pi)$	−0.348
$a_{2u}(\pi)$	−0.240	$e_g(\pi)$	−0.366	−0.365	−0.362	$b_{2u}(\pi)$	−0.352
$a_{1u}(\pi)$	−0.242	$a_{2u}(\pi)$	−0.375	−0.375	−0.373	$a_{2u}(\pi)$	−0.373
$b_{2u}(\pi)$	−0.358	$e_g(\pi)$	−0.392	−0.385	−0.379	$e_g(\pi)$	−0.379
$e_g(\pi)$	−0.361	$a_{1g}(d_{z^2})$	−0.432	−0.432	−0.428	$b_{1u}(\pi)$	−0.444
$a_{2u}(\pi)$	−0.372	$b_{1u}(\pi)$	−0.460	−0.448	−0.443	$b_{2g}(d_{xy})$	−0.516
$e_g(\pi)$	−0.382	$b_{2g}(d_{xy})$	−0.481	−0.483	−0.479	$e_g(d_{xz}, d_{yz})$	−0.519
$b_{1u}(\pi)$	−0.439						

[a] Assumed planar.

[b] Asterisk denotes open-shell orbitals.

[c] Experimental geometry, ruffled.

number of experimental data. The near degeneracy of the highest filled orbitals $a_{1u}(\pi)$ and $a_{2u}(\pi)$ is the key to the striking differences observed in the EPR spectra of porphyrin π cation radicals, with the possibility of either a $^2A_{2u}$ or $^2A_{1u}$ ground state (Dolphin and Felton, 1974). The similarity between the sequence of energy levels for the porphin dianion and various metalloporphyrins is in agreement with the experimental observation that the free-base porphin and its metallic derivatives have surprisingly similar photoelectron spectra (Khandelwal and Roebber, 1975; Kitagawa *et al.*, 1979; Dupuis *et al.*, 1980). A study of the redox potentials of metalloporphyrins has led to the conclusion that upon the introduction of a transition metal into a porphyrin, only the σ shell of the porphyrin (namely, the nitrogen lone pairs) is appreciably shifted in energy (Fuhrhop *et al.*, 1973). This is in agreement with the statement reached by Gouterman (1959) that the interaction between the metal $d(\pi)$ and the porphyrin π orbitals is minimal.

We now turn to a discussion of ionization potentials. At the SCF level, ionization potentials may be calculated in two ways. One method is to use Koopmans' theorem: namely, for a closed-shell system the ionization potential is equal to the negative of the orbital energy. There are two drawbacks to this approach. First, the relationship does not apply to the open-shell systems (however, with the open-shell SCF formalism which we have used, it seems to be approximately valid for the filled orbitals). Next, we have shown that in the case of organometallics, Koopmans' relation is approximately valid for the ligand orbitals but not for the metal 3d orbitals (see, for instance, Coutière *et al.*, 1972; Veillard and Demuynck, 1977) since the reorganization energy remains small for the former but not for the latter, where it amounts to several electron volts. Then the proper way to calculate the ionization potentials is to carry out separate SCF calculations for the molecule and its ion and then subtract the energy of the former from that of the latter. This is usually called the ΔSCF method. We discuss first the ionization potentials on the basis of Koopmans' theorem, and this discussion is obviously restricted to the ionization from the π orbitals of the porphyrin. Next, we shall see how the conclusions are changed when the ionization potentials are obtained from the ΔSCF method.

We have reported in Table XIV the ionization potentials calculated for a number of systems either on the basis of Koopmans' theorem or by the ΔSCF method, together with the experimental values found in the literature. For the two highest π orbitals of the porphyrin ligand, a_{1u} and a_{2u}, both the Koopmans' and the ΔSCF values of the ionizations potentials are in good agreement with the experimental values. Koopmans' values tend to be slightly higher than the experimental potentials, while the ΔSCF

TABLE XIV

THEORETICAL AND EXPERIMENTAL VALUES OF THE IONIZATION POTENTIALS (IP)

Compound	Electronic state	Basis set	Molecular orbital	Calculated IP (eV)		Experimental IP (eV)	Reference
				Koopmans' theorem	ΔSCF		
MnP	$^6A_{1g}$	BSII	$a_{2u}(\pi)$	6.53	—	6.44	Khandelwal and Roebber (1975)
			$a_{1u}(\pi)$	6.58	—	6.61	Khandelwal and Roebber (1975)
FeP	$^3A_{2g}$	BSIII	$a_{1u}(\pi)$	6.37	5.9($^4A_{2u}$)	6.06	Kitagawa (1979)
			$a_{2u}(\pi)$	6.75	6.3($^4A_1$)	6.48	Kitagawa (1979)
			$b_{2u}(\pi)$	9.60	9.3($^4B_{1u}$)	7.29	Kitagawa (1979)
			$a_{1g}(d_{z^2})$	11.6	5.8($^4A_{2g}$)		
			$b_{2g}(d_{xy})$	13.0	6.1($^4B_{1g}$)		
CoP	$^2A_{1g}$	BSIII	$a_{1u}(\pi)$	6.26	5.6($^3A_{1u}$)	6.09	Kitagawa (1979)
			$a_{2u}(\pi)$	6.83	6.2($^3A_{2u}$)	6.58	Kitagawa (1979)
			$a_{1g}(d_{z^2})$	—	8.3($^1A_{1g}$)		
$FePNH_3$	$^5A''$	BSII	$a_{1u}(\pi)$	6.34	—		
			$a_{2u}(\pi)$	6.53	—		
$FePO_2NH_3$	$^1A'$	BSII	$a_{1u}(\pi)$	6.37	—		
			$a_{2u}(\pi)$	6.56	—		

values are slightly lower. For all the systems studied except MnP, our calculations indicate that the a_{1u} orbital has a higher energy than a_{2u}, but the reverse situation occurs for MnP (however, the energy difference is extremely small for this molecule). For the three molecules MnP, FeP, and CoP, the experimental separation between these two states of the ion is well reproduced by the calculation (for MnP theoretical 0.05 vs. 0.17 eV experimental, for FeP theoretical 0.4 vs. 0.4 eV experimental, and for CoP theoretical 0.6 vs. 0.5 eV experimental). On the basis of Koopman's theorem, together with the values of Table XIII, the third π ionization potential for FeP or CoP would be at about 9.6 eV, while Kitagawa *et al.* (1979) report in the photoelectron spectra a band at about 7.3–7.5 eV which they assign to the third π cation state. These authors already mentioned that the theoretical calculation fails to reproduce the experimental gap between the second and the third ionization potentials. They hypothesize that Koopmans' theorem would be applicable for the first two π cation states but not for the following π states.

Ionization potentials calculated by the ΔSCF method for the π orbitals are in good agreement with those obtained from Koopmans' theorem, since the relaxation energy remains small for these orbitals (in the range 0.3–0.6 eV), in agreement with our earlier findings for other organometallics. This is true not only for the a_{1u} and a_{2u} π orbitals but also for the third π orbital b_{2u}. Thus the relaxation does not appreciably reduce the calculated gap between the second and the third π ionization potentials.

According to the ΔSCF calculations for FeP and CoP, the ionization energy of an electron in a filled metal 3d orbital is at 5.8 eV ($3d_{z^2}$) and 6.1 eV ($3d_{xy}$) for FeP and at 8.3 eV ($3d_{z^2}$) for CoP. The d electron bands have not been located in the photoelectron spectra of the metalloporphyrins. However, the ionization from a 3d-like orbital of Fe has been reported at 6.88 eV in the photoelectron spectrum of iron phtalocyanine (Berkowitz, 1979), in rather good agreement with our values of 5.8 and 6.1 eV for FeP.

On the whole, our results regarding ionization potentials are in excellent agreement with those of Ohno (1980). This indicates that the calculation of the ionization potentials is rather insensitive to the details of the basis set used.

D. The Electron-Density Distributions in the Metalloporphyrins

Only recently has it become possible to obtain from X-ray diffraction measurements accurate experimental information on the electron-density distribution in crystals of CoTPP (Stevens, 1981). Since the electron distribution is a sensitive property straightforwardly related to the wave function of the system, it may be used as a critical test against which our calculations may be judged. Stevens has reported the maps of the defor-

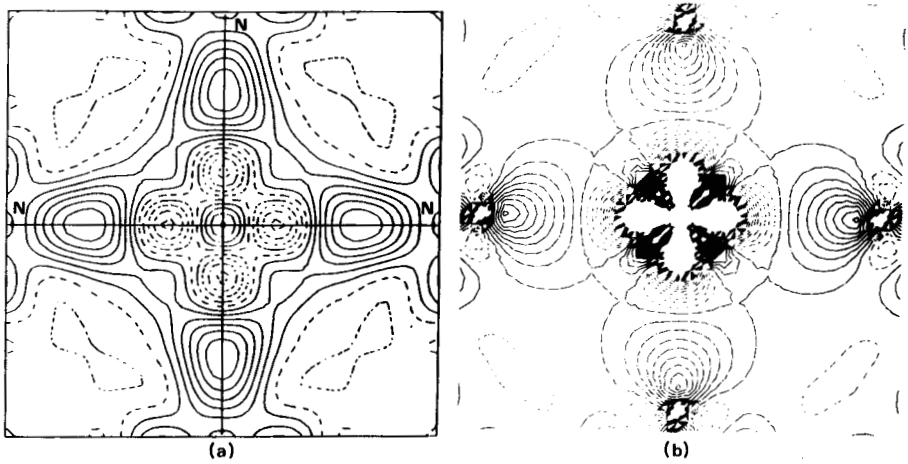

Fig. 12. The deformation density distribution near the cobalt atom in the plane of the CoN_4 core: (a) from the experimental work of Stevens (1981) on CoTTP; (b) from the theoretical work of Bénard (1982) on CoP. The contour intervals are $0.10eA^{-3}$ for experimental maps and $0.10eA^{-3}$ for computed maps.

mation density distribution near the cobalt atom in the plane of the CoN_4 core (Fig. 12a) and in the pyrrole plane (Fig. 13a). Bénard (1982) has computed the theoretical deformation density maps for the cobaltoporphyrin CoP (Fig. 12b and Fig. 13b). Comparison with the experimental maps shows that all the significant features (peaks, pits, and saddle points) obtained from the diffraction experiments are reproduced by the computed wave function. For instance, the two maps of Fig. 13 show the same zone of electron deficiency at the center of the pyrrole ring and the same accumulation regions centered in the middle of the bonds. A better quantitative agreement cannot be expected since (1) the effects of thermal smearing have not been introduced into the wave function; and (2) the experimental and theoretical deformation density in the vicinity of the heavy atoms are equally ill defined (Rees, 1976).

E. Population Analysis and Charge Transfers

For the sake of brevity, we do not report here the detailed results of the population analysis for the systems studied (results for the iron systems have been given by Dedieu *et al.*, 1977). We comment briefly about a few points which are frequently discussed in the literature.

It is commonly accepted that a moderate π back-bonding from metal to porphyrin helps to relieve the charge build-up on the metal atom that results from σ donation. Experimental evidence in support of or against a

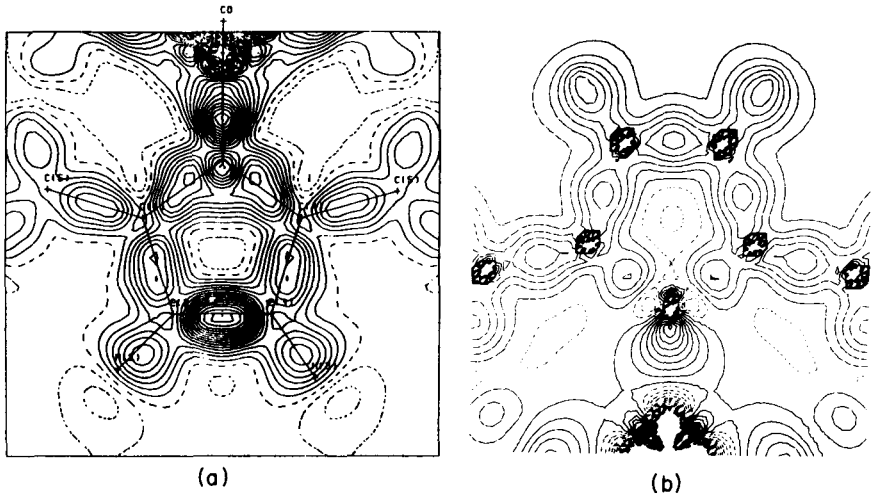

Fig. 13. The deformation density distribution in the pyrrole plane: (a) from the experimental work of Stevens (1981) on CoTPP; (b) from the theoretical work of Bénard (1982) on CoP. The contour intervals are $0.05eA^{-3}$ for experimental maps and $0.10eA^{-3}$ for computed maps.

significant iron-to-porphyrin π back-bonding has been discussed by several authors (see, for instance, Goff and La Mar, 1977; Mispelter *et al.*, 1978; Goff *et al.*, 1977). The π populations of the metal and of the porphyrin ligand are reported in Table XV for some representative systems. The four-coordinate systems show a π charge transfer from the porphyrin to the metal. The five-coordinate system $MnPO_2$ also shows a large π transfer from the porphyrin to the metal, which is understandable in terms of the formal valency $Mn(III)O_2^-$. For the other five-coordinate systems $FePNH_3$, FePCO, and $FePO_2$, the population analysis indicates a depopulation of the π orbitals for both the metal and the porphyrin. A metal-to-porphyrin π back-bonding is found only in the case of the hexacoordinate systems $FePO_2NH_3$ and $FePO_2H_2O$. It has been found that the direction of the charge transfer does not depend on the basis set used, minimal or double zeta (although the double-zeta calculations tend to level off the net charges).

A comparison of the wave functions and of the corresponding population analysis for FeP (low spin) and $FePO_2$ shows that the bonding between the dioxygen ligand and the iron atom may be described in a relatively simple way, which is very close to the original proposal by Pauling (1949). A synergic process involves a charge transfer from the dioxygen orbitals $3\sigma_g$ and π_g^a to the $3d_{z^2}$ orbital of iron, while π back-bonding popu-

TABLE XV

π POPULATIONS OF THE METAL AND OF THE PORPHYRIN[a]

System	S	Porphyrin[c]	Metal[d]	Δ		Nature of the transfer
				Metal[e]	Porphyrin[f]	
MnP	5/2	25.960	2.040	+0.040	−0.040	P → M
FeP	0	25.978	4.022	+0.022	−0.022	P → M
	1	25.962	2.038	+0.038	−0.038	P → M
	2	25.944	2.055	+0.055	−0.056	P → M
$FePNH_3$[b]	2	25.987	2.999	−0.001	−0.013	
$MnPO_2$	3/2	25.904	2.134	+0.134	−0.096	P → M
$FePO_2NH_3$	0	26.038	3.848	−0.152	+0.038	M → P

[a] With BSII except for FeP $S = 0$, which used BSI.
[b] Out-of-plane displacement of the iron atom of 0.25 Å.
[c] Total $2p\pi$ population of the carbon and nitrogen atoms of the porphyrin.
[d] Total $3d\pi + 4p\pi$ population of the metal.
[e] Charge transferred to the metal π orbitals.
[f] Charge transferred to the porphyrin π orbitals.

lates the π_g^b orbital of the dioxygen ligand at the expense of the metal d_{yz} orbital (for the sake of simplicity, we refer to a dioxygen ligand in a $^1\Delta$ state). Both charge transfers are relatively small, of the order of $0.1e$ or less. Acting in the opposite way, they leave the dioxygen ligand quasi-neutral. Since the $3\sigma_g$ orbital is bonding, whereas the orbitals π_g^a and π_g^b are antibonding, it is expected that as a whole the binding of the dioxygen ligand to the ferroporphyrin will weaken the O—O bond. This probably explains the decrease in the O—O stretching frequency, which has been found both experimentally and theoretically.

IV. Geometrical Structure

A. The Deviations from a Planar Metal–Porphyrin Unit in the Deoxy Systems

1. *Ruffling of the Porphyrin*

The tendency of the porphin to complex a great number of metal ions is related to the ability of the porphyrin ring to stretch or to contract. The resulting complexes exhibit variable structures depending on the size of the metal ion and on the nature of the axial ligands (Hoard, 1975). Three different types of geometries have been reported for the porphyrin ring (Fig. 14):

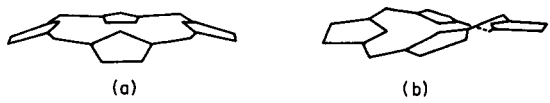

Fig. 14. (a) The domed geometry of the porphyrin; (b) the ruffled geometry of the porphyrin.

(1) A planar geometry with D_{4h} symmetry
(2) A domed geometry with C_{4v} symmetry, usually in the case of five-coordinated porphyrins
(3) A ruffled geometry with D_{2d} symmetry. The ruffling results from a contraction of the porphyrin skeleton occuring when the radius of the metal ion is small

The intrinsic stabilities of these different structures are probably close since, for instance, the octaethylporphinatonickel(II) NiOEP crystallizes in two different forms: tetragonal with the macrocycle highly distorted and having D_{2d} symmetry (Meyer, 1972), and triclinic with the macrocycle effectively planar (Cullen and Meyer, 1974). The four-coordinate porphyrins FeTPP and CoTPP display ruffled structures of S_4 (quasi-D_{2d}) symmetry (Collman *et al.*, 1975a; Madura and Scheidt, 1976).

In order to investigate the energy cost of these deformations, we have considered the metal-free porphin P^{2-} and the iron(II) porphyrin FeP ($S = 1$) with either a planar D_{4h} or a ruffled D_{2d} skeleton (keeping the Ct—N distance equal to the value of 1.97 Å). As seen from Table XVI, the corresponding energy values are close and, furthermore, the results depend on the basis set used. To assess which structure is the most stable would require an extended basis set, together with extensive geometry optimization.

TABLE XVI

RELATIVE ENERGIES OF DIFFERENT STRUCTURES FOR P^{2-} AND FeP

Molecule	Basis set	Structure	
		Planar D_{4h}	Ruffled D_{2d}
P^{2-}	BSI	−978.5215	−978.5495
	BSII	−980.5666	−980.5525
FeP ($^3A_{2g}$)	BSII	−2241.0951	−2241.0755

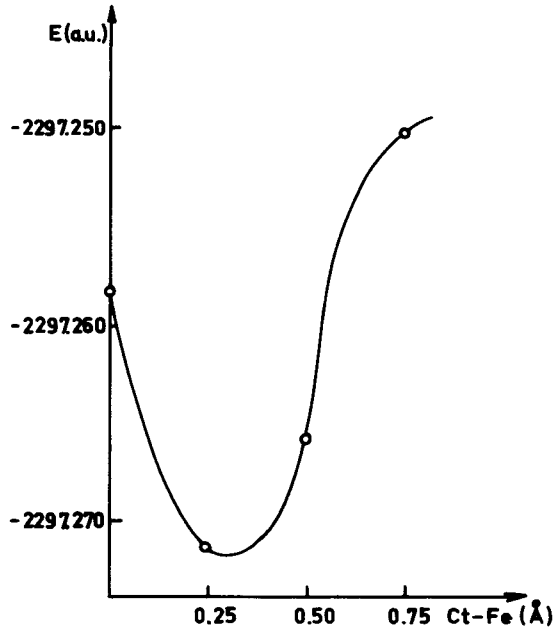

Fig. 15. The potential energy of $FePNH_3$ as a function of the out-of-plane displacement of the iron atom.

2. *The Out-Of-Plane Displacements in the Four- and Five-Coordinate Porphyrins*

a. The five-coordinate porphyrins: $FePNH_3$. As mentioned above, the low affinity of deoxyhemoglobin for molecular oxygen has been related to the out-of-plane displacement of the iron atom since, upon oxygenation, the iron moves into the porphyrin plane. For this reason, we have calculated the potential energy curve for our deoxyheme model $FePNH_3$ as a function of the out-of-plane displacement of the iron (Fig. 15). The curve has a minimum for a displacement of 0.32 Å. This value is intermediate between the EXAFS value of 0.2–0.3 Å for deoxyhemoglobin (Eisenberger *et al.*, 1978) and the displacements of 0.40 and 0.42 Å reported for two synthetic five-coordinate porphyrins with a 2-MeIm ligand (Jameson *et al.*, 1978a). The steric requirements of the 2-MeIm are probably responsible for the increased displacement of about 0.1 Å, compared to our value (as evidenced by the tilting of the ligand). A similar adjustment for the steric hindrance of the 2-MeIm group through a displacement of 0.11–0.12 Å of the iron atom has been reported in the dioxygen complexes of the picket-fence porphyrin (Jameson *et al.*, 1978a). The calcu-

lated displacement of 0.32 Å is also close to the value of 0.28 Å reported on the basis of an X-ray crystal structure for a polymeric "picket-fence" porphyrin with the iron atom of one porphyrin unit coordinated to the pivalamid oxygen atom of another unit, this system being devoid of any short contact between the axial ligand and the porphyrin ring (Jameson *et al.*, 1978b).

b. The out-of-plane displacement in the four-coordinate porphyrins. A question which is frequently addressed is the origin of this out-of-plane displacement of the iron atom (Perutz, 1978). Traditionally, it was said that the radius of the high-spin iron atom is too large to fit into the porphyrin hole (Cotton and Wilkinson, 1972). An equivalent explanation emphasizes the presence of an electron in the antibonding orbital $d_{x^2-y^2}$ since pulling the iron out of the porphyrin plane will reduce the antibonding character of this orbital (Hoard, 1975). For this reason we have calculated the potential energy curve for the high-spin ($S = 2$) four-coordinate system FeP, and we have found that the equilibrium structure corresponds to the iron atom in the porphyrin plane (Veillard *et al.*, 1980). This supports the proposal of Olafson and Goddard (1977) that the out-of-plane displacement of iron in the five-coordinate porphyrins is not due to the size of the high-spin iron(II) but rather to the nonbonded interactions between the electron pair of the fifth ligand and the pyrrole nitrogens of porphyrin.

Further confirmation of the importance of the axial ligand–porphyrin interactions may be found in the following calculations. We have computed the potential energy curves as a function of the out-of-plane displacement for the two systems $Fe(NH_2)_4NH_3$ and $[Fe(NH_2)_4SH]^-$ considered respectively as models of the deoxyheme and of the reduced cytochrome P450. The energy minima correspond respectively to a displacement of 0.45 and 0.65 Å. The increase in the out-of-plane displacement when going from a nitrogen to a sulfur ligand results from an increase of the repulsive interactions between the lone pairs of the fifth ligand and of the pyrrole nitrogens since the lone pair of a mercaptide sulfur is more delocalized than the lone pair of a nitrogen atom.

Although the size of the metal does not seem to be responsible for the out-of-plane displacement in the case of the iron atom, this factor might become dominant for larger atoms. One possible candidate is the manganese atom, since its ionic radius is larger than the one of iron (the difference being in the range 0.03–0.08 Å, depending on the set of ionic radii used). Support for this hypothesis may be found in the results of the X-ray structure for MnTPP (Kirner *et al.*, 1977) with an out-of-plane displacement of 0.19 Å of the manganese atom. For these reasons, we have calculated the potential energy curve of MnP as a function of the out-of-

plane displacement of the manganese atom, for the high-spin ($S = 5/2$) configuration with BSII (Dedieu *et al.*, 1981). The minimum was found for the manganese atom being in the plane. Using the model $MnN_4C_6H_{10}$ we have extended this study with basis set III and additional f-type polarization functions. With this improved basis set the manganese atom is still found to be sitting in the plane of the porphyrin. For this reason, we consider that the *intrinsic* equilibrium position of the manganese atom in MnP is the porphyrin plane and that the out-of-plane displacement reported for MnTPP is the consequence of a weak π-complex formation between a toluene solvate molecule and the metalloporphyrin, as proposed by Kirner *et al.* (1977).

B. The Geometrical Structures of the Oxy and Carboxy Systems

1. *Situation of the Problem*

When this theoretical study began, the X-ray crystal structure of the dioxygen adduct of the picket-fence porphyrin (Collman *et al.*, 1974, 1975b) was the only known structure of a dioxygen adduct of a metalloporphyrin that was of good enough quality to assess unambiguously the geometry of the MO_2 unit. The FeO_2 unit was found to adopt a bent, end-on structure (I) rather than a perpendicular side-on structure (II). The Fe—O—O plane was found to be four-way statistically disordered, bisecting the N—Fe—N right angles of the equatorial porphyrin plane. However, high thermal motion and disorder in many parts of the structures of O_2 adducts of picket-fence porphyrins have apparently precluded precise characterization of the O—O distance and the Fe—O—O angle (see Jameson *et al.*, 1978a, 1980).

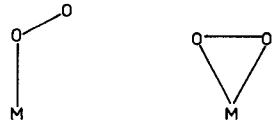

(I) (II)

The structures of two natural oxyhemoproteins have been reported. In oxymyoglobin (Phillips, 1978) the FeO_2 unit is bent ($\angle FeOO = 121°$) but without any disordering and with the Fe—O—O plane eclipsing the Fe—N (pyrrole) bond. These features have been traced to steric hindrance of some distal residues. Again, although further refinements of the structure have apparently been carried out (see Table 20 of Jameson *et al.*, 1980), the bond distances and bond angles within the FeO_2 unit are only known with large standard deviation errors. The structure of oxyerythrocruorin (Weber *et al.*, 1978) indicates an end-on dioxygen ligand

but with a near linear Fe—O—O bond ($\angle$Fe—O—O = 170°). This structure was poorly resolved however, and the large error (30°) on the Fe—O—O angle precludes any definite conclusion. We note simply that the dioxygen unit is found to point approximately between the vinyl-substituted pyrrole residues.

Structures of dioxygen adducts of metalloporphyrins other than iron porphyrins have now been published. A perpendicular structure (II) has been found for the dioxygen complex of the titaniumoctaethylporphyrin (Guilard *et al.*, 1976, 1978) with the O—O unit eclipsing two Ti—N (pyrrole) bonds. In the oxycobaltomyoglobin the MO_2 unit adopts a bent structure (Petsko *et al.*, 1981).

An X-ray crystal structure of a dioxygen adduct of a manganese porphyrin is still to be found. A side-on perpendicular structure has been postulated, originally on the basis of the EPR data (Weschler *et al.*, 1975; Hoffman *et al.*, 1976, 1978). Later, the value of the O—O IR stretching vibration [803 cm^{-1} for $\nu(^{18}O_2)$] was said to be characteristic of such a perpendicular structure (Jones *et al.*, 1979).

Our theoretical study of the geometrical aspects of the dioxygen coordination to the porphyrins of Ti, Mn, Fe, and Co was therefore aimed at the determination and the understanding of (1) the geometrical structure of the MO_2 unit either bent (I) or perpendicular (II), and (2) the stereochemistry of the MPO_2 system by studying the rotational isomerism around the M—O bond, since for each of the two structures, perpendicular or bent, the O—O bond may project either along the M—N bonds [eclipsed structures (III) and (IV)] or along the bisector of the N—M—N angle [staggered structures (V) and (VI)].

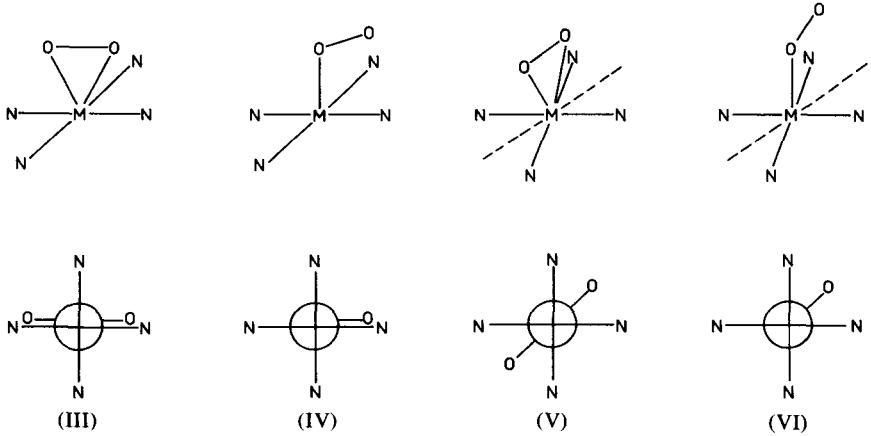

2. *Bent, Kinked, and Perpendicular Structures of the Oxy Systems*

For $TiPO_2$ the perpendicular structure was found to be more stable than the bent structure by 83 kcal/mol (Rohmer *et al.*, 1977). This is in agreement with the X-ray crystal structure which we mentioned above. The energy difference between the two structures is large and our conclusion should therefore be independent of further theoretical refinements such as basis set enlargment, geometry optimization, or the use of a method that goes beyond the SCF level.

For the $MnPO_2$ system the situation is less clear-cut. As evidenced from Table VI, the energy difference between the two basic structures, bent and perpendicular, is highly dependent on the geometry optimization of the MnO_2 unit. Two factors seem to be important: the Ct—Mn distance and the conformation of the O_2 unit with respect to the Mn—N (pyrrole) bonds. For the eclipsed conformation, the bent structure is more stable than the perpendicular structure by about 22 kcal/mol (we consider here only the lowest energy configurations—of the $Mn(III)O_2^-$ superoxo type—in both structures). This difference is reduced to 5 kcal/mol if one compares the bent eclipsed structure to the perpendicular staggered one (with Ct—Mn = 0.62 Å). It seems therefore difficult to assess, on the basis of only our present calculations, the geometry of the MnO_2 unit. This would require a rather careful geometry optimization. Moreover, as we pointed out already, one should probably go beyond the SCF level and consider more than one configuration in the ground-state wave function for each basic structure. Finally, we cannot exclude the possibility of a kinked geometry (VII), somewhat intermediate between the perpendicular structure (observed for $TiPO_2$) and the bent structure (observed for $FePO_2$). This is not an unreasonable assumption: this structure was indeed considered for the dioxygen adduct of iron porphyrins (*vide infra*).

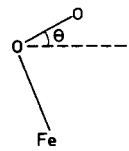

(VII)

The iterative extended Hückel (IEH) calculations of Hanson and Hoffman (1980) are said to favor the perpendicular geometry. This is again based on calculated properties from wave functions which are set according to the experimental EPR data and not based on energy comparison. One may wonder what would have been the result if total energies had been reported. Although we are well aware that the IEH method may not

be reliable for this purpose, it is interesting to note that calculations using this method and carried out on the $FePO_2NH_3$ system (Kirchner and Loew, 1977) had definitely favored—on energy grounds—the kinked and the bent structures over the perpendicular structure, thus in agreement with the experimental data and our *ab initio* calculations (see below).

For $FePO_2NH_3$ the bent structure is more stable than the perpendicular structure by 49 kcal/mol (with the minimal BSI). This is in agreement with the X-ray crystal structure data which we have quoted above. As for $TiPO_2$, the energy difference is sufficiently large that it would survive a calculation carried out with a better basis set. The optimized value of the FeOO angle (128°, Dedieu *et al.*, 1976b) is in agreement with the experimental value found for the dioxygen adduct of picket-fence porphyrins (131°, Jameson *et al.*, 1978a; 129°, Jameson *et al.*, 1980). The optimization of the O—O bond length ended with a value of 1.296 Å. Owing to the use of a minimal basis set, this value is certainly overestimated and we believe that it would fall in the range 1.22–1.26 Å when using better basis sets. A lower bound of 1.21 Å has been recently found (Jameson *et al.*, 1980).

The earlier crystallographic study of the dioxygen adduct of the picket-fence porphyrin (Jameson *et al.*, 1978a) suffered from large disorder and high thermal motion. Since the O—O bond length was found to be unrealistically short (average value 1.16 Å), a kinked structure such as (VII) could not be ruled out. Such a structure was indeed predicted on the basis of IEH calculations by Kirchner and Loew (1977) who found the kinked structure about 15 kcal/mol lower in energy than the bent structure. From our calculations the bent structure is favored over the kinked one (with the geometry corresponding to the lowest energy reported by Kirchner and Loew) by about 6 kcal/mol. The kinked structure seems therefore to be ruled out for the $FePO_2NH_3$ model system (which has an unsubstituted planar ferroporphyrin). The energy difference is sufficiently small, however, that one cannot preclude the occurrence of the kinked structure for the dioxygen adduct of the highly substituted picket-fence porphyrin or of some naturally occuring proteins. Nevertheless, the most recent X-ray crystal structure of the dioxygen adduct of the picket-fence porphyrin (Jameson *et al.*, 1980) indicates that the off-axis displacement of the coordinated oxygen atom (if any) should be small.

For the $CoPO_2NH_3$ system we found the bent structure more stable than the perpendicular one, by about 45 kcal/mol in the minimal basis set calculations. This is again in agreement with the experimental structure of the oxycobaltomyoglobin (Petsko *et al.*, 1981) and with the known structures of several dioxygen adducts of Co(II)–Schiff-base complexes (see Basolo *et al.*, 1975).

The trends in the geometrical structure of the MO_2 unit along the

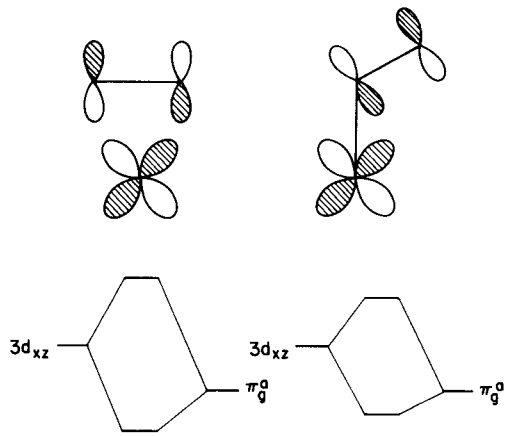

Fig. 16. The $3d_{xz}-\pi_g^a$ interaction for the two structures: perpendicular (left) and bent (right).

transition series (perpendicular for an early transition metal Ti, bent at the end of the series for Fe and Co) have been rationalized as follows. The dominant metal–ligand interaction is $3d_{xz}-1\pi_g^a$ for both structures, bent and perpendicular (or $3d_{Xz}-1\pi_g^a$ depending on the relative orientation of the dioxygen ligand and the porphyrin ring). This interaction shown in Fig. 16 is somewhat larger for the perpendicular structure than for the bent structure (this results from a larger overlap in the perpendicular structure). For $TiPO_2$ only the lowest orbital of Fig. 16 is filled and the interaction is therefore stabilizing. The minimum energy is achieved by maximizing this interaction, hence the preference for the perpendicular structure. On the other hand, for Fe and Co both orbitals of Fig. 16 are filled and the corresponding interaction is destabilizing. The energy will be minimum when this interaction is minimized, and this is achieved in the bent structure. The above analysis, although somewhat simplified (Dedieu *et al.*, 1979a, Refs. 96 and 97), is similar to that proposed by Hoffmann *et al.* (1977) in terms of a Walsh diagram for ML_4XY complexes. In the middle of the series the situation is again less clear-cut (as for the ground-state assignment): this is best illustrated by the $MnPO_2$ system (see Table VI). Since more than one configuration will probably contribute to the ground state, a discussion in terms of orbital interactions is not possible. Moreover, should one consider the lowest energy configuration for each structure, the corresponding dominant interactions are different since the configurations are not the same. In the perpendicular structure [configuration (6)], the dominant interaction between π_g^a(occupied) and d_{xz}, which is empty, is a stabilizing one. In the bent structure [configuration (4)] the

interaction between π_g^a and d_{xz} is a three-electron interaction, thus destabilizing. It is balanced, however, by an interaction between π_g^a(occupied) and d_{z^2}(empty) which is stabilizing. The net result is therefore a small energy difference between both structures. (It should be noted that we have only considered the eclipsed conformation for the bent structure. Staggering the O_2 unit might stabilize the bent structure somewhat since it would reduce the steric contacts between the terminal oxygen atom and the pyrrole nitrogens.)

3. *The Rotational Isomerism around the Metal–Oxygen Bond*

The relative stabilities of the eclipsed and staggered conformations were investigated for two systems, $TiPO_2$ and $FePO_2$ (considered as a model of $FePO_2Im$). In both cases the experimental mode of coordination was retained, perpendicular for $TiPO_2$, bent for $FePO_2$, and the SCF calculations were performed only on the corresponding ground-state configuration. For $TiPO_2$ the eclipsed structure (III) was found more stable than the staggered structure (V) by 5 kçal/mol, in agreement with the crystal structure of $Ti(OEP)O_2$ (Guilard *et al.*, 1976, 1978). Dynamic NMR data have been interpreted in terms of a rotation of the peroxide group with an estimated rotation barrier of 10 kcal/mol (Guilard *et al.*, 1978). The greater stability of the eclipsed structure has been rationalized on the basis of metal–ligand interaction diagrams (see Dedieu *et al.*, 1979a) deduced from the SCF wave functions.

For the $FePO_2$ system the most stable structure corresponds to the staggered structure (VI), the eclipsed structure (IV) being higher in energy by 6 kcal/mol. This is also in agreement with the crystal structure of the dioxygen adduct of picket-fence porphyrins (Collman *et al.*, 1974, 1975b; Jameson *et al.*, 1980). Note that the eclipsed structure which has been found for the dioxygen adduct of oxymyoglobin (Phillips, 1978) has been traced to steric interactions from protein residues. This is consistent with a low rotational barrier, as obtained from these calculations. INDO–SCF calculations (Herman and Loew, 1980) also indicate a rather small barrier in the $FePO_2Im$ system, the staggered geometries being the most stable [on the other hand, the eclipsed structure was found through IEH calculation (Kirchner and Loew, 1977), again with a small rotational barrier]. We traced (see Dedieu *et al.*, 1979a) the greater stability of the staggered conformation to the steric repulsion between the terminal oxygen atom and one of the pyrrole nitrogen atom rather than to the orbital interactions which were found to be rather weak. Using the same arguments, the conformation of the $CoPO_2NH_3$ system was also predicted to be staggered.

We do not have enough calculated data to compare both conformations

in the $MnPO_2$ system. For the lowest energy configuration of the perpendicular structure [configuration (6), $(\pi_g^a)^2(\pi_g^b)^1(xy)^2(Yz)^1(z^2)^1$], the eclipsed configuration appears to be slightly more stable than the staggered configuration (as for $TiPO_2$, this result can be easily explained in terms of orbital interactions). It must be pointed out again that this result only holds for the lowest energy configuration. The definite result may be different once a many-configurational wave function has been used.

4. *The Structure of the* FeCO *unit in* FePCO

This part of our study was initiated by several reports of a bent-structure (VIII) for the Fe—C—O unit in X-ray crystal structures of different carbon monoxide hemoproteins (Huber *et al.*, 1970; Padlan and Love, 1974; Norwell *et al.*, 1975). The bending of the Fe—C—O unit (α being of the order of 135–145°) was traced to the steric interactions with the surrounding proteins. Indeed, using empirical energy functions to calculate interaction potentials, Case and Karplus (1978) showed that a carbonyl ligand linearly bound to the iron atom should have strong repulsive interactions with some protein residues. Heidner *et al.* (1976) have suggested a bending of the entire Fe–CO unit away from the heme normal [as sketched in (IX)], but the carbon atom could not be located. It has been emphasized, however, that the available X-ray and neutron diffraction date did not allow distinguishing between the two structures bent (VIII) and tilted (IX), although this latter possibility was chemically more reasonable (Collman, 1977; Peng and Ibers, 1976). Since both structures were rather unexpected, we decided to investigate the intrinsic structure of the Fe—CO unit in the model system FePCO in the absence of any steric constraints. (For the sake of economy, we considered a model system without a sixth axial ligand.)

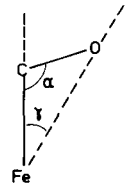

(VIII)

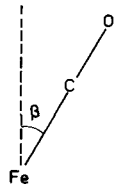

(IX)

Calculations on structures (VIII) and (IX) were carried out for different values of the angle α and β (keeping the Fe—C and C—O bond lengths at 1.77 and 1.16 Å, respectively); α and β were not varied independently but were subject to the constraint $\beta = \gamma$ (i.e., we kept the same angle between the Fe—O axis and the heme normal for both structures). This

allowed us a comparison of the energetics of the two deformations. We found, as expected from the extensive literature on transition metal carbonyl complexes, a linear Fe—C—O bond, but the potential energy appeared to be rather soft (the numerical results may be found in the original publication Dedieu *et al.*, 1976). After the completion of our work, X-ray crystal structures of the FeTPP(CO)(Py) system (Peng and Ibers, 1976) and of the carbonyl complex of the picket-fence porphyrins (see Ref. 5 of Peng and Ibers, 1976) also indicated a linear Fe—C—O bond perpendicular to the heme plane. From our calculated energies it seems very difficult to choose between the two alternatives VIII and IX for the structure of CO in carboxyhemoproteins. A bend of 30° would require 9.2 kcal/mol and the corresponding tilt 11.3 kcal/mol. On the basis of their empirical calculations, Case and Karplus (1978) have tentatively favored the tilting deformation over the bending deformation. They have reported a value of about 7 kcal/mol for the maximum strain energy that can be supported by the protein. At first glance, the values which we report here seem therefore to be still slightly too large to be consistent with the bending (or the corresponding tilting) of 35°–45° which has been found experimentally. It must be pointed out, however, that in order to obtain this level of chemical accuracy, more refined calculations (allowing at least a more complete geometry relaxation) should be performed. But such calculations presently lie beyond our computing possibilities.

Acknowledgments

This work has been supported by the C.N.R.S. through the ATP no. 2240, which is gratefully acknowledged. The computations have been carried out at the Centre de Calcul du C.N.R.S. in Strasbourg-Cronenbourg and we take the opportunity to thank the staff of the Centre. We are greatly indebted to Dr. M. Bénard for his contribution to the development of the computational methods which have made possible these studies. We thank Dr. E. D. Stevens for the communication of results prior to publication. Special thanks are due to Mr. J. Maire for the drawings and to Mrs. L. Koch for the typing.

References

Baldwin, J. E., and Huff, J. (1973). *J. Am. Chem. Soc.* **95,** 5757–5759.
Basolo, F., Hoffman, B. M., and Ibers, J. A. (1975). *Acc. Chem. Res.* **8,** 384–392.
Benard, M. (1976). *J. Chim. Phys.* 413–414.
Benard, M. (1982). *Angew. Chem.* (in press).
Benard, M., and Barry, M. (1979). *Comput. Chem.* **3,** 121–124.
Benard, M., Dedieu, A., Demuynck, J., Rohmer, M.-M., Strich, A., and Veillard, A. (1981). "ASTERIX: A system of Programs for the Univac 1110." Unpublished.
Berkowitz, J. (1979). *J. Chem. Phys.* **70,** 2819–2828.

Brault, D., and Rougee, M. (1974). *Biochemistry* **13,** 4598–4602.
Caron, C., Mitschler, A., Rivière, G., Ricard, L., Schappacher, M., and Weiss, R. (1979). *J. Am. Chem. Soc.* **101,** 7401–7402.
Case, D. A., and Karplus, M. (1978). *J. Mol. Biol.* **123,** 697–701.
Case, D. A., Huynh, B. H., and Karplus, M. (1979). *J. Am. Chem. Soc.* **101,** 4433–4453.
Cerdonio, M., Congiu-Castellano, A., Mogno, F., Pispisa, B., Romani, G. L., and Vitale, S. (1977). *Proc. Natl. Acad. Sci. U.S.A.* **74,** 398–400.
Cerdonio, M., Congiu-Castellano, A., Calabrese, L., Morante, S., Pispisa, B., and Vitale, S. (1978). *Proc. Natl. Acad. Sci. U.S.A.* **75,** 4916–4919.
Cheung, S. K., Grimes, C. J., Wong, J., and Reed, C. A. (1976). *J. Am. Chem. Soc.* **98,** 5028–5030.
Chevrier, B., Weiss, R., Lange, M., Chottard, J. C., and Mansuy, D. (1981). *J. Am. Chem. Soc.* **103,** 2899–2901.
Churg, A. K., and Makinen, M. W. (1978). *J. Chem. Phys.* **68,** 1913–1925.
Collman, J. P. (1977). *Acc. Chem. Res.* **10,** 265–272.
Collman, J. P., Gagne, R. R., Reed, C. A., Robinson, W. T., and Rodley, G. A. (1974). *Proc. Natl. Acad. Sci. U.S.A.* **71,** 1326–1329.
Collman, J. P., Hoard, J. L., Kim, N., Lang, G., and Reed, C. A. (1975a). *J. Am. Chem. Soc.* **97,** 2676–2681.
Collman, J. P., Gagne, R. R., Reed, C. A., Halbert, T. R., Lang, G., and Robinson, W. T. (1975b). *J. Am. Chem. Soc.* **97,** 1427–1439.
Collman, J. P., Brauman, J. I., Halbert, T. R., and Suslick, K. S. (1976). *Proc. Natl. Acad. Sci. U.S.A.* **73,** 3333–3337.
Collman, J. P., Brauman, J. I., Doxsee, K. M., Halbert, T. R., Hayes, S. E., and Suslick, K. S. (1978). *J. Am. Chem. Soc.* **100,** 2761–2766.
Cotton, F. A., and Wilkinson, G. (1972). "Advanced Inorganic Chemistry," p. 871. Wiley, New-York.
Coutière, M.-M., Demuynck, J., and Veillard, A. (1972). *Theor. Chim. Acta* **27,** 281–287.
Cullen, D. L., and Meyer, E. F., Jr. (1974). *J. Am. Chem. Soc.* **96,** 2095–2102.
Dedieu, A., and Rohmer, M.-M. (1977). *J. Am. Chem. Soc.* **99,** 8050–8051.
Dedieu, A., Rohmer, M.-M., and Veillard, A. (1976a). *J. Am. Chem. Soc.* **98,** 5789–5800.
Dedieu, A., Rohmer, M.-M., Veillard, H., and Veillard, A. (1976b). *Bull. Soc. Chim. Belg.* **85,** 953–962.
Dedieu, A., Rohmer, M.-M., Bénard, M., and Veillard, A. (1976c). *J. Am. Chem. Soc.* **98,** 3717–3718.
Dedieu, A., Rohmer, M.-M., and Veillard, A. (1977). *In* "Metal–Ligand Interactions in Organic Chemistry and Biochemistry" (B. Pullman and N. Goldblum, eds.), Part 2, pp. 101–130. Reidel, Dordrecht.
Dedieu, A., Rohmer, M.-M., Veillard, H., and Veillard, A. (1979a). *Nouv. J. Chim.* **3,** 653–667.
Dedieu, A., Rohmer, M.-M., and Veillard, A. (1979b). Unpublished results.
Dedieu, A., Rohmer, M.-M., and Veillard, A. (1981). To be published.
Demuynck, J., Kochanski, E., and Veillard, A. (1979). *J. Am. Chem. Soc.* **101,** 3467–3472.
Dolphin, D., and Felton, R. H. (1974). *Acc. Chem. Res.* **7,** 26–32.
Dolphin, D., Sams, J. R., Tsin, T. B., and Wong, K. L. (1976). *J. Am. Chem. Soc.* **98,** 6970–6975.
Drago, R. S. (1979). *Inorg. Chem.* **18,** 1408–1410.
Dupuis, P., Roberge, R., and Sandorfy, C. (1980). *Chem. Phys. Lett.* **75,** 434–437.
Eaton, W. A., Hanson, L. K., Stephens, P. J., Sutherland, J. C., and Dunn, J. B. R. (1978). *J. Am. Chem. Soc.* **100,** 4991–5003.

Eicher, H., Bade, D., and Parak, F. (1976). *J. Chem. Phys.* **64,** 1446–1455.
Eisenberger, P., Shulman, R. G., Brown, G. S., and Ogawa, S. (1976). *Proc. Natl. Acad. Sci. U.S.A.* **73,** 491–495.
Eisenberger, P., Shulman, R. G., Kincaid, B. M., Brown, G. S., and Ogawa, S. (1978). *Nature (London)* **274,** 30–34.
Enemark, J. H., and Feltham, R. D. (1974). *Coord. Chem. Rev.* **13,** 339–406.
Fermi, G. (1975). *J. Mol. Biol.* **97,** 237–256.
Fuhrhop, J.-H., Kadish, K. M., and Davis, D. G. (1973). *J. Am. Chem. Soc.* **95,** 5140–5147.
Gelin, B. R., and Karplus, M. (1977). *Proc. Natl. Acad. Sci. U.S.A.* **74,** 801–805.
Goff, H., and La Mar, G. N. (1977). *J. Am. Chem. Soc.* **99,** 6599–6606.
Goff, H., La Mar, G. N., and Reed, C. A. (1977). *J. Am. Chem. Soc.* **99,** 3641–3646.
Gonser, U., Maeda, Y., Trautwein, A., Parak, F., and Formanek, H. (1974). *Z. Naturforsch.* **29B,** 241–244.
Gouterman, M. (1959). *J. Chem. Phys.* **30,** 1139–1161.
Gouterman, M. (1978). *In* "The Porphyrins" (D. Dolphin, ed.), Vol. 3, p. 1–165. Academic Press, New-York.
Griffith, J. S. (1958). *Discuss. Faraday Soc.* **26,** 81–86.
Guest, M. F., and Saunders, V. R. (1974). *Mol. Phys.* **28,** 819–828.
Guilard, R., Fontesse, M., Fournari, P., Lecomte, C., and Protas, J. (1976). *J.C.S. Chem. Commun.* 161–162.
Guilard, R., Latour, J.-M., Lecomte, C., Marchon, J.-C., Protas, J., and Ripoll, D. (1978). *Inorg. Chem.* **17,** 1228–1237.
Hall, M. B. (1980). Personal communication.
Hanson, L. K., and Hoffman, B. M. (1980). *J. Am. Chem. Soc.* **102,** 4602–4609.
Heidner, E. J., Ladner, R. C., and Perutz, M. F. (1976). *J. Mol. Biol.* **104,** 707–722.
Herman, Z. S., and Loew, G. H. (1980). *J. Am. Chem. Soc.* **102,** 1815–1821.
Hoard, J. L. (1975). *In* "Porphyrins and Metalloporphyrins" (K. M. Smith, ed.), pp. 317–380. Elsevier, Amsterdam.
Hoard, J. L., and Scheidt, W. R. (1973). *Proc. Natl. Acad. Sci. U.S.A.* **70,** 3919–3922.
Hoffman, B. M., and Petering, D. H. (1970). *Proc. Natl. Acad. Sci. U.S.A.* **67,** 637–643.
Hoffman, B. M., Weschler, C. J., and Basolo, F. (1976). *J. Am. Chem. Soc.* **98,** 5473–5482.
Hoffman, B. M., Szymanski, T., Brown, T. G., and Basolo, F. (1978). *J. Am. Chem. Soc.* **100,** 7253–7259.
Hoffmann, R., Chen, M. M. L., and Thorn, D. L. (1977). *Inorg. Chem.* **16,** 503–511.
Huber, R., Epp, O., and Formanek, H. (1970). *J. Mol. Biol.* **52,** 349–354.
Huynh, B. H., Papaefthymion, G. C., Yen, C. S., Groves, J. L., and Wu, C. S. (1974a). *Biochem. Biophys. Res. Commun.* **60,** 1295–1301.
Huynh, B. H., Papaefthymion, G. C., Yen, C. S., Groves, J. L., and Wu, C. S. (1974b). *J. Chem. Phys.* **61,** 3750–3758.
Huzinaga, S. (1965). *J. Chem. Phys.* **42,** 1293–1302.
Huzinaga, S. (1971). "Approximate Atomic Functions." Tech. Rep. Univ. of Alberta, Canada.
Hyla-Kryspin, I., Bénard, M., Strich, A., and Demuynck, J. (1981). *J. Chem. Phys.* **75,** 3954–3961.
Jameson, G. B., Rodley, G. A., Robinson, W. T., Gagne, R. R., Reed, C. A., and Collman, J. P. (1978a). *Inorg. Chem.* **17,** 850–857.
Jameson, G. B., Robinson, W. T., Collman, J. P., and Sorrell, T. N. (1978b). *Inorg. Chem.* **17,** 858–864.
Jameson, G. B., Molinaro, F. S., Ibers, J. A., Collman, J. P., Brauman, J. I., Rose, E., and Suslick, K. S. (1978c). *J. Am. Chem. Soc.* **100,** 6769–6770.

Jameson, G. B., Molinaro, F. S., Ibers, J. A., Collman, J. P., Brauman, J. I., Rose, E., and Suslick, K. S. (1980). *J. Am. Chem. Soc.* **102,** 3224–3237.
Jones, R. D., Budge, J. R., Ellis, P. E., Jr., Linard, J. E., Summerville, D. A., and Basolo, F. (1979). *J Organomet. Chem.* **181,** 151–158.
Kashiwagi, H., and Obara, S. (1981). *Int. J. Quantum Chem.* **20,** 843–859.
Kashiwagi, H., Takada, T., Obara, S., Miyoshi, E., and Ohno, K. (1978). *Int. J. Quantum Chem.* **14,** 13–27.
Kent, T., Spartalian, K., Lang, G., and Yonetani, T. (1977). *Biochim. Biophys. Acta* **490,** 331–340.
Kent, T., Spartalian, K., and Lang, G. (1979). *J. Chem. Phys.* **71,** 4899–4908.
Khandelwal, S. C., and Roebber, J. L. (1975). *Chem. Phys. Lett.* **34,** 355–359.
Kirchner, R. F., and Loew, G. H. (1977). *J. Am. Chem. Soc.* **99,** 4639–4647.
Kirner, J. F., Reed, C. A., and Scheidt, W. R. (1977). *J. Am. Chem. Soc.* **99,** 1093–1101.
Kitagawa, T., and Teraoka, J. (1979). *Chem. Phys. Lett.* **63,** 443–446.
Kitagawa, S., Morishima, I., Yonezawa, T., and Sato, N. (1979). *Inorg. Chem.* **18,** 1345–1349.
Kobayashi, H., and Yanagawa, Y. (1972). *Bull. Chem. Soc. Jpn.* **45,** 450–456.
Koster, A. S. (1975). *J. Chem. Phys.* **63,** 3284–3286.
Lang, G. (1970). *Q. Rev. Biophys.* **3,** 1–60.
Lang, G., Spartalian, K., Reed, C. A., and Collman, J. P. (1978). *J. Chem. Phys.* **69,** 5424–5427.
Latour, J. M., Marchon, J. C., and Nakajima, M. (1979). *J. Am. Chem. Soc.* **101,** 3974–3976.
Lin, W. C. (1976). *Inorg. Chem.* **15,** 1114–1118.
Lever, A. B. P., Wilshire, J. P., and Quan, S. K. (1979). *J. Am. Chem. Soc.* **101,** 3668–3669.
Lever, A. B. P., Wilshire, J. P., and Quan, S. K. (1981). *Inorg. Chem.* **20,** 761–768.
Loew, G. H., and Kirchner, R. F. (1978). *Biophys. J.* **22,** 179–189.
Madura, P., and Scheidt, W. R. (1976). *Inorg. Chem.* **15,** 3182–3184.
Maeda, Y., Harami, T., Trautwein, A., and Gonser, U. (1976). *Z. Naturforsch.* **31B,** 487–490.
Maggiora, G. M. (1973). *J. Am. Chem. Soc.* **95,** 6555–6559.
Meyer, E. F., Jr. (1972). *Acta Crystallogr. Sect. B* **28,** 2162–2167.
Mispelter, J., Momenteau, M., and Lhoste, J. M. (1977). *Mol. Phys.* **33,** 1715–1728.
Mispelter, J., Momenteau, M., and Lhoste, J. M. (1978). *Chem. Phys. Lett.* **57,** 405–409.
Mispelter, J., Momenteau, M., and Lhoste, J. M. (1980). *J. Chem. Phys.* **72,** 1003–1012.
Moxon, N. T., Fielding, P. E., and Gregson, A. K. (1981). *J.C.S. Chem. Commun.* 98–99.
Muralidharan, S., and Hayes, R. G. (1978). *Chem. Phys. Lett.* **57,** 630–632.
Nakato, Y., Abe, K., and Tsubomura, H. (1976). *Chem. Phys. Lett.* **39,** 358–360.
Neumann, D. B., Basch, H., Kornegay, R. L., Snyder, L. C., Moskowitz, J. W., Hornback, C., and Liebmann, S. P. ( ). "Polyatom (Version 2)," Program 199. Quantum Chemistry Program Exchange, Indiana University, Bloomington, Indiana.
Norwell, J. C., Nunes, A. C., and Schoenborn, B. P. (1975). *Science* **190,** 568–570.
Olafson, B. D., and Goddard, W. A. (1977). *Proc. Natl. Acad. Sci. U.S.A.* **74,** 1315–1319.
Ohno, K. (1979). *In* "Horizons of Quantum Chemistry" (K. Fukui and B. Pullman, eds.), pp. 245–266. Reidel, Dordrecht.
Padlan, E. A., and Love, W. E. (1974). *J. Biol. Chem.* **249,** 4067–4078.
Pauling, L. (1949). "Hemoglobin," p. 57. Butterworths, London.
Pauling, L. (1977). *Proc. Natl. Acad. Sci. U.S.A.* **74,** 2612–2613.
Pauling, L., and Coryell, C. D. (1936). *Proc. Natl. Acad. Sci. U.S.A.* **22,** 210–216.
Peng, S. M., and Ibers, J. A. (1976). *J. Am. Chem. Soc.* **98,** 8032–8036.
Perutz, M. F. (1970). *Nature (London)* **228,** 734–739.

Perutz, M. F. (1972). *Nature (London)* **237,** 495–499.
Perutz, M. F. (1976). *Br. Med. Bull.* **32,** 195–208.
Perutz, M. F. (1978). *Sci. Am.* **239**(6), 68–86.
Petsko, G. A., Rose, D., Tsernoghon, D., Ikeda-Saito, M., and Yonetani, T. (1981). *J. Mol. Biol.*, in press. (Quoted in Jameson *et al.*, 1980.)
Phillips, S. E. V. (1978). *Nature (London)* **273,** 247–248.
Pitzer, R. M. (1973). *J. Chem. Phys.* **59,** 3308–3312.
Rees, B. (1976). *Acta Crystallogr. Sect. A* **32,** 483–488.
Rohmer, M.-M., Barry, M., Dedieu, A., and Veillard, A. (1977). *Int. J. Quantum Chem., Quant. Biol. Symp.* **4,** 337–342.
Roos, B., and Siegbahn, P. (1970). *Theor. Chim. Acta* **17,** 209–215.
Roos, B., Vinot, G., and Veillard, A. (1971). *Theor. Chim. Acta* **20,** 1–11.
Saunders, V. R., and Hillier, I. H. (1973). *Int. J. Quantum. Chem.* **7,** 699–705.
Spangler, D., Maggiora, G. M., Shipman, L. L., and Christoffersen, R. E. (1977). *J. Am. Chem. Soc.* **99,** 7478–7489.
Spiro, T. G., and Burke, J. M. (1976). *J. Am. Chem. Soc.* **98,** 5482–5489.
Stevens, E. D. (1981). *J. Am. Chem. Soc.* **103,** 5087–5095.
Strich, A., and Veillard, A. (1981). *Theor. Chim. Acta,* **60,** 373–383; **61,** 402.
Taketa, H., Huzinaga, S., and O-Ohata, K. (1966). *J. Phys. Soc. Jpn.* **21,** 2313–2324.
Trautwein, A., Zimmermann, R., and Harris, F. E. (1975). *Theor. Chim. Acta* **37,** 89–104.
Veillard, A. (1975). *In* "Computational Techniques in Quantum Chemistry and Molecular Physics" (G. H. F. Diercksen, B. T. Sutcliffe, and A. Veillard, eds.), pp. 201–250. Reidel, Dordrecht.
Veillard, A., and Demuynck, J. (1977). *In* "Modern Theoretical Chemistry. Applications of Electronic Structure Theory" (H. F. Schaefer, ed.), pp. 187–222. Plenum, New-York.
Veillard, A., and Strich, A. (1981). Unpublished results.
Veillard, A., Dedieu, A., and Rohmer, M. -M. (1980). *In* "Horizons of Quantum Chemistry" (K. Fukui and B. Pullman, eds.), pp. 197–225. Reidel, Dordrecht.
Walker, F. A. (1970). *J. Am. Chem. Soc.* **92,** 4235–4244.
Wayland, B. B., and Abd-Elmageed, M. E. (1974). *J. Am. Chem. Soc.* **96,** 4809–4814.
Weber, E., Steigemann, W., Jones, T. A., and Huber, R. (1978). *J. Mol. Biol.* **120,** 327–336.
Weschler, C. J., Hoffman, B. M., and Basolo, F. (1975). *J. Am. Chem. Soc.* **97,** 5278–5280.
Whitman, D. R., and Hornback, C. J. (1969). *J. Chem. Phys.* **51,** 398–402.
Yonetani, T., Yamamoto, H., and Iizuka, T. (1974). *J. Biol. Chem.* **249,** 2168–2174.

Radiation–Molecule Interactions in Chemical Physics

D. P. CRAIG
Research School of Chemistry
The Australian National University
Canberra, Australia

and

T. THIRUNAMACHANDRAN
Department of Chemistry
University College London
London, England

ADVANCES IN QUANTUM CHEMISTRY, VOLUME 16

ISBN 0-12-034816-0

I. Introduction

The development of quantum chemistry beyond its former principal area of molecular structure and properties toward time-dependent processes, kinetics, molecular dynamics, intermolecular forces, and interaction with radiation has renewed interest in methods for dealing with time dependence generally. The use of high-intensity coherent sources has placed new demands on methods for dealing with radiation effects, including nonlinear processes such as two-photon absorption. There is also a range of problems in the study of intermolecular forces which have needed new theoretical approaches.

For the most part calculations of the interaction of molecules and light have been made with the so-called semiclassical method. The quantum properties of the molecule are properly allowed for, while the radiation is treated classically: the Maxwell field, with no quantum conditions imposed, is taken to be an external driving field that is not affected by the system it acts upon. Its effect on the system is treated by perturbation theory. On the other hand, the problem of intermolecular forces is usually treated with no explicit reference at all to fields, although from a physical point of view the electromagnetic field is the vehicle carrying the interaction, and its recognition in the theory gives a better insight. That is even more so in problems where both external and internal fields act, as in circular dichroism induced in one molecule by its coupling to another. In a range of such problems there is the need to include the effects of electromagnetic retardation, which are important at large separations.

We describe here the present status of the application of quantum electrodynamics to such problems, which it unifies from the theoretical point of view. In some cases quantum electrodynamics and semiclassical theory give the same results. In others, such as spontaneous emission, quantum electrodynamics gives the correct result where the semiclassical method fails. In all cases quantum electrodynamics provides a better physical picture and offers a convenient computational technique, aided by a diagrammatic procedure for selecting and evaluating the matrix elements. In dealing with molecule–radiation interactions, quantum electrodynamics is the most successful theory presently known. The quantitative agreements are impressive; for example, the value calculated for the Lamb shift for hydrogen differs from experiment by three parts in 10^5. In this article we give only an outline of the basic theory and representative applications. More detailed accounts of the methods of nonrelativistic quantum electrodynamics are given by Power (1964) and Healy (1982).

The essential step in quantum electrodynamics is to apply quantum

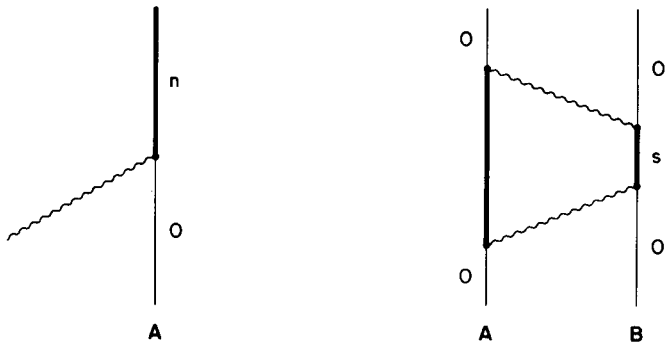

Fig. 1. Time-ordered graphs for real and virtual processes.

conditions to the variables of the radiation field. The particles associated with the quantized field are photons, and the processes of interest are conveniently described as interactions between photons and atoms or molecules. There is a broad division into *real* and *virtual* processes. In real processes one or more photons are lost or gained by the field, as in emission or absorption. In virtual processes photons participate in the formation and destruction of intermediate states, the final state of the electromagnetic field being the same as, or changed from the initial state. The distinction is illustrated in the graphs of Fig. 1. The left-hand graph shows a real process of absorption in which the ground state 0 of a molecule A is excited to state n by absorption of a photon of frequency ω, the photon energy being equal to the energy gap between the states, $\hbar\omega = E_n - E_0$. The right-hand graph is representative of a number of graphs for the dispersion interaction between molecules A and B. Virtual emission of a photon from A leaves it in state r; absorption by B raises B to s. The second virtual process returns both molecules to their ground states. The photons have frequencies unrelated to the molecular excitation energies: energies are conserved overall, but not for the virtual processes, which are conceived as occupying a time so short that the energies of the virtual states are within limits allowed by the uncertainty principle.

Use of quantized fields and photons allows the radiation and the molecules to be treated as a single coupled dynamical system, each part affecting the other. Energy is conserved overall. Moreover, use of the second quantized representation, which does not require conservation in the total number of particles, but allows the number of photons to change, leads to a convenient formalism for (multiple) events of absorption and emission, including the use of the diagrammatic technique already mentioned.

II. The Quantized Radiation Field and Coupling with Molecules

A. Maxwell's Equations

Large-scale electrodynamic phenomena involving unquantized particle motions in electric and magnetic fields are in all known cases described by Maxwell's equations in the four macroscopic field vectors **E**, **B**, **D**, and **H**, together with the Lorentz force

$$\nabla \cdot \mathbf{D} = \rho^{\text{true}} \tag{1}$$

$$\nabla \cdot \mathbf{B} = 0 \tag{2}$$

$$\nabla \times \mathbf{E} = -\partial \mathbf{B}/\partial t \tag{3}$$

$$\nabla \times \mathbf{H} = \partial \mathbf{D}/\partial t + \mathbf{J}^{\text{true}} \tag{4}$$

Maxwell's equations relate the fundamental electric and magnetic field strengths **E** and **B** and the auxiliary fields **D** and **H** with the charge density of free (true) charges ρ^{true} and the current density $\mathbf{J}^{\text{true}}$. In older references **B** is sometimes called the magnetic induction, **H** the magnetic field, and **D** the electric displacement.

The motions of the charged particles in the electromagnetic field are given by the solutions of Newton's equations of motion with an added force term

$$\mathbf{F} = q(\mathbf{E} + \mathbf{v} \times \mathbf{B}) \tag{5}$$

known as the Lorentz force; **v** is the velocity of the particle with charge q. In a region that is charge free, the coupled equations (6) and (7),

$$\nabla \times \mathbf{E} = -\partial \mathbf{B}/\partial t \tag{6}$$

$$\nabla \times \mathbf{B} = (1/c^2)\, \partial \mathbf{E}/\partial t \tag{7}$$

determine the divergence-free field vectors **E** and **B**.

The macroscopic Maxwell's equations apply on the large scale, in which the particle character of elementary charges is smoothed out. Thus in

$$\mathbf{D}(\mathbf{r}) = \epsilon_0 \mathbf{E}(\mathbf{r}) + \mathbf{P}(\mathbf{r}) \tag{8}$$

where the polarization **P** is a continuous function of position; ϵ_0 is the vacuum permittivity. The electrical structure of matter on the microscopic scale is too fine to be dealt with in this averaged way. The microscopic field equations (Maxwell–Lorentz equations) are used instead. The idea of a continuous distribution of charges is abandoned in favor of individual treatment of each charge. A function representing a point-

charge distribution must be zero everywhere except at the position of a charge, and there it is infinite. With the use of the Dirac delta function the density function is for a unit charge,

$$\rho(\mathbf{r}) = \delta(\mathbf{r} - \mathbf{q}) \tag{9}$$

$$\delta(\mathbf{r} - \mathbf{q}) = 0, \qquad \mathbf{r} \neq \mathbf{q} \tag{10}$$

$$\int \delta(\mathbf{r} - \mathbf{q})\, d^3\mathbf{r} = 1 \tag{11}$$

where $\mathbf{q}$ is the position of the charge. For a collection of charges the definitions of charge and current densities are given in Eqs. (12) and (13),

$$\rho(\mathbf{r}) = \sum_i e_i\, \delta(\mathbf{r} - \mathbf{q}_i) \tag{12}$$

$$\mathbf{j}(\mathbf{r}) = \sum_i e_i \dot{\mathbf{q}}_i\, \delta(\mathbf{r} - \mathbf{q}_i) \tag{13}$$

where $\dot{\mathbf{q}}_i$ is the velocity.

We now write field equations for the microscopic field in terms of lower case vectors $\mathbf{e}$, $\mathbf{b}$, $\mathbf{j}$, and ρ.

$$\nabla \cdot \mathbf{e} = \rho/\epsilon_0 \tag{14}$$

$$\nabla \cdot \mathbf{b} = 0 \tag{15}$$

$$\nabla \times \mathbf{e} = -\partial \mathbf{b}/\partial t \tag{16}$$

$$\nabla \times \mathbf{b} = (1/c^2)\, \partial \mathbf{e}/\partial t + (1/\epsilon_0 c^2)\mathbf{j} \tag{17}$$

Inasmuch as each charge is considered individually, with no "background," only the free-field vectors appear, though in applications to be referred to later the microscopic auxiliary fields $\mathbf{d}$ and $\mathbf{h}$ are used. The quantity μ_0, the vacuum magnetic permeability, is suppressed throughout the present article in favor of ϵ_0 and c through $\epsilon_0\mu_0 = 1/c^2$.

B. Electromagnetic Potentials

The procedure for applying quantum conditions to the variables of the electromagnetic field is through the vector potential $\mathbf{a}$, related to the magnetic field $\mathbf{b}$ by

$$\mathbf{b} = \nabla \times \mathbf{a} \tag{18}$$

and, using Eq. (16)

$$\nabla \times (\mathbf{e} + \partial \mathbf{a}/\partial t) = 0 \tag{19}$$

so that

$$\mathbf{e} + \partial \mathbf{a}/\partial t = -\nabla \phi \tag{20}$$

where ϕ is the scalar potential, here defined for convenience with a negative sign; $\mathbf{a}$ and ϕ together define the field variables $\mathbf{e}$ and $\mathbf{b}$. The definition is not unique, since the addition to $\mathbf{a}$ of the gradient of any scalar function $\chi(r, t)$ and the subtraction from ϕ of $\partial\chi/\partial t$ leave the field vectors invariant. This gauge invariance enables a choice of $\mathbf{a}$ to be made adapted to particular problems.

The gauge universally used in atomic and molecular problems is the Coulomb gauge, defined by

$$\nabla \cdot \mathbf{a} = 0 \tag{21}$$

in which the fields are separated into longitudinal and transverse, the former being described by only the scalar potential and the latter by only the vector potential. Equation (21) shows that the $\mathbf{a}$ field is pure transverse, so that $\mathbf{e} = \mathbf{e}^{\perp} = -\partial\mathbf{a}/\partial t$. The $\mathbf{b}$ field is transverse in all gauges. The scalar potential, describing the longitudinal field is (in Coulomb gauge) the Coulombic potential. We thus have the convenient framework that the atomic and molecular Hamiltonians are given as usual with Schrödinger operators for particle coordinates and their canonical momenta as is familiar in quantum chemistry. The Coulomb fields can be treated classically and only the radiation field is quantized and is purely transverse. The particles associated with the quantized field are transverse photons. In the Coulomb gauge we can usefully begin with two limiting cases: one is the free radiation field without sources, and the other is the system of charges only, without the radiation field, as in elementary quantum mechanics. We treat the latter as a solved problem, and discuss the free field and then the interaction of the free field with atomic and molecular systems.

C. The Free Field

In Coulomb gauge, $\nabla \cdot \mathbf{a} = 0$, the scalar potential is a constant which may be taken to be zero. Then from Eqs. (17) and (20) we have

$$\nabla \times (\nabla \times \mathbf{a}) = -c^{-2}(\partial^2\mathbf{a}/\partial t^2) \tag{22}$$

and, since $\nabla \cdot \mathbf{a} = 0$,

$$\nabla^2\mathbf{a} - c^{-2}(\partial^2\mathbf{a}/\partial t^2) = 0 \tag{23}$$

Equation (23) is the equation of motion for $\mathbf{a}$, and it is readily shown that equations of motion identical in form hold for $\mathbf{e}$ and $\mathbf{b}$. A class of solutions to the analog of Eq. (23) for $\mathbf{e}$,

$$\nabla^2\mathbf{e} - c^{-2}(\partial^2\mathbf{e}/\partial t^2) = 0 \tag{24}$$

is the plane wave

$$\mathbf{e} = \mathbf{e}_0 e^{i(\mathbf{k}\cdot\mathbf{r}-\omega t)} \tag{25}$$

where $\mathbf{k}$ is the wave vector and $k/2\pi$ the wave number or number of wavelengths per unit distance along the direction of propagation $\hat{\mathbf{k}}$; $k = \omega/c$ where ω is the angular frequency. The directions of the electric and magnetic fields $\mathbf{e}_0$, $\mathbf{b}_0$ and that of the wave vector $\mathbf{k}$ form a right-handed triad.

Quantization of the radiation field is effected through the vector potential $\mathbf{a}$, for which the wave vector in Eq. (26)

$$\mathbf{a} = \mathbf{a}_0 e^{i(\mathbf{k}\cdot\mathbf{r}-\omega t)} \tag{26}$$

may assume any of an infinite range of values. To get a convenient normalization in the quantum theory it is convenient to normalize by containing the radiation field in a box of arbitrary finite volume V, usually chosen to be a cube. The vector potential is required to obey periodic boundary conditions, taking the same values at opposite sides of the cube. The solutions are Jean's normal modes and are discrete, infinite, and countable.

The condition that the solutions be equal at opposite ends of the cube of volume $V = L^3$ is met if the components k_x, k_y, and k_z are limited to the values in Eq. (27)

$$k_i = (2\pi/L)n_i, \qquad i = x, y, z \tag{27}$$

where the n_i terms are integers including zero. Each solution is described as a field mode, and the complete set of modes is a basis for a Fourier expansion (mode expansion) for the vector potential at any point inside the box. Thus for the vector potential

$$\mathbf{a}(\mathbf{r}, t) = \sum_{\mathbf{k}} \{\mathbf{a}_{\mathbf{k}}(t)e^{i\mathbf{k}\cdot\mathbf{r}} + \bar{\mathbf{a}}_{\mathbf{k}}(t)e^{-i\mathbf{k}\cdot\mathbf{r}}\} \tag{28}$$

where $\mathbf{a}_{\mathbf{k}}(t)$ are amplitude coefficients, the bar denoting the complex conjugate. The mode amplitudes are transverse to the direction of propagation and can be specified in terms of components along mutually orthogonal directions specified by unit vectors $\mathbf{e}^{(\lambda)}(\mathbf{k})$, $\lambda = 1, 2$; $\mathbf{e}^{(1)}$ and $\mathbf{e}^{(2)}$ can be real or complex, the latter choice being adapted to problems involving circularly polarized light. Equation may be written

$$\mathbf{a}(\mathbf{r}, t) = \sum_{\mathbf{k},\lambda} \{\mathbf{e}^{(\lambda)}(\mathbf{k})a_{\mathbf{k}}^{(\lambda)}e^{i\mathbf{k}\cdot\mathbf{r}} + \bar{\mathbf{e}}^{(\lambda)}(\mathbf{k})\bar{a}_{\mathbf{k}}^{(\lambda)}e^{-i\mathbf{k}\cdot\mathbf{r}}\} \tag{29}$$

There are similar mode expansions for $\mathbf{e}$ and $\mathbf{b}$.

D. Quantization of the Free Field

As for particles, quantization is effected by expressing the Hamiltonian in canonically conjugate variables and promoting the variables to quantum

operators. The starting point is the Lagrangian density $\mathscr{L}$, the Lagrangian being this density integrated over the system space,

$$L = \int \mathscr{L}\, d^3\mathbf{r} \tag{30}$$

The property required of the Lagrangian is that it should lead to the correct equations of motion, which are here Maxwell's equations. A suitable Lagrangian density is given in Eq. (31)

$$\mathscr{L} = \tfrac{1}{2}\epsilon_0\{\dot{\mathbf{a}}^2 - (c\nabla \times \mathbf{a})^2\} \tag{31}$$

$$= \tfrac{1}{2}\epsilon_0(\mathbf{e}^2 - c^2\mathbf{b}^2) \tag{32}$$

The momentum density canonically conjugate to $\mathbf{a}$ is given by Eq. (33)

$$\boldsymbol{\Pi}(\mathbf{r}) = \partial\mathscr{L}/\partial\dot{\mathbf{a}} = \epsilon_0\dot{\mathbf{a}} \tag{33}$$

and therefore the Hamiltonian density

$$\mathscr{H} = \boldsymbol{\Pi}\cdot\dot{\mathbf{a}} - \mathscr{L}$$

$$= \tfrac{1}{2}\epsilon_0\{(\boldsymbol{\Pi}/\epsilon_0)^2 + (c\nabla \times \mathbf{a})^2\} \tag{34}$$

$$= \tfrac{1}{2}\epsilon_0(\mathbf{e}^2 + c^2\mathbf{b}^2) \tag{35}$$

also,

$$H = \int \mathscr{H}\, d^3\mathbf{r} \tag{36}$$

By expressing $\mathscr{H}$ in terms of the mode expansion (29) for $\mathbf{a}$, and the analogous expansion for $\boldsymbol{\Pi}$, we find

$$H = 2V\epsilon_0 c^2 \sum_{\mathbf{k},\lambda} k^2 a_{\mathbf{k}}^{(\lambda)}\bar{a}_{\mathbf{k}}^{(\lambda)} \tag{37}$$

By introducing new variables $q_{\mathbf{k}}^{(\lambda)}, p_{\mathbf{k}}^{(\lambda)}$,

$$q_{\mathbf{k}}^{(\lambda)} = (V\epsilon_0)^{1/2}\{a_{\mathbf{k}}^{(\lambda)} + \bar{a}_{\mathbf{k}}^{(\lambda)}\}, \qquad p_{\mathbf{k}}^{(\lambda)} = -ick(V\epsilon_0)^{1/2}\{a_{\mathbf{k}}^{(\lambda)} - \bar{a}_{\mathbf{k}}^{(\lambda)}\} \tag{38}$$

for which $p_{\mathbf{k}}^{(\lambda)} = \dot{q}_{\mathbf{k}}^{(\lambda)}$, we find

$$H = \sum_{\mathbf{k},\lambda} \tfrac{1}{2}\{p_{\mathbf{k}}^{(\lambda)2} + \omega^2 q_{\mathbf{k}}^{(\lambda)2}\} \tag{39}$$

The Hamiltonian for the electromagnetic field is thus decomposed into a sum of harmonic oscillator Hamiltonians, one for each $(\mathbf{k}, \lambda)$ mode, with $\omega = c|\mathbf{k}|$. The electromagnetic field may therefore be quantized in the same way as a system of oscillators. Promoting the variables $q_{\mathbf{k}}^{(\lambda)}$ and $p_{\mathbf{k}}^{(\lambda)}$ to operators, and using the second-quantized representation, we have

$$H = \sum_{\mathbf{k},\lambda} \{a^{\dagger(\lambda)}(\mathbf{k})a^{(\lambda)}(\mathbf{k}) + \tfrac{1}{2}\}\hbar ck \tag{40}$$

where $a^{\dagger(\lambda)}(\mathbf{k})$ and $a^{(\lambda)}$ are creation and annihilation operators for the mode $(\mathbf{k}, \lambda)$ with commutation rules

$$\begin{aligned} [a^{(\lambda)}(\mathbf{k}), \quad a^{\dagger(\lambda')}(\mathbf{k}')] &= \delta_{\mathbf{k}\mathbf{k}'}\,\delta_{\lambda\lambda'} \\ [a^{(\lambda)}(\mathbf{k}), \quad a^{(\lambda')}(\mathbf{k}')] &= [a^{\dagger(\lambda)}(\mathbf{k}), \quad a^{\dagger(\lambda')}(\mathbf{k}')] = 0 \end{aligned} \tag{41}$$

The Bose particles introduced through the commutation properties of Eq. (41) are the photons.

The state of the electromagnetic field is described by listing the occupation numbers $n_{\mathbf{k}}^{(\lambda)} = a^{\dagger(\lambda)}(\mathbf{k})a^{(\lambda)}(\mathbf{k})$ of all occupied modes,

$$|n_1(\mathbf{k}_1, \lambda_1), \quad n_2(\mathbf{k}_2, \lambda_2), \quad \ldots \quad \rangle \tag{42}$$

The kets of Eq. (42) are the number states.

The classical field variables **e**, **b**, **a**, and **Π** now appear as operators,

$$\mathbf{e}(\mathbf{r}) = i \sum_{k,\lambda} \left(\frac{\hbar ck}{2\epsilon_0 V}\right)^{1/2} \{\mathbf{e}^{(\lambda)}(\mathbf{k})a^{(\lambda)}(\mathbf{k})e^{i\mathbf{k}\cdot\mathbf{r}} - \bar{\mathbf{e}}^{(\lambda)}(\mathbf{k})a^{\dagger(\lambda)}(\mathbf{k})e^{-i\mathbf{k}\cdot\mathbf{r}}\} \tag{43}$$

$$\begin{aligned} \mathbf{b}(\mathbf{r}) = i \sum_{k,\lambda} \left(\frac{\hbar k}{2\epsilon_0 cV}\right)^{1/2} &\{(\hat{\mathbf{k}} \times \mathbf{e}^{(\lambda)}(\mathbf{k}))\mathbf{a}^{(\lambda)}(\mathbf{k})e^{i\mathbf{k}\cdot\mathbf{r}} \\ &-(\hat{\mathbf{k}} \times \bar{\mathbf{e}}^{(\lambda)}(\mathbf{k}))a^{\dagger(\lambda)}(\mathbf{k})e^{-i\mathbf{k}\cdot\mathbf{r}}\} \end{aligned} \tag{44}$$

$$\mathbf{a}(\mathbf{r}) = \sum_{k,\lambda} \left(\frac{\hbar}{2\epsilon_0 ckV}\right)^{1/2} \{\mathbf{e}^{(\lambda)}(\mathbf{k})a^{(\lambda)}(\mathbf{k})e^{i\mathbf{k}\cdot\mathbf{r}} + \bar{\mathbf{e}}^{(\lambda)}(\mathbf{k})a^{\dagger(\lambda)}(\mathbf{k})e^{-i\mathbf{k}\cdot\mathbf{r}}\} \tag{45}$$

$$\mathbf{\Pi}(\mathbf{r}) = -i \sum_{k,\lambda} \left(\frac{\hbar ck\epsilon_0}{2V}\right)^{1/2} \{\mathbf{e}^{(\lambda)}(\mathbf{k})a^{(\lambda)}(\mathbf{k})e^{i\mathbf{k}\cdot\mathbf{r}} - \bar{\mathbf{e}}^{(\lambda)}(\mathbf{k})a^{\dagger(\lambda)}(\mathbf{k})e^{-i\mathbf{k}\cdot\mathbf{r}}\} \tag{46}$$

Comparing these expressions with the classical mode expansion one sees that the classical amplitudes $a_{\mathbf{k}}$ and $\bar{a}_{\mathbf{k}}$ have been replaced by the operators $a^{(\lambda)}(\mathbf{k})$ and $a^{\dagger(\lambda)}(\mathbf{k})$; V is the volume of the quantization box, and the normalization is chosen so that the energy of the state of occupation number $n_{\mathbf{k}}^{(\lambda)}$ is $n_{\mathbf{k}}^{(\lambda)}\hbar ck$.

E. Uncertainty Relations for the Radiation Field

One of the consequences of quantization of the radiation field is that the operators for the fields and the Hamiltonian do not commute among themselves. For example,

$$[e_i(\mathbf{r}), b_j(\mathbf{r}')] = (i\hbar/\epsilon_0)\epsilon_{ijk}\,\nabla'_k\,\delta(\mathbf{r} - \mathbf{r}') \tag{47}$$

$$[\mathbf{e}(\mathbf{r}), H] = i\hbar c^2(\nabla \times \mathbf{b}) \tag{48}$$

The noncommutation of operators places restrictions on simultaneous measurements of field strengths and energy. In quantum theory, if A and B are two noncommuting operators representing observables, the uncertainty relation is (see, for example, Merzbacher, 1970)

$$\Delta A\, \Delta B \geq \tfrac{1}{2}|\langle C\rangle| \tag{49}$$

where C is the commutator of A and B; the angular brackets denote the expectation value. There is, of course, no counterpart in classical theory where the observables can all be measured as accurately as desired. From Eq. (48) it follows that for number states, which are eigenstates of the Hamiltonian, the electric field does not have a precise value but only an average value about which it fluctuates. The fluctuations exist in the vacuum state and they can perturb electron motions; these perturbations manifest themselves in, for example, spontaneous emission of an excited atom, Lamb's shift, and intermolecular coupling.

In classical theory an important quantity characterizing a wave is the phase ϕ. The corresponding quantum mechanical operator for a single mode is defined by Eq. (50) (Susskind and Glogower, 1964; Carruthers and Nieto, 1968):

$$a = (n + 1)^{1/2} e^{i\phi}, \qquad a^{\dagger} = e^{-i\phi}(n + 1)^{1/2} \tag{50}$$

where n is the number operator $a^{\dagger}a$. The operator ϕ is not Hermitian and $e^{i\phi}$ is not unitary, however $\cos\phi$ and $\sin\phi$ are Hermitian and may be used together as phase operators. It is easily shown that $\cos\phi$ and $\sin\phi$ do not commute with the number operator n:

$$[n, \cos\phi] = -i \sin\phi, \qquad [n, \sin\phi] = i \cos\phi \tag{51}$$

The uncertainty relations follow from Eq. (49):

$$\Delta n\, \Delta \cos\phi \geq \tfrac{1}{2}|\langle \sin\phi\rangle|, \qquad \Delta n\, \Delta \sin\phi \geq \tfrac{1}{2}|\langle \cos\phi\rangle| \tag{52}$$

For number states,

$$\Delta \cos\phi = \Delta \sin\phi = 1/\sqrt{2}, \qquad n \neq 0 \tag{53}$$

implying that the phase angle ϕ can take random values between 0 and 2π. Thus, even in the large n limit number states do not tend to the classical limit. The proper quantum mechanical states tending to the classical limit for large expectation values of n are the coherent states (Glauber, 1963). They are eigenstates of the annihilation operator a and given by

$$|\alpha\rangle = \exp(-\tfrac{1}{2}|\alpha|^2) \sum_n \frac{\alpha^n}{(n!)^{1/2}} |n\rangle \tag{54}$$

where α is a complex number. They have the properties $\langle n \rangle = |\alpha|^2$ and $\Delta n = |\alpha|$ and are not eigenstates of n. For large photon populations, i.e., large mean values of n, we have $|\alpha|^2 \gg 1$ and

$$\Delta \cos \phi \approx \sin \theta/2|\alpha|, \qquad \Delta \sin \phi \approx \cos \theta/2|\alpha| \tag{55}$$

where θ is defined by $\alpha = |\alpha|e^{i\theta}$ so that

$$\Delta n \, \Delta \cos \phi \approx \tfrac{1}{2} \sin \theta, \qquad \Delta n \, \Delta \sin \phi \approx \tfrac{1}{2} \cos \theta \tag{56}$$

Thus the coherent states are essentially minimum uncertainty states for large n.

The question of phase is important in interpreting scattering experiments. Although the number and phase variables cannot take precise values simultaneously, it is possible to have a definite phase *difference* for a wave scattered by two molecules for single photons or any definite number.

F. Coupling of Electromagnetic Field to Molecules

The Lagrangian for the complete system must be chosen to satisfy the condition that it leads to the correct equations of motion. These are here Maxwell's equations, with sources, for the field, and Newton's equations with the Lorentz force as an added term for the particles.

A Lagrangian obeying this condition may be written as a sum of terms for the particles of the atoms or molecules separately, the radiation field, and a coupling term between them,

$$L = L_{\text{part}} + L_{\text{rad}} + L_{\text{int}} \tag{57}$$

where

$$L_{\text{part}} = \frac{1}{2} \sum_{\alpha} m_\alpha \dot{\mathbf{q}}_\alpha^2 - V(\mathbf{q}) \tag{58}$$

$$L_{\text{rad}} = \tfrac{1}{2} \epsilon_0 \int \{\dot{\mathbf{a}}^2 - (c\nabla \times \mathbf{a})^2\} \, d^3\mathbf{r} \tag{59}$$

$$L_{\text{int}} = \int \mathbf{j}^{\perp}(\mathbf{r}) \cdot \mathbf{a}(\mathbf{r}) \, d^3\mathbf{r} \tag{60}$$

where α runs over the particles of the molecule and $\mathbf{j}^{\perp}$, the transverse current can be related to the total current $\mathbf{j}(\mathbf{r})$,

$$\mathbf{j}(\mathbf{r}) = \sum_{\alpha} e_\alpha \dot{\mathbf{q}}_\alpha \, \delta(\mathbf{r} - \mathbf{q}_\alpha) \tag{61}$$

through the transverse delta function,

$$j_i^{\perp}(\mathbf{r}) = \int j_j(\mathbf{r}') \, \delta_{ij}^{\perp}(\mathbf{r} - \mathbf{r}') \, d^3\mathbf{r}' \tag{62}$$

The passage to the Hamiltonian is effected with the help of the momenta conjugate to the displacement variables $\mathbf{q}_\alpha$ and $\mathbf{a}$ for particles and field,

$$\mathbf{p}_\alpha = \partial L/\partial \dot{\mathbf{q}}_\alpha = m_\alpha \dot{\mathbf{q}}_\alpha + e_\alpha \mathbf{a}(\mathbf{q}_\alpha) \tag{63}$$

$$\mathbf{\Pi}(\mathbf{r}) = \partial \mathscr{L}/\partial \dot{\mathbf{a}} = \epsilon_0 \dot{\mathbf{a}} = -\epsilon_0 \mathbf{e}^\perp \tag{64}$$

Then,

$$\begin{aligned} H &= \sum_\alpha \mathbf{p}_\alpha \cdot \dot{\mathbf{q}}_\alpha + \int \mathbf{\Pi} \cdot \dot{\mathbf{a}}\, d^3\mathbf{r} - L \\ &= \sum_\alpha (2m_\alpha)^{-1}(\mathbf{p}_\alpha - e_\alpha \mathbf{a}(\mathbf{q}_\alpha))^2 + V(\mathbf{q}) \\ &\quad + \frac{1}{2}\int \left\{ \frac{\mathbf{\Pi}^2}{\epsilon_0} + \epsilon_0 (c\nabla \times \mathbf{a})^2 \right\} d^3\mathbf{r} \end{aligned} \tag{65}$$

It is possible to give a general prescription for introducing the coupling between the particles and the radiation field. We first write down the Hamiltonian assuming that there is no interaction between the particles and the field. The coupling is introduced by the substitution $\mathbf{p}_\alpha \rightarrow \mathbf{p}_\alpha - e_\alpha \mathbf{a}(\mathbf{q}_\alpha)$. This is often referred to as the principle of minimal electromagnetic interactions, or minimal coupling (Gell-Mann, 1956). Taking into account the structure of the matter present by grouping the particles into molecules and treating the nuclei as at fixed positions, we write $\mathbf{p}_\alpha(\zeta)$ and $\mathbf{q}_\alpha(\zeta)$ as momentum and position vectors of the electrons of the molecule ζ. The Hamiltonian now is

$$\begin{aligned} H = \sum_\zeta \left\{ \left(\frac{1}{2m}\right) \sum_\alpha \mathbf{p}_\alpha^2(\zeta) + V(\zeta) \right\} + \frac{1}{2}\int \left\{ \frac{\mathbf{\Pi}^2}{\epsilon_0} + \epsilon_0 (c\nabla \times \mathbf{a})^2 \right\} d^3\mathbf{r} \\ - \frac{e}{m} \sum_\zeta \sum_\alpha \mathbf{p}_\alpha(\zeta) \cdot \mathbf{a}(\mathbf{q}_\alpha(\zeta)) + \frac{e^2}{2m} \sum_\zeta \sum_\alpha \mathbf{a}^2(\mathbf{q}_\alpha(\zeta)) + \sum_{\zeta<\zeta'} V(\zeta, \zeta') \end{aligned} \tag{66}$$

where the potential $V(\mathbf{q})$ has been split into intra- and intermolecular parts,

$$V = \sum_\zeta V(\zeta) + \sum_{\zeta<\zeta'} V(\zeta, \zeta') \tag{67}$$

Thus,

$$H = \sum_\zeta H_{\text{mol}}(\zeta) + H_{\text{rad}} + \sum_\zeta \{H_{\text{int}}^{(1)}(\zeta) + H_{\text{int}}^{(2)}(\zeta)\} + V_{\text{int}} \tag{68}$$

in which the first and second terms stand for the leading terms and V_{int} stands for the final term of Eq. (66), and

$$H_{\text{int}}^{(1)}(\zeta) = -(e/m)\sum_{\zeta,\alpha} \mathbf{p}_\alpha(\zeta) \cdot \mathbf{a}(\mathbf{q}_\alpha(\zeta)) \tag{69}$$

$$H_{\text{int}}^{(2)}(\zeta) = (e^2/2m)\sum_{\zeta\alpha} \mathbf{a}^2(\mathbf{q}_\alpha(\zeta)) \tag{70}$$

Quantization of the Hamiltonian is done according to the usual scheme of promoting dynamical variables to operators. For the operators of the radiation field, the commutation properties are those in Eq. (41), and for the particles the usual

$$[q_{i(\alpha)}(\zeta),\ p_{j(\beta)}(\zeta')] = i\hbar\,\delta_{ij}\,\delta_{\alpha\beta}\,\delta_{\zeta\zeta'} \tag{71}$$

G. The Minimal Coupling and Multipolar Hamiltonians

The minimal coupling Hamiltonian (66) contains molecular interactions of both instantaneous and retarded types; $H_{\text{int}}^{(1)}(\zeta)$ and $H_{\text{int}}^{(2)}(\zeta)$ given in Eqs. (69) and (70) are one-center in character. However, they can give rise to intermolecular interactions by the emission and absorption of virtual photons by different molecular centers. Virtual photon exchanges take place with the speed of light and the interactions arising from them are time delayed, or *retarded*. The other coupling term, V_{int}, is *instantaneous* in that at a given time it depends on the charge distribution at that time.

In problems such as absorption and emission and scattering in dilute systems, the interactions between molecules may be neglected. The process depends on the **a** field within the space of a single molecule, within which retardation is of no significance. This is not the case in calculating the forces between molecules where both the retarded and instantaneous forces must be included. Even in the dipole approximation, to which our discussion is limited, the treatment is then clumsy. It is better to make a canonical transformation of the Hamiltonian to a form such as the multipolar Hamiltonian in which the interaction term H_{int} is entirely retarded, all interactions between molecules being mediated by transverse photons.

The transformation of the minimal-coupling Hamiltonian H_{min} to the multipolar H_{mult} is given by

$$H_{\text{mult}} = e^{-iS} H_{\text{min}} e^{iS} \tag{72}$$

with $S = (i/\hbar)\int \mathbf{p}(\mathbf{r}) \cdot \mathbf{a}(\mathbf{r})\, d^3\mathbf{r}$ as the generator; $\mathbf{p}(\mathbf{r})$ is the electric polarization field. Details of the transformation are given in the original papers by Power and Zienau (1959), Woolley (1971), Babiker *et al.* (1974), Power and Thirunamachandran (1978, 1980), and are not reproduced here. In the electric dipole approximation, $\mathbf{p}(\mathbf{r})$ is

$$\mathbf{p}(\mathbf{r}) = \sum_\zeta \mathbf{p}_\zeta(\mathbf{r}) = \sum_\zeta \boldsymbol{\mu}(\zeta)\ \delta(\mathbf{r} - \mathbf{R}_\zeta) \tag{73}$$

where $\boldsymbol{\mu}(\zeta)$ is the dipole moment operator. The transformed Hamiltonian is found to be

$$H = \sum_{\zeta} \left\{ \frac{1}{2m} \sum_{\alpha} \mathbf{p}_{\alpha}^2(\zeta) + V(\zeta) \right\} + \frac{1}{2} \int \left\{ \frac{\boldsymbol{\Pi}^2}{\epsilon_0} + \epsilon_0 c^2 (\boldsymbol{\nabla} \times \mathbf{a})^2 \right\} d^3\mathbf{r} + \frac{1}{\epsilon_0} \sum_{\zeta} \boldsymbol{\mu}(\zeta) \cdot \boldsymbol{\Pi}(\mathbf{R}_{\zeta}) + \frac{1}{2\epsilon_0} \sum_{\zeta} \int |\mathbf{p}_{\zeta}^{\perp}(\mathbf{r})|^2 \, d^3\mathbf{r} \tag{74}$$

An essential point is that the relationship of the field momentum $\boldsymbol{\Pi}(\mathbf{r})$ to the transverse electric field $\mathbf{e}^{\perp}(\mathbf{r})$ is different for the minimal coupling and multipolar Hamiltonians:

$$\boldsymbol{\Pi}(\mathbf{r}) = -\epsilon_0 \mathbf{e}^{\perp}(\mathbf{r}) \qquad \text{(minimal coupling)} \tag{75}$$

$$\boldsymbol{\Pi}(\mathbf{r}) = -\epsilon_0 \mathbf{e}^{\perp}(\mathbf{r}) - \mathbf{p}^{\perp}(\mathbf{r}) \qquad \text{(multipolar)} \tag{76}$$

In terms of the auxiliary field

$$\mathbf{d}(\mathbf{r}) = \epsilon_0 \mathbf{e}(\mathbf{r}) + \mathbf{p}(\mathbf{r}) \tag{77}$$

Eq. (76) becomes

$$\boldsymbol{\Pi}(\mathbf{r}) = -\mathbf{d}^{\perp}(\mathbf{r}) \qquad \text{(multipolar)} \tag{78}$$

Thus in the multipolar Hamiltonian, the canonical field momentum is the auxiliary field $\mathbf{d}^{\perp}(\mathbf{r})$ (apart from sign) and not $\mathbf{e}^{\perp}(\mathbf{r})$. In terms of $\mathbf{d}^{\perp}(\mathbf{r})$ and $\mathbf{b}(\mathbf{r})$, the multipolar Hamiltonian may be written as

$$H = \sum_{\zeta} \left\{ \frac{1}{2m} \sum_{\alpha} \mathbf{p}_{\alpha}^2(\zeta) + V(\zeta) \right\} + \frac{1}{2} \int \left\{ \frac{\mathbf{d}^{\perp 2}}{\epsilon_0} + c^2 \epsilon_0 \mathbf{b}^2 \right\} d^3\mathbf{r} - \frac{1}{\epsilon_0} \sum_{\zeta} \boldsymbol{\mu}(\zeta) \cdot \mathbf{d}^{\perp}(\mathbf{R}_{\zeta}) + \frac{1}{2\epsilon_0} \sum_{\zeta} \int |\mathbf{p}_{\zeta}^{\perp}(\mathbf{r})|^2 \, d^3\mathbf{r} \tag{79}$$

The final term in Eq. (79) is independent of the radiation field and can be dropped except in self-energy problems such as the Lamb shift. The new Hamiltonian can thus be written

$$H = H_{\text{mol}} + H_{\text{rad}} + H_{\text{int}} \tag{80}$$

where

$$H_{\text{mol}} = \sum_{\zeta} \left\{ \frac{1}{2m} \sum_{\alpha} \mathbf{p}_{\alpha}^2(\zeta) + V(\zeta) \right\} \tag{81}$$

$$H_{\text{rad}} = \frac{1}{2}\int \left\{ \frac{\mathbf{d}^{\perp 2}}{\epsilon_0} + c^2\epsilon_0 \mathbf{b}^2 \right\} d^3\mathbf{r} \tag{82}$$

$$H_{\text{int}} = -\frac{1}{\epsilon_0}\sum_{\zeta} \boldsymbol{\mu}(\zeta)\cdot\mathbf{d}^{\perp}(\mathbf{R}_\zeta) \tag{83}$$

It is recalled that the nuclei are fixed. In this Hamiltonian the electrostatic interactions between molecules have been eliminated. The molecules are coupled to each other only *via* the electromagnetic field.

The Hamiltonian (80) is in the dipole approximation, based on the approximation that the vector potential **a** is uniform over each molecule, its value being taken at the molecular center. When this is relaxed the next terms in the Hamiltonian are those for the coupling of the electric quadrupole and the magnetic dipole moments. The Hamiltonian then includes the new H_{int} given in Eq. (84), in place of the dipole form of Eq. (83),

$$H_{\text{int}} = -\frac{1}{\epsilon_0}\sum_{\zeta} \boldsymbol{\mu}(\zeta)\cdot\mathbf{d}^{\perp}(\mathbf{R}_\zeta) - \frac{1}{\epsilon_0}\sum_{\zeta} Q_{ij}(\zeta)\,\Delta_i\, d_j^{\perp}(\mathbf{R}) - \sum_{\zeta} \mathbf{m}(\zeta)\cdot\mathbf{b}(\mathbf{R})$$
$$+ \frac{e^2}{8m}\sum_{\zeta} \{(\mathbf{q}_\alpha(\zeta) - \mathbf{R})\times\mathbf{b}(\mathbf{R})\}^2 \tag{84}$$

The field-independent transverse-polarization term has been dropped, as before. The $Q_{ij}(\zeta)$ terms are the components of the quadrupole-moment operator $\mathbf{Q}(\zeta)$, and $\mathbf{m}(\zeta)$ is the magnetic dipole-moment operator.

H. The Calculation of Transition Rate. The Fermi Golden Rule

In many of the applications of quantum electrodynamics, such as calculating the rate of absorption or emission of photons, the time dependence of the process is dealt with through the time-Schrödinger equation,

$$i\hbar(\partial/\partial t)|\psi(t)\rangle = H|\psi(t)\rangle \tag{85}$$

which describes the evolution of the system $\psi(t)$ in space and time. For a conservative system, where the Hamiltonian is time independent, Eq. (85) may be solved formally to give

$$|\psi(t)\rangle = U(t, t_0)|\psi(t_0)\rangle \tag{86}$$

where

$$U(t, t_0) = \exp[-iH(t - t_0)/\hbar] \tag{87}$$

and $U(t, t_0)$ is the time-evolution operator for the development of the state of a system from an initial time t_0. In cases of practical interest the wave

equation (85) is not soluble exactly; time-dependent perturbation theory in one of the familiar forms is used to obtain approximate solutions. Some standard results are given to prepare for the treatment of applications in following sections.

Typically, in the problems to be treated, the Hamiltonian is partitioned into $H = H_0 + V$, where the unperturbed H_0 is the sum of Hamiltonians for the free radiation field, and for an unperturbed atomic or molecular system; V is their mutual interaction. More generally, H_0 is time independent and defines a solved problem, with eigenvalues E_n and corresponding eigenstates $|n\rangle$. The perturbation V is also time independent, after being switched on at t_0, and causes changes in the unperturbed system, namely, transitions between the eigenstates of H_0. Given that at t_0 the system is in a state $|\psi(t_0)\rangle$, which is one of the states $|n\rangle$, we calculate the effect of V on the time development of the system.

In the interaction representation we put

$$U(t, t_0) = \exp[-iH_0(t - t_0)/\hbar]U_I(t, t_0) \tag{88}$$

and find that (see, for example, Merzbacher, 1970)

$$U_I(t, t_0) = 1 + \sum_{n=1}^{\infty} \left(\frac{1}{i\hbar}\right)^n \int_{t_0}^{t} dt_1 \int_{t_0}^{t_1} dt_2 \cdots \int_{t_0}^{t_{n-1}} dt_n V_I(t_1) \cdots V_I(t_n) \tag{89}$$

where V_I, the perturbation in interaction representation, is time dependent,

$$V_I(t) = \exp[iH_0(t - t_0)/\hbar]V \exp[-iH_0(t - t_0)/\hbar] \tag{90}$$

and $U_I(t, t_0)$ represents the modification in the time evolution due to the interaction V.

With the use of Eq. (89) the probability amplitude can be found for a system which was in the initial state $|i\rangle$ at t_0 to develop into the final state $|f\rangle$ at t. The amplitude is

$$\begin{aligned}\langle f|\exp[iH_0(t - t_0)/\hbar]|\psi(t)\rangle &= \langle f|\exp[iH_0(t - t_0)/\hbar]U(t, t_0)|\psi(t_0)\rangle \\ &= \langle f|U_I(t, t_0)|i\rangle\end{aligned} \tag{91}$$

The probability amplitude, correct to first order in V, is

$$-\hbar^{-1}\langle f|V|i\rangle\{\exp[i\omega_{fi}(t - t_0)] - 1\}/\omega_{fi} \tag{92}$$

where the characteristic frequency ω_{fi} is given by $\omega_{fi} = (E_f - E_i)/\hbar$. The probability of finding the system in state $|f\rangle$ at t is, in this order,

$$P_{fi}(t) = \frac{|\langle f|V|i\rangle|^2}{\hbar^2} 4 \frac{\sin^2 \omega_{fi}(t - t_0)/2}{\omega_{fi}^2} \tag{93}$$

The probability $P_{fi}(t)$ depends on the squared modulus of the appropriate matrix element of the perturbation V weighted by the trigonometric function $4\{\sin^2 \frac{1}{2}\omega_{fi}(t - t_0)\}/\omega_{fi}^2$, which has a sharp peak centered at $\omega_{fi} = 0$ with half-width $2\pi/(t - t_0)$. Thus, so long as $\langle f|V|i\rangle \neq 0$ the transition probability $|f\rangle \leftarrow |i\rangle$ is extremely small unless there is energy conservation within an interval $2\pi\hbar/(t - t_0)$.

If either or both of the initial and final states is part of a continuous-energy spectrum, the probability $P(t)$ is a sum over a range of states. We find this case in light absorption given in Section III,A, where the incident radiation has a continuous distribution over the modes, and there is absorption over a narrow range within this distribution. Supposing the final state to be within a continuum, we have

$$P_{\text{total}}(t) = \sum_f P_{fi}(t) = 4 \sum_f \frac{|\langle f|V|i\rangle|^2}{\hbar^2} \frac{\sin^2 \omega_{fi}(t - t_0)/2}{\omega_{fi}^2} \tag{94}$$

The summation in Eq. (94) is dealt with by introducing the energy density of states ρ_f,

$$dn_f = \rho_f \, dE_f = \hbar \rho_f \, d\omega_f \tag{95}$$

giving the number of states in a small energy interval; ρ_f is allowed to be a function of ω_f, but it is taken to be slowly varying compared with the trigonometric factor in Eq. (94). This applies also to $|V_{fi}|^2$. Treating both as constants with values at the peak $\omega_{fi} = 0$, we find the approximate expression (96), which is the well-known Fermi golden rule giving the transition rate between states $|i\rangle$ and $|f\rangle$:

$$dP/dt = \Gamma = (2\pi/\hbar)|\langle f|V|i\rangle|^2 \rho \tag{96}$$

III. Interactions between Free Molecules and Radiation

A. One-Photon Absorption

Among the simplest processes of interaction between radiation and matter is the absorption of a photon by an atom or molecule, to be calculated in the approximation where the wavelength is long compared with the dimensions of the absorber (dipole approximation). This elementary process is treated in quantum electrodynamics as follows.

For the interaction of a monochromatic beam of polarized light with an assembly of molecules the Hamiltonian is

$$H = \sum_\zeta H_{\text{mol}}(\zeta) + H_{\text{rad}} + \sum_\zeta H_{\text{int}}(\zeta) \tag{97}$$

The first two terms are the H_0 of Section II,H, made up of the sum of free-molecule Hamiltonians for the molecules ζ and the free-field second-quantized Hamiltonian given in Eq. (66). The final term is the perturbation, namely, the coupling of molecule to the radiation field in dipole approximation:

$$H_{\text{int}}(\zeta) = -\epsilon_0^{-1}\boldsymbol{\mu}(\zeta) \cdot \mathbf{d}^{\perp}(\mathbf{R}_\zeta) \tag{98}$$

where $\boldsymbol{\mu}(\zeta)$ is the electric dipole-moment operator. The molecules do not interact with one another, and the Schrödinger equation for H_{mol} is assumed solved, with known eigenvalues and eigenstates. In the initial state all molecules are in the ground state, and the state of the monochromatic beam is specified by an occupation number of n photons in the single mode $(\mathbf{k}, \lambda)$ with wave vector $\mathbf{k}$ and polarization λ. The initial state is thus represented by the product ket

$$|i\rangle = |n(\mathbf{k}, \lambda)\rangle \prod_{\zeta} |E_0(\zeta)\rangle \tag{99}$$

The incident radiation satisfies energy conservation

$$E_m - E_0 \approx \hbar ck \tag{100}$$

where E_{m} is the energy of the final molecular state. In an assembly of N noninteracting molecules (dilute gas), the photon may be absorbed by any molecule, giving an Nfold degeneracy. A typical component of the degenerate set of final states is

$$|(n-1)(\mathbf{k}, \lambda)\rangle |E_m(\zeta)\rangle \prod_{\zeta' \neq \zeta} |E_0(\zeta')\rangle \tag{101}$$

with loss of one photon from the incident beam and excitation of one molecule. Taking $|E_{\text{m}}(\zeta)\rangle$ to be nondegenerate, the matrix element for excitation of molecule ζ is

$$M_{fi}(\zeta) = -\langle E_m(\zeta)|\boldsymbol{\mu}(\zeta)|E_0(\zeta)\rangle \cdot \langle (n-1)(\mathbf{k}, \lambda)|\, \mathbf{d}^{\perp}(\mathbf{R}_\zeta)/\epsilon_0 |n(\mathbf{k}, \lambda)\rangle \tag{102}$$

The first factor is the electric dipole transition moment abbreviated to $\boldsymbol{\mu}^{mo}(\zeta)$. The second factor can be evaluated using the mode expansion of $\mathbf{d}^{\perp}$, equal to that of $-\boldsymbol{\Pi}$ in Section II,D:

$$M_{fi}(\zeta) = -i(n\hbar ck/2\epsilon_0 V)^{1/2}\mathbf{e}^{(\lambda)}(\mathbf{k}) \cdot \boldsymbol{\mu}^{mo}(\zeta) e^{i\mathbf{k}\cdot\mathbf{R}_\zeta} \tag{103}$$

where $\mathbf{R}_\zeta$ is the position of molecule ζ. The total transition rate is found from Fermi's rule, by summing the rates for each of the N degenerate components (101) and allowing for the spread of frequencies of the incident radiation through the energy density ρ,

$$\Gamma = \frac{2\pi}{\hbar}\rho\left(\frac{n\hbar ck}{2\epsilon_0 V}\right)\sum_{\zeta}|\mathbf{e}^{(\lambda)}(\mathbf{k})\cdot\boldsymbol{\mu}^{mo}(\zeta)|^2 \tag{104}$$

In the dilute gas (and in solution) the molecules are randomly oriented, and the last factor of Eq. (104) must be averaged over all molecular orientations. The result

$$\langle\mu_i^{mo}\mu_j^{mo}\rangle = \tfrac{1}{3}\delta_{ij}|\boldsymbol{\mu}^{mo}|^2 \tag{105}$$

leads to the spatially averaged transition rate

$$\langle\Gamma\rangle = \left(\frac{2\pi}{3\hbar}\right)\rho\left(\frac{n\hbar ck}{2\epsilon_0 V}\right)N|\boldsymbol{\mu}^{mo}|^2 \tag{106}$$

The density of field states ρ is related to the incident intensity $\mathcal{I}$, the energy density per unit frequency, by

$$\rho = \mathcal{I}V/2\pi n\hbar^2\omega \tag{107}$$

giving for the spatially averaged transition rate:

$$\langle\Gamma\rangle = (N/6\hbar^2\epsilon_0)|\boldsymbol{\mu}^{mo}|^2\mathcal{I} = NB\mathcal{I} \tag{108}$$

where B is the Einstein B coefficient

$$B = (6\hbar^2\epsilon_0)^{-1}|\boldsymbol{\mu}^{mo}|^2 \tag{109}$$

B. Spontaneous Emission

Spontaneous emission is a leading example of the differences between quantum electrodynamics and the semiclassical theory of the interaction of radiation and matter (Dirac, 1927). In the semiclassical method there is no external field; an excited atomic or molecular state is not perturbed and is a stationary state. The spontaneous emission cannot be accounted for within the semiclassical framework. Interesting attempts, particularly by Jaynes and co-workers (Jaynes and Cummings, 1963; Milonni, 1980), have been made to study radiation processes from a classical point of view.

In quantum electrodynamics the excited molecule is part of a system including the radiation field and is perturbed by the field even where the field is in its vacuum state with no photons present. The perturbation causes radiative decay, in which the molecule drops back to its ground state and a photon is added to the field with conservation of total energy. The initial state is $|0\rangle|E_m\rangle$, where $|0\rangle$ refers to the vacuum state of the radiation field. The final state is $|1(\mathbf{k},\lambda)\rangle|E_0\rangle$, where $\mathbf{k}$ is the resonant photon mode, $\hbar ck = E_m - E_0$. After summing over polarizations and spatial averaging, a straightforward calculation gives for the total emission rate

$$\langle \Gamma \rangle = (\omega^3/3\pi\epsilon_0\hbar c^3)|\boldsymbol{\mu}^{om}|^2 \tag{110}$$

$$= A \tag{111}$$

where A is the Einstein A coefficient, related to B in Eq. (109) by

$$A = (2\hbar\omega^3/\pi c^3)B = (8\pi h\nu^3/c^3)B \tag{112}$$

where ν is the circular frequency for the transition.

C. Circular Dichroism

The calculation of the transition rate for electric dipole-allowed transitions in Section III,A can be extended to the differential rate of absorption for left- and right-circularly polarized light by chiral (optically active) molecules (Power and Thirunamachandran, 1974). Selection rules for chiral molecules allow transitions between at least some pairs of states to be induced by both electric and magnetic dipole radiation. The transition probability is made up of pure electric terms, as given in Section III,A, of pure magnetic terms, closely analogous to them, and electric–magnetic terms. The pure electric and pure magnetic parts are the same for the circularly polarized components, but the crossterm involves interference between the probability amplitudes for the electric and magnetic couplings, and the absorption rates for left- and right-polarized light are different. It was shown in Section III,A that the one-photon rate for an assembly by molecules with random orientations is the sum of rates for individual molecules; it is now sufficient to calculate the single-molecule rates.

The interaction part of the total Hamiltonian (80) must now include the coupling of the molecular magnetic dipole moment $\mathbf{m}$ to the magnetic vector of the radiation field, giving for the new H_{int},

$$H_{\text{int}} = -(1/\epsilon_0)\boldsymbol{\mu}(\mathbf{R}) \cdot \mathbf{d}^{\perp}(\mathbf{R}) - \mathbf{m}(\mathbf{R}) \cdot \mathbf{b}(\mathbf{R}) \tag{113}$$

for a molecule centered at $\mathbf{R}$. Taking a transition $|E_m\rangle \leftarrow |E_0\rangle$ caused by a left-circular photon of mode $(\mathbf{k}, \mathrm{L})$, we have for initial and final states:

$$|i\rangle = |E_0\rangle|n(\mathbf{k}, \mathrm{L})\rangle \tag{114}$$

$$|f\rangle = |E_m\rangle|(n-1)(\mathbf{k}, \mathrm{L})\rangle \tag{115}$$

with a matrix element for absorption:

$$\begin{aligned} M_{fi}^{(\mathrm{L})} = &-\langle E_m|\boldsymbol{\mu}|E_0\rangle \cdot \langle (n-1)(\mathbf{k}, \mathrm{L})|\mathbf{d}^{\perp}(\mathbf{R})/\epsilon_0|n(\mathbf{k}, \mathrm{L})\rangle \\ &-\langle E_m|\mathbf{m}|E_0\rangle \cdot \langle (n-1)(\mathbf{k}, \mathrm{L})|\mathbf{b}(\mathbf{R})|n(\mathbf{k}, \mathrm{L})\rangle \end{aligned} \tag{116}$$

After expanding $\mathbf{d}^{\perp}$ and $\mathbf{b}$ in modes according to Section II,D, we find

$$M_{fi}^{(\mathrm{L})} = -i(n\hbar ck/2\epsilon_0 V)^{1/2}\mathbf{e}^{(\mathrm{L})}(\mathbf{k}) \cdot \{\boldsymbol{\mu}^{mo} - (i/c)\mathbf{m}^{mo}\}e^{i\mathbf{k}\cdot\mathbf{R}} \tag{117}$$

differing from expression (103) only in the appearance of the complex dipole moment $[\boldsymbol{\mu}^{mo} - (i/c)\,\mathbf{m}^{mo}]$ in place of the pure electric part, and in the circular polarization unit vector $\mathbf{e}^{(L)}(\mathbf{k}) = 2^{-1/2}(\mathbf{e}^{(1)}(\mathbf{k}) + i\mathbf{e}^{(2)}(\mathbf{k}))$ in place of linear polarization. However, use of Eq. (117) now gives the golden rule absorption rate

$$\langle \Gamma^{(L)} \rangle = \left(\frac{2\pi}{3\hbar}\right)\left(\frac{n\hbar ck}{2\epsilon_0 V}\right) \rho \left|\boldsymbol{\mu}^{mo} - \left(\frac{i}{c}\right)\mathbf{m}^{mo}\right|^2 \tag{118}$$

which is not the same as that for right-circular photons,

$$\langle \Gamma^{(R)} \rangle = \left(\frac{2\pi}{3\hbar}\right)\left(\frac{n\hbar ck}{2\epsilon_0 V}\right) \rho \left|\boldsymbol{\mu}^{mo} + \left(\frac{i}{c}\right)\mathbf{m}^{mo}\right|^2 \tag{119}$$

the difference being the differential rate

$$\langle \Gamma^{(L)} \rangle - \langle \Gamma^{(R)} \rangle = -\left(\frac{8\pi i}{3\hbar c}\right)\left(\frac{n\hbar ck}{2\epsilon_0 V}\right) \rho \boldsymbol{\mu}^{om} \cdot \mathbf{m}^{mo} \tag{120}$$

where use is made of the fact that $\boldsymbol{\mu}^{mo}$ and $\mathbf{m}^{om}$ are real and imaginary, respectively, for real wave functions. With Eq. (107) for the density of states,

$$\langle \Gamma^{(L)} \rangle - \langle \Gamma^{(R)} \rangle = -\frac{2\mathcal{J}i}{3\hbar^2 c\epsilon_0}\,\boldsymbol{\mu}^{om} \cdot \mathbf{m}^{mo} = \frac{2\mathcal{J}}{3\hbar^2 c\epsilon_0} R^{mo} \tag{121}$$

where R^{mo} is the optical rotatory strength

$$R^{mo} = \mathrm{Im}\ \boldsymbol{\mu}^{om} \cdot \mathbf{m}^{mo} \tag{122}$$

where $\boldsymbol{\mu}$ is polar and $\mathbf{m}$ is axial; R is pseudoscalar and takes opposite signs for enantiomeric forms of a chiral molecule. It follows that the absorption rate difference is of opposite sign for enantiomers. In most examples, except where $\boldsymbol{\mu}^{mo}$ happens to be very small, the dominant contribution to the absorption rate is made by the electric moment and is the same for left and right photons: the dichroism is a small modulation on this common rate. Equation (121) has been adapted to the theory of vibrational circular dichroism (Craig and Thirunamachandran, 1978). The theory of magnetic circular dichroism, namely, circular dichroism induced by an external magnetic field, has been studied by Healy (1976) using quantum electrodynamics.

Although the coupling of the molecular quadrupole moment with the gradient of the radiation electric field is of the same order as the magnetic dipole coupling, the latter does in fact give the leading term in circular dichroism. The reason is that the interference between the electric quadrupole and dipole amplitudes vanishes from the orientational average, as may be demonstrated by arguments on the symmetry of the dipole–

quadrupole tensor $\mu_i^{om}Q_{jk}^{mo}$, which is the analog of the rotatory tensor $\mu_i^{om}m_j^{mo}$.

D. Laser-Induced Circular Dichroism

An optically inactive (achiral) system in an ordinary circular dichroism experiment gives a null result. If, however, the achiral substance is irradiated by an auxiliary intense beam of circularly polarized light from a laser, it becomes chiral and shows the typical chiroptical properties of optical rotation, circular dichroism, and circular differential scattering. Liao and Bjorklund (1976, 1977) have observed optical rotation by sodium vapor in the presence of polarized laser light. Also, neon gas shows circular dichroism under laser irradiation (Delsart and Keller, 1978). The theory to which we refer has been given by Thirunamachandran (1979). We discuss only circular dichroism.

In the semiclassical picture the laser field would be seen as causing a time-dependent circular polarization in the achiral absorber, thus giving it chiral character. This chirality would then lead to circular dichroism. In quantum electrodynamics the leading term comes from interference between three-photon and one-photon contributions to the transition matrix element for the absorption rate. The typical graphs are shown in Fig. 2. The right-hand three-photon graphs are representative of a total of six for the various time sequences of the events.

Let the nonresonant laser beam be of mode ($\mathbf{k}_1$, L) and the probe beam be of mode ($\mathbf{k}_2$, L/R). The probe beam is assumed to be resonant with the one-photon-allowed transition $m \leftarrow 0$; *i.e.*, $E_{mo} = \hbar c k_2$. The initial and final states of the system are $|E_0; n_1(\mathbf{k}_1, \text{L}), n_2(\mathbf{k}_2, \text{L/R})\rangle$ and $|E_m; n_1(\mathbf{k}_1,$

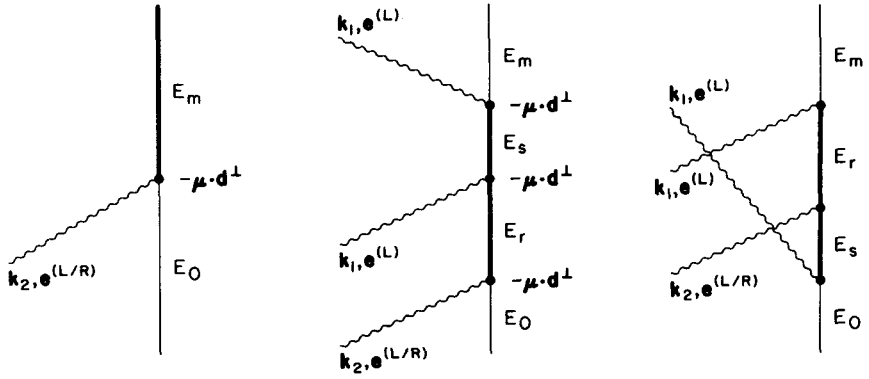

Fig. 2. Left-hand graph: one-photon absorption. Right-hand graphs: one-photon absorption in the presence of an auxiliary chiral field.

L), $(n_2 - 1)(\mathbf{k}_2, \text{L/R})\rangle$; the state of the laser beam is not changed. With no intense beam, the first-order element for the $m \leftarrow 0$ transition is (left-hand graph)

$$M_1^{\text{L/R}} = -i\left(\frac{n_2\hbar ck_2}{2\epsilon_0 V}\right)^{1/2} e_k^{(\text{L/R})}(\mathbf{k}_2)\mu_k^{mo} \tag{123}$$

When the coupling is taken into account, the leading new contribution to the matrix element is of third order, given by

$$M_3^{\text{L,L/R}} = -i\left(\frac{n_2\hbar ck_2}{2\epsilon_0 V}\right)^{1/2}\left(\frac{n_1\hbar ck_1}{2\epsilon_0 V}\right) e_i^{(\text{L})}(\mathbf{k}_1)e_j^{(\text{L})}(\mathbf{k}_1)e_k^{(\text{L/R})}(\mathbf{k}_2)\beta_{ijk}^{mo} \tag{124}$$

where

$$\begin{aligned}\beta_{ijk}^{mo} = \sum_{r,s}\Bigg[&\frac{\mu_i^{ms}\mu_j^{sr}\mu_k^{ro}}{(E_{sm} - \hbar\omega_1)(E_{ro} - \hbar\omega_2)} + \frac{\mu_j^{ms}\mu_i^{sr}\mu_k^{ro}}{(E_{sm} + \hbar\omega_1)(E_{ro} - \hbar\omega_2)} \\ &+ \frac{\mu_j^{ms}\mu_k^{sr}\mu_i^{ro}}{(E_{sm} + \hbar\omega_1)(E_{ro} + \hbar\omega_1)} + \frac{\mu_i^{ms}\mu_k^{sr}\mu_j^{ro}}{(E_{sm} - \hbar\omega_1)(E_{ro} - \hbar\omega_1)} \\ &+ \frac{\mu_k^{ms}\mu_i^{sr}\mu_j^{ro}}{E_{so}(E_{ro} - \hbar\omega_1)} + \frac{\mu_k^{ms}\mu_j^{sr}\mu_i^{ro}}{E_{so}(E_{ro} + \hbar\omega_1)}\Bigg]\end{aligned} \tag{125}$$

The tensor β_{ijk}^{mo} is not symmetric with respect to any pair of indices, in contrast with the β tensor to be introduced for hyper-Rayleigh and hyper-Raman scattering (Section III,H), which is symmetric in one pair. The differential absorption rate is

$$\Gamma^{\text{LL}} - \Gamma^{\text{LR}} = (2\pi/\hbar)\{|M_1^{\text{L}} + M_3^{\text{LL}}|^2 - |M_1^{\text{R}} + M_3^{\text{LR}}|^2\}\rho \tag{126}$$

The induced circular dichroism depends on interference between the one- and three-photon terms. It is convenient to express it as a ratio with the total absorption,

$$\Delta = \frac{\Gamma^{\text{LL}} - \Gamma^{\text{LR}}}{\Gamma^{\text{LL}} + \Gamma^{\text{LR}}} \approx \frac{\langle M_1^{\text{L}}\overline{M}_3^{\text{LL}} + \overline{M}_1^{\text{L}}M_3^{\text{LL}} - M_1^{\text{R}}\overline{M}_3^{\text{LR}} - \overline{M}_1^{\text{R}}M_3^{\text{LR}}\rangle}{\langle|M_1^{\text{L}}|^2 + |M_1^{\text{R}}|^2\rangle} \tag{127}$$

Substituting Eqs. (123) and (124) for M_1 and M_3 and performing a rotational average, we get

$$\Delta = \frac{I_1}{4\epsilon_0 c}(\hat{\mathbf{k}}_1 \cdot \hat{\mathbf{k}}_2)\frac{\mu_\lambda^{mo}\beta_{\mu\lambda\mu}^{mo} - \mu_\lambda^{mo}\beta_{\lambda\mu\mu}^{mo}}{|\boldsymbol{\mu}^{mo}|^2} \tag{128}$$

where I_1 is the irradiance of the laser beam. The differential ratio is linearly proportional to the irradiance and the cosine of the angle between the directions of propagation of the two beams. As expected, the ratio

(128) tends to zero as I_1 tends to zero. Alternative methods of calculating Δ are given in the reference cited above.

In natural circular dichroism, the differential absorption rate depends on the pseudoscalar $\boldsymbol{\mu} \cdot \mathbf{m}$ and its sign is opposite for two enantiomers. In laser-induced circular dichroism, the enantiomeric equivalents are the two possible circular polarizations of the nonresonant laser beam of the molecule–laser system. A change of helicity of the beam is the same as the change of sign of $\mathbf{k}_1$ in Eq. (128), leading to a change in sign of the differential ratio.

E. Two-Photon Absorption

1. *Two-Photon Absorption from a Single Beam*

High-intensity coherent radiation from lasers can cause transitions between molecular states involving two or more photons. Typical simple examples are multiphoton ionization processes and two-photon absorption in the UV spectrum of hydrocarbons such as benzene, where the selection rules, including g ← g, u ← u, enable new insight into symmetry assignments and cognate problems. There are also many more complex processes known which involve multiple-photon events from two or more different beams. Quantum electrodynamics allows compact descriptions in which, as in earlier sections, changes in state of the radiation are followed, along with those of the molecule, with improved physical insight (Power and Thirunamachandran, 1975).

The description of two-photon absorption in this and the following section calls for the mediation in the overall process of intermediate (virtual) states. Absorption of one photon creates a virtual state of the molecule and absorption of another completes the transition. The overall two-photon process is energy conserving, but the energy of the virtual state is not restricted and all molecular states can participate. For a two-photon process the leading contribution to the matrix element is the second-order term of $U_I(t, t_0)$, Eq. (89). The probability amplitude for $|f\rangle \leftarrow |i\rangle$, assuming that the frequency of the incident photons (from a single beam) is not resonant with any one-photon molecular transition, is

$$\frac{1}{i\hbar} \sum_I \frac{\langle f|V|I\rangle\langle I|V|i\rangle}{E_{iI}} \int_{t_0}^{t} \exp[i\omega_{fi}(t_1 - t_0)]\, dt_1 \tag{129}$$

where $E_{iI} = E_i - E_I$. The summation is over a complete set of eigenstates of $H_0 = H_{\text{mol}} + H_{\text{rad}}$ that is complete with respect both to molecular and radiation field states. The usual argument leads to a transition rate (96) by the Fermi golden rule with the matrix element

$$M_{fi} = \sum_I \frac{\langle f|V|I\rangle\langle I|V|i\rangle}{E_{iI}} \tag{130}$$

As before, it is sufficient to calculate the rate for one molecule and multiply by the number of molecules to obtain the total rate.

Let the single incident beam from which two photons are to be absorbed be monochromatic in the mode $(\mathbf{k}, \lambda)$. The initial and final states are

$$|i\rangle = |E_0\rangle|n(\mathbf{k}, \lambda)\rangle \tag{131}$$

$$|f\rangle = |E_m\rangle|(n-2)(\mathbf{k}, \lambda)\rangle \tag{132}$$

$$M_{fi} = \sum_I \frac{(1/\epsilon_0)^2 \langle f| -\boldsymbol{\mu}\cdot\mathbf{d}^\perp|I\rangle\langle I| -\boldsymbol{\mu}\cdot\mathbf{d}^\perp|i\rangle}{E_{iI}} \tag{133}$$

In the intermediate state, one photon has been transferred from the radiation field and a new molecular (virtual) state produced:

$$|I\rangle = |E_r\rangle|(n-1)(\mathbf{k}, \lambda)\rangle \tag{134}$$

the standard graphical representation of the process is shown in the time-ordered diagram of Fig. 3.

As usual, the vertical solid line shows the changes in molecular state produced by photons through interactions labeled at the vertices. It is conventional not to show the state of the radiation field, but to show changes in its state caused by incoming (absorbed) and outgoing (emitted) photons. The initial state of the system is read off at line 1, with the molecule in its ground state $|E_0\rangle$ and with two $(\mathbf{k}, \lambda)$ photons. The intermediate state is at line 2 ($|E_r\rangle$ and one photon less in the radiation field), and the final state at line 3, with overall energy conservation $E_m - E_0 = 2\hbar ck$. The energy interval between initial and intermediate states is $E_{iI} = E_0 - E_r + \hbar ck$; excitation of the intermediate state is not energy conserv-

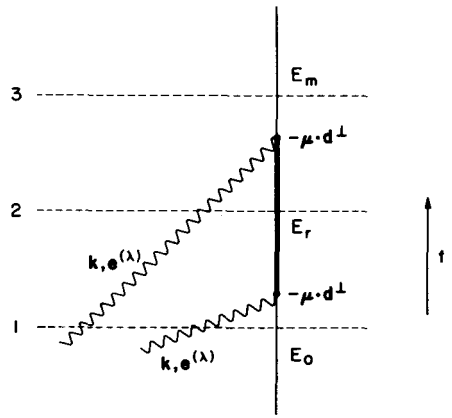

Fig. 3. Time-ordered graph for two-photon absorption from a single beam.

ing so that $E_{ro} \neq \hbar ck$. As in other applications of second-order and higher order perturbations, the intermediate states are reached by virtual processes, not by real ones. There is no violation of energy conservation; one can say that the lifetime of the system in the intermediate state is so short that the uncertainty in its energy allows any molecular level to be involved.

With the mode expansion for $\mathbf{d}^{\perp}$ the matrix element for the time-ordered diagram in Fig. 3 is readily found:

$$M_{fi} = \left(\frac{\hbar ck}{2\epsilon_0 V}\right) \{n(n-1)\}^{1/2} e_i^{(\lambda)}(\mathbf{k}) e_j^{(\lambda)}(\mathbf{k}) \frac{1}{2} \sum_r \left\{ \frac{\mu_i^{mr}\mu_j^{ro}}{E_{ro} - \hbar\omega} + \frac{\mu_j^{mr}\mu_i^{ro}}{E_{ro} - \hbar\omega} \right\} \tag{135}$$

a form that has been simplified by using the i, j symmetric property of the polarization tensor $e_i^{(\lambda)}(\mathbf{k}) e_j^{(\lambda)}(\mathbf{k})$.

Defining the molecular second-rank tensor

$$\alpha_{ij}^{mo}(\pm\omega_1, \pm\omega_2) = \sum_r \left\{ \frac{\mu_i^{mr}\mu_j^{ro}}{E_{ro} \mp \hbar\omega_1} + \frac{\mu_j^{mr}\mu_i^{ro}}{E_{ro} \mp \hbar\omega_2} \right\} \tag{136}$$

the Fermi golden rule absorption rate is

$$\Gamma = \left(\frac{2\pi N}{\hbar}\right) |M_{fi}|^2 \rho = \frac{1}{4} \left(\frac{2\pi N}{\hbar}\right) \left(\frac{\hbar ck}{2\epsilon_0 V}\right)^2 \times \rho n(n-1) e_i^{(\lambda)}(\mathbf{k}) e_j^{(\lambda)}(\mathbf{k}) \bar{e}_k^{(\lambda)}(\mathbf{k}) \bar{e}_l^{(\lambda)}(\mathbf{k}) \alpha_{ij}^{mo}(\omega, \omega) \bar{\alpha}_{kl}^{mo}(\omega, \omega) \tag{137}$$

where the frequency $\omega = ck$ is that of the absorbed photons. Rotational averaging (Andrews and Thirunamachandran, 1977) for molecules in gases or liquids gives

$$\langle \Gamma \rangle = \left(\frac{2\pi N}{\hbar}\right) \left(\frac{\hbar ck}{2\epsilon_0 V}\right)^2 \rho n(n-1) \times \frac{1}{60} \left[\left\{ 2|\mathbf{e}^{(\lambda)}(\mathbf{k}) \cdot \mathbf{e}^{(\lambda)}(\mathbf{k})|^2 - 1 \right\} \alpha_{\lambda\lambda}^{mo}(\omega, \omega) \bar{\alpha}_{\mu\mu}^{mo}(\omega, \omega) - \left\{ |\mathbf{e}^{(\lambda)}(\mathbf{k}) \cdot \mathbf{e}^{(\lambda)}(\mathbf{k})|^2 - 3 \right\} \alpha_{\lambda\mu}^{mo}(\omega, \omega) \bar{\alpha}_{\lambda\mu}^{mo}(\omega, \omega) \right] \tag{138}$$

Subscripts i, j, k, and l in Eq. (137) refer to the laboratory frame and λ and μ in Eq. (138) to the molecular frame.

In one-photon absorption (Section III,A), the photon polarization disappeared from the transition rate on averaging over molecular orientations, so that the rate does not depend on the polarization of the incident light. This is not true of two-photon absorption; inasmuch as $\mathbf{e}^{(\lambda)}(\mathbf{k}) \cdot \mathbf{e}^{(\lambda)}(\mathbf{k})$ is unity for linear polarization and zero for circular polarization, it is clear that there is polarization dependence. For example, the atomic transition

$n'S \leftarrow nS$ is two-photon allowed for linear polarization but forbidden for circular polarization, as is readily seen by angular momentum conservation. The polarization dependence of absorption rates may be exploited to evaluate the molecular tensor products $\alpha^{mo}_{\lambda\lambda}(\omega, \omega)\bar{\alpha}^{mo}_{\mu\mu}(\omega, \omega)$ and $\alpha^{mo}_{\lambda\mu}(\omega, \omega)\bar{\alpha}^{mo}_{\lambda\mu}(\omega, \omega)$. The α tensors are molecular properties characteristic of a transition (here, $m \leftarrow 0$) and functions of the beam frequency ω. However, as two-photon absorption is confined to a narrow frequency range, close to one-half of the transition-frequency $(E_m - E_0)/2\hbar$, values of the tensor products can only be found close to that frequency.

The two-photon transition rate can be given, analogously to that for the one-photon rate [Eq. 108], in terms of field-dependent and molecular factors,

$$\langle \Gamma \rangle = N \mathcal{I} I g^{(2)} B^{(2)} \tag{139}$$

where N is the number of absorbers, $\mathcal{I}$ the energy density per unit frequency, I the energy flux per unit area (irradiance), $g^{(2)}$ the coherence factor for two-photon correlation [Eq. 140], and $B^{(2)}$, defined in Eq. (141), the two-photon analog of the Einstein B coefficient,

$$g^{(2)} = \langle n(n-1) \rangle / \langle n \rangle^2 \tag{140}$$

In the expression for $g^{(2)}$, the average is over the state of the radiation field, and n is the occupation number referring to the operator $a^\dagger a$. Here, the field is represented by number states and the average is $g^{(2)} = (n-1)/n$, giving near to unity for large occupation number (very intense beam); $B^{(2)}$ is given for plane, circular, and unpolarized absorption in Eq. (141).

$$\begin{aligned}
B^{(2)}_{\text{plane}} &= (240\hbar^2 c \epsilon_0^2)^{-1} \{\alpha^{mo}_{\lambda\lambda}(\omega, \omega)\bar{\alpha}^{mo}_{\mu\mu}(\omega, \omega) \\
&\quad + 2\alpha^{mo}_{\lambda\mu}(\omega, \omega)\bar{\alpha}^{mo}_{\lambda\mu}(\omega, \omega)\} \\
B^{(2)}_{\text{circular}} &= (240\hbar^2 c \epsilon_0^2)^{-1} \{-\alpha^{mo}_{\lambda\lambda}(\omega, \omega)\bar{\alpha}^{mo}_{\mu\mu}(\omega, \omega) \\
&\quad + 3\alpha^{mo}_{\lambda\mu}(\omega, \omega)\bar{\alpha}^{mo}_{\lambda\mu}(\omega, \omega)\} \\
B^{(2)}_{\text{unpolarized}} &= (960\hbar^2 c \epsilon_0^2)^{-1} \{\alpha^{mo}_{\lambda\lambda}(\omega, \omega)\bar{\alpha}^{mo}_{\mu\mu}(\omega, \omega) \\
&\quad + 7\alpha^{mo}_{\lambda\mu}(\omega, \omega)\bar{\alpha}^{mo}_{\lambda\mu}(\omega, \omega)\}
\end{aligned} \tag{141}$$

2. *Two-Photon Absorption from Different Beams*

Much more versatile two-photon experiments are possible when two different monochromatic high-intensity beams are incident on a system in modes $(\mathbf{k}_1, \lambda_1)$ and $(\mathbf{k}_2, \lambda_2)$. The absorbed photons can have different frequencies and polarizations. The calculation of the matrix element for the process is made with the help of the time-ordered diagrams in Fig. 4. Two diagrams are now required, because two different sets of virtual

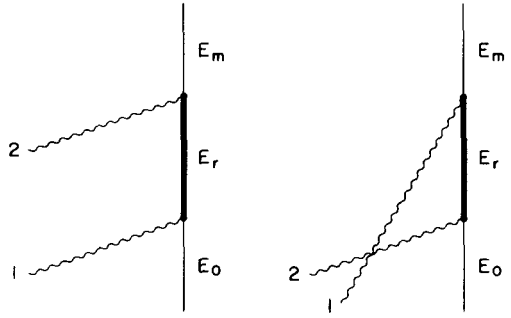

Fig. 4. Absorption of two photons $(\mathbf{k}_1, \lambda_1)$ and $(\mathbf{k}_2, \lambda_2)$ from two beams.

states occur, according to whether photon 1 is absorbed before or after photon 2. The matrix element is

$$M_{fi} = (\hbar c/2\epsilon_0 V)(k_1 k_2 n_1 n_2)^{1/2} e_i^{(\lambda_1)}(\mathbf{k}_1) e_j^{(\lambda_2)}(\mathbf{k}_2) \alpha_{ij}^{mo}(\omega_1, \omega_2) \qquad (142)$$

Whereas α_{ij}^{mo} in the single-beam case is a tensor symmetric in its indices, that does not apply in Eq. (142) either to $\boldsymbol{\alpha}$ or to the polarization tensor $e_i^{(\lambda_1)}(\mathbf{k}_1) e_j^{(\lambda_2)}(\mathbf{k}_2)$. By choosing different polarizations for the two beams, it is possible to characterize fully the two-photon transition. Frequency variations are also possible subject to $\hbar c k_1 + \hbar c k_2 = E_m + E_0$, and to the condition that there are no resonances with molecular energy intervals $E_r - E_0$. (Details are given in a review by McClain, 1974.)

The theory is easily adapted to the situation where the final state is an ionized state. A comprehensive review of multiphoton ionization of atoms has been given by Lambropoulos (1976). In a molecular example, multiphoton ionization techniques have been used to detect bound–bound multiphoton transitions in benzene (Johnson, 1976).

A novel application of two-photon absorption is in Doppler-free spectroscopy (Grynberg and Cagnac, 1977). By using split beams counterpropagating through the absorption cell, it is possible to eliminate first-order Doppler broadening and achieve high resolution. Suppose the frequency of the atomic transition is 2ω. If an atom interacts with counterpropagating light beams with wave vectors $\mathbf{k}$ and $-\mathbf{k}$ ($\omega = c|\mathbf{k}|$), the Doppler-shifted frequencies are $\omega(1 \pm v/c)$ where v is the velocity component in the direction of the observer. If the atom absorbs a photon from each, we find that energy conservation $E_{mo} = 2\hbar\omega$ is satisfied irrespective of thermal motions because of a cancellation of the velocity-dependent terms. Such Doppler-free absorption was first observed in the 5S $\leftarrow$ 3S transition of atomic sodium (Biraben *et al.*, 1974; Levenson and Bloembergen, 1974).

F. Raman Scattering

In quantum electrodynamics, Rayleigh scattering (elastic) and Raman scattering (inelastic) are two-photon processes. In the latter, the final state of the molecule is different from the initial state: the difference between the frequencies of the incident and scattered photons is equal to a characteristic frequency of the molecule, usually a rotational, vibrational, or, in rather rare cases thus far, an electronic transition frequency.

Raman scattering, like two-photon absorption, is an incoherent process, so that the total rate is found by calculating the scattering rate for a single molecule and multiplying by the number of molecules. The leading contribution to the scattering-matrix element is of second order and can be found from the time-ordered diagrams in Fig. 5. The incident and scattered photons are in states $|n(\mathbf{k},\lambda);0(\mathbf{k}',\lambda')\rangle$ and $|(n-1)(\mathbf{k},\lambda);1|(\mathbf{k}',\lambda')\rangle$ and the initial and final molecular states $|E_0\rangle$ and $|E_m\rangle$. The expression for the matrix element in the dipole approximation is

$$-\left(\frac{\hbar c}{2\epsilon_0 V}\right)(nkk')^{1/2}e_i'e_j\sum_r\left\{\frac{\mu_i^{mr}\mu_j^{ro}}{E_{ro}-\hbar ck}+\frac{\mu_j^{mr}\mu_i^{ro}}{E_{ro}+\hbar ck'}\right\} \tag{143}$$

The sum in Eq. (143) is the tensor $\alpha_{ij}^{mo}(\omega,-\omega')$ defined in Eq. (136). With the Fermi rule we find for the scattering rate into the solid angle $d\Omega'$ around $\hat{\mathbf{k}}'$

$$d\Gamma=\left(\frac{2\pi}{\hbar}\right)\left(\frac{\hbar c}{2\epsilon_0 V}\right)^2\frac{nkk'^3\,d\Omega' V}{(2\pi)^3\hbar c}\,\bar{e}_i'e_je_k'\bar{e}_l\alpha_{ij}^{mo}\bar{\alpha}_{kl}^{mo} \tag{144}$$

Expressing the rate in terms of the radiant density $I(\mathbf{k}')$, namely, the energy radiated along $\hat{\mathbf{k}}'$ with polarization λ' per unit solid angle per unit time,

$$I(\mathbf{k}')=\frac{d\Gamma}{d\Omega'}\hbar ck'=\frac{NIk'^4}{(4\pi\epsilon_0)^2}\,\bar{e}_i'e_je_k'\bar{e}_l\alpha_{ij}^{mo}\bar{\alpha}_{kl}^{mo} \tag{145}$$

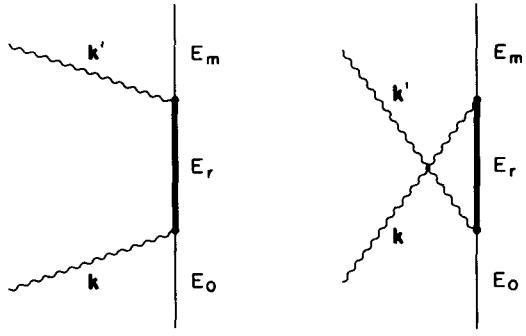

Fig. 5. Raman scattering.

The molecular states $|E_0\rangle$ and $|E_m\rangle$ are thus far unspecified. Let us adopt the Born–Oppenheimer approximation and write for the excited state,

$$|E_m\rangle = \phi_m(\mathbf{q}, \mathbf{Q})\chi_{mv}(\mathbf{Q}) \tag{146}$$

where $\phi_m(\mathbf{q}, \mathbf{Q})$ is the electronic wave function with electronic coordinates $\mathbf{q}$ for a particular set of values of nuclear normal coordinates $\mathbf{Q}$ treated as parameters; $\chi_{mv}(Q_k)$ is the vibrational wave function for the vth level of an oscillator in the normal coordinate Q_k. In vibrational Raman scattering the molecule is in its electronic ground state in initial and final states, but changes its vibrational state from v to v'. The molecular tensor α_{ij}^{gm} in Eq. (144) now becomes

$$\alpha_{ij}^{ov',ov} = \sum_{r,v''} \left\{ \frac{\langle \chi_{ov'}| \langle \phi_0|\mu_i|\phi_r\rangle |\chi_{rv''}\rangle \langle \chi_{rv''}| \langle \phi_r|\mu_j|\phi_0\rangle |\chi_{ov}\rangle}{E_{ro} + e_{rv'',ov} - \hbar ck} \right.$$
$$\left. + \frac{\langle \chi_{ov'}| \langle \phi_0|\mu_j|\phi_r\rangle |\chi_{rv''}\rangle \langle \chi_{rv''} \langle \phi_r|\mu_i|\phi_0\rangle |\chi_{ov}\rangle}{E_{ro} + \epsilon_{rv'',ov} + \hbar ck'} \right\} \tag{147}$$

where E_{ro} is the pure electronic energy separation and $\epsilon_{rv'',ov}$ the vibrational energy difference. Conventional Raman experiments are done with incident frequencies chosen to be far from any resonance, $|E_{ro} - \hbar ck| \gg |\epsilon_{rv'',vo}|$, and the quantities ϵ in the denominators of Eq. (147) can be dropped. For the same reason, k' may be approximated by k. Thus,

$$\alpha_{ij}^{ov',ov} = \sum_{r,v''} \left\{ \frac{\langle \chi_{ov'}|\mu_i^{or}|\chi_{rv''}\rangle \langle \chi_{rv''}|\mu_j^{ro}|\chi_{ov}\rangle}{E_{ro} - \hbar ck} \right.$$
$$\left. + \frac{\langle \chi_{ov'}|\mu_j^{or}|\chi_{rv''}\rangle \langle \chi_{rv''}|\mu_j^{ro}|\chi_{ov}\rangle}{E_{ro} + \hbar ck} \right\} \tag{148}$$

The Q dependence of the transition moments, though not explicit in Eq. (148), is important.

With closure on the vibrational sum

$$\alpha_{ij}^{ov',ov} = \left\langle \chi_{ov'} \middle| \sum_r \left\{ \frac{\mu_i^{or}\mu_j^{ro}}{E_{ro} - \hbar ck} + \frac{\mu_j^{or}\mu_i^{ro}}{E_{ro} + \hbar ck} \right\} \middle| \chi_{ov} \right\rangle$$
$$\equiv \langle \chi_{ov'}|\alpha_{ij}|\chi_{ov}\rangle \tag{149}$$

where α_{ij} is the usual frequency-dependent polarizability except for any consequences of the Q dependence already mentioned. Equation (149) has acquired i, j symmetry through neglect of the vibrational energies. In resonance Raman scattering where the incident radiation is close to one of the molecular energy intervals, the vibrational energy intervals cannot be dropped; closure of the vibrational sum is then not possible, and the

tensor has an i,j antisymmetric part which causes relaxation of the usual Raman selection rules.

For the Raman intensity for a system in random orientation we need the rotational average of the molecular part of Eq. (145), giving

$$I(\mathbf{k}') = \frac{N_v I k'^4}{30(4\pi\epsilon_0)^2}\left[A\alpha_{\lambda\lambda}^{ov',ov}\bar{\alpha}_{\mu\mu}^{ov',ov} + B\alpha_{\lambda\mu}^{ov',ov}\bar{\alpha}_{\lambda\mu}^{ov',ov}\right] \tag{150}$$

where the polarization-dependent coefficients A and B are given by

$$A = 4|\mathbf{e}\cdot\bar{\mathbf{e}}'|^2 - |\mathbf{e}\cdot\mathbf{e}'|^2 - 1, \qquad B = -2|\mathbf{e}\cdot\bar{\mathbf{e}}'|^2 + 3|\mathbf{e}\cdot\mathbf{e}'|^2 + 3 \tag{151}$$

and N_v is the number of molecules in the initial vibrational state v. For a given polarization of the scattered radiation, A and B are the same for left- and right-circularly polarized incident light. Thus in electric dipole approximation the scattered intensity is independent of the handedness of the incident radiation. However, higher multipole coupling terms can lead to intensities dependent on the helicity of the incident photon and can be invoked to account for the phenomenon of circular differential Raman scattering, as described later.

In terms of the irreducible parts of $\alpha_{\lambda\mu}$, the intensity expression (150) becomes

$$I(\mathbf{k}') = \frac{N_v I k'^4}{90(4\pi\epsilon_0)^2}\Big[(3A + B)\alpha_{\lambda\lambda}^{ov',ov(0)}\alpha_{\mu\mu}^{ov',ov(0)} + 3B\alpha_{\lambda\mu}^{ov',ov(2)}\alpha_{\lambda\mu}^{ov',ov(2)}\Big] \tag{152}$$

where $\alpha_{\lambda\lambda}^{(0)}$ and $\alpha_{\lambda\mu}^{(2)}$ transform as a scalar (weight 0) and a symmetric traceless second-rank tensor (weight 2), respectively. Expressions for reversal and depolarization ratios follow directly.

G. Circular Differential Raman Scattering

Efforts have been made for a long time to measure differential Raman scattering of left- and right-circularly polarized light by optically active molecules. The early work was unsuccessful (Bhagavantam and Venkateswaran, 1930; Kastler, 1930), but lasers and improved detection methods have made observation possible (Barron *et al.*, 1973).

Extension of the discussion given in the previous section leads to an understanding of this property (Barron and Buckingham, 1971; Andrews, 1980). As for circular dichroism it is necessary to go beyond the electric dipole approximation and to include the coupling associated with the spatial variation of the vector potential. In the multipolar formalism, the leading terms from the variation are the magnetic dipole and electric quadrupole interactions. The appropriate interaction energy operator is

$$H_{\text{int}} = -\epsilon_0^{-1}\boldsymbol{\mu}\cdot\mathbf{d}^{\perp} - \epsilon_0^{-1}\mathbf{Q}:\nabla\mathbf{d}^{\perp} - \mathbf{m}\cdot\mathbf{b} \tag{153}$$

The time-ordered graphs have the same structure as those for the conventional Raman effect (Section III,F) but are now supplemented to include all possible combinations of vertex interactions of the three terms of H_{int} in Eq. (153). We have seen in the previous section that if both vertices are of the electric dipole type, there is no discrimination in the scattered intensity. However, matrix elements from graphs with one electric dipole vertex and one magnetic dipole or electric quadrupole vertex can give contributions that depend on the handedness of the incident beam. Proceeding as before, the electric dipole–magnetic dipole contribution to the transition matrix element is found to be

$$M_{fi}(G) = -(\hbar k/2\epsilon_0 V)n^{1/2}G_{ij}^{ov',ov}\{(\bar{e}_i'(\hat{\mathbf{k}}\times\mathbf{e})_j - e_i(\hat{\mathbf{k}}'\times\mathbf{e}')_j\} \tag{154}$$

where

$$G_{ij}^{ov',ov} = \langle\chi_{ov'}|G_{ij}|\chi_{ov}\rangle \tag{155}$$

and χ_{ov} is the vth quantum state of a normal vibration in the ground electronic state and G_{ij} is the electric–magnetic analog of the electric dipole polarizability tensor α_{ij},

$$G_{ij} = \sum_r \left\{\frac{\mu_i^{or}m_j^{ro}}{E_{ro} - \hbar ck} + \frac{m_j^{or}\mu_i^{ro}}{E_{ro} + \hbar ck}\right\} \tag{156}$$

There is an analogous expression for the combination of electric dipole and electric quadrupole interactions

$$M_{fi}(A) = -\left(\frac{i\hbar ck^2}{2\epsilon_0 V}\right)n^{1/2}A_{ijk}^{ov',ov}\left\{\bar{e}_i'e_j\hat{k}_k - e_i\bar{e}_j'\hat{k}_k'\right\} \tag{157}$$

where

$$A_{ijk}^{ov',ov} = \langle\chi_{ov'}|A_{ijk}|\chi_{ov}\rangle \tag{158}$$

and A_{ijk} is the electric dipole–quadrupole polarizability tensor

$$A_{ijk} = \sum_r \left\{\frac{\mu_i^{or}Q_{jk}^{ro}}{E_{ro} - \hbar ck} + \frac{Q_{jk}^{or}\mu_i^{ro}}{E_{ro} + \hbar ck}\right\} \tag{159}$$

The scattering rate is proportional to the squared modulus of the contributions to the matrix element and is given by

$$\begin{aligned}\Gamma &= (2\pi/\hbar)|M_{fi}(\alpha) + M_{fi}(G) + M_{fi}(A)|^2\rho \\ &\approx (2\pi/\hbar)\{|M_{fi}(\alpha)|^2 + M_{fi}(\alpha)\bar{M}_{fi}(G) + \bar{M}_{fi}(\alpha)M_{fi}(G) \\ &\quad + M_{fi}(\alpha)\bar{M}_{fi}(A) + \bar{M}_{fi}(\alpha)M_{fi}(A)\}\rho\end{aligned} \tag{160}$$

where $M_R(\alpha)$ is the electric dipole–dipole matrix element already given for the conventional Raman effect in Eq. (143). Thus we see that in Eq. (160), the first term is the pure electric dipole contribution, and following terms contain the leading interferences between the different transition amplitudes. The pure magnetic dipole and pure electric quadrupole terms are of higher order and have been omitted. Following the procedure of Section III,F, including use of the radiant density I and taking the random orientational average, we find from Eq. (160) that the scattered intensity may be partitioned into a pure electric part (first term, independent of handedness) and two terms which change sign between left- and right-handed light:

$$I = I(\alpha\alpha) + I(\alpha G) + I(\alpha A) \tag{161}$$

where

$$\begin{aligned} I(\alpha G) = &- \frac{2N_v I k'^4}{c(4\pi\epsilon_0)^2} \bar{e}_i' e_j \{ e_k' (\hat{\mathbf{k}} \times \bar{\mathbf{e}})_l \\ &- \bar{e}_k (\hat{\mathbf{k}}' \times \mathbf{e}')_l \} \langle \alpha_{ij}^{ov',ov} G_{kl}^{ov',ov} \rangle \end{aligned} \tag{162}$$

$$I(\alpha A) = \frac{2iN_v I k'^5}{(4\pi\epsilon_0)^2} \bar{e}_i' e_j (e_k' \bar{e}_l \hat{k}_m - \bar{e}_k e_l' \hat{k}_m') \langle \alpha_{ij}^{ov',ov} A_{klm}^{ov',ov} \rangle \tag{163}$$

In experiments on differential scattering, observations are usually made for the case where the polarization of the scattered photon $\mathbf{e}'$ is either in the $\hat{\mathbf{k}}\hat{\mathbf{k}}'$ plane or normal to it. We denote the former by $\mathbf{e}^{\parallel}$ and the latter by $\mathbf{e}^{\perp}$. The three unit vectors $\mathbf{e}^{\parallel}$, $\mathbf{e}^{\perp}$, and $\hat{\mathbf{k}}'$ form a right-handed triad. The differential scattering intensity,

$$\Delta_\mu I(\theta) = I_\theta(\mathrm{R} \rightarrow \mu) - I_\theta(\mathrm{L} \rightarrow \mu) \tag{164}$$

is linearly dependent on the intensity of the incident radiation. $I_\theta(\mathrm{L/R} \rightarrow \mu)$ denotes the intensity of light with polarization μ scattered from a left/right-hand incident beam; θ is $\cos^{-1}(-\hat{\mathbf{k}} \cdot \hat{\mathbf{k}}')$. The experimental results are commonly given as the ratio of the circular intensity differential (165), independent of incident intensity,

$$\Delta_\mu(\theta) = [I_\theta(\mathrm{R} \rightarrow \mu) - I_\theta(\mathrm{L} \rightarrow \mu)]/[I_\theta(\mathrm{R} \rightarrow \mu) + I_\theta(\mathrm{L} \rightarrow \mu)] \tag{165}$$

In terms of the parallel and perpendicular photon polarizations the differential ratios are

$$\Delta_\parallel(\theta) = \frac{\alpha + \beta \cos\theta + \gamma \cos^2\theta}{\delta + \epsilon \cos^2\theta}, \qquad \Delta_\perp(\theta) = \frac{\alpha + \gamma + \beta \cos\theta}{\delta + \epsilon} \tag{166}$$

where

$$\alpha = (4/3c)(9\alpha_{\lambda\mu}^{(2)} \tilde{G}_{\lambda\mu}^{(2)} - \omega\alpha_{\lambda\mu}^{(2)} A_{\lambda,\mu}^{(2)})$$

$$\beta = (2/3c)(-10\alpha^{(0)}_{\lambda\lambda}\tilde{G}^{(0)}_{\mu\mu} + 15\alpha^{(2)}_{\lambda\mu}\tilde{G}^{(2)}_{\lambda\mu} + 3\omega\alpha^{(2)}_{\lambda\mu}A^{(2)}_{\lambda\mu})$$

$$\gamma = (2/3c)(10\alpha^{(0)}_{\lambda\lambda}\tilde{G}^{(0)}_{\mu\mu} + 3\alpha^{(2)}_{\lambda\mu}\tilde{G}^{(2)}_{\lambda\mu} + 3\omega\alpha^{(2)}_{\lambda\mu}A^{(2)}_{\lambda\mu})$$

$$\delta = 6\alpha^{(2)}_{\lambda\mu}\alpha^{(2)}_{\lambda\mu}, \qquad \epsilon = \tfrac{1}{3}(10\alpha^{(0)}_{\lambda\lambda}\alpha^{(0)}_{\mu\mu} + 3\alpha^{(2)}_{\lambda\mu}\alpha^{(2)}_{\lambda\mu})$$

with $A_{\lambda\mu} = \epsilon_{\lambda\rho\sigma}A_{\rho\sigma\mu}$ and $\tilde{G}_{\lambda\mu} = \text{Im } G_{\lambda\mu}$. From a knowledge of these constants it is possible to evaluate the molecular tensor products $\alpha^{(0)}_{\lambda\lambda}\tilde{G}^{(0)}_{\mu\mu}$, $\alpha^{(2)}_{\lambda\mu}\tilde{G}^{(2)}_{\lambda\mu}$, and $\alpha^{(2)}_{\lambda\mu}A^{(2)}_{\lambda\mu}$, which may also be calculated theoretically, as for example, using an atom–dipole interaction model (Prasad and Burow, 1979a,b).

H. Hyper-Raman Scattering

The usual Rayleigh (elastic) and Raman (inelastic) scattering from molecules are two-photon processes, the latter of which has been discussed in Section III,F. When the incident beam is sufficiently intense, as in a coherent laser beam, there are in addition higher order nonlinear processes. The best known is second-harmonic generation in a noncentrosymmetric system, in which light of an incident frequency ω causes some light emission at 2ω in a three-photon process, two ω photons being absorbed and one 2ω photon emitted in the forward direction.

A related nonlinear effect is hyper-Raman scattering where the scattered photon has frequency ω', approximately twice the incident frequency ω. The mismatch $|2\omega - \omega'|$ equals a vibrational or rotational transition frequency of the molecule or a lattice vibrational frequency in a crystal. Such a nonlinear scattering process was first considered by Decius and Rauch (1959) and the first experimental observations made by Terhune *et al.* (1965). For a beam of intensity 10^{15} Wm^{-2} the ratio of hyper-Raman to Raman intensity is in the order of 10^{-6}, and pulsed lasers have made observations of hyper-Raman scattering feasible. Also, multichannel spectrometers have much reduced the time required to record a hyper-Raman spectrum. Molecules that have been studied include methane, ethane, and ethylene (Verdieck *et al.*, 1970), carbon tetrachloride, chloroform and water (French and Long, 1975), and tetrachloroethylene (Schmid and Schrötter, 1977). Hyper-Raman spectroscopy can be a source of molecular information not normally available from IR or Raman studies, by exploiting different selection rules, governed by the symmetry properties of the hyperpolarizability tensor. Hyper-Raman scattering in quantum electrodynamics is a three-photon process, the leading contribution to the transition matrix element being of third order in the interaction (Andrews and Thirunamachandran, 1978c). The time-ordered graphs in Fig. 6 show the absorption of two identical photons $(\mathbf{k}, \lambda)$ and the emission of one photon $(\mathbf{k}', \lambda')$, where $\omega = \hbar ck$ and

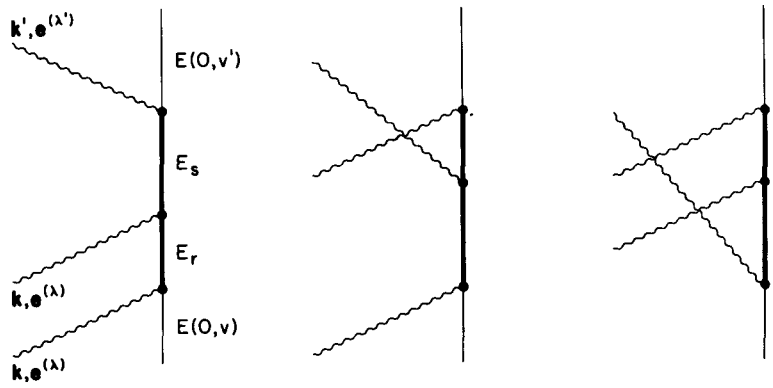

Fig. 6. Hyper-Raman scattering.

$\omega' = \hbar ck'$. As for the Raman effect, we use the Born–Oppenheimer approximation for the molecular states. In the initial and final states $|0, v\rangle$ and $|0, v'\rangle$, the molecule is in its ground electronic state and has v and v' quanta of a particular vibrational mode. The populations of all other modes are unchanged. The radiation field states are $|n(\mathbf{k}, \lambda); 0(\mathbf{k}', \lambda')\rangle$ and $|(n-2)(\mathbf{k}, \lambda); 1(\mathbf{k}', \lambda')\rangle$, with energy conservation:

$$E_{ov'} - \epsilon_{ov} = \hbar(2\omega - \omega')$$

The matrix element in the electric dipole approximation is

$$\begin{aligned} M_{fi} = -i \left[\frac{\hbar^3\omega^2\omega' n(n-1)}{8\epsilon_0^3 V^3}\right]^{1/2} & \bar{e}_i' e_j e_k \\ \times \sum_{\substack{r,R \\ s,S}} \Bigg\{ & \frac{\langle \chi_{ov'}|\mu_i^{os}|\chi_{sS}\rangle\langle\chi_{sS}|\mu_j^{sr}|\chi_{rR}\rangle\langle\chi_{rR}|\mu_k^{ro}|\chi_{ov}\rangle}{(E_{so} + \epsilon_{sS,ov} - 2\hbar\omega)(E_{ro} + E_{rR,ov} - \hbar\omega)} \\ + & \frac{\langle \chi_{ov'}|\mu_j^{os}|\chi_{sS}\rangle\langle\chi_{sS}|\mu_i^{sr}|\chi_{rR}\rangle\langle\chi_{rR}|\mu_k^{ro}|\chi_{ov}\rangle}{(E_{so} + \epsilon_{sS,ov'} + \hbar\omega)(E_{ro} + \epsilon_{rR,ov} - \hbar\omega)} \\ + & \frac{\langle \chi_{ov'}|\mu_j^{os}|\chi_{sS}\rangle\langle\chi_{sS}|\mu_k^{sr}|\chi_{rR}\rangle\langle\chi_{rR}|\mu_i^{ro}|\chi_{ov}\rangle}{(E_{so} + \epsilon_{sS,ov'} + \hbar\omega)(E_{ro} + \epsilon_{rR,ov'} + 2\hbar\omega)} \Bigg\} \end{aligned} \tag{167}$$

If none of the denominators is small compared with a vibrational spacing, we can simplify the expression as in the theory of the ordinary Raman effect (Section III,F) by neglecting the vibrational intervals ϵ. Closure on the vibrational levels in the sums over intermediate states gives for the matrix element

$$M_{fi} = -i \left[\frac{\hbar^3\omega^2\omega' n(n-1)}{8\epsilon_0^3 V^3}\right]^{1/2} \bar{e}_i' e_j e_k \langle \chi_{ov'}|\beta_{ijk}|\chi_{ov}\rangle \tag{168}$$

where

$$\beta_{ijk} = \frac{1}{2}\sum_{r,s}\left[\frac{\mu_i^{os}\mu_j^{sr}\mu_k^{ro}}{(E_{so}-2\hbar\omega)(E_{ro}-\hbar\omega)} + \frac{\mu_j^{os}\mu_i^{sr}\mu_k^{ro}}{(E_{so}+\hbar\omega)(E_{ro}-\hbar\omega)}\right.$$
$$+ \frac{\mu_j^{os}\mu_k^{sr}\mu_i^{ro}}{(E_{so}+\hbar\omega)(E_{ro}+2\hbar\omega)} + \frac{\mu_i^{os}\mu_k^{sr}\mu_j^{ro}}{(E_{so}-2\hbar\omega)(E_{ro}-\hbar\omega)}$$
$$\left. + \frac{\mu_k^{os}\mu_i^{sr}\mu_j^{ro}}{(E_{so}+\hbar\omega)(E_{ro}-\hbar\omega)} + \frac{\mu_k^{os}\mu_j^{sr}\mu_i^{ro}}{(E_{so}+\hbar\omega)(E_{ro}+2\hbar\omega)}\right] \tag{169}$$

With the form chosen for the hyperpolarizability tensor β_{ijk} the matrix element as a whole is symmetric to interchange of the indices j, k. It is now readily found that the scattered radiant intensity, calculated from the Fermi rule and the matrix element (168) is

$$I(\mathbf{k}') = \frac{2\pi}{105c}\frac{N_v k'^4 \bar{I}^2 g^{(2)}}{(4\pi\epsilon_0)^3}$$
$$\times\{[30(\bar{\mathbf{e}}'\cdot\mathbf{e})(\mathbf{e}\cdot\mathbf{e}')(\bar{\mathbf{e}}\cdot\bar{\mathbf{e}}) - 12(\bar{\mathbf{e}}'\cdot\mathbf{e})(\mathbf{e}'\cdot\bar{\mathbf{e}})$$
$$-12(\mathbf{e}\cdot\mathbf{e}')(\bar{\mathbf{e}}'\cdot\bar{\mathbf{e}}) - 10(\mathbf{e}\cdot\mathbf{e}) - (\bar{\mathbf{e}}\cdot\bar{\mathbf{e}}) + 8]\beta_{\lambda\lambda\mu}\beta_{\mu\nu\nu}$$
$$+[-12(\bar{\mathbf{e}}'\cdot\mathbf{e})(\mathbf{e}\cdot\mathbf{e}')(\bar{\mathbf{e}}\cdot\bar{\mathbf{e}}) + 16(\bar{\mathbf{e}}'\cdot\mathbf{e})(\mathbf{e}'\cdot\bar{\mathbf{e}})$$
$$+2(\mathbf{e}\cdot\mathbf{e}')(\bar{\mathbf{e}}'\cdot\bar{\mathbf{e}}) + 4(\mathbf{e}\cdot\mathbf{e})(\bar{\mathbf{e}}\cdot\bar{\mathbf{e}}) - 6]\beta_{\lambda\lambda\mu}\beta_{\nu\nu\mu}$$
$$+[-10(\bar{\mathbf{e}}'\cdot\mathbf{e})(\mathbf{e}\cdot\mathbf{e}')(\bar{\mathbf{e}}\cdot\bar{\mathbf{e}}) + 4(\bar{\mathbf{e}}'\cdot\mathbf{e})(\mathbf{e}'\cdot\bar{\mathbf{e}})$$
$$+ 4(\mathbf{e}\cdot\mathbf{e}')(\bar{\mathbf{e}}'\cdot\bar{\mathbf{e}}) + 8(\mathbf{e}\cdot\mathbf{e})(\bar{\mathbf{e}}\cdot\bar{\mathbf{e}}) - 5]\beta_{\lambda\mu\mu}\beta_{\lambda\nu\nu}$$
$$+[8(\bar{\mathbf{e}}'\cdot\mathbf{e})(\mathbf{e}\cdot\mathbf{e}')(\bar{\mathbf{e}}\cdot\bar{\mathbf{e}}) - 6(\bar{\mathbf{e}}'\cdot\mathbf{e})(\mathbf{e}'\cdot\bar{\mathbf{e}})$$
$$-6(\mathbf{e}\cdot\mathbf{e}')(\bar{\mathbf{e}}'\cdot\bar{\mathbf{e}}) - 5(\mathbf{e}\cdot\mathbf{e})(\bar{\mathbf{e}}\cdot\bar{\mathbf{e}}) + 11]\beta_{\lambda\mu\nu}\beta_{\lambda\mu\nu}$$
$$+[-12(\bar{\mathbf{e}}'\cdot\mathbf{e})(\mathbf{e}\cdot\mathbf{e}')(\bar{\mathbf{e}}\cdot\bar{\mathbf{e}}) + 2(\bar{\mathbf{e}}'\cdot\mathbf{e})(\mathbf{e}'\cdot\bar{\mathbf{e}})$$
$$+16(\mathbf{e}\cdot\mathbf{e}')(\bar{\mathbf{e}}'\cdot\bar{\mathbf{e}}) + 4(\mathbf{e}\cdot\mathbf{e})(\bar{\mathbf{e}}\cdot\bar{\mathbf{e}}) - 6]\beta_{\lambda\mu\nu}\beta_{\mu\lambda\nu}\} \tag{170}$$

where $g^{(2)}$ is the second-degree coherence (140) and $\bar{I}$ the mean irradiance of the incident beam. The superscripts of the molecule tensors have been suppressed:

$$\beta_{\lambda\mu\nu} = \langle\chi_{ov'}|\beta_{\lambda\mu\nu}|\chi_{ov}\rangle \tag{171}$$

Selection rules for activity in the hyper-Raman effect of vibrations of the various symmetry species can be found from the transformation properties of the tensor $\beta_{\lambda\mu\nu}$. A general tensor of rank 3 has 27 independent components, which are reduced to 18 by μ, ν symmetry. Reduction to irreducible components, according to their weights (orders of the covering associated Legendre polynomials in a spherical system), gives two terms of weight 1, one of weight 2, and one of weight 3, with six, five, and seven

irreducible components, respectively. Explicit expressions for these components may be found in the reference cited above. The irreducible representations spanned by these components for molecules of point group symmetry D_{5h}, D_{6h}, D_{4d}, D_{6d}, O_h, I_h, and $D_{\infty h}$ are listed in Table I. For comparison, the irreducible representations of the electric dipole moment and polarizability are also listed in Table I. The corresponding representations for point groups of lower symmetry are easily obtained from correlation tables (Wilson *et al.*, 1955). Thus, for example, in group D_{2h} which applies to the common hydrocarbons naphthalene, anthracene, and tetracene, the components of weight 1 are $2B_{1u} + 2B_{2u} + 2B_{3u}$, those of weight 2 are $2A_{2u} + B_{1u} + B_{2u} + B_{3u}$, and those of weight 3 are $A_u + 2B_{1u} + 2B_{2u} + 2B_{3u}$. Some interesting points emerge: all IR active modes are also hyper-Raman active because the weight-1 components of the β-tensor transform like the electric dipole moment; for centrosymmetric molecules, hyper-Raman active modes are of *ungerade* symmetry and are therefore Raman inactive. For noncentrosymmetric molecules, vibrational modes with the same symmetry as a weight-2 component of the β-tensor can be Raman active. This is a necessary requirement, but is not sufficient because the weight-2 components of the Raman and hyper-Raman tensors, in general, transform differently under reflection. For example, the symmetry properties of the weight-2 components for a molecule belonging to D_{4d} show that only E_2 is both Raman and hyper-Raman active. However in pure rotation (chiral) groups hyper-Raman active modes with weight-2 symmetry are also Raman active. Hyper-Raman active modes may be classified into six types, and by measuring the hyper-Raman spectra for five specified configurations, it is possible to assign an active mode to one of the six classes. (Details may be found in the paper cited earlier.)

The possibility that chiral molecules may exhibit a circular differential effect in hyper-Raman scattering has been discussed by Andrews and Thirunamachandran (1979). The theory follows the same lines as that for circular differential Raman scattering and uses Eq. (153) for the interaction term in the calculation of the circular intensity differential ratios.

IV. Interactions between Molecules

A unifying feature of quantum electrodynamics is its power to deal with the interactions between atoms and molecules in the same theoretical framework as for interactions between radiation and matter. We saw earlier that in the multipolar framework two molecules A and B interact only *via* the exchange between them of transverse photons real or virtual and that this process is on exactly the same theoretical footing as the interac-

TABLE I

SELECTION RULES FOR INFRARED, RAMAN, AND HYPER-RAMAN ACTIVITY[a]

Group	Infrared, μ (weight 1)	Raman		Hyper-Raman		
		α (weight 0)	α (weight 2)	β (weight 1)	β (weight 2)	β (weight 3)
D_{5h}	$A_2'' + E_1'$	A_1'	$A_1' + E_2' + E_1''$	$2A_2'' + 2E_1'$	$A_1'' + E_1' + E_2''$	$A_2'' + E_1' + E_2' + E_2''$
D_{6h}	$A_{2u} + E_{1u}$	A_{1g}	$A_{1g} + E_{1g} + E_{2g}$	$2A_{2u} + 2E_{1u}$	$A_{1u} + E_{1u} + E_{2u}$	$A_{2u} + B_{1u} + B_{2u} + E_{1u} + E_{2u}$
D_{4d}	$B_2 + E_1$	A_1	$A_1 + E_2 + E_3$	$2B_2 + 2E_1$	$B_1 + E_1 + E_2$	$B_2 + E_1 + E_2 + E_3$
D_{6d}	$B_2 + E_1$	A_1	$A_1 + E_2 + E_5$	$2B_2 + 2E_1$	$B_1 + E_1 + E_4$	$B_2 + E_1 + E_3 + E_4$
O_h	T_{1u}	A_{1g}	$E_g + T_{2g}$	$2T_{1u}$	$T_{2u} + E_u$	$A_{2u} + T_{1u} + T_{2u}$
I_h	T_{1u}	A_g	H_g	$2T_{1u}$	H_u	$T_{2u} + G_u$
$D_{\infty h}$	$\Sigma_u^+ + \Pi_u$	Σ_g^+	$\Sigma_g^+ + \Pi_g + \Delta_g$	$2\Sigma_u^+ + 2\Pi_u$	$\Sigma_u^- + \Pi_u + \Delta_u$	$\Sigma_u^+ + \Pi_u + \Delta_u + \Phi_u$

[a] The irreducible representations of the dipole moment $\boldsymbol{\mu}$, the polarizability $\boldsymbol{\alpha}$, and hyperpolarizability $\boldsymbol{\beta}$, are listed in key symmetry groups (Andrews and Thirunamachandran, 1978c).

tion between a molecule and a radiation field, as in a real emission or absorption. Thus if we write for the Hamiltonian of molecules A and B coupled to a radiation field in dipole approximation (Section II,G),

$$H = H_{\text{rad}} + H_{\text{A}} + H_{\text{B}} - \epsilon_0^{-1}\boldsymbol{\mu}(\text{A})\cdot\mathbf{d}^{\perp}(\mathbf{R}_{\text{A}}) - \epsilon_0^{-1}\boldsymbol{\mu}(\text{B})\cdot\mathbf{d}^{\perp}(\mathbf{R}_{\text{B}})$$

we find that the energy calculated for a state contains a term for the coupling of A to B that is not from a direct coupling operator in the Hamiltonian but appears in second order as a consequence of their being individually coupled to common modes of the electromagnetic field. Such interactions do not involve an overall change in the state of the radiation, but there are other processes where there is a net change, such as induced circular dichroism, in which circular dichroism appears in one molecule as the result of its interactions with a second molecule, and radiation-induced contributions to the intermolecular energy; both types are considered later.

Intermolecular forces such as the dispersion interaction were first found by perturbation theory in the electrostatic limit (molecular separation much less than a characteristic molecular transition wavelength). The importance of electromagnetic interactions (those mediated by the electromagnetic field propagated with the speed of light) was by the calculation of long-range dispersion interactions by Casimir and Polder (1948) which gave the remarkable result that, for distances beyond that of a characteristic wavelength, the short-range behavior according to R^{-6}, where R is the molecular separation, was replaced at long range by R^{-7}. The change is associated with retardation, namely, the delay by time R/c between the emission and absorption of the transverse photons "conveying" the interactions. Earlier, experimenters (see Vervey, 1947) had suggested the need for a shorter range force to explain observations in colloid science; and after Casimir and Polder's work the correctness of the R^{-7} law was confirmed (Tabor and Winterton, 1969). The dispersion interaction result and its experimental confirmation give the most direct evidence for the reality of retardation effects, which are illustrated first in the simplest case, that of resonance coupling.

A. Resonance Coupling in Dipole Approximation

Two identical molecules, one in an excited state, are coupled together by the exchange of the single excitation. One cannot say which molecule is excited; there is an excited molecule pair which may exist in two distinct states. In some cases the states have different symmetry properties, and it may be that only one of the two can be directly produced by photon absorption. The transfer of excitation is often given a formalism that is analogous to that for the motion of particles and is described as the motion

of an *exciton*. It has a particular practical importance in the excited states of molecular crystals, the exciton being delocalized over a large number of identical molecules with quantization governed by a wave vector and described by Bloch waves.

The simple system of two identical atoms also has practical importance; for example, in work on superradiance (Dicke, 1954). In some applications the two-body system appears in absorption, i.e., where a photon is absorbed by the pair and one wants to know the nature of the final state with one quantum of excitation. In other applications the problem (e.g., superradiance) is the emission from a pair which has been excited at some earlier time. Here we shall not consider the absorption process, but assume that the pair already has one unit of excitation, calculate the matrix element for excitation transfer, and so find the energy shift.

To illustrate one aspect, the effect of retardation, we at first suppress the quantum aspects and use a classical argument. If the excitation energy of each coupled system is $\hbar\omega = \hbar ck$, the classical analog is an oscillating electric dipole of frequency ω. We now calculate the interaction energy of excited system A with the unexcited system B, which has the same characteristic frequency ω. First making the calculation without allowing retardation, i.e., infinitely fast propagation of electric influences, we find for the electric field at B produced by the oscillating dipole at A,

$$E_i^{(B)} = -(4\pi\epsilon_0)^{-1}\mu_j(A)(\delta_{ij} - 3\hat{R}_i\hat{R}_j)/R^3 \tag{172}$$

The time dependence $e^{i\omega t}$ is not included; R is the A–B distance; and $\boldsymbol{\mu}(A)$ is the polarization for excited A.

The energy of coupling of this field to the system B is

$$\Delta E = (4\pi\epsilon_0)^{-1}R^{-3}\mu_i(A)\mu_j(B)(\delta_{ij} - 3\hat{R}_i\hat{R}_j) \tag{173}$$

which has the same form as the familiar dipole–dipole coupling of permanent moments.

Retardation is allowed for by calculating in place of the static field (172) the full Maxwell field at B caused by the classical oscillating charge at A. Then

$$\begin{aligned} E_i^{(B)} = (4\pi\epsilon_0)^{-1}\mu_j(A)e^{ikR}\{&(k^2/R)(\delta_{ij} - \hat{R}_i\hat{R}_j) \\ &+ [(ik/R^2) - R^{-3}](\delta_{ij} - 3\hat{R}_i\hat{R}_j)\} \end{aligned} \tag{174}$$

The retarded interaction with system B is

$$\begin{aligned} \Delta E_{\text{ret}} = -(4\pi\epsilon_0)^{-1}\mu_i(A)\mu_j(B)\Bigg\{&\frac{k^2\cos kR}{R}(\delta_{ij} - \hat{R}_i\hat{R}_j) \\ &- \left(\frac{\cos kR}{R^3} + \frac{k\sin kR}{R^2}\right)(\delta_{ij} - 3\hat{R}_i\hat{R}_j)\Bigg\} \end{aligned} \tag{175}$$

This result is the same as that obtained properly through quantum electrodynamics, as shall be seen. For small kR (the "near zone"), ΔE_{ret} is indistinguishable from the static ΔE. For large kR (the "wave zone"), the only first term remains, giving a coupling that falls off as R^{-1}. From the angular dependence it is seen that only the components of moments transverse to the join $\mathbf{R}$ contribute; the electric field in Eq. (175) is pure transverse at large enough distances from A, being the pure radiation field of classical electromagnetism. Clasically one can speak of a change of phase proportional to the distance between the field of the emitter and the response it causes in the absorber, and there is sometimes an attempt to explain the effects of retardation as coming from "dephasing." In quantum theory, however, the (absolute) phase and the number of photons in a mode are noncommuting variables and care is required. In this particular case only the phase difference between two systems is at issue, and there is no difficulty.

To deal with resonance coupling in quantum electrodynamics, we suppose A and B to be identical molecules,with nondegenerate ground and excited states $|E_0\rangle$ and $|E_n\rangle$ connected by an electric dipole transition with moment $\boldsymbol{\mu}^{0n}$. The states $|E_n^{\text{A}}, E_0^{\text{B}}\rangle$ and $|E_0^{\text{A}}, E_n^{\text{B}}\rangle$ of the molecular pair are degenerate, the rate of excitation transfer between the two states, from a time-dependence point of view, and the energy shift, from a stationary state point of view, both depend on the matrix element

$$M = \langle E_n^{\text{B}}, E_0^{\text{A}}|H_{\text{int}}(E - H_0)^{-1}H_{\text{int}}|E_n^{\text{A}}, E_0^{\text{B}}\rangle \tag{176}$$

where

$$H_{\text{int}} = -\epsilon_0^{-1}\boldsymbol{\mu}(\text{A})\cdot\mathbf{d}_{\perp}(\mathbf{R}_{\text{A}}) - \epsilon_0^{-1}\boldsymbol{\mu}(\text{B})\cdot\mathbf{d}^{\perp}(\mathbf{R}_{\text{B}}) \tag{177}$$

The frequency Ω of excitation exchange is $|M|/\hbar$; where Ω is less than the frequencies of other processes in the two molecules, such as intra- or intermolecular vibrations, or the emission rate, the role of H_{int} as a time-dependent perturbation is important. Where Ω^{-1} is short compared with these processes, or with the resolving time of an experiment, H_{int} is a stationary perturbation. In this case the excitation is delocalized over the coupled molecules, and the states are given in the linear combinations

$$\Phi_{\pm} = 2^{-1/2}\{|E_n^{\text{A}}, E_0^{\text{B}}\rangle \pm |E_0^{\text{A}}, E_n^{\text{B}}\rangle\} \tag{178}$$

To find the matrix element M the usual procedure is followed, using the graphs in Fig. 7. From the left-hand graph,

$$\sum_{\mathbf{p},\lambda}\left(\frac{\hbar cp}{2\epsilon_0 V}\right)\bar{e}_i^{(\lambda)}(\mathbf{p})e_j^{(\lambda)}(\mathbf{p})\mu_i^{0n}(\text{A})\mu_j^{n0}(\text{B})\frac{e^{i\mathbf{p}\cdot\mathbf{R}}}{E_{n0} - \hbar cp} \tag{179}$$

where $\mathbf{R} = \mathbf{R}_{\text{A}} - \mathbf{R}_{\text{B}}$ is the intermolecular separation. The sum over the photon wave vectors $\mathbf{p}$ is converted to an integral,

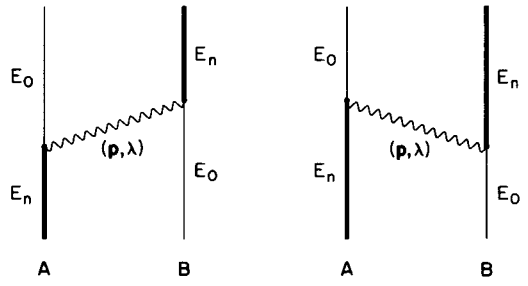

Fig. 7. Resonance coupling.

$$\frac{1}{V}\sum_{\mathbf{p}} \rightarrow \frac{1}{(2\pi)^3}\int d^3\mathbf{p} \tag{180}$$

and the λ sum (polarization sum) is

$$\sum_{\lambda} e_i^{(\lambda)}(\mathbf{p})\bar{e}_j^{(\lambda)}(\mathbf{p}) = \delta_{ij} - \hat{p}_i\hat{p}_j \tag{181}$$

so that the contribution (178) to the matrix element becomes

$$\frac{\mu_i^{0n}(\mathrm{A})\mu_j^{n0}(\mathrm{B})}{2\epsilon_0}\int p(\delta_{ij} - \hat{p}_i\hat{p}_j)\frac{e^{i\mathbf{p}\cdot\mathbf{R}}}{k-p}\frac{d^3\mathbf{p}}{(2\pi)^3} \tag{182}$$

where $k = E_{n0}/\hbar c$. For the right-hand graph the denominator is $-(E_{n0} + \hbar cp)$, and the total matrix element is

$$M = \frac{\mu_i^{0n}(\mathrm{A})\mu_j^{n0}(\mathrm{B})}{2\epsilon_0}\int p(\delta_{ij} - \hat{p}_i\hat{p}_j)\left(\frac{e^{i\mathbf{p}\cdot\mathbf{R}}}{k-p} - \frac{e^{-i\mathbf{p}\cdot\mathbf{R}}}{k+p}\right)\frac{d^3\mathbf{p}}{(2\pi)^3} \tag{183}$$

Integration leads to

$$M = \mu_i^{0n}(\mathrm{A})\mu_j^{n0}(\mathrm{B})V_{ij}(k, \mathbf{R}) \tag{184}$$

in which $V_{ij}(k, \mathbf{R})$ is the tensor potential for the retarted interaction (McLone and Power, 1964),

$$\begin{aligned} V_{ij}(k, \mathbf{R}) = (4\pi\epsilon_0 R^3)^{-1}[&(\delta_{ij} - 3\hat{R}_i\hat{R}_j)(\cos kR + kR\sin kR) \\ &- (\delta_{ij} - \hat{R}_i\hat{R}_j)k^2R^2\cos kR] \end{aligned} \tag{185}$$

The stationary states (178) apply when other internal processes, such as molecular vibrations, are slow compared with the excitation transfer rate. Likewise, if the system is probed by a pulse of picosecond width, the response will be approximately that of localized systems for transfer rates less than 10^{12} sec^{-1} and of pair stationary states for higher transfer rates.

Where transfer is fast compared with the spontaneous emission rate of the free molecule, and no other processes intervene, the emitting species are the stationary states (178). If the symmetry allows emission only from one such state, the line strength is twice that of the free molecule, and the natural lifetime is reduced to one-half, the pair being superradiant (Stephen, 1964; Power, 1967b).

An interesting feature of Eq. (185) for the resonance coupling energy is that as either the separation distance R or the wave number k or both decrease, so that $kR \ll 1$, we have

$$\lim_{kR\to 0} V_{ij}(k, \mathbf{R}) = (4\pi\epsilon_0 R^3)^{-1}(\delta_{ij} - 3\hat{R}_i\hat{R}_j)$$

which is the near-zone interaction. For $k = 0$ the transition moments go over into permanent moments and Eq. (185), as $V_{ij}(0, \mathbf{R})$, is the well-known static coupling of permanent dipoles. The result can be found directly, without recourse to a limit argument, from the graphs of Fig. 7 after replacing the state $|E_n\rangle$ by the ground state $|E_0\rangle$. The calculation is a striking reminder that in the multipolar framework all intermolecular interactions are via transverse photons (here virtual), which include interactions between permanent moments.

In the far zone, $kR \gg 1$, the potential is given by

$$V_{ij}(k, \mathbf{R}) \simeq -\frac{k^2}{4\pi\epsilon_0 R}(\delta_{ij} - \hat{R}_i\hat{R}_j)\cos kR \tag{187}$$

in which the distance dependence is as R^{-1} with a modulation of period $2\pi/k$.

B. The Dispersion Interaction

In resonance coupling (Section IV,A) the effect of retardation on the range of the interaction is to add terms in R^{-2} and R^{-1}, the latter becoming dominant at long distance. Thus the range becomes longer, mirroring the increasing importance in the emitting molecule's Maxwell field of the transverse component ($\sim R^{-1}$). In the dispersion interaction, however, at long distance an R^{-7} dependence on distance replaces the R^{-6} dependence characteristic of the contribution by static dipolar coupling.

The attraction between molecules in their ground state was discussed by London (1930) in terms of virtual molecular transitions. A spontaneous dipolar fluctuation in molecule A induced a dipole moment in B, which in turn acted back on A with an overall distance dependence of R^{-6}.

From the quantum electrodynamical viewpoint the dispersion interaction arises from two-photon exchange. The energy shift is fourth order in H_{int} and is given by

$$E = -\sum_{\mathrm{I,II,III}}{}' \frac{\langle 0|H_{\mathrm{int}}|\mathrm{III}\rangle\langle \mathrm{III}|H_{\mathrm{int}}|\mathrm{II}\rangle\langle \mathrm{II}|H_{\mathrm{int}}|\mathrm{I}\rangle\langle \mathrm{I}|H_{\mathrm{int}}|0\rangle}{(E_{\mathrm{I}} - E_0)(E_{\mathrm{II}} - E_0)(E_{\mathrm{III}} - E_0)}$$
$$+ \sum_{\mathrm{I,II}} \frac{\langle 0|H_{\mathrm{int}}|\mathrm{II}\rangle\langle \mathrm{II}|H_{\mathrm{int}}|0\rangle\langle 0|H_{\mathrm{int}}|\mathrm{I}\rangle\langle \mathrm{I}|H_{\mathrm{int}}|0\rangle}{(E_{\mathrm{I}} - E_0)^2(E_{\mathrm{II}} - E_0)} \tag{188}$$

the second term arising from wave-function renormalization. For nonpolar molecules this term does not contribute to intermolecular coupling and attention is confined to the first term. The ket vector $|0\rangle$ is the unperturbed ground state of the system where both molecules are in their ground states and the radiation field is in the vacuum state. The intermediate states I, II, and III are of four types: (1) both molecules excited and no photons present, (2) one molecule excited with one virtual photon present, (3) both molecules in the ground state with two virtual photons present, and (4) both molecules excited with two virtual photons present. The graphs in Fig. 8 contribute to the fourth-order interaction energy. From graph (i) the contribution to the energy shift is

$$-\sum_{\substack{\mathbf{p},\mathbf{p}'\\ \lambda,\lambda'\\ r,s}} \left(\frac{\hbar cp}{2\epsilon_0 V}\right)\left(\frac{\hbar cp'}{2\epsilon_0 V}\right) \bar{e}_j^{(\lambda)}(\mathbf{p})\bar{e}_j^{(\lambda')}(\mathbf{p}')e_k^{(\lambda)}(\mathbf{p})e_l^{(\lambda')}(\mathbf{p}')\mu_i^{or}\mu_j^{ro}\mu_k^{qs}\mu_l^{so}$$
$$\times \frac{e^{i(\mathbf{p}+\mathbf{p}')\cdot\mathbf{R}}}{(E_{so} + \hbar cp)(\hbar cp + \hbar cp')(E_{ro} + \hbar cp')} \tag{189}$$

where the molecule labels are implicit: r is associated with molecule A and s with B. There are similar expressions for the contributions from the other graphs; the associated energy denominators are listed in Table II. For the coupling of ground-state molecules the intermediate states are higher than the ground state. All denominators are positive and the interaction is attractive. For excited molecules the interaction may be attractive or repulsive.

In the classical description, charge fluctuations in one molecule provided an excitation field for the second molecule. In Q.E.D. the corresponding description is that of virtual molecular transitions the energy for which is "borrowed" from (or "lent" to) the vacuum radiation field for periods short enough to be allowed within the uncertainty principle limit $\Delta E\, \Delta t \geq \hbar$.

In Eq. (189), the sum over polarizations may be carried out with Eq. (181) to give

$$-\sum_{\substack{\mathbf{p},\mathbf{p}'\\ r,s}} \left(\frac{\hbar cp}{2\epsilon_0 V}\right)\left(\frac{\hbar cp'}{2\epsilon_0 V}\right) (\delta_{ik} - \hat{p}_i\hat{p}_k)(\delta_{jl} - \hat{p}_j'\hat{p}_l')\mu_i^{or}\mu_j^{ro}\mu_k^{qs}\mu_l^{so}$$
$$\times e^{i(\mathbf{p}+\mathbf{p}')\cdot\mathbf{R}}/D_i \tag{190}$$

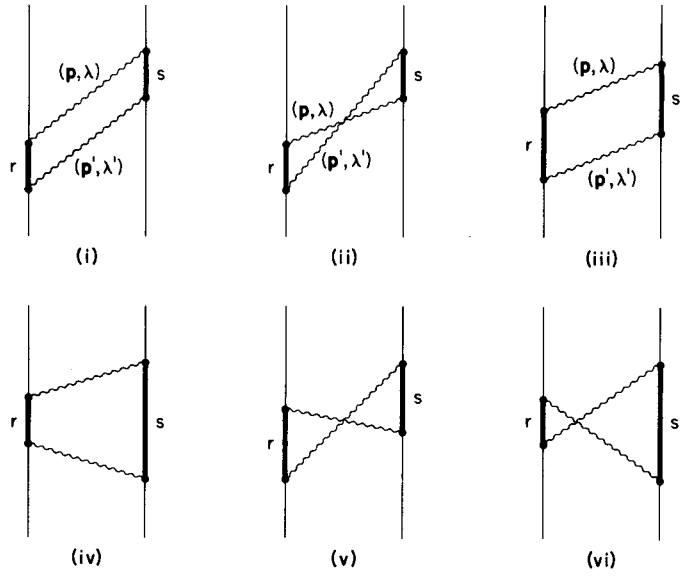

Fig. 8. The dispersion interaction. There are six additional graphs numbered (vii)–(xii) obtained from (i)–(vi) by interchange of A and B.

where D_{i} is the energy denominator for graph (i). The contributions from other graphs are added, giving the total

$$-\sum_{\substack{\mathbf{p},\mathbf{p}'\\ r,s}} \left(\frac{\hbar cp}{2\epsilon_0 V}\right)\left(\frac{\hbar cp'}{2\epsilon_0 V}\right)(\delta_{ik}-\hat{p}_i\hat{p}_k)(\delta_{jl}-\hat{p}_j'\hat{p}_l')\mu_i^{or}\mu_j^{ro}\mu_k^{os}\mu_l^{so}$$

$$\times e^{i(\mathbf{p}+\mathbf{p}')\cdot\mathbf{R}}\sum_{a=\text{i}}^{\text{xii}}\frac{1}{D_a} \tag{191}$$

TABLE II

ENERGY DENOMINATORS D_a

(i)	$(E_{so}+\hbar cp)(\hbar cp+\hbar cp')(E_{ro}+\hbar cp')$	(vii)	$(E_{ro}+\hbar cp)(\hbar cp+\hbar cp')(E_{so}+\hbar cp')$
(ii)	$(E_{so}+\hbar cp')(\hbar cp+\hbar cp')(E_{ro}+\hbar cp')$	(viii)	$(E_{ro}+\hbar cp)(\hbar cp+\hbar cp')(E_{so}+\hbar cp)$
(iii)	$(E_{so}+\hbar cp)(E_{ro}+E_{so})(E_{ro}+\hbar cp')$	(ix)	$(E_{ro}+\hbar cp)(E_{ro}+E_{so})(E_{so}+\hbar cp')$
(iv)	$(E_{so}+\hbar cp)(E_{ro}+E_{so})(E_{so}+\hbar cp')$	(x)	$(E_{ro}+\hbar cp)(E_{ro}+E_{so})(E_{ro}+\hbar cp')$
(v)	$(E_{so}+\hbar cp')(E_{ro}+E_{so}+\hbar cp+\hbar cp')\times(E_{ro}+\hbar cp')$	(xi)	$(E_{ro}+\hbar cp)(E_{ro}+E_{so}+\hbar cp+\hbar cp')\times(E_{so}+\hbar cp)$
(vi)	$(E_{so}+\hbar cp')(E_{ro}+E_{so}+\hbar cp+\hbar cp')\times(E_{so}+\hbar cp)$	(xii)	$(E_{ro}+\hbar cp)(E_{ro}+E_{so}+\hbar cp+\hbar cp')\times(E_{ro}+\hbar cp')$

where the fact is used that the preexponential factor is unchanged by the substitution $\mathbf{p} \rightarrow -\mathbf{p}$ and/or $\mathbf{p}' \rightarrow -\mathbf{p}'$, so that the exponential factor can always be written as $e^{i(\mathbf{p}+\mathbf{p}')\cdot\mathbf{R}}$. The wave-vector sums in Eq. (191) may be converted to integrals using Eq. (180), and after integration we get the complete Casimir–Polder result (1948; see also Power, 1967a). In the following sections the limiting cases of the potentials in the wave zone and the near zone are discussed.

1. *The Wave-Zone Limit: Casimir–Polder Potential*

At distances longer than any molecular transition wavelength the virtual field of one molecule at the position of the other is purely transverse, and the retardation (R/c at distance R) causes phase changes varying with the frequencies of the virtual field components. The complex interferences leave a residual interaction with distance dependence R^{-7}, falling off more quickly than the static (R^{-6}) term that it has replaced. It is not difficult to see that the reason is that the virtual fields, which convey the interaction, have R^{-1} dependence and therefore are very long range in nature; the interferences cause the much faster rate of change in the mutual coupling.

Within the methods of the last section we can calculate the short- and long-range potentials by appealing to a physical argument to limit the number of graphs to be included in each case. In the uncertainty relation $\Delta E > \hbar/\Delta t$ let us equate the time uncertainty to twice the retardation R/c, the time required for photon transit and return between molecules. The energy uncertainty ΔE, the energy "borrowed" for virtual excitation, cannot be less than $\hbar/\Delta t$. Thus for molecules close together the high-energy virtual photons must be responsible and low-energy photon contributions may be ignored. In the near zone, inspection of the denominators then shows that D_{iii}, D_{iv}, D_{ix}, and D_{x} are smaller than the others, and the corresponding graphs dominate in the near zone (see the following section). In the wave zone, for molecules separated by distances large compared with a wavelength, the energy uncertainty can be very small, and very low-frequency photons $\mathbf{p}$ and $\mathbf{p}'$ contribute. The dominating graphs are (i), (ii), (vii), and (viii), for which the denominators in the limit are smaller than any others, and may each be approximated by $E_{\mathrm{ro}}E_{\mathrm{so}}(\hbar cp + \hbar cp')$. The expression for the energy shift, from these four graphs only, and with freely rotating molecules, is

$$\Delta E = -\frac{4}{9}\sum_{\substack{\mathbf{p},\mathbf{p}'\\ r,s}} \left(\frac{\hbar cp}{2\epsilon_0 V}\right)\left(\frac{\hbar cp'}{2\epsilon_0 V}\right)\{1 + (\hat{\mathbf{p}}\cdot\hat{\mathbf{p}}')^2\}$$

$$\times \frac{|\boldsymbol{\mu}^{ro}|^2|\boldsymbol{\mu}^{so}|^2}{E_{ro}E_{so}} \frac{e^{i(\mathbf{p}+\mathbf{p}')\cdot\mathbf{R}}}{(\hbar cp + \hbar cp')} \tag{192}$$

Converting the $\mathbf{p}$ and $\mathbf{p}'$ sums to integrals and using

$$\alpha(\mathrm{A}) = \frac{2}{3}\sum_r \frac{|\boldsymbol{\mu}^{ro}|^2}{E_{ro}}, \qquad \alpha(\mathrm{B}) = \frac{2}{3}\sum_s \frac{|\boldsymbol{\mu}^{so}|^2}{E_{so}} \tag{193}$$

for the isotropic polarizabilities we get

$$\Delta E = -\frac{\hbar c\,\alpha(\mathrm{A})\alpha(\mathrm{B})}{4\epsilon_0^2}\int \{1 + (\hat{\mathbf{p}}\cdot\hat{\mathbf{p}}')^2\}\,\frac{pp'e^{i(\mathbf{p}+\mathbf{p}')\cdot\mathbf{R}}}{(p+p')}\,\frac{d^3\mathbf{p}\,d^3\mathbf{p}'}{(2\pi)^6} \tag{194}$$

The nature of the R dependence is easily deduced from dimensional arguments. The coefficient of the integral has dimensions (energy) $\times$ (length)^7, and the integral must therefore have dimensions (length)$^{-7}$. Since R is the only parameter in the integral it follows that the integral on evaluation must give R^{-7}, apart from a numerical factor which is found by integration. Integration of Eq. (194) gives

$$\Delta E = -\frac{23\hbar c}{64\pi^3\epsilon_0^2}\,\frac{\alpha(\mathrm{A})\alpha(\mathrm{B})}{R^7} \tag{195}$$

which is the Casimir–Polder potential for large intermolecular separations (Casimir, 1948; Casimir and Polder, 1948).

Other approaches also lead to the wave-zone limit (195). For example, a second canonical transformation gives an alternative form of the Hamiltonian (Craig and Power, 1969).

$$H = H_{\mathrm{rad}} + H_{\mathrm{A}} + H_{\mathrm{B}} - (2\epsilon_0^2)^{-1}\alpha_{ij}(\mathrm{A})\,d_i^{\perp}(\mathbf{R}_{\mathrm{A}})\,d_j^{\perp}(\mathbf{R}_{\mathrm{A}}) - (2\epsilon_0^2)^{-1}\alpha_{ij}(\mathrm{B})\,d_i^{\perp}(\mathbf{R}_{\mathrm{B}})\,d_j^{\perp}(\mathbf{R}_{\mathrm{B}}) \tag{196}$$

where $\alpha_{ij}(\mathrm{A})$ is the static polarizability tensor for molecule A. The calculation, now in the second instead of the fourth order of perturbation theory, gives Eq. (195) based on graphs with two-photon vertices (Fig. 9). Another viewpoint, due to Power (1972), is to treat the final terms in the Hamiltonian (196) as perturbing the ground state of the radiation field, so that the distance-dependent potential energy appears as a change in the field parts of the total energy.

2. *Near-Zone Limit: the London Potential*

The work of the previous section indicated that for the near zone the graphs corresponding to the denominators D_{iii}, D_{iv}, D_{ix}, and D_{x} are dominant. The energy denominators may each be approximated by $(\hbar cp)(\hbar cp')\,(E_{ro} + E_{so})$. The energy shift is then given by

$$\Delta E = -(\epsilon_0^{-2})^{-1}\sum_{r,s}\frac{\mu_i^{or}\mu_j^{ro}\mu_k^{os}\mu_l^{so}}{E_{ro}+E_{so}}\int(\delta_{ik}-\hat{p}_i\hat{p}_k)e^{i\mathbf{p}\cdot\mathbf{R}}\,\frac{\mathbf{d}^3\mathbf{p}}{(2\pi)^3}\int(\delta_{jl}-\hat{p}_j'\hat{p}_l')\times e^{i\mathbf{p}'\cdot\mathbf{R}}\,\frac{\mathbf{d}^3\mathbf{p}'}{(2\pi)^3} \tag{197}$$

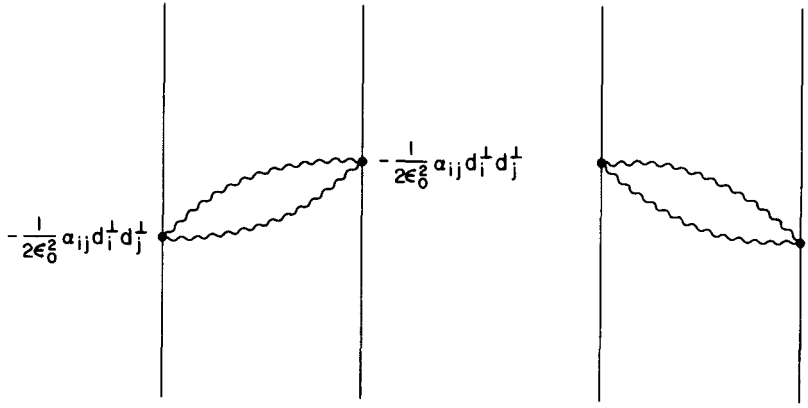

Fig. 9. Far-zone dispersion coupling. Vertices are two-photon effective interactions.

which after $\mathbf{p}$ and $\mathbf{p}'$ integration gives the familiar London result,

$$\Delta E = -\frac{1}{(4\pi\epsilon_0)^2 R^6}\sum_{r,s}\frac{\mu_i^{or}\mu_j^{ro}\mu_k^{os}\mu_l^{so}}{E_{ro}+E_{so}}(\delta_{ik}-3\hat{R}_i\hat{R}_k)(\delta_{jl}-3\hat{R}_j\hat{R}_l) \quad (198)$$

as conventionally obtained using second-order perturbation theory with the dipolar interaction operator,

$$V_{mn} = \frac{\mu_m(\mathrm{A})\mu_n(\mathrm{B})}{4\pi\epsilon_0 R^3}(\delta_{mn}-3\hat{R}_m\hat{R}_n) \quad (199)$$

For freely rotating molecules, the energy shift (198) becomes

$$\Delta E = \frac{1}{24\pi^2 e_0^2 R^6}\sum_{r,s}\frac{|\boldsymbol{\mu}^{ro}|^2|\boldsymbol{\mu}^{so}|^2}{E_{ro}+E_{so}} \quad (200)$$

A commonly used alternative to (Eq. 200) for the energy shift is in terms of dynamic polarizabilities over imaginary frequencies (see Margenau and Kestner, 1969). By using the identity

$$\frac{1}{E_{ro}+E_{so}} = \frac{1}{\pi}\int_{-\infty}^{\infty}\frac{E_{ro}E_{so}}{(E_{ro}^2+u^2)(E_{so}^2+u^2)}\,du \quad (201)$$

Eq. (200) can be transformed to

$$\Delta E = -\frac{3}{32\pi^3\epsilon_0^2 R^6}\int_{-\infty}^{\infty}\alpha^{\mathrm{A}}(u)\alpha^{\mathrm{B}}(u)\,du \quad (202)$$

where $u = i\hbar\omega$. A knowledge of the polarizabilities as analytic functions of u will then enable us to calculate the dispersion energy exactly.

C. Intermolecular Contributions to Dynamic Stark Shifts

The energy levels of an atom or molecule acted on by a radiation field undergo a shift, known as the dynamic Stark shift. The radiation perturbs the levels through its coupling to the electrons; the dominant contribution to the shift can be found by second-order perturbation theory. For monochromatic radiation in mode $(\mathbf{k}, \lambda)$ and molecular state $|m\rangle$, the graphs are given to the left of Fig. 10. The energy shift ΔE is given by

$$\Delta E = -\left(\frac{n\hbar ck}{2\epsilon_0 V}\right) e_i \bar{e}_j \sum_n \left\{\frac{\mu_i^{mn}\mu_j^{nm}}{E_{nm} - \hbar ck} + \frac{\mu_j^{mn}\mu_i^{nm}}{E_{nm} + \hbar ck}\right\}$$

$$= -\left(\frac{I}{2c\epsilon_0}\right) e_i \bar{e}_j \alpha_{ij}^{mm}(k) \tag{203}$$

where $\alpha_{ij}^{mm}(k)$ is the dynamic polarizability and I the irradiance. As in earlier examples (see Section IV,B), the result may alternatively be recovered as a first-order perturbation with an effective interaction (204), which can be found by a canonical transformation of the usual Hamiltonian

$$H_{\text{int}}^{\text{eff}} = -(2\epsilon_0^2)^{-1} \alpha_{ij}^{mm}(k)\, d_i^{\perp}(\mathbf{k})\, d_j^{\perp}(\mathbf{k}) \tag{204}$$

The corresponding graph is shown in Fig. 10.

If the system acted on by the radiation is made up of two (or more) molecules the energy shift is changed by their mutual interaction. The shift becomes that for radiation acting on the coupled pair. In the semiclassical picture one would say that the dipole moments induced in two nonpolar molecules with fixed orientations interact through the instantaneous dipole–dipole coupling, giving an energy shift that is proportional to R^{-3}. Such a result could hold only at distances short compared with the incident wavelength; at longer range there is a change due to retardation.

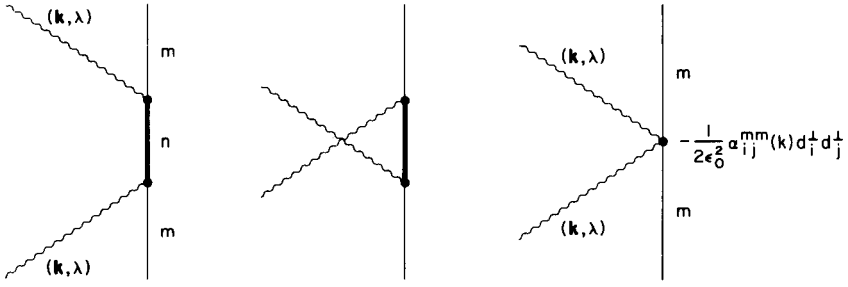

Fig. 10. Left-hand graphs: dynamic molecular Stark shift with one-photon vertex interactions $(1/\epsilon_0)\boldsymbol{\mu} \cdot \mathbf{d}^{\perp}$. Right-hand graph: with two-photon effective interaction.

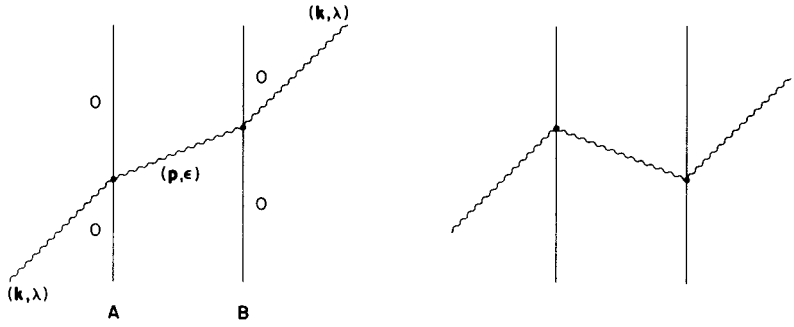

Fig. 11. Intermolecular contribution to dynamic Stark shift (plus graphs with A and B interchanged).

Applying quantum electrodynamics to find the intermolecular contribution to the ground-state energy shift we seek an expression correct for all separation distances (Thirunamachandran, 1980). The coupling is now described by one-photon exchange. After canonical transformation of the Hamiltonian we find an effective two-photon interaction operator

$$H_{\mathrm{int}}^{\mathrm{eff}}(\zeta) = -\epsilon_0^{-2}\alpha_{ij}^{\zeta}(k)\, d_i^{\perp}(\mathbf{k})\, d_j^{\perp}(\mathbf{p}) \tag{205}$$

where $\mathbf{p}$ is the wave vector of the virtual photon coupling the two molecules, and $\mathbf{k}$ that of the single-mode incident on the system; ζ designates the pair of molecules A and B. There is no factor 1/2 in Eq. (205), in contrast to Eq. (204), because $\mathbf{k}$ and $\mathbf{p}$ appearing in the creation and annihilation are different. The appropriate graphs are given in Fig. 11.

The energy shift after summation over the polarization of the virtual photon, isotropic polarizabilities being assumed for simplicity, is

$$\Delta E = \left(\frac{n\hbar ck}{2\epsilon_0 V}\right) \bar{e}_i^{(\lambda)}(\mathbf{k}) e_j^{(\lambda)}(\mathbf{k})\alpha^{\mathrm{A}}(k)\alpha^{\mathrm{B}}(k)(e^{i\mathbf{k}\cdot\mathbf{R}} + e^{-i\mathbf{k}\cdot\mathbf{R}})$$
$$\times \frac{1}{2\epsilon_0}\int (\delta_{ij} - \hat{p}_i\hat{p}_j)\left\{\frac{p}{k-p}e^{i\mathbf{p}\cdot\mathbf{R}} - \frac{p}{k+p}e^{-i\mathbf{p}\cdot\mathbf{R}}\right\}\frac{d^3\mathbf{p}}{(2\pi)^3} \tag{206}$$

After integration over $\mathbf{p}$,

$$\Delta E = (I/2c\epsilon_0)\bar{e}_i^{(\lambda)}(\mathbf{k})e_j^{(\lambda)}(\mathbf{k})\alpha^{\mathrm{A}}(k)\alpha^{\mathrm{B}}(k)V_{ij}(k, \mathbf{R})$$
$$\times (e^{i\mathbf{k}\cdot\mathbf{R}} + e^{-i\mathbf{k}\cdot\mathbf{R}}) \tag{207}$$

where $V_{ij}(k, \mathbf{R})$ is the retarded dipole–dipole interaction tensor (185).

The expression holds for the complete range of R up to distances of molecular overlap. It has a particularly useful application to the radiation-induced shift in an oriented crystal where pairwise summation can be expected to extend into regions of R where retardation can be important.

In the near zone ($kR \ll 1$), $V_{ij}(k, \mathbf{R})$ tends to the static dipole–dipole interaction tensor (186), and Eq. (207) becomes

$$\Delta E = (I/2c\epsilon_0)\bar{e}_i^{(\lambda)}(\mathbf{k})e_j^{(\lambda)}(\mathbf{k})\alpha^{\mathrm{A}}(k)\alpha^{\mathrm{B}}(k)(2\pi\epsilon_0 R^3)^{-1}(\delta_{ij} - 3\hat{R}_i\hat{R}_j) \quad (208)$$

Comparing Eq. (208) with Eq. (203) for the energy shift for a single molecule we see that the structures are the same if we introduce an effective polarizability for the coupled pair:

$$\alpha_{ij}^{\mathrm{pair}}(k) = -(2\pi\epsilon_0 R^3)^{-1}(\delta_{ij} - 3\hat{R}_i\hat{R}_j)\alpha^{\mathrm{A}}(k)\alpha^{\mathrm{B}}(k) \quad (209)$$

Although the individual molecular polarizabilities are isotropic by assumption, the pair polarizability is anisotropic because the direction of the intermolecular join $\hat{\mathbf{R}}$ is kept fixed relative to the direction of propagation of the incident radiation. It is evident from Eq. (209) that the isotropic part of the pair polarizability is zero and the energy shift is zero if the molecular pair is allowed to tumble with respect to the direction of propagation of light.

In the general expression (207), averaging over all directions $\hat{\mathbf{R}}$ with respect to the propagation direction $\hat{\mathbf{k}}$ of the incident beam, we find for the shift,

$$\Delta E = -\left(\frac{I}{8\pi c\epsilon_0^2}\right)\left(\frac{\alpha^{\mathrm{A}}(k)\alpha^{\mathrm{B}}(k)}{R^3}\right)\left(kR\ \sin 2kR + 2\ \cos 2kR - \frac{5\ \sin 2kR}{kR} - \frac{6\ \cos 2kR}{k^2R^2} + \frac{3\ \sin 2kR}{k^3R^3}\right) \quad (210)$$

If this expression is approximated for small kR we find

$$\Delta E = -\left(\frac{11I}{60\pi c\epsilon_0^2}\right)\left(\frac{k^2\alpha^{\mathrm{A}}(k)\alpha^{\mathrm{B}}(k)}{R}\right) \quad (211)$$

The energy shift (211) approaches zero as $kR \to 0$ in agreement with the behavior of the Coulombic expression (208) found by taking the $kR = 0$ limit of the potential before averaging over orientations. This interaction, because of its R^{-1} dependence, is effective out to large distances. Thus in an assembly of molecules the total energy shift has contributions from a large number of pairs. Also, when the incident frequency is close to a molecular transition frequency, so that there is a near resonance, there is an "amplification" effect as the dynamic polarizability in Eq. (211) increases sharply. In practical cases the dynamic polarizability could be three orders of magnitude larger than the static polarizability.

The radiation-induced energy shift (210) involves a single-photon interchange between the coupled systems, as does the resonance interaction (real one-photon exchange) in Section IV,A. Both fall off with distance in the same way as the Maxwell field (R^{-1}). The contrast with the wave-zone

dispersion interaction is striking: there are in that case two virtual photons which interfere, leaving an R^{-7} dependence in the leading term. Other properties such as "collision-induced" multipole moments can be calculated in a similar manner (Craig and Thirunamachandran, 1981).

D. Interactions of Functional Groups in a Single Molecule

The theory of coupling of molecules by exchange of virtual photons, discussed in the previous sections, is applicable to large molecules with several functional groups. The groups are assumed to be independent in the first instance, and electron exchange between groups is neglected. The molecular skeleton, which keeps the relative orientations of the chromophores fixed, does not interact with the radiation field, but the functional groups couple by exchange of virtual photons just as if they were separate molecular systems.

Such a many-group model is well suited to studying the optical activity of large molecules where the variation of electromagnetic fields over the entire molecule must be taken into account because the overall molecular size may be comparable to the wavelength of the incident radiation. The functional group sizes are small, however, compared with the wavelength, and a local point–dipole approximation at the various chromophore centres may be used. The model has been used to study optical rotation (Atkins and Woolley, 1970), two-photon circular dichroism (Andrews, 1976), and circular differential Rayleigh and Raman scattering (Andrews and Thirunamachandran, 1978a,b).

E. Chiral Discrimination

The account of molecular interactions given in Sections IV,A and IV,B is easily extended to deal separately with left- and right-handed forms of chiral systems. The dominant contributions are governed by electric dipole forces and are nondiscriminating; but there are extra terms, albeit small, which are not the same for left-hand–left-hand as for left-hand–right-hand pairs. Theoretical and experimental aspects of such discriminatory interactions have been recently reviewed by Craig and Mellor (1976). The discriminating terms are from electric dipole–magnetic dipole coupling; H_{int} must now include coupling with both electric and magnetic fields. For a pair of chiral molecules A and B located at $\mathbf{R}_A$ and $\mathbf{R}_B$,

$$H_{\text{int}} = -\epsilon_0^{-1}\boldsymbol{\mu}(\text{A}) \cdot \mathbf{d}^{\perp}(\mathbf{R}_A) - \epsilon_0^{-1}\boldsymbol{\mu}(\text{B}) \cdot \mathbf{d}^{\perp}(\mathbf{R}_B) - \mathbf{m}(\text{A}) \cdot \mathbf{b}(\mathbf{R}_A) - \mathbf{m}(\text{B}) \cdot \mathbf{b}(\mathbf{R}_B)$$

In the following sections we describe chiral discrimination in resonance and dispersion interactions.

1. *Discrimination in the Resonance Interaction*

Let A and B be the enantiomers of a neutral, chiral molecule. The calculation of the discriminating term differs from Section IV,A in that one of the vertices in the time-ordered graphs is the magnetic interaction. The matrix element, after summation over the virtual photon polarizations, is

$$M = (2\epsilon_0 c)^{-1}\epsilon_{ijk}\{\mu_i^{gn}(\mathrm{A})m_j^{no}(\mathrm{B}) + m_j^{gn}(\mathrm{A})\mu_i^{no}(\mathrm{B})\} \times \int p_k \left\{\frac{e^{ip\cdot R}}{k-p} - \frac{e^{-ip\cdot R}}{k+p}\right\}\frac{d^3p}{(2\pi)^3} \tag{212}$$

where ϵ_{ijk} is the alternating tensor and $k = E_{no}/\hbar c$. On integration we find (Craig *et al.*, 1971)

$$M = \mathrm{Im}\{\mu_i^{gn}(\mathrm{A})m_j^{no}(\mathrm{B}) + m_j^{gn}(\mathrm{A})\mu_i^{no}(\mathrm{B})\}U_{ij}(k, \mathbf{R}) \tag{213}$$

where $U_{ij}(k, \mathbf{R})$ is the retarded electric dipole–magnetic dipole interaction tensor,

$$U_{ij}(k, \mathbf{R}) = \epsilon_{ijk}(\hat{R}_k/4\pi\epsilon_0 cR^3)\{kR\cos kR + k^2R^2\sin kR\} \tag{214}$$

Comparing Eqs. (213) and (184), the electric dipole–electric dipole counterpart, we see that instead of the electric moment appearing quadratically, Eq. (213) is bilinear in the electric and magnetic moments. The resonance discrimination is about five orders of magnitude smaller than the electric dipole–electric dipole interaction. Even in the near zone, the discrimination is k dependent:

$$U_{ij}(k, \mathbf{R}) \simeq \epsilon_{ijk}(k\hat{R}_k/4\pi\epsilon_0 cR^2), \qquad kR \ll 1 \tag{215}$$

In the pure electric resonance case, $V_{ij}(k, \mathbf{R})$ is k independent in the near zone.

2. *Discriminating Dispersion Interactions in the Wave Zone*

In Section IV,B we gave the theory of dispersion interactions within the electric dipole approximation, finding that in the wave-zone limit the dispersion energy has R^{-7} dependence on distance R. For chiral systems this term still is the most important, but there are corrections arising from the inclusion of magnetic dipole coupling. The leading correction has opposite signs for $d(\mathrm{A}) - d(\mathrm{B})$ and $d(\mathrm{A}) - l(\mathrm{B})$ pairs. The calculation of the chiral discrimination energy is essentially similar to the calculation of the Casimir–Polder potential in Section IV,B. Graphs with the structure of (i) and (ii), and their reflections, of Fig. 8 contribute, with the difference that for each center one of the vertices is replaced by a magnetic dipole interaction. Thus each one of the four wave-zone graphs branches into four others for the four different orderings of the electric and magnetic vertices.

The fourth-order contribution to the energy shift from the graphs derived from (i) of Fig. 8 is

$$-\frac{1}{4\hbar c^3\epsilon_0^2}\mu_i^{or}m_j^{ro}\mu_k^{os}m_l^{so}\int pp'\{(\delta_{ik}-\hat{p}_i\hat{p}_k)(\delta_{jl}-\hat{p}_j'\hat{p}_l')$$
$$+(\delta_{ij}-\hat{p}_i'\hat{p}_k')(\delta_{jl}-\hat{p}_j\hat{p}_l)-\epsilon_{ilm}\epsilon_{kjn}(\hat{p}_m\hat{p}_n'+\hat{p}_m'\hat{p}_n)\}$$
$$\times\frac{e^{i(\mathbf{p}+\mathbf{p}')\cdot\mathbf{R}}}{(k_r+p')(k_s+p)(p+p')}\frac{d^3\mathbf{p}}{(2\pi)^3}\frac{d^3\mathbf{p}'}{(2\pi)^3} \tag{216}$$

where $k_r = E_{ro}/\hbar c$ and $k_s = E_{so}/\hbar c$. In obtaining Eq. (216) we have used the fact that $\mu_i^{or}m_j^{ro} = -m_j^{or}\mu_i^{ro}$ and $\mu_k^{os}m_l^{so} = -m_l^{os}\mu_k^{so}$. Similar expressions hold for the contributions from the graphs obtained from (ii), (vii), and (viii), giving a total discrimination energy

$$\Delta E = \frac{1}{4\hbar c^3\epsilon_0^2}\mu_i^{or}m_j^{ro}\mu_k^{os}m_l^{so}\int\{(\delta_{ij}-\hat{p}_i\hat{p}_k)(\delta_{jl}-\hat{p}_j'\hat{p}_l')$$
$$+(\delta_{ij}-\hat{p}_i'\hat{p}_k')(\delta_{jl}-\hat{p}_j\hat{p}_l)-\epsilon_{ilm}\epsilon_{kjn}(\hat{p}_m\hat{p}_n'+\hat{p}_m'\hat{p}_n)\}$$
$$\times\frac{pp'(p-p')^2e^{i(\mathbf{p}+\mathbf{p}')\cdot\mathbf{R}}}{(p+p')(k_r+p)(k_r+p')(k_s+p)(k_s+p')}\frac{d^3\mathbf{p}}{(2\pi)^3}\frac{d^3\mathbf{p}'}{(2\pi)^3} \tag{217}$$

In the wave zone, as we have already seen, p and p' are much smaller than k_r and k_s and may be neglected in the denominator. For freely rotating molecules, a rotational average of the molecular part of Eq. (217) gives

$$\langle\mu_i^{or}m_j^{ro}\mu_k^{os}m_l^{so}\rangle = \tfrac{1}{9}\delta_{ij}\delta_{kl}(\boldsymbol{\mu}^{or}\cdot\mathbf{m}^{ro})(\boldsymbol{\mu}^{os}\cdot\mathbf{m}^{so}) = -\tfrac{1}{9}\delta_{ij}\delta_{kl}R^{or}R^{os} \tag{218}$$

where R^{or} and R^{os} are the rotatory strengths. Using Eq. (218) in Eq. (217) and completing the $\mathbf{p}$ and $\mathbf{p}'$ integrals we obtain

$$\Delta E = \frac{\hbar^3 c}{3\pi^3\epsilon_0^2R^9}\sum_r\frac{R^{or}}{E_{ro}^2}\sum_s\frac{R^{os}}{E_{so}^2} \tag{219}$$

It is evident that Eq. (219) changes sign when one of the molecules is replaced by its enantiomer. Thus chemically identical molecules with the same handedness repel and with opposite handedness attract. When A and B are chemically different it is not possible to assign an absolute sign to the energy because the rotatory strengths can be either positive or negative.

3. *Discriminating Dispersion Energies in the Near Zone*

Follwing Section IV,B it is easily seen that the interaction in the near zone can be calculated using second-order perturbation theory with $H_{\text{int}} = H_E + H_M$, where

$$H_E = \frac{\mu_i(\mathrm{A})\mu_j(\mathrm{B})}{4\pi\epsilon_0 R^3}(\delta_{ij} - 3\hat{R}_i\hat{R}_j) \tag{220}$$

$$H_M = \frac{m_i(\mathrm{A})m_j(\mathrm{B})}{4\pi\epsilon_0 c^2 R^3}(\delta_{ij} - 3\hat{R}_i\hat{R}_j) \tag{221}$$

There is no dipolar coupling between an electric and magnetic moment in the near zone because the limit of $U_{ij}(k, \mathbf{R})$ is k dependent. The dispersion energy is

$$\Delta E = -\sum_{r,s} \frac{\langle E_0^{\mathrm{B}}, E_0^{\mathrm{A}}|H_E + H_M|E_r^{\mathrm{A}}, E_s^{\mathrm{B}}\rangle\langle E_s^{\mathrm{B}}, E_r^{\mathrm{A}}|H_E + H_M|E_0^{\mathrm{A}}, E_0^{\mathrm{B}}\rangle}{E_{ro} + E_{so}} \tag{222}$$

The electric–magnetic cross term of Eq. (220) is discriminating as seen by replacing the molecule B by its chiral enantiomer generated by inversion at the origin; the electric dipole changes sign but not the magnetic dipole, and the energy changes sign between $d - d$ and $d - l$ interactions. In terms of optical rotatory strength tensors, the discriminating energy is

$$\Delta E_{\mathrm{disc}} = (8\pi^2\epsilon_0^2 c^2 R^6)^{-1}(\delta_{ik} - 3\hat{R}_i\hat{R}_k)(\delta_{jl} - 3\hat{R}_j\hat{R}_l) \times \sum_{r,s} \frac{R_{ij}^{or} R_{kl}^{os}}{E_{ro} + E_{so}} \tag{223}$$

which, for freely rotating molecules, becomes (Mavroyannis and Stephen, 1962; Craig *et al.*, 1971)

$$\Delta E_{\mathrm{disc}} = \frac{1}{12\pi^2\epsilon_0^2 c^2 R^6} \sum_{r,s} \frac{R^{or} R^{os}}{E_{ro} + E_{so}} \tag{224}$$

Again, as in the wave zone, chemically identical molecules of the same chiral form repel and those of opposite form attract. If A and B are nonidentical chemically no general statement can be made. It should be remembered that in all cases the dominating electric–electric dispersion gives attraction, which is slightly increased or decreased by the discriminating terms. The magnitudes are several orders of magnitude down, and experimental checks have not yet been reported.

F. Molecule-Induced Circular Dichroism

Circular dichroism (CD) (Section III,C) is a property of free chiral molecules, but may appear in achiral molecules acted upon by an intense circularly polarized laser beam (Section III,D). Also, achiral molecules in the field of one or more chiral molecules, either present together in an achiral solvent, or dissolved in a chiral solvent, may develop optical activity, including CD. The effect is thus intermolecular in character. The typical experiment is to detect and measure circular dichroism at a transi-

tion frequency characteristic of the achiral molecule, the chiral molecule being transparent at that frequency. For example, CD can be made to appear in $n-\pi^*$ transitions in achiral aromatic ketones, nitro, and azo compounds by dissolving them in one enantiomeric form of pinene as solvent (see, for example, Bosnich, 1967; Hayward and Totty, 1971). We give a brief account of the theory of dynamical contributions to induced CD due to Craig *et al.* (1976) using quantum electrodynamics. There are also static contributions to induced CD which can in principle be treated by quantum electrodynamics, but in practice have been calculated by other means.

Let us suppose that the incident beam for the detection of induced CD is of mode (**k**, L/R), with frequency matching a dipole-allowed transition of the achiral molecule A, $\hbar ck = E_m - E_0$. The levels of the molecule C causing the induction are $\{|E_r\rangle\}$, and since C is chiral some of the transitions $r \leftarrow 0$ are allowed to both electric and magnetic dipole radiation. To quantify the induced CD we need the difference in absorption rates of left- and right-circularly polarized light for the transition $|E_m^A; E_0^C\rangle \leftarrow |E_0^A; E_0^C\rangle$ in the A–C molecule pair. The overall process is a change of state only of A, but there are intermediate states involving virtual transitions of C. However, the leading contribution to the matrix element for the pair transition is of the first order, since the transition in A is electric dipole allowed. The corresponding graph is (a) of Fig. 12. There is no participation by C, and the contribution to the matrix element is

$$M_{fi}^{(1)(\mathrm{L/R})} = -i(n\hbar ck/2\epsilon_0 V)^{1/2} e_i^{(\mathrm{L/R})}(\mathbf{k})\mu_i^{mo} e^{i\mathbf{k}\cdot\mathbf{R}_A} \tag{225}$$

There being no coupling between the achiral and chiral molecules, the transition rate based on the matrix element (225) is independent of the helicity of the incident radiation. We need to include higher order terms to take into account the coupling between A and C. The leading correction term is of third order. The relevant time-ordered graphs are (b)–(g) of Fig. 12. The third-order terms involve virtual excitation of the chiral molecule, the interaction between A and C being mediated by a virtual photon. In the final state of the system, C is in its ground state and A is excited to $|E_m^A\rangle$. The total contribution from a graph is obtained by summing over the virtual states $|E_r^C\rangle$, and virtual photon modes ($\mathbf{p}$, λ), the sum of the contributions from graphs (b)–(d) being

$$i\left(\frac{n\hbar k}{8\epsilon_0^3 cV}\right)^{-1/2} e_i^{(\mathrm{L/R})}(\mathbf{k})\mu_k^{mo} \int \frac{p}{k-p}[(\delta_{ik} - \hat{p}_j\hat{p}_k)(c\alpha_{ij} \mp iG_{ji}) + \epsilon_{jkl}\hat{p}_l G_{ij}]e^{i(\mathbf{k}+\mathbf{p})\cdot\mathbf{R}} \frac{d^3\mathbf{p}}{(2\pi)^3} \tag{226}$$

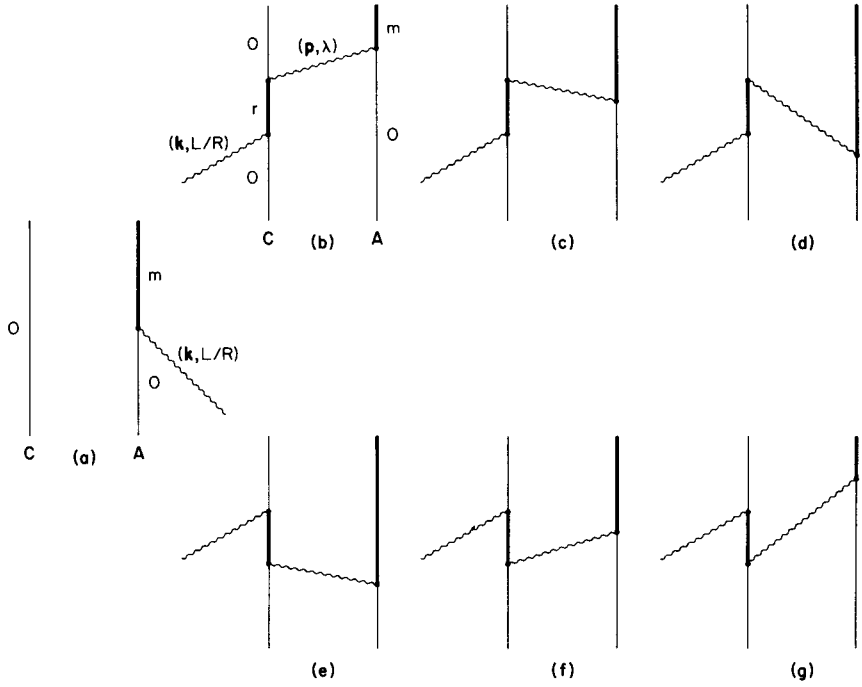

Fig. 12. Induced circular dichroism.

where the upper and lower signs refer to L and R, respectively; the tensors α and $\mathbf{G}$ for the chiral molecule are given as before by

$$\alpha_{ij} = \sum_r \left\{ \frac{\mu_i^{or}\mu_j^{ro}}{E_{ro} - \hbar ck} + \frac{\mu_j^{or}\mu_i^{ro}}{E_{ro} + \hbar ck} \right\} \tag{227}$$

$$G_{ij} = \sum_r \left\{ \frac{\mu_i^{or} m_j^{ro}}{E_{ro} - \hbar ck} + \frac{m_j^{or}\mu_i^{ro}}{E_{ro} + \hbar ck} \right\} \tag{228}$$

In Eq. (226), $\mathbf{R} = \mathbf{R}_C - \mathbf{R}_A$. Similarly, the sum of the contributions from graphs (e)–(g) is

$$i\left(\frac{n\hbar k}{8\epsilon_0^3 cV}\right)^{1/2} e_i^{(L/R)}(\mathbf{k})\mu_k^{mo} \int \frac{p}{-k-p}[(\delta_{jk} - \hat{p}_j\hat{p}_k)(c\alpha_{ij} \mp iG_{ji}) + \epsilon_{jkl}\hat{p}_l G_{ij}]e^{i(\mathbf{k}-\mathbf{p})\cdot\mathbf{R}} \frac{d^3\mathbf{p}}{(2\pi)^3} \tag{229}$$

The forms of Eqs. (226) and (229) suggest that the two one-photon vertices of C in the graphs may be "collapsed" to an effective two-photon

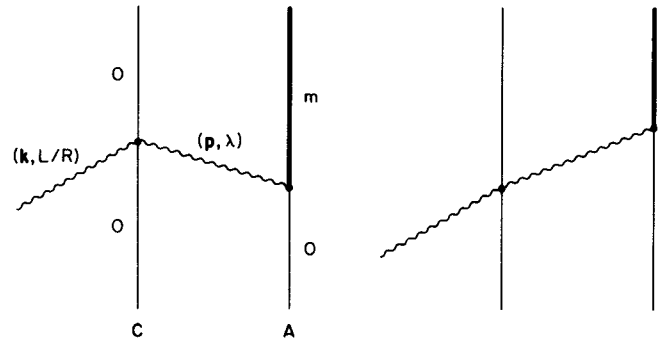

Fig. 13. Induced circular dichroism with an effective two-photon vertex.

vertex leading to graphs of the type shown in Fig. 13. As shown by Craig *et al.* (1976), the change corresponds to a canonical transformation; there is the advantage that with the effective two-photon vertex for C, the leading term containing the intermolecular coupling may be calculated by second-order perturbation theory.

The sum of Eqs. (226) and (229) after integration over **p** is given by

$$M_{fi}^{(3)(\mathrm{L/R})} = i(n\hbar ck/2\epsilon_0 V)^{1/2} e_i^{(\mathrm{L/R})}(\mathbf{k})\mu_k^{mo} e^{i\mathbf{k}\cdot\mathbf{R}} \times \{[\alpha_{ij} \mp (i/c)G_{ji}]V_{jk} + iG_{ij}U_{jk}\} \tag{230}$$

where V_{jk} and U_{jk} are the retarded intermolecular tensors (185) and (214) encountered earlier. The total matrix element correct to third order for absorption of a photon of mode (**k**, L/R) from the incident beam is the sum of Eqs. (225) and (230). The difference in absorption rate between left- and right-circularly polarized light is then found from the Fermi golden rule,

$$\Gamma^{(\mathrm{L})} - \Gamma^{(\mathrm{R})} = (2\pi/\hbar)\{|M_{fi}^{(1)(\mathrm{L})} + M_{fi}^{(3)(\mathrm{L})}|^2 - |M_{fi}^{(1)(\mathrm{R})} + M_{fi}^{(3)(\mathrm{R})}|^2\}\rho \tag{231}$$

The leading contribution to the differential absorption rate comes from the first-order–third-order interference term:

$$\Gamma^{(\mathrm{L})} - \Gamma^{(\mathrm{R})} = (\mathcal{I}i/2\hbar^2\epsilon_0 c)\mu_k^{mo}\mu_r^{mo}[(\delta_{ir} - \hat{k}_i\hat{k}_r)G_{ji}V_{jk}(e^{i\mathbf{k}\cdot\mathbf{R}} + e^{-i\mathbf{k}\cdot\mathbf{R}}) + c\epsilon_{irs}\hat{k}_s(\alpha_{ij}V_{jk} + iG_{ij}U_{jk})(e^{i\mathbf{k}\cdot\mathbf{R}} - e^{-i\mathbf{k}\cdot\mathbf{R}})] \tag{232}$$

which applies to an A–C pair for which **R** is fixed relative to $\hat{\mathbf{k}}$ and with orientations of A and C fixed relative to **R**.

An application of Eq. (232) is to pairs of molecules on known sites and known relative orientations in a crystal. To deal with induced CD in solution we need the average with respect to the orientation of the join **R** of the molecules to the probe beam **k** and also with respect to the angular

orientation of C relative to A at fixed **R**. The first average, the "tumbling" average (all orientations equally probable), is given by

$$\langle \Gamma^{(L)} \rangle - \langle \Gamma^{(R)} \rangle$$
$$= \left(\frac{\mathcal{J}i}{\hbar^2 \epsilon_0 c}\right) \mu_k^{mo} \mu_r^{mo} \Bigg[\left\{ (\delta_{ir} - \hat{R}_i \hat{R}_r) \frac{\sin kR}{kR} + (\delta_{ir} - 3\hat{R}_i \hat{R}_r) \right.$$
$$\times \left(\frac{\cos kR}{k^2 R^2} - \frac{\sin kR}{k^3 R^3} \right) \Bigg\} G_{ji} V_{jk} - ic \epsilon_{irs} \hat{R}_s \left(\frac{\cos kR}{kR} - \frac{\sin kR}{k^2 R^2} \right)$$
$$\times (\alpha_{ij} V_{jk} + i G_{ij} U_{jk}) \Bigg] \tag{233}$$

which in the $kR \ll 1$ limit tends to

$$\langle \Gamma^{(L)} \rangle - \langle \Gamma^{(R)} \rangle$$
$$\simeq -\left(\frac{\mathcal{J}}{12\pi\hbar^2 \epsilon_0^2 c} \right) \frac{\mu_k^{mo} \mu_r^{mo}}{R^3} (\delta_{jk} - 3\hat{R}_j \hat{R}_k)$$
$$\times (ckR \epsilon_{irs} \hat{R}_s \alpha_{ij} - 2i\delta_{ir} G_{ji}) \tag{234}$$

The average over relative angles must allow for the potential V_{AC} opposing relative motion and must include a Boltzmann factor as in Eq. (235)

$$\ll \Gamma^{(L)} - \Gamma^{(R)} \gg$$
$$= \frac{\iint d\Omega \, d\Omega' \langle \Gamma^{(L)} - \Gamma^{(R)} \rangle \exp\{-V_{AC}(R, \Omega, \Omega')/kT\}}{\iint d\Omega \, d\Omega' \exp\{-V_{AC}(R, \Omega, \Omega')/kT\}} \tag{235}$$

where $V_{AC}(R, \Omega, \Omega')$ is a function of the separation R and of sets of Eulerian angles Ω and Ω'. The potential V_{AC} is the complete potential function for the coupling of A and C. In the high-temperature limit, assumed here, the leading term of Eq. (235) is simply the unweighted average over all orientations. Under these conditions the average of Eq. (233) is

$$(\mathcal{J}/12\pi\hbar^2 \epsilon_0^2 c) |\boldsymbol{\mu}^{mo}|^2 \{\text{Im } G_{ii}\} R^{-3} \left[\cos 2kR \left(4 - \frac{6}{k^2 R^2} \right) \right.$$
$$\left. + \sin 2kR \left(2kR - \frac{6}{kR} + \frac{3}{k^3 R^3} \right) \right] \tag{236}$$

which for small kR gives

$$(\mathcal{J}k^2/15\pi\hbar^2 \epsilon_0^2 c) |\boldsymbol{\mu}^{mo}|^2 (\text{Im } G_{ii}) R^{-1} \tag{237}$$

as the leading contribution. It may be noted that replacement of C by its enantiomer changes the sign of G, and the induced CD takes the opposite sign.

One can visualize the differential absorption result (234) in the near zone in a simple manner (Craig *et al.*, 1974). The interaction between A and C is Coulombic, and the perturbed energy levels may be calculated according to stationary-state perturbation theory. The perturbed wave functions are obtained by the mixing of excited-state wave functions $|E_0^A; E_r^C\rangle$ and $|E_m^A; E_0^C\rangle$ and of the doubly-excited-state wave functions $|E_m^A; E_r^C\rangle$ with the ground state $|E_0^A; E_0^C\rangle$ according to

$$|E_m^A; E_0^C\rangle' = |E_m^A; E_0^C\rangle - \sum_r \frac{\langle E_r^C; E_0^A|V|E_m^A; E_0^C\rangle}{E_{ro} - E_{mo}} |E_0^A; E_r^C\rangle \quad (238)$$

$$|E_0^A; E_0^C\rangle' = |E_0^A; E_0^C\rangle - \sum_r \frac{\langle E_r^C; E_m^A|V|E_0^A; E_0^C\rangle}{E_{ro} + E_{mo}} |E_m^A; E_r^C\rangle \quad (239)$$

which in the electric dipole approximation become

$$|E_m^A; E_0^C\rangle' \approx |E_m^A; E_0^C\rangle - \frac{(\delta_{ij} - 3\hat{R}_i\hat{R}_j)}{4\pi\epsilon_0 R^3} \sum_r \frac{\mu_i^{om}\mu_j^{ro}}{E_{ro} - E_{mo}} |E_0^A; E_r^C\rangle \quad (240)$$

$$|E_0^A; E_0^C\rangle' \approx |E_0^A; E_0^C\rangle - \frac{(\delta_{ij} - 3\hat{R}_i\hat{R}_j)}{4\pi\epsilon_0 R^3} \sum_r \frac{\mu_i^{om}\mu_j^{or}}{E_{ro} + E_{mo}} |E_m^A; E_r^C\rangle \quad (241)$$

where the primes denote the perturbed wave functions. The transition rate for the absorption of circularly polarized light by the perturbed system is

$$\frac{\mathcal{I}}{6\hbar^2\epsilon_0} |\langle E_0^C; E_m^A|\boldsymbol{\mu}_1 + \boldsymbol{\mu}_2 \mp (i/c)(\mathbf{m}_1 + \mathbf{m}_2)|E_0^A; E_0^C\rangle'|^2 \quad (242)$$

where $\mathcal{I}$ is the energy density per unit frequency. The upper and lower signs apply to absorption of left- and right-circularly polarized photons, respectively. The origin-dependent nature of the magnetic dipole operator $\mathbf{m}$ must be borne in mind: with moments referred to the local molecular centers, the differential absorption rate is

$$\langle \Gamma^{(L)} - \Gamma^{(R)} \rangle = -\left(\frac{2\mathcal{I}i}{3\hbar^2\epsilon_0 c}\right) \langle E_0^C; E_0^A|\boldsymbol{\mu}_1 + \boldsymbol{\mu}_2|E_m^A; E_0^C\rangle' \cdot \langle E_0^C; E_m^A|\mathbf{m}_2 - (e/2m)\mathbf{R} \times \mathbf{p}_2|E_0^A; E_0^C\rangle' \quad (243)$$

Using Eqs. (240) and (241) and retaining the leading terms, we recover the near-zone result (234).

A model closely related to the graphs in Fig. 12 is that the circular dichroism induced in A is the result of the interference between the di-

rectly absorbed wave [graph (a)] and the wave scattered by the chiral molecule, the interference being constructive or destructive depending on the helicity of the incident photons. In this model the moments induced in C by the incident wave act as sources of an auxiliary field at A. The induced electric moment through the G term provides the discriminatory component of the electric field at A.

V. Conclusion

In this review we have shown how a wide range of phenomena involving interactions between molecules and radiation, or interactions between molecules themselves, may be viewed in a unified way within the framework of quantum electrodynamics. The primary interaction between an atom or molecule and the quantized radiation field is the absorption or emission of real or virtual photons. Coupling between molecules is treated as the result of the coupling of each molecule to the radiation field, which mediates the interaction. It is then possible to understand a variety of complex processes and calculate observables such as transition rates, scattering probabilities, level shifts, and intermolecular energy shifts. We have attempted to be representative rather than exhaustive in the coverage of applications. Others are described in the original papers and in the case of multiphoton processes there is a compilation by Eberly and Karczewski (1977) together with the annual supplements.

The examples chosen to illustrate the methods of quantum electrodynamics are from chemical physics and quantum chemistry. They refer to bound electrons of low binding energy where relativistic effects can be neglected. It is interesting, however, to note that early relativistic calculations such as electron–electron scattering due to the exchange of a virtual photon (Coulomb scattering) and photon–electron scattering (Compton scattering) showed remarkable agreement with experiment, but higher order corrections led to divergences and infinities. These difficulties stimulated the major advances made in the late 1940s that led to a covariant formulation of quantum electrodynamics and the development of renormalization techniques [see Schwinger (1958) for a collection of classic papers on the subject]. In the renormalization program, the infinities are identified in a systematic way and incorporated in the redefined physical constants of the electron, namely, the observed charge and mass. With this procedure it has been possible to calculate radiative corrections to high precision.

Despite these successes the impression should not be left that the methods are without problems. It is not obvious whether renormalization is a fundamental requirement of theory or whether it is simply a mathe-

matical artifice concealing deeper defects in the foundations. There is also the question of reliance throughout on perturbation techniques, no non-perturbation techniques having been developed. In the problems treated in this review perturbation methods are applicable so long as the radiation field strengths are much smaller than the Coulomb fields within a molecule. Except for very intense fields this requirement is satisfied: the field of a 1 W cm^{-2} continuous laser is about 10^3 V m^{-1}; for a pulsed laser of 10^6 W cm^{-2} the field is about 10^6 V m^{-1}. These fields can be compared with the field $\approx 10^{11}$ V m^{-1} acting on a ground-state electron in atomic hydrogen. Thus as long as the laser power per unit area is well below 10^{16} W cm^{-2} (field strength 10^{11} V m^{-1}), pertubation methods in molecular quantum electrodynamics are satisfactory. Such considerations inspire confidence that whatever refinements or modifications to the theory may be required the practical value of the methods for making calculations yielding agreement with experiment to very high precision is unlikely to be affected. In this sense, the theory as known at present can be said to have a lasting value.

References

Andrews, D. L. (1976). *Chem. Phys.* **16,** 419.

Andrews, D. L. (1980). *J. Chem. Phys.* **72,** 4141.

Andrews, D. L., and Thirunamachandran, T. (1977). *J. Chem. Phys.* **67,** 5026.

Andrews, D. L., and Thirunamachandran, T. (1978a). *Proc. R. Soc. London Ser. A* **358,** 297.

Andrews, D. L., and Thirunamachandran, T. (1978b). *Proc. R. Soc. London Ser. A* **358,** 311.

Andrews, D. L., and Thirunamachandran, T. (1978c). *J. Chem. Phys.* **68,** 2941.

Andrews, D. L., and Thirunamachandran, T. (1979). *J. Chem. Phys.* **70,** 1027.

Atkins, P. W., and Woolley, R. G. (1970). *Proc. R. Soc. London Ser. A* **314,** 251.

Babiker, M., Power, E. A., and Thirunamachandran, T. (1974). *Proc. R. Soc. London Ser. A* **338,** 235.

Barron, L. D., and Buckingham, A. D. (1971). *Mol. Phys.* **20,** 1111.

Barron, L. D., Bogaard, M. P., and Buckingham, A. D. (1973). *J. Am. Chem. Soc.* **95,** 603.

Bhagavantam, S., and Venkateswaran, S. (1930). *Nature (London)* **125,** 237.

Biraben, F., Cagnac, B., and Grynberg, G. (1974). *Phys. Rev. Lett.* **32,** 643.

Bosnich, B. (1967). *J. Am. Chem. Soc.* **89,** 6143.

Carruthers, P., and Nieto, M. M. (1968). *Rev. Mod. Phys.* **40,** 411.

Casimir, H. B. G. (1948). *Proc. K. Ned. Akad. Wet.* **51,** 793.

Casimir, H. B. G., and Polder, D. (1948). *Phys. Rev.* **73,** 360.

Craig, D. P., and Mellor, D. P. (1976). *Top. Curr. Chem.* **63,** 1.

Craig, D. P., and Power, E. A. (1969). *Int. J. Quantum Chem.* **3,** 903.

Craig, D. P., and Thirunamachandran, T. (1978). *Mol. Phys.* **35,** 825.

Craig, D. P., and Thirunamachandran, T. (1981). *Chem. Phys. Lett.* **80,** 14.

Craig, D. P., Power, E. A., and Thirunamachandran, T. (1971). *Proc. R. Soc. London Ser. A* **322,** 165.

Craig, D. P., Power, E. A., and Thirunamachandran, T. (1974). *Chem. Phys. Lett.* **27,** 149.

Craig, D. P., Power, E. A., and Thirunamachandran, T. (1976). *Proc. R. Soc. London Ser. A* **348**, 19.
Decius, J. C., and Rauch, J. E. (1959). *Ohio State Symp. Mol. Struct. Spectrosc.*
Delsart, C., and Keller, J.-C. (1978). *J. Appl. Phys.* **49**, 3662.
Dicke, R. H. (1954). *Phys. Rev.* **93**, 99.
Dirac, P. A. M. (1927). *Proc. R. Soc. London Ser. A* **114**, 243.
Eberly, J. H., and Karczewski, B. (1977). "Multiphoton Bibliography 1970–76." Univ. of Rochester Press, Rochester, New York.
French, M. J., and Long, D. A. (1975). *J. Raman Spec.* **3**, 391.
Gell-Mann, M. (1956). *Nuovo Cimento* **4** (Suppl. 2), 848.
Glauber, R. J. (1963). *Phys. Rev.* **131**, 2766.
Grynberg, G., and Cagnac, B. (1977). *Rep. Prog. Phys.* **40**, 791.
Hayward, L. D., and Totty, R. N. (1971). *Can. J. Chem.* **49**, 624.
Healy, W. P. (1976). *J. Chem. Phys.* **64**, 3111.
Healy, W. P. (1982). "Non-Relativistic Quantum Electrodynamics." Academic Press, New York.
Jaynes, E. T., and Cummings, F. W. (1963). *Proc. I.E.E.E.* **51**, 89.
Johnson, P. M. (1976). *J. Chem. Phys.* **64**, 4143.
Kastler, A. (1930). *C.R. hebd. Seance Acad. Sci. Paris* **191**, 565.
Lambropoulos, P. (1976). *Adv. At. Mol. Phys.* **12**, 87.
Levenson, M. D., and Bloembergen, N. (1974). *Phys. Rev. Lett.* **32**, 645.
Liao, P. F., and Bjorklund, G. C. (1976). *Phys. Rev. Lett.* **36**, 584.
Liao, P. F., and Bjorklund, G. C. (1977). *Phys. Rev. A* **15**, 2009.
London, F. (1930). *Z. Phys.* **63**, 245.
McClain, W. M. (1974). *Acc. Chem. Res.* **7**, 129.
McLone, R. R., and Power, E. A. (1964). *Mathematika* **11**, 91.
Margenau, H., and Kestner, N. R. (1969). "Theory of Intermolecular Forces." Pergamon, Oxford.
Mavroyannis, C., and Stephen, M. J. (1962). *Mol. Phys.* **5**, 629.
Merzbacher, E. (1970). "Quantum Mechanics." Wiley, New York.
Milonni, P. W. (1980). *In* "Foundations of Radiation Theory and Quantum Electrodynamics" (A. O. Barut, ed.), p. 1. Plenum, New York.
Power, E. A. (1964). "Introductory Quantum Electrodynamics." Longmans, London.
Power, E. A. (1967a). *Adv. Chem. Phys.* **12**, 167.
Power, E. A. (1967b). *J. Chem. Phys.* **46**, 4297.
Power, E. A. (1972). *In* "Magic Without Magic: John Archibald Wheeler" (J. R. Klauder, ed.), p. 135. Freeman, San Francisco, California.
Power, E. A., and Thirunamachandran, T. (1974). *J. Chem. Phys.* **60**, 3695.
Power, E. A., and Thirunamachandran, T. (1975). *J. Phys. B* **8**, L170.
Power, E. A., and Thirunamachandran, T. (1978). *Am. J. Phys.* **46**, 370.
Power, E. A., and Thirunamachandran, T. (1980). *Proc. R. Soc. London Ser. A* **372**, 265.
Power, E. A., and Zienau, S. (1959). *Philos. Trans. R. Soc. Ser. A* **251**, 427.
Prasad, P. L., and Burow, D. F. (1979a). *J. Am. Chem. Soc.* **101**, 800.
Prasad, P. L., and Burow, D. F. (1979b). *J. Am. Chem. Soc.* **101**, 806.
Schmid, W. J., and Schrötter, H. W. (1977). *Chem. Phys. Lett.* **45**, 502.
Schwinger, J. (1958). "Quantum Electrodynamics." Dover, New York.
Stephen, M. J. (1964). *J. Chem. Phys.* **40**, 669.
Susskind, L., and Glogower, J. (1964). *Physics* **1**, 49.
Tabor, D., and Winterton, R. H. S. (1969). *Proc. R. Soc. London Ser. A* **312**, 435.
Terhune, R. W., Maker, P. D., and Savage, C. M. (1965). *Phys. Rev. Lett.* **14**, 681.

Thirunamachandran, T. (1979). *Proc. R. Soc. London Ser. A* **365,** 327.
Thirunamachandran, T. (1980). *Mol. Phys.* **40,** 393.
Verdieck, J. F., Peterson, S. H., Maker, P. D., and Savage, C. M. (1970). *Chem. Phys. Lett.* **7,** 219.
Vervey, E. J. W. (1947). *J. Phys. Colloid Chem.* **51,** 631.
Wilson, E. B., Decius, J. C., and Cross, P. C. (1955). "Molecular Vibrations." McGraw-Hill, New York.
Woolley, R. G. (1971). *Proc. R. Soc. London Ser. A* **321,** 557.

Problems of Nonlinear Radiationless Processes in Chemistry

A. A. OVCHINNIKOV
L. Ya. Karpov Physico-Chemical Research Institute
Moscow, USSR

and

M. YA. OVCHINNIKOVA
Institute of Chemical Physics of the Academy of Sciences of the USSR
Moscow, USSR

I. Introduction

Numerous processes of relaxation and transformation of electronic and vibrational excitation energy in the condensed phase or in large molecules and nonadiabatic chemical reactions of electron transfer in polar

ADVANCES IN QUANTUM CHEMISTRY, VOLUME 16

ISBN 0-12-034816-0

liquids are described in terms of radiationless transition (RLT) theory. The RLT theory in its modern form has been developed by Huang and Rhys (1950), Lax (1952), Krivoglaz (1953), Pekar (1954), Kubo and Toyozawa (1955) for electronic transitions in solids. Since then the RLT theory has been often used for description of relaxation processes and elementary chemical steps in the condensed phase. The concepts of RLT theory are close to those of the theory of nonadiabatic processes in the gas phase (Nikitin and Umanskii, 1979; Child, 1974). Both theories are based on the Franck–Condon (FC) principle for electronic transition. The RLT theory first derived for a harmonic system is now generalized for much more complicated nonlinear systems and processes.

The present article deals with the above new problems of RLT theory and their relation to the semiclassical methods (Miller, 1974, 1975a), with a number of chemical processes considered from a unique point of view and with some unsolved problems. Further progress in this field will need considerable efforts, first of all in the quantum chemical calculations of fundamental energetic parameters of the processes and of the potential energy surfaces (PES) in molecular systems. In particular, the region of PES far from the equilibrium configuration might appear to be most important for the RLT rate. Therefore this article also tries to draw the attention of quantum chemists to the necessity of calculating the PES of excited states, intermolecular potentials for close collisions, and the structure of fluid adjacent to the reactant.

We hope that the discussion of partly known and partly new methods and applications of the RLT theory in chemistry from a unique point of view will be a useful addition to a number of recently published excellent reviews on the specific problems of the RLT theory. These are the reviews by Schlag *et al.* (1971), Freed (1976, 1980), and Lin (1980), which are devoted to relaxation of electronic excitation in large molecules; the reviews by Heller (1969), Rice (1975), and Plotnikov and Ovchinnikov (1978) on photochemical processes; and the reviews by Diestler (1976, 1980), Oxtoby (1979), Brus and Bondybey (1980), and Lin (1980), which treat a vibrational relaxation of the impurity molecules in the condensed phase. Note also the reviews by Marcus (1964), Levich (1970), Dogonadze (1971), Dogonadze and Kuznetsov (1975, 1978), Bockris and Khan (1979), Ulstrup (1979), and Benderski and Ovchinnikov (1980) on the theory of electron transfer reactions in polar liquids, whereas a wider discussion of mechanisms of such reactions can be found in the monographs by Reynolds and Lumry (1966) and Bassolo and Pearson (1967). The review by Goldansky (1977) deals with low-temperature reactions; the tunnel and isotope effects in chemical reactions are discussed by Bell (1973); and the

model studies of tunnel-reaction dynamics are reviewed by Ovchinnikova (1982).

The simultaneous discussion of many types of relaxation processes and reactions presented below permits revealing the general features as well as the specificity of each process. The present review is concerned mainly with the slow (in molecular time scale) processes due either to the high transition energy or requiring a large rearrangement of the molecular environment (high reaction barriers). The small probability of these processes may be connected with the fact that the energy exchange between vibrations and translation or the transformation of great electronic energy into many vibrational and rotational quanta of a molecular system is classically forbidden. All these tunnel processes in fact involve many degrees of freedom. Joint use of the familiar RLT theory together with the semiclassical methods of studying multidimensional tunnel dynamics provides new possibilities for generalization of the RLT theory to the nonlinear or anharmonic systems. Such an approach connects the RLT probability with the optimal tunnel trajectory of the process and often permits discovery of the most probable distribution of converted energy between different degrees of freedom.

Three classes of problems are considered in which nonlinearity is of great importance, and the familiar RLT theory of harmonic models fails.

The first class involves almost local relaxation in which a large portion of electronic energy transforms into a relatively small number of modes or local bonds. For instance, dissipation of the impurity molecule vibrational energy in a solid matrix where the interaction is of a local nature since only close pair collisions are important here and only adjacent intermolecular "bonds" are the initial acceptors of energy. Very exact calculations of anharmonic dynamics (both classical and tunnel) are needed. A discussion of such a process is given in Section III, together with a brief review of the theory of electronic transitions in large molecules.

The second class involves charge transfer processes in polar liquids where the reorientation of molecular dipoles is the most essential motion of fluid particles and can by no means be reduced to harmonic dynamics. Nevertheless, under certain conditions the RLT theory can also be extended to this case, due to its cooperative statistical character. Namely, these transitions are accompanied by rearrangement of a large number of molecules, i.e., of a large solvent region, so that a large interaction energy is imparted by small interactions with each molecule. This permits using as first approximation the continuum model and the linear dielectric medium response to the electric field. These processes are discussed in Section IV.

The third class of problem is concerned with low-temperature reactions. A semiclassical formulation of the tunnel RLT, together with the quantum transition-state method (Miller, 1975b), provides a unified approach both to first-order nonadiabatic processes and to the adiabatic tunnel chemical reactions. Roughly speaking, the reaction rate is determined in this approach by optimal FC overlap of the product and reactant wave functions connected with the optimal "tunnel classical" trajectory of the system. These problems are discussed briefly in Sections II,E–II,G.

Section II outlines the main concepts and characteristic features of various types of radiationless processes. Part of the results presented there are well known and have been derived independently by many authors. Therefore only certain relevant references are given there. We hope to compensate for this in Sections III and IV with the discussion of specific problems. A number of related problems are not considered here, such as electronic relaxation in small molecules, the irreversibility problem, vibrational dephasing. These are discussed in reviews which will be quoted in corresponding sections. We try to avoid wherever possible mathematical treatments that are too complicated. Thus many variants of the RLT theory without simple physical interpretation are not reflected here. Partly they can be found in reviews by Freed (1976, 1980), Diestler (1976, 1980), and Lin (1980).

Something must be said about the transition-state theory (TST) and the RLT theory in general. It is known that in chemical kinetics the TST becomes inaccurate when the dynamic behavior is essential. But the greatest inadequacy occurs when the dynamics are essentially quantal, in particular if the chemical process represents quantum mechanical tunnel transfer of the electron or of light hydrogen or proton particles. The quantal effects may be important for heavy reactants also if the temperature is sufficiently low. In all these cases the formal transmission coefficient can differ by a few orders of magnitude, so that there is no sense in introducing it. The general criterion of the TST validity can be expressed by inequalities $kT\tau_i/h \gg 1$ where τ_i are characteristic motion times of the reactant particles.

Another limitation of the TST application appears in the case of fast chemical reactions or slow relaxation to equilibrium parameters between the elementary step. For example, in fast gas-phase reactions the nonequilibrium vibrational or rotational distributions are possible. In solids the fast reactions lead to accumulation of lattice deffects and to interesting macroscopic effects. However, in this review we deal only with the first type of deviation from the simple TST.

To conclude this section we note that the use of simplified physical models for many complex chemical processes is not unjustified here as

long as it is considered only as a first step and not as a universal theory. For even a simple reaction, quantum chemical calculations are needed in order to overcome the semiempirical character of the theory, and new possibilities of the nonlinear RLT theory from using such quantum chemical information are discussed here.

II. Physical Principles and Methods of the Radiationless Processes Theory

A. Original Formulation of the Radiationless Transition Problem

In each electronic state (1 or 2) involved in RLT, the nuclear motion of a molecular system is described by its own Hamiltonian

$$H_{1(2)} = T + U_{1(2)}(R) + \mathscr{E}_{1(2)} \tag{1}$$

where T is the kinetic energy of atoms $U_k + \mathscr{E}_k$, $k = 1, 2$, are the electronic terms of system at fixed nuclear coordinates R with their minimal values $\mathscr{E}_k$ for states 1 and 2, respectively. The PESs, $U_{1(2)}(R)$ and the corresponding electronic functions $\psi^e_{1(2)}(R, r)$ can be calculated taking account of the whole electronic interaction (adiabatic terms) or neglecting some part V_e of this interaction (diabatic terms). In each case the specific perturbation V causes transition. This interaction may be either a nonadiabacity operator

$$(V_{NO})_{12} = \langle \psi^e_1 \nabla_R \psi^e_2 \rangle M^{-1} \nabla_R - \langle \psi^e_1 \nabla_R M^{-1} \nabla_R \psi^e_2 \rangle \tag{2}$$

i.e., the operator of nuclear kinetic energy applied to electronic functions, or a matrix element of the neglected interaction V_e,

$$V_{12} = \langle \psi^e_1 V_e \psi^e_2 \rangle + (V_{NO})_{12} \tag{3}$$

For example, V_e is the spin–orbit (SO) coupling for the triplet–singlet ($T \rightarrow S$) transition in molecules, or V_e is due to the overlap of the electronic functions localized on different centers for charge transfer transition. In all cases the Born–Oppenheimer separation of the electronic and nuclear motions is assumed: The eigenfunctions of Hamiltonians $(H - V_{NO})$ or $(H - V_{NO} - V_e)$ are presented in the form $\Psi_{1(2)}(rR) = \Psi^e_{1(2)}(rR)\psi_{1(2)}(R)$ where $\psi_{1(2)}(R)$ are the nuclear wave functions in corresponding electronic states.

In the first-order perturbation theory (with respect to the interaction V_{12} causing transition), the RLT probability per unit time is given by the well-known Golden-rule expression

$$W = 2\pi/\hbar \sum_{if} |\langle \psi_{1i}(R) V_{12} \psi_{2f}(R) \rangle|^2 e^{-\beta E_i} \delta(E_i - E_f) \tag{4}$$

here $\beta = 1/kT$ is the inverse temperature. This is roughly the density of final states with the energy $E_f = E_i$ of initial state weighted with the FC factors and averaged over the Gibbs distribution of initial states. The replacing of the delta function in Eq. (4) by its Fourier transform reduces the probability W to a known expression via the generating function $G(t)$ (Kubo and Toyozawa, 1955)

$$W = \hbar^{-2} \int_{-\infty}^{\infty} G(t)\, dt \tag{5}$$

$$G(t) = Z^{-1}\, \mathrm{Sp}\{\exp[-iH_1(t - i\beta')/\hbar]V \exp[iH_2 t/\hbar]V\} \tag{6}$$

Here $\beta' = \hbar\beta = \hbar/kT$, $Z = \mathrm{Sp}(e^{-\beta H})$ is the partition function, and Sp denotes the integration over all nuclear coordinates. A similar expression

$$I(\nu) = Z^{-1} \int_{-\infty}^{\infty} e^{-2\pi i\nu t}\, \mathrm{Sp}\{e^{-iH_1(t-i\beta')/\hbar} M e^{iH_2 t/\hbar} M\} \tag{7}$$

replacing V by the dipole moment operator describes the contour $I(\nu)$ of the emission or absorption accompanying radiative transition.

The RLT between the nondegenerate electronic states with an energy gap $\Delta\mathscr{E} = \mathscr{E}_1 - \mathscr{E}_2$ can occur only if the PESs U_1, U_2 depend on the electronic state (1 or 2) (electron–nuclear or vibronic coupling) or if the perturbation V_{12} depends essentially on the nuclear coordinates. Conversion of the electronic energy to the nuclear motion energy would be impossible without such couplings.

Equations (4)–(7) are valid for a system described by arbitrary the Hamiltonian operators H_1, H_2. The aim here is to outline the main principles and features of different types of relaxation processes and reactions. Historically, the initial advances in RLT theory were related to electronic transitions in ionic crystals where the harmonic models are adequate. These models describe the transition from one stable electronic state to another with little change in the equilibrium nuclear configuration and without a considerable change of the PESs form; they are discussed in next section.

B. RLT in Harmonic Systems

The vibrational Hamiltonians are such a system described by the coordinate vector $\mathbf{R}$ are

$$H_l = (\dot{\mathbf{R}}\mathbf{M}\dot{\mathbf{R}})/2 + (\mathbf{R} - \mathbf{R}_l^e)\mathbf{M}^{1/2}\boldsymbol{\Omega}_l^2\mathbf{M}^{1/2}(\mathbf{R} - \mathbf{R}_l^e)/2, \qquad l = 1, 2 \tag{8}$$

where the mass and frequency matrixes are denoted by $\mathbf{M}$ and $\boldsymbol{\Omega}$ and the vectors of equilibrium positions in each electronic state (1 or 2) by $\mathbf{R}_{i(2)}^e$.

An analytical expression for the generating function [Eq. (6)] of this system was obtained by Kubo and Toyozawa (1955). In a simple case of displaced but undistorted ($\Omega_1 = \Omega_2$) oscillators and constant interaction $V = V_{12}$, the RLT rate is

$$W = \hbar^{-1}|V|^2 \int_{-\infty}^{\infty} G(t)\, dt, \qquad G(t) = \exp[\Phi(t)] \tag{9}$$

$$\Phi(t) = -i\,\Delta\mathscr{E}t/\hbar + \Phi_0, \qquad \Delta\mathscr{E} = \mathscr{E}_1 - \mathscr{E}_2 \tag{10}$$

The matrix expression obtained by Kubo and Toyozawa for ϕ_0 is equivalent to summing over all normal modes

$$\Phi_0 = \sum_k s_k \frac{\cosh \omega_k(it + \beta'/2) - \cosh \omega_k\beta'/2}{\sinh \beta'\omega_k/2} \tag{11}$$

Here s_k is due to the change δq_k of the equilibrium value of a normal-mode coordinate q_k in the transition

$$s_k = m_k\omega_k(\delta q_k)^2/2 \tag{12}$$

where m_k and ω_k are the reduced mass and the frequency of this mode. Another very important quantity, the reorganization energy E_R, must be introduced

$$E_R = \sum_k \hbar\omega_k s_k \tag{13}$$

Consider now the dependence of RLT probability on the temperature, energy gap $\Delta\mathscr{E}$, average vibrational quantum $\hbar\bar{\omega}$, and the vibronic coupling parameter E_R. The corresponding dimensionless parameters are

$$kT/\hbar\bar{\omega}, \qquad N = \Delta\mathscr{E}/\hbar\bar{\omega}, \qquad \bar{s} = E_R/\hbar\bar{\omega} \tag{14}$$

where N is the order of the multiphonon process. With this aim consider the oversimplified one-frequency model in which the vibrational spectrum of the molecular system is replaced by one characteristic frequency $\bar{\omega}$ with the average coupling parameters $\bar{s}$. Then the probability [Eq. (9)] is

$$W = 2\pi V^2/\hbar \sum_n \exp[N\beta'\bar{\omega}/2 - \bar{s}\,\tanh^{-1}\beta'\bar{\omega}/2]$$
$$\times I_n(\bar{s}\,\sinh^{-1}\beta'\bar{\omega}/2)\,\delta(\Delta\mathscr{E} - n\hbar\bar{\omega}) \tag{15}$$

Leaving aside here the problem of discreteness of the vibrational spectrum of such a one-frequency model, we replace the sum in Eq. (15) by an integral (or the δ function by its mean value $1/\hbar\bar{\omega}$) and consider according to Kubo and Toyozawa the limits of Eq. (15), which can be readily interpreted.

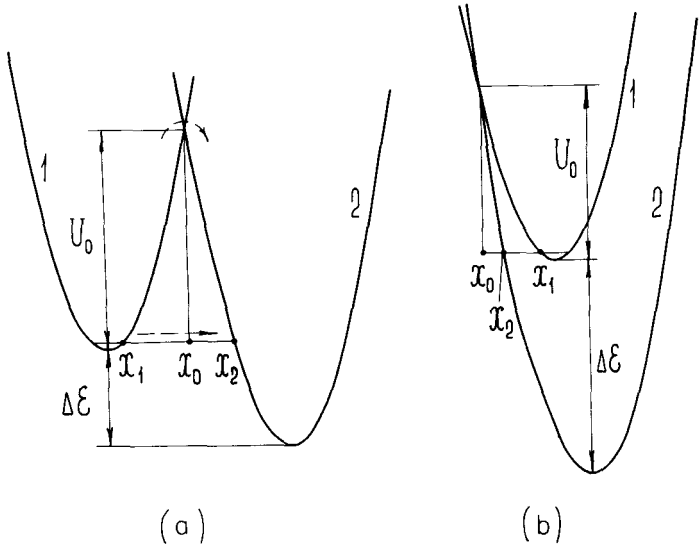

Fig. 1. Electronic terms for a harmonic model with the coordinate x_0 and potential U_0 of the crossing point and turning points x_1, x_2. (a) Strong vibronic coupling limit. The dotted lines show the activation and tunnel paths of transitions for high and low temperatures. (b) The weak coupling limit with large $\Delta\mathcal{E}$.

1. *The Strong Coupling Limit, $E_R \gg \hbar\bar{\omega}$*

It is observed for a wide class of charge transfer reactions in polar media and corresponds to the effective oscillator diagram (a) in Fig. 1 for the case $E_R \gg \hbar\bar{\omega}$. At high temperatures $kT > \hbar\bar{\omega}/2$, the RLT rate [Eq. (15)] becomes

$$W = \frac{1}{\hbar} V^2 \left(\frac{\pi}{kTE_R}\right)^{1/2} \exp\left[-\frac{(E_R - \Delta\mathcal{E})^2}{4E_R kT}\right] = \frac{\bar{\omega}}{2\pi} P e^{-E_a/kT} \qquad (16)$$

The transition is seen to occur classically with an activation energy E_a equal to the potential at the crossing point of two electronic terms. The preexponential factor in Eq. (16) is equal to the mean frequency $\bar{\omega}/2\pi$ of attaining the crossing point multiplied by the transmission coefficient P. The latter is the Landau–Zener transition probability averaged over the Maxwellian velocity distribution above the crossing point

$$P = 4\pi\overline{\xi(v)}, \qquad \xi(v) = V^2/(\hbar v\, \Delta F) \qquad (17)$$

where ξ is the corresponding Massey parameter and ΔF is the difference between the potential slopes at the crossing point. Equation (16) has the form typical for the transition-state theory, and it can immediately be

generalized for the adiabatic case of large interaction $V = V_{12}$ by replacing the transmission coefficient by 1 and the activation energy E_a by the barrier height $U^{\#}$ of the adiabatic surface.

At low temperatures, $kT < \hbar\bar{\omega}/2$, the RLT rate becomes

$$W_{1\to 2} = e^{\beta\Delta\mathscr{E}} W_{2\to 1} = \frac{2\pi}{\hbar\bar{\omega}} V^2 \exp\left[\frac{\Delta\mathscr{E}}{\hbar\bar{\omega}} \ln \frac{E_R e}{\Delta\mathscr{E}} - \frac{E_R}{\hbar\omega}\right] \tag{18}$$

This result corresponds to quantum tunneling of the system from the zero vibrational level of the initial electronic state to the potential well of the final state. Indeed, this expression coincides with

$$W_{1\to 2} = \frac{\bar{\omega}}{2\pi} P_t \exp\left\{-\frac{2}{\hbar}\left[\left|\int_{x_1}^{x_0} p_1(x)\,dx\right| + \left|\int_{x_0}^{x_2} p_2(x)\,dx\right|\right]\right\} \tag{19}$$

$$p_{1(2)}(x) = \{2m[E - U_{1(2)}(x)]\}^{1/2}$$

with accuracy to the factor ~ 1. Here the exponent defines the barrier penetrability of the particle with mass m and energy $E = \mathscr{E}_1 + \hbar\bar{\omega}/2$ and P_t is the tunnel transmission coefficient

$$P_t = \pi V^2/(\hbar\,\Delta F v_0) = \pi\xi(v_0), \qquad v_0 \simeq (2E_a/m)^{1/2}$$

This expression is valid for weak interaction V ($\xi < 1$). The general expression for P_t has been obtained by Ovchinnikova (1965). In particular, for strong interaction $P_t \to 1$ and the tunnel penetrability factor is to be simultaneously calculated for the exact adiabatic barrier instead of the diabatic one. At intermediate temperatures the activation energy varies from E_a to zero as $T \to 0$, and a relatively simple expression for RLT can be obtained.

Note that both the classical [Eq. (16)] and the quantum [Eq. (19)] RLT rates have a maximum at $\Delta\mathscr{E} = E_R$ when the potential surface U_2 intersects U_1 in the region of the U_1 equilibrium configuration.

2. *Weak Coupling Limit*

Another physically important case of the tunnel process is the relaxation of large electronic energy ($N = \Delta\mathscr{E}/\hbar\omega \gg 1$) for small and moderate coupling ($\bar{s} \lesssim 1$). Such a situation corresponding to Fig. 1b is typical for relaxation of electronically excited molecules. Previously, for the above-mentioned strong coupling limit at low temperatures, the system undergoes tunneling motion between two configurational regions separated by the barrier. Unlike this in the weak coupling limit $E_R \ll \Delta\mathscr{E}$, the classically allowed regions in each electronic state overlap and the tunnel character of the process is connected with the large difference between the momenta p_1 and p_2 in the overlap region. The corresponding asymptotics

of the exact result [Eq. (15)] in the one-frequency model give the following expression for the RLT rate at zero temperature.

$$W = \frac{2\pi}{\hbar}\left(\frac{2\pi}{\Delta\mathscr{E}\hbar\bar{\omega}}\right)^{1/2} \exp\left[-\bar{s} - \frac{\Delta\mathscr{E}}{\hbar\bar{\omega}} \ln\frac{\Delta\mathscr{E}}{\hbar\bar{\omega}s}\right] = \frac{\bar{\omega}}{2\pi} p_t e^{-\Phi} \qquad (20)$$

where Φ is the difference between classical action integrals up to the crossing point x_0 on each term with energy $E = \mathscr{E}_1 + \hbar\bar{\omega}/2$

$$\Phi = 2\left[\left|\int_{x_0}^{x_1} p_1(x)\,dx\right| - \left|\int_{x_0}^{x_2} p_2(x)\,dx\right|\right]\Big/\hbar \qquad (21)$$

The definition of x_1, x_2 is shown in Fig. 1b. A generalization of tunnel transmission coefficient P_t for strong interaction V is known from the solution of the tunnel transition problem in the system of two linear crossing terms (Bykhovski *et al.*, 1964). The tunnel assymptotics [Eq. (20)] can be written immediately using the semiclassical procedure for the matrix-element estimation (Landau and Lifshitz, 1974).

The main feature of relaxation is the rapid exponential decrease in the RLT rate with increasing energy gap $\Delta\mathscr{E}$. Note that for a harmonic model, transition is allowed only in the Nth order in vibronic coupling parameter s ($W \sim s^N$) where N is the multiphonon-process order. This is due to the fact that the action $\Phi \sim N \ln(N/s)$ tends to infinity as $s \to 0$. For an anharmonic system it will be shown further that the transition is already allowed in the first order in s, though the exponential dependence of $W(\Delta\mathscr{E})$ is retained.

The simple-model results in this section confirm the important general FC principle of conservation of nuclear momenta and coordinates in transitions: The potential crossing region (or the points of the potential singularities) might appear to be the one most important for the transition, and the RLT is controlled by the probability of classical or quantum fluctuation of the system to this region. The same principles are the basis of the nonadiabatic transition theory in inelastic atomic collisions (Nikitin and Umanski, 1979). A specific requirement of the large molecular systems discussed below is the necessity of choosing the optimal fluctuation from among those occuring in multidimensional systems. Some solutions of this problem in a harmonic system are described in the next section.

C. Steepest Descent Method in the RLT Theory. Weak Coupling Limit

Note that asymptotic results [Eqs. (16), (18), and (20)] can be obtained without using the exact result [Eq. (15)] valid for the one-frequency model only. It is sufficient for this purpose to apply the steepest descent method (SDM) (or the stationary-phase method) directly to calculation of the integral [Eq. (9)]. The application of this very important method to RLT

seems to have been first suggested by Holstein (1953). It appears to be decisive for the study of relaxation and reactions in multidimensional, multifrequency systems at large energy gap $\Delta\mathscr{E} \gg \hbar\omega$ or at large reorganization energy $E_R \gg \hbar\omega$. We consider first the harmonic systems.

The condition $\Phi'(t_0) = 0$ for determination of the saddle point $t_0 = i\tau_0$ of the integrand in Eq. (9) with the derivative of action function (11) has the form

$$\Delta\mathscr{E} = \sum_k \bar{E}_k = \sum_k s_k \hbar\omega_k \frac{\sinh \omega_k(\beta'/2 - \tau_0)}{\sinh \omega_k \beta'/2} \tag{22}$$

and the RLT rate according to the steepest descent estimation of the integral of Eq. (9) is

$$W = [(2\pi)^{1/2}/\hbar]V^2 |d^2\Phi/dt^2|^{-1/2} \exp[\Phi(t_0)] \tag{23}$$

Moreover, this method gives additional information about the most probable distribution of the electronic energy over various vibrational degrees of freedom $\Delta\mathscr{E} \to \Sigma\bar{E}_k$ according to Eq. (22) and the dispersion of this distribution on the modes q_k for final vibrational energy

$$\langle (E_k - \bar{E}_k)^2 \rangle = (\hbar\omega_k)^2 s_k \frac{\cosh \omega_k(\beta'/2 - \tau_0)}{\sinh \bar{\omega}_k \beta'/2}$$

Here, the averaging is performed over all possible final channels with a fixed total energy $E_f = E_i$ and over Gibbs distribution of initial energies.

The physical meaning of the result of Eq. (23) and the ranges of its validity can be readily demonstrated for weak and strong coupling. In this section the case of weak coupling ($E_R \leqslant \hbar\omega$), large energy gap ($\Delta\mathscr{E} \gg \hbar\omega$), and low temperature is considered. It is typical for electronic relaxation in large molecules. The RLT theory was first applied to this problem by Lin (1966), Siebrand (1966, 1967a,b), Lin and Bersohn (1968), and Bixon and Jortner (1968). The SDM was first used for such transitions by Ovchinnikova (1968) and Fisher (1970).

According to Eq. (23), the RLT rate is determined by the action function $\Phi(t_0)$ at the saddle point

$$\begin{aligned} \Phi(t_0 = iy) &= -\Delta\mathscr{E}y/\hbar + \sum_k [\tilde{s}_k e^{\omega_k y} + \tilde{\alpha}_k/2e^{2\omega_k y}] \\ \Phi''(t_0) &= \sum_k (\tilde{s}_k \omega_k^2 e^{\omega_k y} + 2\omega_k^2 \tilde{\alpha}_k e^{2\omega_k y}) \end{aligned} \tag{24}$$

where ϕ'' is the second derivative of action and

$$\begin{aligned} \tilde{s}_k &= s_k(1 - e^{-\beta\hbar\omega_k})^{-1}, \qquad \tilde{\alpha}_k = \alpha_k(1 - e^{-2\beta\hbar\omega_k})^{-1} \\ \alpha_k &= \left(\frac{\omega_{1k} - \omega_{2k}}{\omega_{1k} + \omega_{2k}}\right)^2 \end{aligned} \tag{25}$$

Different from Eq. (11), Eq. (24) accounts for the small frequency change ($\alpha_k \ll 1$) of normal modes without their mixing. The saddle point $t_0 = iy$ is determined by equation

$$\hbar\Phi'(t_0) = -\Delta\mathscr{E} + \sum_k (\tilde{s}_k e^{\omega_k y} + \tilde{\alpha}_k e^{2\omega_k y})\hbar\omega_k = 0 \tag{26}$$

Freed (1976) gave a very clear derivation and a physical interpretation of this result for undistorted transition ($\alpha_k = 0$) at zero temperature. For such a case, FC factors $\langle\{0\}_1|\{n_k\}_2\rangle$ needed are known and the RLT rate [Eq. (4)] is

$$W = \frac{2\pi}{\hbar} V^2 \sum_{n_k} \prod_k e^{-s_k} s_k^{n_k} \frac{1}{k!} \delta\left(\sum_k n_k\hbar\omega_k - \Delta\mathscr{E}\right)$$

A search for the optimal distribution n_k^* providing the maximum contribution to the rate with fixed-energy constraint leads to the equations (if $n_k > 1$) $n_k^* = n_k(y) = \exp(\omega_k y)$ and $\sum_k s_k n_k(y) = \Delta\mathscr{E}$, which are identical to Eq. (26), determining the saddle point $t_0 = iy$.

Thus for a multidimensional system and for nonzero temperature the SDM gives the possibility of finding the optimal initial and final states and of estimating the RLT rate from the width of the FC factors distribution close to the optimal state n_k^*. The formal conditions of SDM validity for a harmonic system are

$$\Delta\mathscr{E} \gg \hbar|\Phi''(t_0)|^{1/2} \sim (\Delta\mathscr{E}\hbar\omega)^{1/2} \gg \hbar\omega$$

This means that the region of final states close to the optimal state n_k^* with significant contribution of the RLT rate must include many states. At the same time, the energy width of this region must be less than $\Delta\mathscr{E}$. Further, as seen for an anharmonic system the FC factors behave in such a way that SDM might be inapplicable.

The most general method for investigation of the system with separable variables (either harmonic or anharmonic) is the factorization-variable method. It can be illustrated by a simple system with two independent groups of variables a and b and with $V = V_{12} = \text{const}$. Assume that for each of the subsystems a or b the dependences of the FC-weighted state density are known and are

$$I_a(\mathscr{E}_a) = Z_a^{-1} \sum_{n,m} \exp(-\beta E_{1m}^a)|\langle\psi_{1m}^a|\psi_{2n}^a\rangle|^2 \delta(E_{1m}^a - E_{2n}^a - \mathscr{E}_a) \tag{27}$$

and the same expression holds for $I_b(\mathscr{E}_b)$ (Z is a partition function here). Then the electronic transition probability with the transition energy (energy gap) $\Delta\mathscr{E}$ is

$$W(\Delta\mathscr{E}) = V^2 I_{ab}(\Delta\mathscr{E}), \qquad I_{ab} = \int F(\mathscr{E}_a)\, d\mathscr{E}_a$$
$$F(\mathscr{E}_a) = I_a(\mathscr{E}_a) I_b(\Delta\mathscr{E} - \mathscr{E}_a) \tag{28}$$

This feature of the mode factorization permits extension of RLT theory to systems where some degree of freedom either sharply changes the character of the motion or has an essentially anharmonic character. Such a program was first suggested by Gelbart *et al.* (1970) to account for the role of torsial vibrations in molecules undergoing cis–trans isomerization during transitions.

The relation (28) permits studying the distribution of electronic energy over two or more subsystems. Two different types of energy distribution are possible and can be illustrated by a simple system with two identical degrees of freedom a and b. In the harmonic case the use of Eq. (18) for calculation of both functions $I_a(\mathscr{E}_a)$ and $I_b(\Delta\mathscr{E} - \mathscr{E}_a)$ in the integral of Eq. (28) yields the maximum in the integrand $F(\mathscr{E}_a, \Delta\mathscr{E})$ for the optimal equiprobable (in this case) distribution $\mathscr{E}_a^* = \mathscr{E}_b^*$ of the transition energy $\Delta\mathscr{E} = \mathscr{E}_a^* + \mathscr{E}_b^*$. This is seen from Fig. 2a. It can be verified that $F(\mathscr{E}_a^*)/F(0) = 2^N$, where $N = \Delta\mathscr{E}/\hbar\omega$ is the order of the multiphonon process, and that only

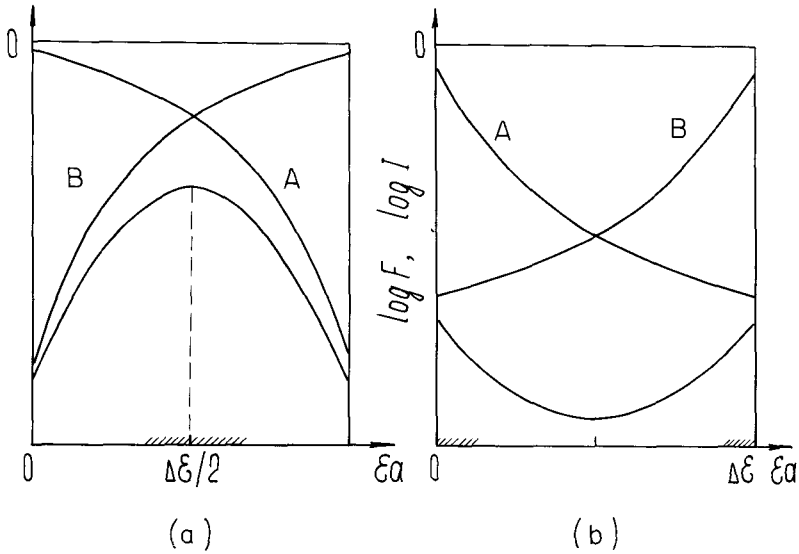

Fig. 2. The logarithms of the FC weighted-state density $I_a(\mathscr{E}_a)$, $I_b(\Delta\mathscr{E} - \mathscr{E}_a)$ (curves A and B) and of their product $F(\mathscr{E}_a) = I_a(\mathscr{E}_a) I_b(\Delta\mathscr{E} - \mathscr{E}_a)$ defining the distribution of energy between two equivalent degrees of freedom: for harmonic potentials (a) and for anharmonic Morse potentials with small displacement (b). The regions of most probable distribution are shown on the energy axis.

the small region $\Delta\mathscr{E}/N$ around the optimal value $\mathscr{E}_a^*$ contributes to the RLT rate [Eq. (28)]. An essentially different situation takes place for two anharmonic oscillators with small vibronic coupling parameters $s_a = s_b \ll 1$. Then the rate of the $0, 0 \to n_a, n_b$ transition is nonzero, even in the first order with respect to the parameter s (see Section III,B)

$$I(\mathscr{E}(n)) = \delta_{n,0} + s\tilde{I}(\mathscr{E}(n)) + O(s^2)$$

where the functions $\tilde{I}_a(\mathscr{E}_a)$ and $\tilde{I}_b(\mathscr{E}_b)$ behave as shown in Fig. 2b (the second derivative of $\ln \tilde{I}(\mathscr{E})$ is negative, different from the harmonic case). This leads to a more probable localization of the total energy of only one of the anharmonic oscilators but not on both as for the harmonic case. It is seen from Fig. 2b that the SDM is invalid for the anharmonic case and the saddle point $\mathscr{E}_a^*$ corresponds to the minimum in the integrand in Eq. (28).

The mode-factorization method was of great help in studying the relative rates of decay from single vibronic levels (Heller *et al.*, 1972; Prais *et al.*, 1974; Kühn *et al.*, 1977; Freed, 1976). Indeed, such a decay rate $W(n_a, \Delta\mathscr{E})$ of the vibrational state of n_a of the mode a can be written as (the assumption V = const is retained)

$$W(n_a, \Delta\mathscr{E}) = \sum_m |\langle n_{a1}|m_{a2}\rangle|^2 W_b(\Delta\mathscr{E} - \hbar\omega_a(n_a - m_a)) \qquad (29)$$

where the subscript b denotes the remaining modes of the molecule. Use of the exponential dependence $W_b(\mathscr{E}_b)$ (calculated or empirical) permits us to obtain the simple relation for the single-vibronic-level decay rates $W(n_a)/W(0)$. The detailed theory and its applications are reviewed by Freed (1976).

The following general conclusions about the relaxation of large electronic energy in complex molecular systems are now reiterated:

(1) The RLT rate, as for the one-frequency model, is exponentially decreasing with increasing energy gap

$$W \sim \exp[-\Delta\mathscr{E} f(\Delta\mathscr{E})] \qquad (30)$$

(2) The high-frequency modes appear to be more effective acceptors of the electronic energy compared to the low-frequency ones, and the role of the former becomes more important for large values of $\Delta\mathscr{E}$. The average final quantum number n_k^* of the given mode exponentially increases with the mode frequency [see Eq. (26)]. Taking account of anharmonicity the best acceptors might appear to be the most anharmonic bonds, as shown below (Section III,B).

(3) The RLT rate increases with temperature according to Eqs. (23)–(25).

D. Dependence of the RLT Rate on Temperature and Transition Energy $\Delta\mathscr{E}$. Strong Coupling Limit

This limit corresponds to a large reorganization energy $E_R \gg \hbar\omega$. Historically, such processes in ionic crystals stimulated the development of the RLT theory. These processes are also related to the hopping mechanism of the mobility of the small-size polarons (Holstein, 1953). An example of strong coupling transitions in chemical processes is given by the wide and very important class of reactions with charge transfer in polar media. An essential feature of such transitions is their statistical or cooperative character: These processes are accompanied by the rearrangement of a large number K of degrees of freedom so that the strong overall interaction of electronic state with medium

$$E_R/\hbar\omega = \left(\sum_k s_k\omega_k\right)\Big/\omega \gg 1$$

is provided by a large number of sufficiently weak interactions with a single mode or a single degree of freedom ($s_k \lesssim 1$). Therefore, as before the coordinates of the medium particles undergo small fluctuations or rearrangement near their equilibrium positions. This often provides a basis for describing such a transition either in the harmonic approximation or using a more general linear response theory.

Consider now the characteristic RLT rate dependence on the electronic transition energy (or the reaction heat) for the harmonic model. This dependence $W(\Delta\mathscr{E})$ may be quite measurable. For example, the probability of radiative transition is defined by Eq. (7) which is an analog of the RLT rate $W(\Delta\mathscr{E})$ with $\Delta\mathscr{E}$ replaced by $\Delta\mathscr{E} - h\nu$, (where ν is the radiation frequency. Other examples of a similar measurable dependence $W(\Delta\mathscr{E})$ are provided by electrochemical reactions in which a change of the electrode potential causes variations in the reaction energetics. The dependence $W(\Delta\mathscr{E})$ can also be studied in a series of reactions of the same type with a small variation of their energetics.

As shown by the one-frequency model, the RLT rate [Eq. (16) or (18)], both in classical and quantum cases, has a maximal value when the PES of the final state intersects the initial PES in the region of its equilibrium configuration. This maximal quantity W_{max} may be very close to the maximal frequency of the system $W_{max} \sim 10^{14}$–10^{13} sec^{-1} if transition is not forbidden. For both sides around $\Delta\mathscr{E}_{max}$, the RLT probability decreases by the exponential law which is in general determined by the frequency properties of the system and can be studied by SDM. There is a wide variety of possible situations, and for harmonic models a detailed classification has been done by Dogonadze and Kuznetsov (1975) and Ulstrup (1979). We consider here only two cases: a nearly thermoneutral

reaction and a reaction in the region $\Delta\mathscr{E} \sim E_R$ close to the maximal RLT rate.

In the first case $\Delta\mathscr{E} \ll E_R$, Eq. (21) gives the value $t_0 = i\tau_0 \simeq i\beta/4$ for the saddle point and the RLT rate [Eq. (22)] is

$$W(\Delta\mathscr{E} = 0) = A \exp\left[-\sum_k \tanh(\beta\hbar\omega_k/2)\right] \tag{31}$$

It is seen that the RLT rate temperature dependence is determined only by "classical" low-frequency degrees of freedom $k < k_0$ for which $h\omega_k < 4kT$. At the same time the "quantum" high-frequency modes $k > k_0$ ($h\omega_k > 4kT$) give only the tunnel factor in W but not the contribution to the activation energy of the RLT rate

$$W \sim V^2(E_a\hbar\omega_{cl})^{-1/2} \exp\left(-\sum_{k>k_0} s_k\right) \exp(-\beta E_a) \tag{32}$$

When $\Delta\mathscr{E} \ll E_R$ the activation energy depends on the classical mode reorganization only

$$E_a \simeq (E_R^{cl} - \Delta\mathscr{E})^2/4E_R^{cl}, \qquad E_R^{cl} = \sum_{k<k_0} s_k\hbar\omega_k \tag{33}$$

This important classification of all modes as quantum or classical was proposed by Dogonadze and Kuznetsov.

In the region $|\Delta\mathscr{E} - E_R| \ll E_R$ close to the maximal value of the RLT rate, the SDM, just as the method of semi-invariants (Kubo and Toyozawa, 1955) give the Gaussian dependence

$$W(\Delta\mathscr{E}) = W_0 \exp[-(\Delta\mathscr{E} - E_R)^2/\sigma_2(T)] \tag{34}$$

Here the preexponential factor is almost independent of temperature and of $\Delta\mathscr{E}$, and the width of the maximum of the function [Eq. (34)] is determined by the quantity

$$\sigma_2(T) = 2\sum_k s_k(\hbar\omega_k)^2 \tanh^{-1}\beta\hbar\omega_k/2 \simeq a + bkT \tag{35}$$

where the constants a and b are contributed only by quantum or classical degrees of freedom, respectively,

$$a = 2\sum_{k>k_0} s_k(\hbar\omega_k)^2, \qquad b = 4E_R^{cl} \tag{36}$$

If the system has low-frequency modes only, then in the entire range of $\Delta\mathscr{E}$ the RLT rate is described by the Arrhenius-type dependence

[Eq. (32)] with the activation energy [Eq. (33)] quadric in $\Delta\mathscr{E}$ and controlled by the parameter $E_R = E_R^{cl}$ only, but not influenced by the frequency characteristics of the system. For the strong coupling transitions discussed [$E_R kT \gg (\hbar\bar{\omega})^2$, $E_R/h\bar{\omega} \gg 1$], the SDM is always valid.

For the description of the absorption and emission line shape in radiative transitions with strong vibronic coupling, a similar treatment also gives the Gaussian curves

$$I(\nu) \sim \exp[-(h\nu - \Delta\mathscr{E} \mp E_R)^2/\sigma_2] \tag{37}$$

for which the difference of the absorption and the emission maxima is $2E_R$ and at high temperatures the linewidth shows a typical dependence $\sigma_2^{1/2} = (4E_R kT)^{1/2}$. However, Eq. (37) cannot describe one important feature of experimental spectra in such a classical system as F centers in ionic crystals: the strong temperature dependence of $h\nu_{max}$. The large value of the temperature shift $d(h\nu_{max})/d(kT) \sim 15$ has been interpreted by the changes not accounted for in the phonon frequencies of the excited states (Huang and Rhys, 1950). This shift is much greater than expected for one mode. Therefore, it means that the transition is accompanied by rearrangement of a very large number of modes.

E. Semiclassical Approach in RLT Theory for Anharmonic Systems

The classical or semiclassical interpretation of the exact harmonic model results [Eqs. (14)–(17)] demonstrate the possibility of a similar description of essentially anharmonic systems. Such a treatment is based on the known relation between the quantum process amplitudes and the characteristics of specific classical trajectory of the system under semiclassical conditions (Feynman and Hibbs, 1965). For quantum effects in the atom–molecule scattering, such a description [the classical S-matrix method (CSMM)] has been developed by Miller, Marcus, and others (see reviews by Miller, 1974, 1975a,b). A similar approach to transitions between the electronic states with arbitrary PES is given below. It permits application of the classical trajectory method to essentially quantum relaxation processes and to low-temperature tunnel reactions.

Turning again to the basic expression [Eqs. (5) and (6)] for the RLT rate, we use the well-known semiclassical representation of the propogator

$$\langle x'|e^{-iHt}|x\rangle = (2\pi)^{-n/2}\left|\mathrm{Det}\left\|\frac{\partial^2 S}{\partial x\,\partial x'}\right\|\right|^{1/2}\exp[iS(x'xt)] \tag{38}$$

where S is the action integral along the classical trajectory $x(t')$ of the system with the boundary values x and x' of the coordinate vectors at time moments $t' = 0$ and $t' = t$. Then for an n-dimensional system with

arbitrary PES $U_1(x)$, $U_2(x)$, and for the interaction of a sufficiently general form

$$V_{12} = V(x) = V_0 e^{-\alpha x} \tag{39}$$

the RLT rate [Eq. (5)] becomes

$$W = 2\pi Z^{-1} \int\int\int dt\, dx\, dx' V(x')V(x)A \exp[\phi(xx't)] \tag{40}$$

$$\phi = iS_1(x'x, t_1, -t_1) + iS_2(xx', t_2, -t_2) \tag{41}$$

$$t_1 = (t - i\beta)/2, \qquad t_2 = -t/2 \tag{42}$$

Here S_1 and S_2 correspond to U_1 and U_2, A is expressed via the matrices of the action second derivatives, and x, x' are the boundary values of trajectories $x_1(t')$, $x_2(t')$ at the ends of time intervals $(-t_1, t_1)$, $(-t_2, t_2)$. For convenience, the points $t' = 0$ are chosen in the middle of intervals. The SDM estimation of integrals [Eq. (40)] over all integration variables yields equations for the boundary coordinates x, x' and for the time value $t = 2t_2 = 2t_1 - i\beta$ of the optimal trajectory determining the directions of maximal overlap of the initial and final states in the multidimensional space. These equations are

$$\begin{aligned} x' &= x_1(t_1) = x_2(-t_2), & p_1(t_1) &= p_2(-t_2) + i\alpha/\hbar \\ x &= x_1(-t_1) = x_2(t_2), & p_1(-t_1) &= p_2(t_2) - i\alpha/\hbar \\ E_1 &= E_2, & t_1 + t_2 &= -i\beta/2 \end{aligned} \tag{43}$$

Here E_1, E_2 are the energies of two trajectories; p_1, p_2 are the momenta related to action derivatives with respect to x, x'; and α is the vector defining the interaction dependence [Eq. (39)] on the coordinate. The trajectories $x_1(t')$, $x_2(t')$ are seen to be symmetric with respect to the turning point $t = 0$,

$$x_{1(2)}(t) = x_{1(2)}(-t), \qquad x = x', \qquad \dot{x}_1(0) = \dot{x}_2(0) = 0 \tag{44}$$

Thus the RLT probability is controlled by the contribution of the optimal trajectory

$$W = V^2(\hbar^2 Z)^{-1} A' \exp[\Phi(xx't)] \tag{45}$$

where A' depends on the second derivatives of S_1, S_2, Φ over x, x', t and Φ is the action [Eq. (41)] along this trajectory $x_1(t')$, $x_2(t')$.

For constant interaction V [if $\alpha = 0$ in Eq. (39)], Eqs. (43) simultaneously require an equality of the boundary coordinates and momenta of the two parts of the trajectory on both surfaces U_1 and U_2. This can be fulfilled only if $x(=x')$ is the crossing point of PES. Thus two parts $x_1(t')$

and $x_2(t')$ of the optimal trajectory form a unique continuous periodic trajectory with period $T = -i\beta$. Half of this trajectory connects the turning points x_{01} and x_{02} on both surfaces. Moreover, the substitution of the pure imaginary quantities $[t \to -i\tau,\ p(t) \to i\pi(\tau)]$ for time and momenta transforms the complex-valued trajectory to the real-valued classical trajectory $z(\tau), \pi(\tau)$ in reversed PES ($U \to -U, E \to -E$). Then the RLT rate is

$$W \sim \exp\left(-\beta E - 2\left|\int_0^{\beta/2} \pi(\tau)\dot{z}(\tau)\, d\tau\right|\right) \tag{46}$$

where the real-valued trajectory $z(\tau)$ connects the turning points on both reversed potential surfaces in the whole time $\tau_1 + \tau_2 = \beta/2$. The energy $E = E(\beta)$ of the optimal trajectory coincides with the activation energy $E_a = d \ln W/d\beta$.

The optimal tunnel trajectories have various forms for the two different types (a) or (b) of the tunnel processes corresponding to schemes (a) and (b) in Fig. 1. At $E_R < \Delta\mathscr{E}$ or $E_R > \Delta E$, the equilibrium configurations x_{e1}, x_{e2} of electronic states 1 and 2 lie on the same or on different sides of the terms crossing surface. Consequently, for case (a) the time increment has the same sign in two parts of the trajectory and the corresponding contributions to the total action integral add

$$\tau_1 + \tau_2 = |\tau_1| + |\tau_2| = \beta/2, \qquad \Phi = -(|S_1| + |S_2|) \tag{47}$$

At the same time for case (b) we have

$$\tau_1 + \tau_2 = |\tau_1| - |\tau_2| = \beta/2, \qquad \Phi = -(|S_1| - |S_2|) \tag{48}$$

For multidimensional harmonic models the tunnel trajectory method (TTM) readily gives the same results as those of the SDM application to the generating-function expression [Eq. (5)]. However, the interesting applications of TTM are expected for the anharmonic system for which there is no similar analytical expression. The example of such an application to the anharmonic vibrational relaxation is discussed in Section III,C.

F. Classical *S*-Matrix Method and Quantum Transition-State Method for Chemical Tunnel Reactions

The previous discussion is concerned solely with nonadiabatic reactions, i.e., transitions between different electronic states. We consider here an adiabatic reaction which occurs on the unique adiabatic PES of the system. For high temperatures the transition-state theory (TST) gives the reaction rate as a flow in phase space through the critical surface dividing the product and reactant channels, assuming an equilibrium distribution of the systems in the transition state. For low temperatures an

essential quantum correction and a study of the multidimensional tunnel dynamics are needed. In this connection two semiclassical methods are important: the quantum transition-state theory (QSTS) for calculating the equilibrium rate constant, and the classical S-matrix method (CSMM) (or the complex-valued trajectory method) for calculating the partial state-to-state reaction rates. These methods have been proposed by George and Miller (1972) and Miller (1974, 1975a,b).

To illustrate the ideas of these methods we consider a simple one-dimensional barrier. When the energy E is lower than the barrier height, the barrier penetrability for a particle with mass m is known to be

$$P(E) = \exp[-\phi(E)] \tag{49}$$

$$\phi(E) = (2/\hbar) \int_{x_1}^{x_2} \{2m[U(x) - E]\}^{1/2}\, dx \tag{50}$$

where x_1, x_2 are the turning points. The quantity $\frac{1}{2}\Phi$ is none other than the imaginary part of the action along the trajectory from one channel to another satisfying the classical motion equations in the potential $U(x)$ with energy E and an imaginary time increment

$$\mathrm{Im}(t_2 - t_1) = \tau_0 = \int_{x_1}^{x_2} dx\{2[U(x) - E]/m\}^{-1/2} \tag{51}$$

Using Eq. (50) the thermally average reaction rate can be expressed as

$$P(T) = \beta \int_0^\infty e^{-\beta E - \Phi(E)}\, dE \simeq (\pi/\Phi'')^{1/2} \beta e^{-\beta E^* - \Phi(E^*)} \tag{52}$$

where $E^* = E^*(T)$ corresponds to the maximum of the integrand. This optimal energy of tunneling at a given temperature $kT = \beta^{-1}$ is found from the condition $\Phi'(E) = -\beta$ which connects the time of tunnel motion through the barrier with the inverse temperature

$$\mathrm{Im}(t_2 - t_1) = \tau(E^*) = \hbar/2kT \tag{53}$$

The value $E^*(T)$ coincides with the activation energy $E_a = d \ln P(T)/d\beta$ at a given temperature.

In a similar way the average probability of a tunnel hydrogen atom transfer reaction of the type

$$\mathrm{AH} + \mathrm{B} \rightarrow \mathrm{A} + \mathrm{HB} \tag{54}$$

from the initial state n_1 of the reactant to the product state n_2 is expressed, according to CSMM, via the characteristics of classical complex-valued trajectory with specific boundary conditions: with the given value n_1 and n_2 of vibration and rotation actions corresponding to quantum numbers of the reactions and products. Therefore the reaction rate is

$$P_{n_1 n_2}(T) \sim A \exp[-2 \operatorname{Im} S(n_1 n_2) - \beta E] \tag{55}$$

where E and $S(n_1 n_2)$ are the energy and the action integral along the desired trajectory with condition (53). Such a formulation was first proposed and applied to a collinear model of the H_2 + H reaction by George and Miller (1972). They succeeded in overcoming the difficulties connected with double boundary conditions for the complex-valued trajectory and with the proper choice of the integration contour in the complex plane of time. This rather complicated method is needed to obtain the partial state-to-state rate [Eq. (55)] of a tunnel reaction.

However, the problem is simplified if the average rate constant of a reaction at an initial equilibrium reactant distribution to all final product states is of interest. The QTST proposed by Miller (1975b) is quite appropriate for obtaining such a tunnel reaction rate. It can be explained in the following way.

Assuming that the reaction barrier is sufficient high, the whole space can be divided by critical surface into two regions: the reactant A and the product B. The initial equilibrium density matrix of reactants is

$$\hat{\rho}(0) = \rho(x'x0) = Z_A^{-1} \langle x' e^{-\beta H} x \rangle, \qquad x', x \in A \tag{56}$$

where Z_A is the partitition function of the reactant, the Hamiltonian H is discribed by adiabatic PES, and the coordinates x', x belong to reactant region A. The reaction rate $K(T)$ may be found from the probability $N(t)$ of the system to be in the product channel B at a sufficiently long time t,

$$K(T) = \lim_{t \to \infty} N(t)/t, \qquad N(t) = \int_{y \in B} \rho(yyt)\, dy \tag{57}$$

$$\rho(y'yt) = \langle y' | e^{-iHt} \rho(0) e^{iHt} | y \rangle \tag{58}$$

where y belongs to channel B. Miller used a somewhat different but equivalent definition of the reaction rate. In both ways the use of the semiclassical representation [Eq. (38)] for the propagators gives the reaction rate expression through the characteristics of the periodic classical tunnel trajectory with period $T_0 = -i\beta$ (see Appendix 1). Namely, in time $t = -i\beta/2$ a half of this trajectory will connect two turning points x_0 and y_0 in the reactant and product channels. (The concepts "classical" and "tunnel" trajectories exclude each other for a real-valued one, but are compatible with the complex-valued trajectory.) For the optimal periodic trajectory discussed, the replacement $t \to i\tau$, $\dot{x}_t \to -i\dot{x}_\tau$ make it a real-valued classical trajectory in the reversed potential.

Thus for an adiabatic reaction, the boundary conditions of the optimal trajectory appear to be the same as for a nonadiabatic one, but the preexponential factor depends on the trajectory characteristics only. The rate

constant derived by Miller is

$$K = (dE/d\beta)^{1/2} A_0 \exp(\Phi) \tag{59}$$

Here Φ is the total action integral along the needed periodic trajectory

$$\Phi = 2 \operatorname{Im} S = -\beta E - 2 \left| \int_{x_0}^{y_0} p(t)\dot{x}(t)\, dt \right| \tag{60}$$

The value $E = E(\beta)$ is the energy of this trajectory with the period $-i\beta$, and the preexponential factor A_0 is expressed via the second derivatives of the action over x_0, y_0, or via the stability parameters responsible for evolution of transverse perturbation around the periodic trajectory (Miller, 1975b). An elegant interpretation holds for this result: The exponent in Eq. (59) characterizes the factor of tunneling under multidimensional barrier, and the preexponent is defined by the width of a bundle of significant tunnel trajectories around the optimal one and characterizes the partition function of the quantum "transition state" for the system with nonseparable variables. The integration of the tunnel trajectory from points x_0, y_0 to classically allowed regions A, B with real-time increments might help to obtain additional information about the optimal distribution of the reaction heat over various degrees of freedom or about the efficiency of some sort of initial excitation in accelerating the reaction, if such experimental information is available.

G. Tunnel Dynamics of Low-Temperature Reactions

The low-temperature chemical reactions reviewed by Goldanski (1977) and Le Roy *et al.* (1980) involve both those with sufficiently complicated mechanisms (not discussed here) and simple ones such as H abstraction from hydrocarbon molecules by hydrogen atoms or by methyl radicals

$$RH + H \rightarrow R + H_2, \qquad RH + CH_3 \rightarrow R + CH_4 \tag{61}$$

At temperatures less than 70 K, the experiments show small activation energies compared to values 6–10 kcal/mol for high temperatures, a large isotope effect (up to 10^4), and the existence of a constant limit on the reaction rate at $T \rightarrow 0$.

The result of a model theoretical study of elementary steps of tunnel reactions reviewed in detail by Ovchinnikova (1982) is discussed here in brief.

The first steps in interpreting the non-Arrhenius temperature dependence of reaction rate and large isotope effects were done by Bell (1933, 1959), Christov (1958), and Goldanski (1959a,b) in terms of the tunnel penetrability of one-dimensional potential barriers. They derived a criterion of a dominant contribution of the tunnel pathway of reaction

$\hbar\Omega_i/2\pi kT > 1$ for the frequency of inverted barrier. (For H transfer reactions, the tunneling greatly contributes to the rate constant at temperatures less than 300 K). However, the concept of a static one-dimensional barrier is questionable, since the barrier for H motion depends on the distance R between the reactants (it disappears if the reactants approach the saddle point of PES). A treatment of multidimensional tunnel dynamics as first pointed out by Johnston and Rapp (1961) is needed here. The multidimensional harmonic models of reactions (see Ulstrup, 1979, and the references therein) seems to be too crude for a quantitative study. But even the three-atomic collinear model with realistic PES permits revealing the main coordinates requiring the dynamic description and realizing that the essential feature of tunnel reactions the competing of the small probability for close approach of the reactant with the tunnel factor $\exp[-S(R)]$, for H transfer, sharply decreases with distance R between the reactants.

First of all note that even for a collinear model, direct quantum calculations of tunnel reactions down to probability values of about 10^{-10} have been carried out by now for the reaction $H_2 + H$ only. These calculations show that the CSMM proposed by George and Miller (1972) is sufficiently accurate. This method was later applied by Ovchinnikova (1977, 1979) in a model study of tunnel reactions [Eq. (61)]. It was shown that collinear models with realistic PES actually permit to obtain an agreement about the great height of the reaction barrier (≥ 10 kcal/mol) following from high-temperature data and the small activation energy (<1 kcal/mol) at $T < 70$ K. Moreover, the saddle point potential $U^{\#}$ in collinear models appears to be essentially higher than the barrier height in a one-dimensional description of the same effects. The calculated isotope effects are also close to the experimental values for the reactions RD + H, RH + D, and RD + CH_3.

Besides direct applications of CSMM to model reaction calculations, this method is also useful for checking our simple notion about tunnel dynamics and estimating the accuracy of some approximate approach in its description.

First of all a comparison of the tunnel reaction probability by CSMM with the penetrability of a vibrationally adiabatic barrier along the reaction path for the RH + H reactions shows that if energy decreases down to 8 kcal/mol below the barrier height (~ 12 kcal/mol), the difference becomes greater than 10^3, the overall probability being 10^{-9}. (Note that the discrepancies are much more for H transfer between heavy reactants). The difference is due to the fact that the tunnel trajectories "cut off" an angle of the reaction path near the saddle point of PES. In this connection Marcus and Cotrin (1977) have proposed a recipe for finding the $H_2 + H$ reaction probability as the penetrability of the barrier along the path displaced relative to the reaction path by a zero vibration amplitude. A more

exact dynamic approach dealing with real-valued trajectories (instead of complex-valued ones in CSMM) has been proposed by Altkorn and Schatz (1980).

A quite simple approach has been derived for H transfer between heavy reactants (Ovchinnikova, 1979). It takes into account the competing of small probability for the tunnel or classical approach of the reactants up to a distance R with the small tunnel H-transfer factor $\exp[-S(R)]$ sharply decreasing with R. This factor can be calculated using the PES cross-section profile at a fixed distance R. Thus it is possible to reproduce accurately not only the CSMM reaction probability, but also to predict the optimal distance $R(T)$ of the H transfer at the given temperature. Both the approximate and the CSMM calculations show that the optimal distance $R(T)$ is still close to the saddle point $R^{\#}$ of PES even if the temperature decreases to zero: The value $R(T = 0) - R^{\#}$ is about 0.2–0.3 Å for reactions [Eq. (61)] compared to $R_e - R^{\#} \sim 0.9$ Å, where R_e is the equilibrium van der Waals distance between the reactants. In this connection the analytical result for the tunnel reaction rate derived by Klochikhin *et al.* (1979) and Trakhtenberg *et al.* (1980), in terms of harmonic reactant vibrations with linear expansion of the action $S(R) = S(R_e) + S'(R)(R - R_e)$ in the tunnel H-transfer factor $\exp(-S)$, needs further comparison with realistic models (in particular, $S(R^{\#}) > 0$ in this approximation). A more reasonable behavior of the $S(R)$ is given by the two-dimensional harmonic model involving the distance between the reactant and the coordinate of the transfered atom valence vibration. This model has been used by Ovchinnikov and Benderski (1978, 1979) for interpretation of the low-temperature reaction $R + Cl_2 \rightarrow RCl + Cl$.

One common conclusion follows from both harmonic models and from the approximate dynamic approach: The temperature dependence of the tunnel reaction rate at $T \rightarrow 0$ is controlled by the equilibrium distance R_e and the frequency of intermolecular vibrations of reactants. This permits use of the harmonic model analytical results with empirical parameters to describe the temperature dependence of the set of low-temperature reactions. Now, the question arises of the matrix influence (Ovchinnikov and Benderski, 1979).

Many other problems must also be solved to make the tunnel reaction modeling more reasonable and predictive, such as independently obtaining PES parameters; clearing up the meaning of the collinear model PES in the presence of other degrees of freedom [for example, the bending vibrations of CH_3 in reaction (61)]; the role of the resonance of quantum hydrogen levels in reactant and product channels for exothermic reactions, discussed by Pshenichnov and Sokolov (1967).

III. Mechanisms of Electronic and Vibrational Energy Relaxation

A. Relaxation of Electronic Excitation in Large Molecules

Photoprocesses and radiationless processes in large molecules have been the object of many reviews (Schlag *et al.*, 1971; Nurmukhamedov, 1971; Birks, 1973, 1975; Lin, 1976; Plotnikov, 1980). A variety of the experimental methods (classical decay-rate studies, single-vibronic-level excitation, double-resonance technique, polarization luminescent studies, nanosecond and picosecond spectroscopy) provide detailed information about excited states of molecules and their decay mechanisms. The aim of this section is to summarize briefly the basic conclusions for the RLT theory applications to electronic relaxation in large molecules.

Typical classes of molecules studied are aromatic hydrocarbons, their carbonyl derivatives, nitrogen heterocyclic compounds, etc. The photoprocesses involve states of different types: $S_{\pi\pi^*}$, $T_{\pi\pi^*}$, $S_{n\pi^*}$, $S_{\sigma\pi^*}$, etc., in accordance with the multiplet and orbital nature of the excited states (σ, π, or n orbitals). A more detailed assignment and the systematics of molecules and their spectral properties are discussed by Birks (1973), Plotnikov (1980).

For the RLT theory the decay processes of lowest excited states are of interest (internal conversion $S_1 \rightarrow S_0$ and intersystem crossing $S_1 \rightarrow T_1$ or $T_1 \rightarrow S_0$) in view of the very rapid (10^{-11} sec) radiationless conversion between the higher excited states (Kasha law). Characteristic radiative decay times of the singlet states are about 10^{-6}–10^{-8} or 10^{-6}–10^{-5} sec for π–π^* or for n–π^* transitions, respectively. The lifetime of the lowest $T_{\pi\pi^*}$ or $T^{n}{}_{\pi^*}$ are about 0.1–30 or 10^{-2}–10^{-3} sec. Radiationless decays of the lowest excited states successfully compete with radiative channels and their rate depends on the orbital nature of the transition, the energy gap, and on other factors such as temperature and environment.

For the large molecules discussed with the great transition energy $\Delta\mathscr{E} \gg \hbar\omega$, the density of final excited vibrational states is so high and their broadening due to anharmonicity so large that the RLT rate will appear to be independent of intermolecular relaxation processes. This will occur even if the intramolecular vibrational relaxation dephasing provides for the irreversible behavior during the times sufficient for interfering with the external effect. This situation corresponds to the statistical limit when the RLT rate is determined only by intramolecular characteristics such as the shapes of PES U_1, U_2; the energy gap $\Delta\mathscr{E}$; the electronic coupling; and the temperature. The interpretation of RLT in molecules as an intramolecular process has been since the early works by Hunt and McCoy (1962)

and Robinson and Frosh (1963a,b). The foundation of the statistical limit as well as of the opposite limit of isolated molecules (when the external level broadening or the vibrational relaxation rate are significant) has been discussed, for example, by Medvedev and Osherov (1968), Jortner *et al.* (1969), Konoplev *et al.* (1974), and Freed (1976, 1980), and will not be considered here.

Although the complete PES of the excited states are unknown, some data concerning the relative arrangement of their equilibrium configurations and frequencies [the parameters α_k and s_k of vibronic coupling in Eq. (25)] can be obtained from the vibronic structure of absorption and luminescent spectra. The corresponding parameters depend on the orbital nature of transition. In π–π^* spectra the skeleton C—C vibrations of the aromatic rings are active so that for two characteristic groups of the C—C and C—H stretching vibrations with frequencies $\omega_{CC} \simeq 900$–1500 cm^{-1} and $\omega_{CH} \simeq 3000$ cm^{-1}, the characteristic values of vibronic parameters are $s_{CC} \sim 1$–1.5 and $s_{CH} \sim 0.03$ with $\Delta\mathscr{E} \sim (1.5 - 2.8) \cdot 10^4$ cm^{-1} for $S_1 \to S_0$ and $T_1 \to S_0$ transitions (for $S_1 \to T_1$ the s_k values are lower). For $\pi^* \to$ n transitions with their localized character, the most active vibrations in the spectra are the stretching vibrations of the C=O group for carbonyls ($\omega \sim 1800$ cm^{-1} for S_0 and ~ 1200 for nπ^* states, $s \sim 1 - 1.5$), or C=S vibrations for tiocarbonyl compounds ($\omega \sim 1200, s \sim 1$), or bending vibrations of the CNS group in azoaromatic compounds, etc. (Plotnikov *et al.*, 1977, and references therein). A discussion of various types of electronic coupling and detailed references may be found in reviews by Schlag *et al.* (1971), Freed (1976), and Plotnikov (1980). Note only that the electronic coupling is usually estimated for equilibrium molecular configuration, but here it is needed for distorted configuration corresponding to the crossing-terms region. This may result in another value as well as in other selection rules for electronic coupling. The equilibrium characteristic values of spin–orbit coupling are $V \lesssim 0.3$ cm^{-1} or $V \sim 10$ cm^{-1} for the singlet–triplet $\pi^* \to \pi$ and n $\to \pi^*$ transition in the absence of heavy atoms.

It is seen from the characteristic vibronic parameter values that RLT in molecules belongs to the case of weak coupling and of high transition energy $E_R \sim \bar{s}\hbar\bar{\omega} \sim \hbar\bar{\omega} \ll \Delta\mathscr{E}$. The general conclusion of the RLT theory for such transition concerning the exponential dependence of the RLT rate on the $\Delta\mathscr{E}$ (energy-gap law) is experimentally confirmed. For example, strict verification of the energy-gap law has been obtained for $T_1 \to S_0$ transition in aromatic molecules (Siebrand, 1967b), or for $S_2 \to S_1$ relaxation in azulene derivatives (Murata *et al.*, 1972a,b), or for internal conversion $S_1 \to S_0$ of aromatic molecules (Huang and Lim, 1975). First, the

energy-gap law was established empirically, in particular a more accurate linear correlation

$$\log W(\Delta \mathscr{E}) = -k'(\Delta \mathscr{E} - E_0)N_H/(N_H + N_C)$$

has been proposed for aromatic molecules, where N_C and N_H are the number of C and H atoms in a molecule (Henry and Siebrand, 1973). The exponential law was then interpreted by Siebrand as a sequence of the exponential decrease of the average FC factor F with the use of the factorized Golden-rule expression (the so-called density-of-state model)

$$W = (2\pi/\hbar)V^2\bar{F}\rho_{\text{eff}} \tag{62}$$

where ρ_{eff} is the effective density of the final states. However, the value ρ_{eff} can not be identified with the total density of final states since only a small number of modes can represent efficient acceptors of the electronic energy. The use of SDM for electronic transitions in molecules proposed by Ovchinnikova (1968), Fisher (1970), and Englman and Jortner (1970) permits revealing the meaning of ρ_{eff}.[1] The SDM results [Eqs. (23) and (24)] can be presented in the form of Eq. (62) if $\bar{F}$ is equal to the optimal FC factor $F(n^*)$ and ρ_{eff} is evaluated as

$$\rho_{\text{eff}} = \left[\sum_k s_k(\hbar\omega_k)^2 e^{\omega_k \nu}\right]^{-1/2} \sim (\hbar\bar{\omega}\,\Delta\mathscr{E})^{-1/2}$$

The SDM approach is usually called a dynamic one. It gives the possibility of estimating not only the absolute rate constant but also the different mode efficiencies in accepting the electronic energy. Classification of molecular modes as accepting or promoting modes was first proposed by Lin (1966) (see also Lin and Bersohn, 1968). (The promoting mode allows forbidden transition in accordance with nonadiabatic or vibronic couplings and simultaneously leads to a decrease by the value of its quantum the electronic energy which transforms into the main accepting modes.) According to Eqs. (23)–(26), the highest frequency modes are the best acceptors. The RLT rate calculations with different model parameters (often unsufficiently realistic) demonstrate the important role of both the C—C and C—H stretching vibrations. The role of the latter and the relative part $\mathscr{E}_{CH}/\Delta\mathscr{E}$ of energy transformed into the C—H modes increases with the energy gap (Ovchinnikova, 1968; Fisher, 1970). However, for the CH modes the harmonic approximation is insufficient, as shown by Fisher

[1] The validity of the first saddle-point approximation, called here SDM, and its extension has been discussed, for example, by Nitzan and Jortner (1973) and Medvedev *et al.* (1977).

(1971b). Definitive conclusions would require a more rigorous treatment of anharmonic dynamics (see the next section). The account for the high-frequency C—H modes often permits obtaining an agreement of calculated and experimental decay rates, but gives isotope effects too strong for deuterated molecules compared to the observed one.

In agreement with RLT theory, the strong increase in RLT rate with excess excitation energy has been found by Schlag and Weysenhoff (1969) and Ware *et al.* (1970). This effect has been interpreted in terms of the one-frequency model [Eq. (62)] by Siebrand (1971) or as the result of the increase in the effective vibrational temperature of the excited state (communicating system model with fast rearrangement of the excess energy proposed by Fisher *et al.*, 1971) where the number of modes involved in energy exchange appeared to be significantly less than the total number of molecular modes.

The most informative and promising methods in RLT studies are laser-induced single vibronic excitation ones (see Guttman and Rice, 1974; Freed, 1976, and references therein) in combination with the theory of lifetimes of the single vibronic levels. Among the various versions of the theory (Heller *et al.*, 1972; Prais *et al.*, 1974; Pagitsas and Freed, 1977; Kühn *et al.*, 1977) the most readily interpreted is based on the mode-factorization rule [Eq. (29)]. The calculations of relative efficiency of $S_1 \rightarrow T_1$ transitions from the single vibronic level in benzene and its derivatives and comparison with experiment have been discussed in detail by Freed (1976).

Some conclusions can be made from the results obtained by applying the RLT theory to the absolute decay rate. The theory permits prediction to an order of magnitude of the observed RLT rates with reasonable values of the vibronic coupling parameters. This concerns especially the $T_{n\pi^*} \rightarrow S_0$ transitions characterized by a relatively simple vibrational structure of phosphorescence spectra. For example, in benzophenone the experimental decay time 5×10^{-2} sec of the $T_{n\pi^*}$ state is satisfactorily described by $V \sim 10\,\text{cm}^{-1}$ and coupling with one stretching mode $\omega = 1800$ cm^{-1} of the C=O group with parameter $s = 1.5$ found from the phosphorescence spectra. The model results for the $T_1 \rightarrow S_0$ transition in naphthalene and anthracene molecules also do not contradict experiment, assuming that the main coupling is with C—C stretching modes (Ovchinnikova, 1968).

For many compounds the interconversion $S_1 \rightarrow T_1$ rate of the $\pi^*\pi$ and $n\pi^*$ molecule states has been studied theoretically by Plotnikov *et al.* (1977), Plotnikov and Dolgikh (1978), Dolgikh and Plotnikov (1978), and Plotnikov (1979). The luminescent structure of π^*–π and n–π^* transitions in aromatic molecules and their derivatives containing groups with *n* elec-

trons permits working out characteristic models for vibronic coupling involving high-frequency C—C vibrations for $S_{\pi\pi^*}$–$T_{\pi\pi^*}$ and additional vibrations of characteristic groups for $S_{\pi\pi^*} \rightarrow T_{n\pi^*}$ (or $S_{n\pi^*} \rightarrow T_{\pi\pi^*}$) transitions. An account for different SO and vibronic couplings leads to the ration 10^{-2}–10^{-4} for the rates of these types of transitions. The influence of level positions, the conjugation length, the vibronic coupling with higher excited states, and the heteroatom effect on the decay rate have been studied. A similar estimate of the T_1–S_0 conversion rate has been carried out by Dolgikh and Plotnikov (1979) for many compounds. The rate expression used by Plotnikov is proportional to the factor $\langle \Gamma/(\Delta^2 + \Gamma^2/4) \rangle \sim 0.4/\Gamma$, depending on the parameter $\Gamma \sim 1$ cm^{-1} of the vibrational relaxation rate and exceeding by 1–2 orders of magnitude a similar factor in the SDM result.

At the same time, the benzene molecule most often used in theoretical tests appeared to be the one most difficult to describe. Along with the relative rate calculations of single-vibronic-level decays (Freed, 1976; Kühn *et al.*, 1977), the absolute rates of the $T_1(^3B_{1u}) \rightarrow S_0(A)$, $S_1(^1B_{2u}) \rightarrow T_1$, and $S_1 \rightarrow S_0$ transitions are considered in many papers using various versions of SDM or the mode-factorization method (Nitzan and Jortner, 1973; Fisher and Schneider, 1971; Medvedev *et al.*, 1977), as well as a direct calculation of the state density weighted with FC factors (Metz, 1976; Kühn and Metz, 1978). [In the latter case an additional empirical parameter $\Delta \sim 20$–200 cm^{-1} of the vibrational level width is introduced, and the study of the rate dependence on Δ and on the line shape permits obtaining more explicit conditions of the statistical limit validity. For small Δ an essentially nonmonotonic dependence $W(\Delta\mathscr{E})$ has been found]. Nevertheless, for benzene molecules and at least for $T_1 \rightarrow S_0$ and $S_1 \rightarrow S_0$ transitions, there is no unique point of view about either the electronic or the vibronic coupling mechanisms (Metz, 1976; Siebrand and Zgierski, 1975). Attempts to describe the rate of these transitions with account taken for only two totally symmetric vibrations $\nu_1 = 992$ and $\nu_2 = 3070$ cm^{-1} with $s_{CC} \sim 1.03$ and $s_{CH} \sim 0.035$ for $T_1 \rightarrow S_0$ were not successful (these parameters s_k were found by Burland and Robinson, 1969 on the basis of phosphorescence analysis). The theory gives an RLT rate lower than the experimental one by many orders of magnitude. An account taken for anharmonicity of the local CH mode or an assumption about the large s_{CH} parameter increases the decay rate but still insufficiently (Kühn *et al.*, 1977). Moreover, it leads to an isotope effect much greater than that observed for deutero derivatives (Martin and Kalantar, 1969). Note also that the model of vibronic coupling with two modes ν_1 and ν_2 only cannot also describe the integral intensity of the phosphorescence spectra in the long-wave range. To cope with these contradictions an effect of strong

linear vibronic mixing of close electronic states $^3B_{1u}$ and $^3E_{1u}$ by the e_{2g} vibrations (ν_6 and ν_8) has been assumed (de Groot and van der Waals, 1963; Ovchinnikova, 1968; Scharf, 1979). This assumption was confirmed by the experimental structure of phorescence spectra (Burland *et al.*, 1970). At the present time only rough estimates of the effect of e_{2g} vibration frequency changes on the $T_1 \rightarrow S_0$ transition rate have been made by Ovchinnikova (1968) and Scharf (1979), and the experimental lifetimes might be interpreted in this way. For nitrogen heterocyclic and aromatic carbonyl compounds, the effect of a similar strong distortion of PES due to vibronic mixing of close-lying $n\pi^*$ and $\pi\pi^*$ states (in particular, by the out-of-plane C—H vibrations) is known and has been widely studied (Lim, 1977). It is called the "proximity effect" and results in increasing the RLT rate if the levels are approaching each other. A further study of vibronic coupling between the excited states is needed. Some theoretical models have been proposed in this connection (see Siebrand and Zgierski, 1980, and references therein).

Incomplete knowledge of the excitation decay mechanisms is clear from the absence of full interpretation of the strong temperature and solvent dependences of the decay rate at low temperatures (Birks, 1973). For the $S_1 \rightarrow T_1$ transition such temperature dependences are often connected uniquely with a parallel channel—the thermally activated transition $S_1 \rightarrow T_q$ to higher triplet states. However, it is difficult to interpret it for the $T_1 \rightarrow S_0$ transition. Some theoretical hypotheses which connect this temperature effect with intramolecular factors have been proposed by Fisher (1971a) and Makshantsev (1980), but these are still questionable. More detailed studies of this temperature dependence are needed, since it might be due to the release of some hindered diffusion processes in solids. For example, the sharp quenching of the aromatic molecule phosphorescence in the paraffin matrix at $T \sim 100$ K was found to be due to the diffusion of oxygen molecules in the matrix (Grebenshchikov and Personov, 1969).

The problem of the interference of excited molecular states leading to nonexponential decays or to their dependence on the excitation conditions is not discussed here. The rotational effect in RLT recently discovered will only be briefly mentioned here (see reviews by Howard and Schlag, 1980; and Novak *et al.*, 1980). Two mechanisms of the rotation effect on the RLT rate of isolated molecules have been proposed. The first involves a nonequilibrium rotational distribution of the excited molecule and its change with exciting radiation frequency, together with nonmonotonic behavior of FC factors, and results in a lifetime dependence on radiation frequency in the range of the rotational center of single vibronic line (Howard and Schlag, 1980). The other mechanism is connected with the

direct influence of molecular rotation on electronic coupling via the Coriolis or spin–rotation interaction and was discussed by Novak *et al.* (1980).

B. Role of Local Bond Anharmonicity in RLT and Overtone Spectra

The important role of the anharmonicity in RLT has often been emphasized (Henry and Siebrand 1973, 1975; Fisher, 1976; Lawetz *et al.*, 1972; Kühn *et al.*, 1977), and the FC factors for Morse oscillators used for interpretation of RLT. We consider briefly the validity conditions of the harmonic approximation. According to Eq. (20) the rate of the transformation of high electronic energy into vibrations is determined by minimal tunnel action [Eq. (21)] up to the crossing region of two PES. For a harmonic one-dimensional model, Fig. 1b, the crossing point is

$$|x_0| \simeq a_0\, \Delta\mathscr{E}[(2s)^{1/2}\hbar\bar{\omega}]^{-1} \gg |x_2| = a_0(\Delta\mathscr{E}/\hbar\bar{\omega})^{1/2}$$

where a_0 is the zero vibrational amplitude. This means that the harmonic approach is valid if the PES are harmonic over a wide region of tunnel motion (not only in classically allowed regions) up to energies $U(x_0) = \Delta\mathscr{E}^2/(4\bar{s}\hbar\bar{\omega}) \gg \Delta\mathscr{E}$, significantly higher than the dissociation energy D. Therefore, a study of the FC factors for anharmonic potentials is needed.

The analytical expressions for FC factors for Morse potentials were obtained by Makshantsev and Perstnev (1971a,b), Makshantsev (1972), Lawetz *et al.* (1972), Ovchinnikov and Ploutnikov (1977), and Plotnikov and Dolgikh (1977). These studies led to an important conclusion: The maximal overlap integral appears to be that for the most anharmonic potentials which take place at the maximal localization of energy $\Delta\mathscr{E}$ on one of the local bonds rather than on the normal mode (Lawetz *et al.*, 1972; Kühn *et al.*, 1977). This property of the Morse potential

$$U_M(x) = D(e^{-\alpha x} - 1)^2 \tag{63}$$

is illustrated here. For two displaced Morse potentials the FC factor $\langle 0_1|v_2\rangle$ of multiphonon transition ($v_2 \gg 1$) is nonzero even in the small first-order displacement Δx_e of equilibrium coordinates, and for large $\Delta\mathscr{E}$ it is

$$|\langle 0_1|v_2(\Delta\mathscr{E})\rangle|^2 = (\alpha\, \Delta x_e)^2 A \exp[-\phi_m(\Delta\mathscr{E})]$$

$$A = \frac{8\pi D^2}{(\hbar\omega)^2}\left[\frac{u(u-1/2)}{1-u}\right]^2, \qquad u = (1 - \Delta\mathscr{E}/D)^{1/2} \tag{64}$$

Here the tunnel action ϕ_m may be calculated (and has a finite value) for

undisplaced and undistorted potentials $U_1 = U_2 + \Delta\mathscr{E}$,

$$\phi_m = \lim_{x_0 \to -\infty} 2\left|\int_{x_0}^{x_1} p(x, 0)\, dx - \int_{x_0}^{x_2} p(x, \Delta\mathscr{E})\right| = \frac{\Delta\mathscr{E}}{\hbar\omega}\psi\left(\frac{\Delta\mathscr{E}}{D}\right)$$

$$p(x, E) = (2m)^{1/2}(U_m(x) - E)^{1/2}, \qquad \omega = (2D\alpha^2/m)^{1/2} \tag{65}$$

$$\psi(\kappa) = 2/\kappa[\ln 4/\kappa - 2(1 - \kappa)^{1/2} \arccos(1/\kappa)^{1/2}] \tag{66}$$

This situation essentially differs from the harmonic expression [Eq. (20)] where the transition $0 \to N$ is allowed only in the Nth order in the parameter s: $I(\Delta\mathscr{E} = N\hbar\omega) \sim s^N$. It is seen from Eqs. (64) and (65) that the action Φ_M in Eq. (64) decreases with increasing anharmonicity, i.e., with decreasing dissociation energy or increasing of parameter α of the Morse potential. More general but elaborate analytical dependences of anharmonic FC factors were derived by Makshantsev (1972), and the general semiclassical calculations were worked out by Medvedev (1982).

The qualitative difference in the weighted state density $I_M(\Delta\mathscr{E})$ at small Δx_e and that for the harmonic case consists in the opposite signs of the second derivatives ($d^2I_M(E)/dE^2 > 0$). According to the arguments in Section II,C (see Fig. 2b), this means that for a few equivalent independent accepting bonds the localization of energy on one bond is most probable, i.e., the limiting step of RLT is the transfer of electronic energy to one local bond vibration. According to Plotnikov and Dolgikh (1977), internal conversion occurs as the transformation of the electronic energy into one C—H bond vibration due to the nonadiabacity operator. However, further accurate analyses of the excited-state PES and of electronic coupling for large molecule distortion are needed to draw the final conclusion about the relative role of C—H and skeletal C—C vibrations in $S_1 \to S_0$ and $T_1 \to S_0$ transitions. Though the simple one-dimensional anharmonic models (the effective C—C oscillator assumed by Makshantsev, 1980, or the C—H oscillator) can be chosen so as to reproduce the experimental lifetime, the real RLT mechanism often remains unclear.

The important role of the local-mode anharmonicity in the RLT is directly connected with the local-mode concept in overtone spectroscopy (Henry, 1974, 1976). Over the past years the development of very sensitive thermal-lensing spectroscopy (Albrecht, 1978) and the intracavity CW dye-laser technique (Reddy *et al.* 1978) have permitted measuring highly forbidden transitions, particularly the high overtones of C—H, N—H, O—H vibrations in molecules containing few identical bonds. The dominant absorption was found to correspond to transitions into the excited state only with localization of energy on one local bond (and not on a few bonds simultaneously). This hypothesis and the local mode representation were first proposed by Henry and Siebrand (1968) for the interpreta-

tion of the overtone spectrum in benzene. Ovchinnikov and Erikhman (1973a,b) independently predicted the effect of an anomalously large lifetime of the bond-localized highly excited vibrational states in molecules like H_2O and H_2S. Earlier similar effects—the existence of long-lived highly excited localized vibrational states in molecular crystals (CH_4, N_2, etc.) at low temperatures have been discussed by Ovchinnikov and Erikhman (1971, 1972a,b).

The physical reason for the long lifetime of such states can be readily seen. Due to the strong bond anharmonicity, the energy $E(v, 0, 0, \ldots)$ of the vibrational state with excitation localized on one bond appears to be less than the energy $E(v-1, 1, 0, \ldots)$ of the closest combination state with transfer of one quantum to the identical local bond. For example, the energy levels corresponding to v-quantum excitation of a H_2O molecule with quantum distribution (v_1, $v_2 = v - v_1$) over two bonds are

$$E(v_1, v - v_1) - E(0, 0) = \hbar\omega_0 - \omega_0 x_0 (V^2 - 2vv_1 + 2v_1^2) \pm \delta E_v(v_1)/2 \quad (67)$$

where ω_0 and $\omega_0 x_0$ are the frequency and anharmonicity parameters of the local bond, and the splitting δE of symmetric and antisymmetric states $|v_1, v - v_1\rangle \pm |v - v_1, v_1\rangle$ sharply decreases with $v_1 \to 0$,

$$\delta E_v(v_1) = (-1)^{v+1} \frac{2(v - v_1)!2\omega_0 x_0}{v_1![(v - 2v_1 - 1)!]^2} \left(\frac{\beta}{2\omega_0 x_0}\right)^{v-2v_1}, \qquad v_1 < v/2 \quad (68)$$

where β is the normal-mode splitting for the one-quantum excitation (Ovchinnikov and Erikhman, 1973a,b). Therefore, the time $1/\delta E$ of energy transfer from one bond to another would be very long for small v_1. The values of such splitting for totally localized states $|0, v\rangle \pm |v, 0\rangle$ of a H_2O molecule are given as an example in Table I. Simultaneously, the intensity of the radiative transition to a state with a given number of quanta $v = v_1 + v_2$ sharply increases with the degree of energy localization on one of the bonds. For example, the relative intensities $I(v_1, v_2)$ of the fifth overtone of H_2O are

$$I(1, 4)/I(0, 5) = 2.5 \times 10^{-2}, \qquad I(2, 3)/I(0, 5) = 1 \times 10^{-2}$$

(Ovchinnikov and Erikhman, 1981). Similar intensity relations for benzene have been obtained experimentally by Bray and Berry (1979) and theoretically by Burberry and Albrecht (1979) [for example, $I(0, 7)/I(6, 1) = 50$]. Thus the main observed patterns of overtone spectra of such polyatomic molecules with identical bonds are the most intensive lines for absorption into localized states. These lines have a very simple structure

$$\nu(v) = Av + Bv^2 \quad (69)$$

which coincides with Eq. (67) for $v_1 = 0$, $v_2 = v$, $\delta E = 0$.

TABLE I

THE LOCALIZED-STATE SPLITTINGS OF H_2O

	$\delta E_V(0)$ (cm^{-1})	
V	Eq. (68)[a]	Wallace (1975)[b]
2	11	18
3	1	2
4	−0.45	0
5	2×10^{-3}	

[a] The calculation with the use of Eq. (68): $\omega_0 = 3300\ cm^{-1}$, $x_0 = 0.025$.

[b] The numerical results of Wallace (1975) with a slightly different set of parameters.

Much experimental evidence for the local-mode concept has been obtained by Henry and Siebrand (1968), Bray and Berry (1979), Swofford *et al.* (1977), Henry and Hung (1978), and Fang and Swofford (1980a,b). (For more detailed referencing, see the above papers and the reviews by Albrecht, 1978 and Reddy *et al.*, 1978). This evidence includes the simple structure [Eq. (69)] of overtone spectrum, the latter independence of the substitution of the adjacent identical bonds, the agreement of the calculation and observed intensities, etc. Thus a very important phenomenon is proved, namely the excitation of states with the most nonequilibrium distribution of vibrational energy. Such a distribution essentially differs from the statistical distribution usually discussed in unimolecular reactions. This attracts attention to such states and to the attempts to get some information about their lifetimes (or about the duration of the intramolecular vibrational energy exchange) from the observed forms of the overtone lines in the gas phase (Bray and Berry, 1979). For many small molecules (NH_3, CH_3, and others), the sharp rotational structure of the overtone lines is in agreement with the conclusion about the long lifetime of such states. For benzene molecules Bray and Berry have given the estimate 0.6×10^{-13} sec for the lifetime of such a state with $v = 5$–8. In this connection with the interpretation of overtone spectra many new problems arise about classical and quantal dynamics of such highly excited anharmonic vibrational states (see for example, Ovchinnikov, 1972; Sage, 1979; Fang and Swofford, 1980a,b).

From the point of view of the RLT theory this strongly forbidden absorption is interesting because its intensity, like that of the RLT rate, is determined by the matrix element $\langle 0|d|v \rangle$ of the FC type but is weighted

with the dipole moment function and corresponds to one (ground) electronic state. In this connection it would be of great interest to further investigate not only the separate C—H overtone lines, but also the continuous background of absorption observed for benzene by Bray and Berry (1979) and Albrecht (1978). If the transition to C—C skeletal vibrational states could be assigned as responsible for this absorption, then it would be important to realize the principal factor allowing the transition with such a large change of the vibrational number (~ 18–20).

The problem about rearrangement of electronic energy among vibrational modes or local bonds is important for the study of photo- and radiation stability of the molecules, in particular relative to H abstraction, the most widespread photochemical reaction of hydrogen-containing molecules. The probability of H abstraction as a result of direct electronic–vibrational energy transfer to one of the C—H bonds has been obtained by Ovchinnikov and Plotnikov (1977) and Makshantsev and Fleurov (1980). The comparison with other mechanisms of photoabstraction (such as electronic relaxation followed by redistribution of vibrational energy and unimolecular decay, or the predissociation mechanism due to crossing of attractive and repulsive triplet states) shows that direct dissociation of the C—H bond is dominant only for molecules with weak C—H bonds ($D_{CH} \lesssim$ 2 eV) such as the radical cations (Plotnikov and Ovchinnikov, 1978).

Now for the photodissociation of relatively small molecules (H_2CO, XCN, HCCX, X = Br, Cl, I, etc.) the detailed information about the vibrational and rotational distribution of products is available and is interpreted in terms of excited-state PES and the fragmentation dynamic models reviewed by Freed and Band (1977) and Gelbart *et al.* (1980).

C. Role of Anharmonic Dynamics and Pair Interactions in Vibrational Relaxation of Impurity Molecules in Solids

The process of vibrational energy relaxation (VER) of the impurity molecules in a solid matrix has many features in common with electronic energy relaxation and its treatment widely uses the RLT theory.

The characteristic times of VER of small-impurity molecules vary over a large range: from 10^{-12} to 10^{-10} sec (as for ω_{CH} in CH_3Cl, CH_3I, and for other molecular liquids) up to tens of seconds for diatomic molecules in the noble-gas matrix (Diestler, 1976, 1980). The experimental methods for VER study (direct spectroscopic and time-resolved measurements, transient picosecond and active spectroscopy of Raman scattering, etc.) have been reviewed by Brus and Bondebey (1980), Laubereau and Kaiser (1978), and Pogorelov *et al.* (1979). These methods provide the possibility of measuring both the VER and the rate of vibrational dephasing. The relation of the observed characteristics with the correlation properties of

molecular motion and dephasing have been described by Oxtoby (1979) and are not considered here. As to VER, the general situation is very complicated. Even in four- and five-atom molecules the lifetimes of vibrational levels are influenced by many factors: the resonance energy transfer, the Coriolis and rotational couplings, the Fermi resonance, the intermode anharmonicity, etc., and the mechanisms of relaxation appear to be very specific for various levels and for different molecules (see, for example, Laubereau *et al.*, 1978; Velsko and Oxtoby, 1980). A more simple situation takes place for diatomic molecules in simple monoatomic matrices, and it can be hoped that for such molecules it will be possible to reveal some general mechanisms of relaxation and to verify its agreement with theoretical models (Diestler, 1976, 1980; Lin, 1980). When the vibrational relaxation is not enhanced by the step-ladder vibronic transitions between different electronic states as in some electronically excited molecules (Brus and Bondebey, 1980), then the VER of impurity diatomics is a very slow process. This is connected with conversion of the large intramolecular vibrational quantum $\hbar\omega$ to a large number $N = \hbar\omega/\hbar\Omega$ of intermolecular vibrational quanta or to rotation of impurity molecules. The main theoretical models of VER of diatomics, their accuracy, the role of anharmonic dynamics of system, and pair interactions in VER are discussed here (a more complete description of all reported VER theories can be found in the review by Diestler, 1980).

1. *The Multiphonon and Pair-Collision Mechanisms*

Two approaches have been suggested for calculation of the VER rate of impurity diatomics. One describes VER as a multiphon process with the use of the RLT theory and harmonic approximation for the lattice phonons. In the framework of this approach two variants of such RLT mechanisms have been proposed. In the first one (entirely similar to electronic transition), the VER is caused by changing δq_k of the equilibrium coordinates of the phonon oscillators when the vibrational state of a diatomic molecule changes from $|v\rangle$ to $|v-1\rangle$ (Fong *et al.* 1972; Diestler, 1974). Such a mechanism is probably adequate for the step-ladder VER via internal conversion (Brus and Bondebey, 1980). However, for purely vibrational transitions in one electronic state the s_k parameters estimated from pair atom–atom potentials appeared to be too small and could not explain the observed VER rates. In this connection Nitzan and Jortner (1973) (see also Nitzan *et al.*, 1974, 1975; Lin, 1974, 1976; Ovchinnikov and Erikhman, 1975; Sakun, 1976) have proposed another mechanism for the multiphonon process caused by essentially anharmonic interaction V of the molecule X_M with the adjacent lattice atoms X_j. If expanded in an

intramolecular coordinate y the interaction causing relaxation has the form

$$V = yV_0 \exp[-\alpha|X_j - X_M|] = yV_0 \exp\left[-\sum_k \alpha_k q_k\right] \tag{70}$$

where q_k are the normal-mode coordinates of the lattice. In this case a closed analytical expression was obtained for the probability $W_{v,v-1} = vW_{1,0}$ of the impurity molecule transition $v \to v - 1$. It gives the characteristic exponential energy-gap dependence

$$W_{1,0} = \frac{8\pi V_0^2}{\mu\omega} \frac{\bar{\alpha}^2}{4} \left(\frac{8\pi}{\Omega\omega}\right)^{-1/2} \exp\left\{-\frac{\omega}{\Omega} \ln\left[\frac{2m\omega}{\hbar\bar{\alpha}^2 e}(1 - e^{-\beta\hbar\Omega})\right]\right\} \tag{71}$$

This equation is similar to the probability [Eq. (20)] for the displaced PES except that the parameter s is replaced by $s_\alpha = \hbar\alpha^2/(2m\Omega)$. Equation (71) is given for one mean matrix frequency Ω and parameter $\alpha(=\alpha_k)$, though the rate expression has been obtained for arbitrary phonon spectra (Nitzan *et al.*, 1974, 1975; Lin, 1974, 1976). This result means that the local impurity vibrational modes with a relatively high frequency Ω_k and a large-parameter α_k play a very important role in VER and that the VER rate has a strong temperature dependence. The similarities and differences in the VER temperature dependence for the displaced PES or anharmonic mechanisms are discussed by Lin *et al.* (1979).

Note that the anharmonic interaction [Eq. (70)] is the first-order term in the expansion of the real anharmonic pair interaction potential $U_{jM}(X_j - X_M - y)$ between the matrix and molecule atoms in the intramolecular vibration coordinate y. Nevertheless, in the derivation of Eq. (71) the dynamics of these atoms (i.e., of the same coordinates X_j, X_M) are assumed to be harmonic, i.e., the surface $\sum_j U_{jM}(X_j - X_M)$ (the zero term of expansion in y) is assumed to be quadric. It will be shown that such an approximation can give errors of several orders of magnitude in the VER rate due to its high sensitivity to delicate details of the dynamics. Similar difficulties also arise in the classical treatment of VER in liquids and in solid matrices where the VER rate is defined by the Fourier transform F_ω of the force acting on the oscillator. However, there is no reliable method so far for estimating F_ω at high frequencies (Oxtoby and Rice, 1976; Metieu *et al.* 1977).

A different approach to VER is based, as in the gas phase, on the concept of individual pair collisions of an impurity molecule with fluid atoms. It uses the realistic anharmonic pair potentials (Madigosky and Litovitz, 1961; Sun and Rice, 1965; Davis and Oppenheim, 1972). This model has been criticized in terms of statistical arguments in connection

with the unclear definition of the effective collision energy, particularly at low temperatures when essentially quantum considerations are needed. The calculation of the frequency of close collisions needed for VER and the relative velocity distribution have been carried out by Sun and Rice (1965) with use of the harmonic Slater model. But questions remain about the choice of the core radius for a close collision.

2. *Tunnel-Trajectory Method in Generalized Langevin Equations*

For an estimation of the accuracy of both approaches one needs to use a method which would reflect the anharmonic dynamics of the adjacent atoms as well as the specific interaction with the other lattice atoms. For the VER of the classical oscillator the progress of the theory is connected with the generalized Langevin equations (GLE) approach developed by Adelman and Doll (1976; see also Adelman, 1980) and with the stochastic classical trajectory approach (SCTA) (Shugard *et al.*, 1978). Both take into account the exact classical dynamics of the closest adjacent atoms and the damping and fluctuating forces due to other lattice atoms. However, this method is adequate only for high temperatures (classical system), and it requires considerable computational efforts, mainly for two reasons. First, the SCTA uses equations involving the fluctuating force $F(t)$ which represents a stochastic process and needs to be averaged over the realizations of this process. Second, the VER time (and, consequently, the computational time) increases exponentially with increasing $N = \omega/\Omega$. Nikitin and Ovchinnikova (1980) have proposed a tunnel-trajectory method of treating both the classical and quantal VER with account for exact anharmonic dynamics of adjacent atoms and for the phonon frequency properties of a solid matrix. The method consists of a search for the optimal tunnel classical trajectories of the system which control the rate of the quantal relaxation process according to Eq. (45). There are significant advantages of the tunnel-trajectory method compared to SCTA. First, only one tunnel trajectory corresponding to the unique (optimal for VER) realization of the stochastic force is needed. Second, the integration-time interval is on the order of $1/\Omega$ and does not increase with $N = \omega/\Omega$, and as before the possibility of dealing with the real-valued tunnel trajectory remains. Finally, the method can be applied to classical as well as to quantal low-temperature relaxation. For the harmonic lattice and the interaction [Eq. (70)], such trajectories have been found explicitly and give the known result [Eq. (71)].

For a simple estimation of the anharmonicity effect, consider the rate of vibration–translation energy transfer for the complex of atom C and molecule AB interacting through the Morse potential $U_M(X_B - X_C)$ and having a reduced mass $m = (m_{AB}^{-1} + m_C^{-1})^{-1}$. Just this problem arises in

calculating the vibrational predissociation (VP) rate of the linear van der Waals molecules which have been widely studied (see review by Le Roy and Scott Carley, 1980, and references therein). The VP rate as a function of the relative AB–C energy has been investigated using an exact matrix element with the wave functions of the Morse oscillator (Allen and Feuer, 1964; Child, 1976; Beswick and Jortner, 1977). The semiclassical trajectory method for the VP rate calculation is illustrated here for a linear van der Waals molecule AB–C and will be further used for the multidimensional problem of VER in solids.

Thus the relaxation rate of the vibrational AB excitation

$$\mathrm{AB}(v = 1) — \mathrm{C} \rightarrow \mathrm{AB}(v = 0) + \mathrm{C} \tag{72}$$

with dissociation of the van der Waals collinear complex AB–C is of interest. A typical relation $\omega = \omega_{AB} \gg \Omega = (2D\alpha^2/m)^{1/2}$ for the frequencies is valid here. The transition is caused by perturbation of the first order in

$$V_{10} = 2\alpha\langle 1|y|0\rangle(e^{-2\alpha X} - e^{-\alpha X}) \tag{73}$$

in which the main contribution to the transition probability is given by the first repulsive term. According to Eq. (45), the thermally averaged probability of the quantal process [Eq. (72)] is determined by the action integral along two parts $X_1(\tau)$, $X_2(\tau)$ of the optimal classical trajectory with boundary conditions [Eq. (43)], energies $E_1 = E_2 + \hbar\omega$, and imaginary times of the tunnel motion $2\tau_1$, $2\tau_2 = 2\tau_1 + \hbar\beta$. For the Morse potential the analytical expression for the VER rate $W(T)$ as a function of temperature has been derived by Nikitin and Ovchinnikova (1980). It varies from the typical Landau–Teller dependence $\sim\exp(aT^{1/3})$ at high temperatures to a constant value if $T \rightarrow 0$. The probability depends on the following dimensionless parameters: $b = ND/kT$, $\kappa = \hbar\omega/D$. and $N = \omega/\Omega$. At zero temperature it is

$$W(b \rightarrow \infty, \kappa) = (m_A/m_{AB})^2(\omega m/4\mu)(2\pi N^3/\kappa^3)^{1/2} \exp[-N\psi(\kappa)] \tag{74}$$

where m_{AB} and μ are the total and reduced masses of molecule AB. Here the function $\psi(\kappa)$ is given by Eq. (66) for $\kappa < 1$ and

$$\psi(\kappa) = (2/\kappa)[\ln(4/\kappa) - 2(1 - \kappa)^{1/2} \text{ arc } \cos(1/\kappa)^{1/2}] \tag{75}$$

for $\kappa > 1$. It can be readily verified that if $N = 5$, the probability [Eq. (74)] is many orders of magnitude higher than that obtained by replacing the intermolecular Morse potential by a harmonic one with the same frequency Ω and the same anharmonic interaction V_{01} causing relaxation.

A similar study of the quantal VER probability of the impurity molecule in solids requires obtaining the optimal multidimensional tunnel trajectories, and it has been done by Nikitin and Ovchinnikova (1980).

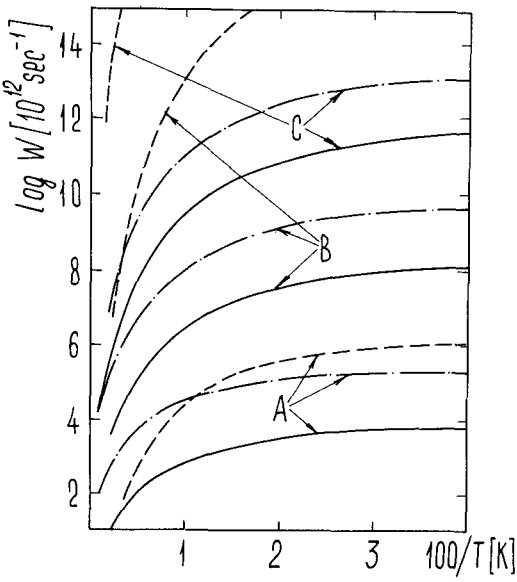

Fig. 3. The VER rate dependences on inverse temperature for a Cl_2-type molecule in the Ar matrix with $N = \omega/\Omega_D = 5, 10, 15$ (curves A, B, C, respectively). Unbroken curves refer to tunnel dynamic calculations for an anharmonic five-particle model; dashed curve refers to the result for the same harmonic model; dash–dot curves refer to pair-collision quantum approximation (Nikitin and Ovchinnikova, 1980).

The model is described by Morse potentials with adjacent lattice atoms and harmonic interactions with other lattice atoms characterized by the parameters describing the phonon spectrum of the solid matrix according to the method of Shugard *et al.* (1977). It has been verified that at high temperatures when the lattice motion is classical, the tunnel-trajectory method gives a result very close to that of SCTA. The VER rate results are presented in Fig. 3 for a five-particle linear model imitating relaxation of the Cl_2-type molecule with frequencies $\omega = 5\Omega_D, 10\Omega_D, 15\Omega_D$ in an argon matrix where Ω_D denotes the Debye frequency of the lattice. The full curves correspond to the tunnel dynamic approach, the dashed ones to relaxation in a harmonic system with the same force matrix near the equilibrium configuration and with the same anharmonic perturbation causing transition. Finally, the VER results for the pair-collision approximation are also presented. The pair-collision approximation is seen to be much more adequate for the exact dynamic result than the harmonic phonon approximation. The reason for this is as follows. The VER in solids (like the gas-phase VER) is controlled by close collisions, where the exponential repulsive pair potential dominates. In classical mechanics the

trajectories of the system at low temperatures correspond on the average to harmonic motion; nevertheless, the high-frequency component F_ω of the force (acting on the oscillator and defining the VER) is contributed by rare close collisions, and the contributions from different collisions are additive (Oxtoby, 1977). The binary nature of VER in liquids is proved by the successful description of the pressure and temperature dependence of VER in liquid hydrogen (Delalande and Gale, 1979). At low temperatures the VER rate is limited by tunnel motion with minimal reduced mass to the region of sharpest increase in potential, and this determines the almost binary character of the quantal process as well. It would be interesting to describe the pressure and temperature VER effects in liquid hydrogen (Chateau *et al.*, 1979) as quantal processes.

The tunnel-trajectory method (as well as the SDM in harmonic models) also provides information about the most probable distribution of vibrational energy $\hbar\omega$ over various local or lattice modes. The dynamic results, as well as the pair-collision results, correspond to a more gentle temperature dependence than that for the harmonic phonon approximation.

Experimental observation of the discussed multiphonon VER mechanism (different from the rotational or stepladder vibronic mechanisms) is often complicated, due to the energy-exchange processes and to radiative transitions (Dubost and Charneau, 1978). Nevertheless, such a mechanism has been associated by Rossetti and Brus (1979) and Brus and Bondebey (1980) with the observed VER of the O_2, NO, C_2^- molecules in Ar, Kr, Xe matrices for which a strong temperature dependence of the VER rate was found. The authors have discussed the most probable distribution of vibrational energy over the local or lattice mode. Note that the tunnel-trajectory method predicts initial localization of this energy on one of the atom–molecule bonds (i.e., for a certain combination of the modes) and the same isotope effect of the VER rate as in quantal pair collision model.

3. *The Rotational Mechanism of VER*

This mechanism involves vibrational energy transfer to the rotation of the impurity molecule. In the gas phase it is dominant for asymmetric diatomics with a small moment of inertia (Nikitin, 1974). Experiments by Bondebey and Brus (1975) and Wiesenfeld and Moore (1976) have shown that the multiphonon energy-gap law of the VER is strongly violated for diatomic hybrids NH, OH, HCl, etc., and it has been suggested that VER occurs by the rotational mechanism. For these molecules a simple empirical dependence $W \sim \exp(-cJ)$ of the VER rate on the final rotational quantum number was found by Legay (1978). This dependence was derived theoretically by Freed and Metiu (1977), Berkowitz and Gerber

(1977, 1979), Diestler *et al.* (1978), and Lin *et al.* (1979). This derivation is illustrated here for a hydride molecule HX.

At fixed position $\mathbf{R}_i$ of the matrix atoms, the characteristic dependence of the potential energy on the molecular axis orientation $\mathbf{n}$ can be described by the sum of pair interactions with adjacent atoms. The repulsive part of these interactions most important for VER has the form

$$U_r(n, y) = \sum_i U(R_i) \exp[-\gamma(r_e + y) \cos \varphi_i], \qquad \cos \varphi_i = \mathbf{n}_i \mathbf{R}_i / R_i \quad (76)$$

where r_e is the equilibrium distance and y is the intramolecular vibrational coordinate. (For simplicity, the mass center of HX is associated with the position of X.) At low temperatures the rate of VER due to rotational transition is defined by the expression

$$W_J(T = 0) = 2\pi J^{-1} |\langle v = 1, J' = 0 | U_r | v = 0, J \rangle|^2 f(\Delta E_J) \quad (77)$$

where $J \sim (\hbar\omega/B_e)^{1/2}$ is the final rotational quantum number, B_e is the rotational constant of HX, and f describes the anharmonic relaxation of remaining energy $\Delta E = \hbar\omega - B_e J(J + 1)$ to the local mode or to the phonon. If the molecule rotation in the matrix is assumed to be free, then the rate W_J in the first order in y contains the following matrix element between the free rotational function $\psi_{J,M=0} = \varphi_J(\theta)/(2\pi)^{1/2}$,

$$M_{0J} = \frac{d}{d\eta} I_{0J}, \qquad I_{0J} = \int_{-\pi}^{\pi} \varphi_0(\theta) \exp(\eta \cos \theta) \varphi_J(\theta) \, d\theta \quad (78)$$

where $\eta = \gamma r_e$ is connected with the potential parameters in Eq. (76). Exact calculation of the integral [Eq. (78)] carried out by Berkowitch and Gerber (1977) and Lin *et al.* (1979), or a simple semiclassical estimation (Appendix II), leads to an exponential VER dependence on the final

$$W \sim J \exp[-2J \ln(2J/e\gamma r_e)] \quad (79)$$

Using the pair-potential parameters, Berkowitz and Gerber (1979) have calculated the VER rate of an NH molecule in an Ar matrix and obtained good agreement with the observed rate.

Other VER calculations for a number of systems (NH, ND, HCl, DCl, CO in an Ar matrix; OH, OD in a Ne matrix) have been carried out by Diestler *et al.* (1978), who had taken into account the hindered character of the low rotational states. They have obtained reasonable agreement between calculated and observed isotope effects, though the absolute rate value appeared to be greater by an order of magnitude than observed one. One of the reasons for this difference might be the high sensitivity of the result to the potential used. In particular, in accordance with the assumed

symmetry of the environment, the approximation $U \sim \exp(a \cos 4\varphi)$ has been used instead of the more reliable one, $U \sim \sum_{k=1}^{4} \exp[a' \cos(\varphi - 2\pi k/4)]$.

Accounting for hindered rotation is very important in solving the question about the completion of the local mode (L) with the molecule rotation (R). If these modes are assumed to be independent acceptors of the vibrational energy $\hbar\omega = E_R + E_L$, the factorization rule, together with the specific dependences of the rates in Eqs. (74) and (79) on E_L and $E_R \sim B_e J^2$ respectively show preferential localization of the transfered energy on one of these modes (R or L) according to Fig. 2b. However, such an independence disappears if the hindered character of the rotation is taken into account because the anisotropy parameters $U_m(R)/B_e$ of the potential $U = \Sigma_m U_m(R) P_m(\cos\theta)$ increases with decreasing R. Therefore the role of the pair collision can appear to be important even for rotational VER. Further, dynamic treatment and efforts to obtain reliable potentials are needed to turn from the empirical to a predictive theory and to get information from abundant experimental data (see, for example, Bondebey and English, 1980).

In connection with the very high sensitivity of the VER rate to potential and dynamic approximations, one incorrect method of obtaining the observed rate values should be mentioned. It uses the far tail of broadened Lorentz lines, which is equivalent to a one-phonon process with a very high frequency. However, all the experience of the RLT theory shows that the high-frequency component of fluid motion decreases exponentially with frequency, but not like a slow Lorentz-type function.

IV. Charge-Transfer Reactions in Polar Liquids

A. Introduction

There is a wide and important class of chemical processes that can be considered as RLT with strong coupling or with large solvent reorganization in transition. This class comprises the oxidation–reduction reactions in polar liquids involving electron transfer (ET) (Reynolds and Lumry, 1966; Bassolo and Pearson, 1967). Many important aspects of the elementary steps of these reactions are now understood because of the pioneering treatments by Gurney, Libby, Zwolinski, R. J. Marcus, Eyring, Weiss, Laidler, R. A. Marcus, Hush, Halpern and Orgel, Platzman, Frank, Levich, Dogonadze, McConnel, Conway, Bockris, Christov, and others. A most detailed and critical description of all the theories and references has been given by Bockris and Khan (1979; see also reviews by Marcus, 1964; Levich, 1970; Dogonadze and Kuznetsov 1975, 1978; Ulstrup, 1979).

The aim of this section is to connect this specific problem with RLT theory and to illuminate the less known and new problems and models of the charge-transfer processes in polar liquids. A review of the known ET models by Marcus, Hush, Levich, Dogonadze is given in Sections IV,B and IV,C. The theory of the charge-transfer radiationless processes in polar liquids proposed by Ovchinnikov and Ovchinnikova (1969a,b) is then considered, which takes into account the spectral dielectric properties of the solvent and the fact that the reorientation dynamics of the solvent molecules does not reduce to the harmonic ones used in the familiar RLT theory. Some general conclusions following from reported comparisons (Bockris *et al.*, 1974) of theory and experiment are discussed in Section IV,D. Finally, a new derivation of both the Kirkwood temperature-dependent expression for a dielectric constant and the Marcus-type ET rate is given (Ovchinnikov, 1981). It demonstrates the limitation on the continuum macroscopic model of structured liquids. This model is insufficient for the quantitative description of the absolute rate of the ET reactions, so a calculation of the structure of the liquid near the reactant is needed. However, it is possible to explain the behavior of the reaction rates as a function of temperature and reaction heat.

The ET reactions in polar media are characterized by a very strong solvent influence on the energetics as well as on the kinetics of the processes. Due to the polar solvent, there exist multicharged ions stabilized mainly by strong interaction with the ligands, the closest molecules of the first-coordination shell constituting the ion complex. The contribution from the long-range ion–dipole electrostatic interaction with external solvent molecules is usually estimated using the Born expression for solvation energy in which the dielectric continuum model is assumed for the solvent outside the ion complex.

The observed ET reactions vary over a large range of rates (twelve orders of magnitude) and over a wide variety of mechanisms (Bassolo and Pearson, 1967). There are intrasphere ET reactions in which two ions taking part in ET have a common ligand, and the ET is accompanied by changes in the first-coordination sphere. In this case the rate depends on the substitutional lability of the ligands and the properties of the bridge groups (Halpern and Orgel, 1960). Another outersphere mechanism takes place for the ET reactions without alteration of the complex structure. The rate of these reactions are greatly increased by ions of the opposite sign. But even in noncatalyzed, slow reactions the ET is possible either at a van der Waals contact of the ion complexes or if these complexes are hydrogen bonded. Often the ET is indistinguishable from a proton transfer. Therefore before theoretical interpretation and description of the outersphere reaction models, some warning is needed: The role of many

chemical factors not discussed here (the bridge groups, symmetry and energetics of electronic states, substitutional lability of ligands, the solvent structure, etc.) may appear to be dominant, and the simple physical models considered below would be inapplicable to certain reactions. Nevertheless, many concepts of modern ET theory remain general for all mechanisms, for example, the FC concept about the necessity of preliminary rearrangement of the solvent molecules and the tunnel character of electron motion.

B. Classical Theory of Adiabatic Reactions

Only the slow outersphere reactions for which the ET step (but not the reactant diffusion) is rate determining will be considered here. The ET reaction of type

$$A^{z_a} + B^{z_b} \rightarrow A^{z'_a} + B^{z'_b} \tag{80}$$

where z_a, z_b, z'_a, z'_b are the charges of ion complexes, is induced by the interaction $V = V_{12}$ due to overlap the reactant electronic orbitals and the ET rate sharply decreases with increasing distance R between the reactants. Therefore the bimolecular rate constant is defined by the product

$$K(T) \simeq W(R_0)v_0 \exp[-F_z(R_0)/kT], \qquad F_z = z_a z_b/\epsilon_s R_0 \tag{81}$$

where W is the ET probability at the fixed minimal distance R_0 between reactants, $v_0 = 4\pi R_0^2 \Delta R_0$ is the characteristic reaction volume, and $F_z(R_0)$ is the free-energy change as a result of approaching of reactants with Coulomb interaction in a medium with dielectric constant ϵ_s.

The ET transition $1 \rightarrow 2$ from the initial to the final electronic states in reaction (80) is governed by the FC principle (this was first realized by Libby, 1952). Therefore the transition rate $W(R)$ is limited by the small probability of such fluctuations of the ion complex coordinates and of the solvent polarization which provide the intersection of electronic terms 1 and 2. Let the ion complexes in reaction (80) be characterized by a set of vibrational coordinates $Q = (Q_A, Q_B)$ and the external solvent be considered as a continuum dielectric medium described by the polarization vector $\mathbf{P}(\mathbf{r})$. Then if the Q vibrations and polarization fluctuations are assumed to be independent, the terms of each electronic state are

$$U_{1(2)} = U^{c}_{1(2)}(Q) + U^{d}_{1(2)} + J_{1(2)} \tag{82}$$

where indices c and d refer to ion complexes and the external dielectric solvent, respectively, and the values $J_{1(2)}$ are the minimal potentials of each electronic state.

Consider now the derivation of Marcus and Hush for the adiabatic ET reaction rate in a classical medium (Marcus, 1956, 1957; Hush, 1961).

According to the transition-state theory the reaction probability is

$$W = A \exp(-F^{\ddagger}/kT) \tag{83}$$

where A is the frequency factor, estimated by Marcus as $kT/\hbar$ (see the discussion in Sections IV,C and IV,D), and $F^{\ddagger}$ is the free energy of the transition state referred to the free energy of equilibrium state 1. Here the transition state corresponds to the fluctuation $Q^{\ddagger}$, $\mathbf{P}^{\ddagger}(\mathbf{r})$ of vibrational coordinates and the solvent polarization with minimal free energy

$$F^{\ddagger} = F_1(Q^{\ddagger}, \mathbf{P}^{\ddagger}) = \min[F_1^{c}(Q) + F_1^{d}(\mathbf{P})] \tag{84}$$

chosen out of the possible fluctuations $\tilde{Q}$, $\tilde{\mathbf{P}}$ providing the resonance of the electronic levels

$$U_1 - U_2 = \Delta U_c(\tilde{Q}) + \Delta U_d(\tilde{\mathbf{P}}) + \Delta J = 0 \tag{85}$$

The potentials U_c are usually assumed to be quadric in Q. Their parameters can be found from electrostatic models of ion complexes describing these complexes in terms of ion–dipole, repulsive and ligand field forces, and reproducing the observed equilibrium distances in complexes before and after transition (Bassolo and Pearson, 1966; Hush, 1961). The frequencies and the equilibrium distances can also be obtained from spectroscopic and structural data for such ion complexes in crystals (Kestner *et al.*, 1974).

Thus it remains for us to find the free-energy $F_1^{d}(\mathbf{P})$ and the potential energy difference U_d for the dielectric medium with nonequilibrium polarization $\mathbf{P}(\mathbf{r})$. This has been done by Marcus (1954, 1956) who developed a quantitative theory of nonequilibrium dielectrics (see also Pekar, 1954). Following this theory, divide the solvent polarization $\mathbf{P}(\mathbf{r})$ into two parts $\mathbf{P} = \mathbf{P}_e + \mathbf{P}_n$ in accordance with the time scales 10^{-15} and 10^{-13}–10^{-11} sec of electronic and nuclear (vibrational and orientational) motion. The first electronic part of polarization $\mathbf{P}_e$ always follows the electric field E variation in the medium: $\mathbf{P}_e = \alpha_e \mathbf{E}$ with $\alpha_e = (\epsilon_{op} - 1)/4\pi$ defined by the optical dielectric constant. The nuclear polarization P_n followed by the slow component $\delta\mathbf{P}_e = (1/\epsilon_{op} - 1)\mathbf{P}_n$ of the electric polarization constitutes, together with $\delta\mathbf{P}_e$, the inertial polarization $\mathbf{P}_{in}(\mathbf{r}) = \mathbf{P}_n/\epsilon_{op}$ defined by Pekar (1954). Owing to the thermal motion of solvent molecules, the inertial polarization $\mathbf{P}_{in}(\mathbf{r})$ fluctuates about its equilibrium value $\mathbf{P}_{in}^{eq}(\mathbf{r})$. The free-energy $F^{d}(\mathbf{P})$ of the nonequilibrium state of dielectric medium has been calculated by Marcus as being equal to the work needed for creating this state. It is

$$\begin{aligned} F_1^{d}(\mathbf{P}_{in}) - F_1^{d}(\mathbf{P}_{in}^{eq}) &= 2\pi/c_0 \int [\mathbf{P}_{in}(\mathbf{r}) - \mathbf{P}_{in}^{eq}(\mathbf{r})]^2 \, dv \\ \mathbf{P}_{in}^{eq}(\mathbf{r}) &= (c_0/4\pi)\mathbf{D}_1(\mathbf{r}) \end{aligned} \tag{86}$$

Here $\mathbf{D}_1$ denotes the dielectric displacement vector (the field of the first state charge ρ_1 in vacuum), and the constant

$$c_0 = (1/\epsilon_{op} - 1/\epsilon_s) \tag{87}$$

is defined by optical and static dielectric constants. At the same time, the difference $\Delta U_d = U_1^d - U_2^d$ between the potential energies in two states with the same fixed-solvent-molecule coordinates is equal only to that between electrostatic interaction energies of charges ρ_1 (or ρ_2) with inertial polarization

$$\Delta U_d = -\int [\mathbf{D}_1(\mathbf{r}) - \mathbf{D}_2(\mathbf{r})]\mathbf{P}_{in}(\mathbf{r})\, dv \tag{88}$$

The minimization of the free energy [Eq. (84)] under the additional condition of Eq. (85) gives the known Marcus expression for the transition probability

$$W = A \exp[-(\Delta J + E_R)^2/4E_R kT], \qquad E_R = E_c + E_d \tag{89}$$

where the ion complexes and dielectric contributions to the reorganization energy E_R are

$$E_c = \sum_k m\omega_k^2\, \Delta Q_k^2/2 \tag{90}$$

$$E_d = c_0/8\pi \int [D_1(r) - D_2(r)]^2\, dv \tag{91}$$

Here the inner shell contribution (90) is due only to changes in bond lengths and angles but not in frequencies (a more general expression was used by Hush, 1961). The difference ΔJ between the electronic terms minima can be expressed in terms of the observed quantity ΔF_0 [change of the free energy during the overall reaction (80)] and of the Born solvation energy

$$\Delta J = \Delta F_0 + (z_a z_b - z_a' z_b')/(\epsilon_s R) \tag{92}$$

where R is the distance between the ions. For a simple spherical model of two ions with radii a and b (radius of an ion plus the inner coordination shell), the parameter E_d of the continuum theory is

$$E_d = c_0(z_a - z_a')^2[(2a)^{-1} + (2b)^{-1} - R^{-1}]$$

It can be verified that the ratio of the total rates of the direct and inverse reactions (80) is equal to the equilibrium constant $K = \exp(-\Delta F_0/kT)$.

Note that Hush has obtained the result (89) in a way that contradicts the Born–Oppenheimer principle. He assumed that the reaction involves a stage with partial charge transfer. But for linear dielectrics and for a linear dependence of inner shell properties on $\lambda\, \Delta z$ (the part of transferred

charge), the minimization of the free energy over λ gives the same result as does the Marcus theory. At the same time, Hush was the first to take into account both the inner shell and the dielectric continuum and to perform the absolute rate calculations (see below).

Many correlations between the rate constants of various reactions (including electrochemical ones) have been predicted by Marcus. These correlations were verified by Ford-Smith and Sutin (1961), Candlin *et al.* (1964), Endicott and Taube (1964), and others and summarized by Marcus (1964) and Albery (1980). These correlations were based on the fact that the contributions from the rearrangement of each reactant environment are almost additive. For many series of similar reactions the quadric correlation of $\ln k(T)$ and ΔF_0 has been demonstrated for a normal reaction regime $\Delta F_0 < E_R$ (for example, Suga *et al.* 1973); the best correlation was for an empirical value E_R. The absolute rate calculations and a comparison with experiment are discussed below (Section IV).

C. Quantum Mechanical Theory of Nonadiabatic Electron-Transfer Reactions

A further essential progress with a new point of view on the ET was achieved by Levich and Dogonadze (1959, 1960) and Dogonadze and Kuznetsov (1973) who formulated the problem in terms of the RLT and polaron theories. It permitted extension of the theory to nonadiabatic reactions (small V_{12}) and to description of quantum (instead of classical activation) mechanism with respect to polarization modes of dielectric continuum when its characteristic frequencies are greater than $2kT/\hbar$. Consider briefly only the idea of the Levich–Dogonadze theory. More detailed presentations are given in the reviews by Levich (1970), Dogonadze and Kuznetsov (1973, 1978), Bockris and Khan (1979), and Ulstrup (1979).

Let the dielectric medium be modeled by a set of oscillators $\mathbf{x}_j = \mathbf{P}_j(\Delta v_j)^{1/2}$ with one frequency ω where $\mathbf{P}_j = \mathbf{P}(\mathbf{r}_j)$ is the mean polarization of a small macrovolume Δv_j. If free energy (87) is identified with the potential energy of the polarization modes, the force constant K_j of these oscillators and the "vibronic coupling" parameter $\Delta\mathbf{x}_j^{eq}$ (i.e., the shift in equilibrium positions of the modes) must be taken as $K_j = 4\pi/c_0$ and $\Delta\mathbf{x}_j^{eq} = c_0[\mathbf{D}_1(r_j) - \mathbf{D}_2(r_j)](\Delta v_j)^{1/2}$ according to Eq. (88). The "momentum" corresponding to the coordinate x_j and the kinetic energy operator $K_j\dot{x}_j^2/2\omega^2$ are defined uniquely by the force constant K_j and the frequency

[2] The force constant $4\pi/c_0$ really characterizes only the longitudinal component of the polarization. But the result of such primitive local treatment appears to be correct since only this component interacts with the charges $\rho_{1(2)}$. The original Levich–Dogonadze treatment using the spacial Fourier components of polarization is more rigorous.

ω.[2] In terms of such a model the quantal transition probability in the first-order perturbation theory in $V = V_{12}$ has been found. It is given by Eq. (15) in which $s = E_d/\hbar\omega$, $\Delta\mathscr{E} = \Delta J$ and the parameters E_d and ΔJ are the same as in the Marcus theory and defined by Eqs. (91) and (92). The high- and low-temperature approximations (16) and (18) for $\hbar\omega < 2kT$ or $\hbar\omega > 2kT$ correspond to classical or quantum limits. In the first case the exponent in the transition probability $W(R)$ exactly coincides with the Marcus expression (89). The preexponential factor A in Eq. (89) for the nonadiabatic limit.

$$\xi = 2\pi V^2/[\hbar\omega(E_d kT)^{1/2}] < 1$$

or adiabatic limit $\xi > 1$ in these models becomes

$$A_{na} = \pi V^2/[\hbar(E_d kT)^{1/2}], \qquad A_a = \omega/2\pi \tag{93a,b}$$

Note that the interaction $2V$ represents small splitting of electronic levels $\psi_1 \pm \psi_2$ in the resonance situation $U_1(QP) - U_2(QP) = 0$ due to the overlap of initial and final orbitals of the transferred electron. It may be obtained by quantum chemical calculations or semiclassical evaluation of the under-barrier tunnel penetrability widely discussed in earlier papers (for example, Zwolinski *et al.*, 1955; Sacher and Laidler, 1964). A crude estimate gives $V \sim \hbar\omega_e \exp(-\alpha R)$ where $\omega_e \sim 10^{15}$ sec^{-1} is the characteristic electronic frequency and $\alpha = (2m_e I_e)^{1/2}/\hbar$ depends on the depth I_e of the electronic level relative to the conduction zone in liquid (m_e is the electron mass). For a system like Fe^{2+}–Fe^{3+} in water, a simple estimation with $R = 7$ Å, $\alpha = 1.4$–2 Å^{-1} gives $V = 1$–0.03 cm^{-1}, $A = 0.5\ 10^{10}$–$1.6\ 10^6$ sec^{-1} ($\xi = 10^{-4}$–10^{-8}). It means that in the usual representation of the rate as $W = (kT/\hbar)\exp(-F/kT)$, the free-energy $\bar{F} = F^{\ddagger} + F_{tun}$ thus defined is contributed by the "tunnel free energy" $F_{tun} = -TS_{tun} = -kT \ln(A\hbar/kT)$. This has been studied for various distances R by Sacher and Laidler (1964; see also Kestner *et al.*, 1974).

One remark about the electron tunneling must be made. For the reaction (80) the typical distance R is about 7 Å and the tunneling time τ_e is much shorter than the characteristic solvent times $1/\omega$. Therefore the potential barrier for the electron must be calculated with fixed molecular coordinates and cannot contain the static dielectric constant ϵ_s. However, for long-range tunneling of electrons in a solid matrix, the value $\omega\tau_e$ may be about 1 and then the barrier as such becomes dependent on the initial and final molecular states. An elegant theory of such nonadiabatic tunneling has been worked out by Ivanov and Kozhushner (1978).

Thus, the Levich *et al.* approach in terms of the RLT theory takes into account both the FC principle and the tunnel character of electron motion, which have been considered separately in earlier

theories. This approach makes it possible to account for the quantum effects.

A number of more complicated multifrequency solvent models for ET reactions have been worked out by Dogonadze and Kuznetsov (1973, 1975, 1978, and references therein). The main results of these studies are important rules for dividing of all degrees of freedom into slow (classical) and fast (quantum), which can or cannot contribute to the activation energy and the general oscillator modeling and classification of various ET regimes such as normal ($|\Delta J| < E_R$) or abnormal, activationless ($\Delta J \sim E_R$) or barrierless ($\Delta J \sim -E_R$), characterized by different values of "transfer coefficient" $\alpha = d \ln W(\Delta J)/d\,\Delta J$. A similar quantum mechanical description of the ET reaction with account for quantal effects in the inner shell vibrations and polarization modes was considered by many authors (Ovchinnikov and Ovchinnikova, 1969a; Schmidt 1973, 1974; Schmickler 1973, 1976; Efrima and Bixon, 1974; Kestner *et al.*, 1974; Van Duyne and Fisher 1974, 1977; Ulstrup and Jortner, 1975). Before discussing the inner shell contribution, the more realistic theory of dielectric media is considered.

D. Influence of the Dielectric Absorption Spectrum on Electron Transfer

The spectra of dielectric absorption in real liquids are continuous. In such a situation the determination of the contribution from different modes to the dielectric reorganization is rather uncertain. Moreover, the reorientational dynamics of the molecular dipoles in liquid can never be reduced to the harmonic ones used in the familiar RLT theory. Nevertheless, the theory of ET transition in polar liquids with account for the real dielectric absorption spectrum has been worked out by Ovchinnikov and Ovchinnikova (1969a,b). It is constructed in a form close to the RLT theory but without the harmonic dynamics approximation, using the linearity of an unsaturated dielectric medium only. This is possible because of the statistical character of transition. Namely, the strong electrostatic interaction U of charges z_a, z_b with the solvent outside the inner shell is contributed from interaction with a very large number N of molecular dipoles. But for each dipole the interaction appears to be weak ($\sim U/N$) compared to the intermolecular forces defining the molecular dynamics and the short-range dipole correlations. Moreover, since the interaction U is long-range relative to the molecular size, the time correlations of macroscopic polarization will determine the ET rate. But the same correlations determine the linear response of the dielectric continuum to the electric field, described in terms of the macroscopic dielec-

tric susceptibility $\epsilon(r, \omega)$. A simplified derivation of the transition rate is presented here.

Similar to the above considerations the inner shell vibrations and polarization fluctuations are assumed to be independent. Then, for a nonadiabatic reaction with the use of the Golden-rule expression (4) and the mode-factorization rule (28), the whole problem can be reduced to solving two independent problems: the RLT with taking into account inner shell reorganization only, and the RLT with taking into account dielectric-medium rearrangement only. This means that the total generating function $G(t)$ in the Golden-rule expression (5) is a product of the following independent factors:

$$G(t) = V^2 g_c(t) g_d(t) \exp(i\,\Delta J t) \tag{94}$$

Here $g_c = G_c(t)/|V|^2$ is the known generating function of the inner shell complex in the harmonic approximation [see Eqs. (9)–(11)]. Therefore it remains to investigate the function

$$g_d(t) = \langle \exp(-iH_1^d t/\hbar) \exp(iH_2^d t/\hbar) \rangle_1 \tag{95}$$

referred to external dielectrics with Hamiltonians $H_{1(2)}^d$ in each electronic state. The averaging in (95) is accomplished over the equilibrium solvent state on the first electronic term. The function (95) can be rewritten as

$$g_d(t) = \left\langle T \exp\left[-i \int_0^t \Delta H_d(t)\, dt\right]\right\rangle_1 \tag{96}$$

Here $\langle T, \ldots \rangle_1$ is the averaged time-ordered exponent and $H(t)$ is the difference $\Delta H = H_1 - H_2$ in the Heisenberg representation. But for a polar medium, H coincides with the difference between the electrostatic potential energies (88), so that

$$\Delta H_d(t) = -\int [\mathbf{D}_1(\mathbf{r}) - \mathbf{D}_2(\mathbf{r})]\mathbf{P}(\mathbf{r}t)\, dv = \sum_j \Delta H_j(t) \tag{97}$$

where $\mathbf{P}(\mathbf{r}t)$ is the polarization operator in the same representation and $\mathbf{D}_1$, $\mathbf{D}_2$ are dielectric displacements. The long-range character of the interaction permits ΔH_d to be represented as the sum of contributions ΔH_j from a large number of small macrovolumes Δv_j and to assume that the polarization fluctuations of different volumes are independent. Then, at the time scale t_d of the generating function $g_d(t)$ (when $\langle \Delta H_d^2 t_d^2 \rangle \sim 1$, but $\langle \Delta H_j^2 t_d^2 \rangle \ll 1$), the average exponent in (96) can be approximated by the exponent from averaged quantities for each volume v_j:

$$g_d(t) = \exp\left\{ -i \langle \Delta H_d \rangle_1 t - \int_0^t dt' \int_0^t dt'' \sum_j \langle T\, \Delta H_j(t')\, \Delta H_j(t'') \rangle_1 \right\} \tag{98}$$

But the averages $\mathbf{P}_i^{eq}(r) = \langle \mathbf{P}(r_j) \rangle$ and the correlation functions $M_T(t' - t'') = \langle T\, \delta\mathbf{P}(r't')\, \delta\mathbf{P}(r''t'') \rangle$ needed here can be connected with observed properties of the medium. Indeed, the linear response of the dielectric medium to the external periodic field can be expressed on the one hand through the Fourier transform of a similar retarded correlation function $M_R(t' - t'')$ (Kubo, 1957), and on the other hand through the complex-valued dielectric susceptibility $\epsilon(r, \omega)$ of the fluid. Using further the fluctuation-dissipation theorem (Kubo, 1957) for relating $M_T(\omega)$ with $M_R(\omega) = -\delta(r' - r'')[1 - 1/\epsilon(r, \omega)]$, we obtain the final result for the transition probability

$$W = |V|^2 I(\Delta J)/\hbar, \qquad I = \int dt\, \exp[-i\, \Delta J t + \Phi_c(t) + \Phi_d(t)] \tag{99}$$

where Φ_c refers to ion complexes and is described by Eq. (11), and the function Φ_d is[3]

$$\phi_d(t) = \frac{1}{8\pi} \int dv\, \Delta D^2(r) \int \frac{d\omega}{\omega^2} \frac{\epsilon''(r, \omega)}{|\epsilon(r, \omega)|^2} \frac{ch(i\omega t - \beta'\omega/2) - ch\beta'\omega/2}{sh\beta'\omega/2} \tag{100}$$

Here $\beta' = \hbar\beta$, $\Delta\mathbf{D} = \mathbf{D}_1 - \mathbf{D}_2$, and $\epsilon''(r, \omega) = \mathrm{Im}\, \epsilon(r, \omega)$ is the imaginary part of the dielectric susceptibility defining the dielectric absorption at frequency ω.

The obtained result for charge-transfer RLT in an arbitrary linear polar quantal medium connects the ET probability with parameters δQ_k, ω_k of ion-complex reorganization and with the spectrum $\epsilon''(r, \omega)$ of the dielectric absorption of the medium. This result was first derived (in a more rigorous manner) by Ovchinnikov and Ovchinnikova (1969a,b), and was later repeated by Dogonadze *et al.* (1969), Dogonadze and Kuznetsov (1971), and Dogonadze and Kornyshev (1972), and more recently has readily been repeated once more by Kuznetsov (1981).

We now summarize the main properties of ET probability W_d with taking into account dielectrics, but without the ion-complex reorganization [this quantity can be directly used for the overall rate calculation using Eq. (28)].

At very high temperatures when all dielectric absorption frequencies in Eq. (100) satisfy the condition $\omega < 2kT/\hbar$, the activation energy and entropy are independent of the spectrum form and of the nature (vibrational or orientational) of dielectric absorption but depend on the parameter c_0 only according to the dispersion relation (see footnote 3):

$$c_0 = 1/\epsilon_{op} - 1/\epsilon_s = \int_0^\infty d\omega \epsilon''(\omega)/[\omega|\epsilon(\omega)|^2] \tag{101}$$

[3] Since the correlations of the inertial polarization P_m only are of interest for ET, the contribution of the optical absorption must be omitted in the integral (100). Accordingly, the dispersion relation (101) for $1/\epsilon(\omega)$ involves the value $1/\epsilon_{op}$ instead of unity as is usual.

In this case the ET probability coincides with Marcus expressions (89) and (91) except in the preexponential factor defined by Eq. (93a).

The role of quantum effects in the dielectric reorganization with account for the complete absorption spectrum was investigated by Ovchinnikov and Ovchinnikova (1969a) for the ET reaction in water. The dielectric properties of water are well known (Saxton, 1952). There are two broad absorption bands in liquid water: the Debye dispersion region ($\tau_D \sim 0.85 \times 10^{-11}$ sec) and the resonance absorption ($\tau_r \sim 3.8 \times 10^{-14}$ sec), corresponding to reorientations and vibrations of water molecules, respectively. In the first region the dielectric constant $\epsilon'(\omega) = \mathrm{Re}\,\epsilon(\omega)$ drops from the static value $\epsilon_s = 78$ to an intermediate one, $\epsilon_{in} = 4.9$, and in the second from 4.9 to $\epsilon_{op} = 1.8$. The reorientational and vibrational motions have been shown from (100) to make similar contributions to the dielectric reorganization energy E_d. Choosing convenient analytical expressions for $1/\epsilon(\omega)$ in water and using the stationary-phase method, one can obtain the probability for a small value of $\Delta J/E_d < 1$ at 300 K,

$$W_d \sim \exp\{-[0.81E_d^2 - 2\,\Delta J E_d + \Delta J^2/0.85 + O(\Delta J^3)]/4E_d kT\} \quad (102)$$

It is close to the Marcus-type probability with replacing E_d by about $0.8E_d$; i.e., the quantum corrections to the continuum reorganization energy in water are about 20%.

Attempts have been made to find the effective frequency ω_{eff} defining the preexponential factor $A_d = \omega_{eff}/2\pi$ of an adiabatic ET reaction in a dielectric medium (Kuznetsov, 1971; Zusman, 1975, 1980; Aleksandrov, 1980; Burshtein and Kofman, 1979; Yakobson and Burshtein, 1980). For a classical medium ($kT \gg \hbar/\tau_D$) with the simple Debye spectrum $\epsilon(\omega) = \epsilon_s + (\epsilon_s - \epsilon_{op})/(1 + i\omega\tau_D)$, in the absence of the ion complex reorganization it becomes possible to match the nonadiabatic and adiabatic limits in the following way (Zusman, 1980; Aleksandrov, 1980). For such a system the difference $X(t) = \Delta U_d(P(r, t))$ between electronic terms 1 and 2 is a stochastic quantity with simple correlation properties

$$\langle X(t)X(t')\rangle_{1(2)} = [X_{1(2)}^{eq}]^2 + 2kTE_d e^{-|t-t'|/\tau}, \qquad \tau = \tau_D \epsilon_{op}/\epsilon_s \quad (103)$$

But the problem about transitions between the levels with a fluctuating energy difference $X(t)$ possessing such properties is equivalent to the nonadiabatic transition problem in a system with two parabolic "terms" $U_{1(2)}^{eff} = (X - X_{1(2)}^{eq})^2/(4E_R)$ in the course of diffusion over X with the "diffusion coefficient" $D = 2kTE_d/\tau$. Thus in the adiabatic case $V^2/(kTE_R) > \hbar/\tau$, the reaction rate is limited by a stationary diffusion flow to the crossing point rather than by the transition rate at this point. As a result the preexponential factor for the adiabatic limit is proportional to the Debye frequency τ_D^{-1}. This would mean an additional activation energy in the rate constant due to the activation dependence of τ_D^{-1}. However, in the real

situation when the reorganization of ion complexes essentially contributes to the total E_R, such a regime with $W \sim \tau_D^{-1} \exp(-F^{\ddagger}/kT)$ becomes improbable (Ovchinnikova, 1981).

The theory discussed can be applied both to the RLT and to the broad absorption spectrum for the radiative charge-transfer transitions in a polar medium. The application of Eqs. (99) and (100) to the calculation of the absorption spectrum of solvated electrons in water and ammonia (Ovchinnikova and Ovchinnikov, 1970) shows good agreement of the linewidth, asymmetry, and their temperature dependences with experimental quantities, but the calculated temperature shift of the absorption maximum appears to be smaller by an order of magnitude than that observed. The same is valid for the absorption spectra of anions (Br^-, I^-, etc.) and some cations (Kestner, 1976). This might mean that the continuum model is inadequate. It is not clear at present whether these effects can be understood in terms of the nonlinear continuum or whether taking into account the discrete structures of liquids is needed. In any case, the discrete structure-model treatment of hydrated electron spectra gives good results (Byakov *et al.*, 1973, 1974). The interpretation of the temperature spectral shift in terms of the temperature dependence of the cavity radius (Jortner, 1959; Kestner, 1976) can also be understood only as an entropy effect, i.e., as the result of radius averaging over many structures of liquids. (For detailed theories and references on solvated electron studies see reviews by Kestner, 1976; Bockris and Khan, 1979; Brodsky and Tsarevsky, 1980).

E. Comparison with Experiment. Relative Ion Complexes and Continuum Contributions

The quantum corrections to outer dielectric contributions were shown to be relatively small at 300 K, but such corrections to ion complexes are essential. The specific models of the reorganization of ion complexes with quantum corrections were considered by Ovchinnikov and Ovchinnikova (1969a), Kestner *et al.* (1974), and Van Duyne and Fisher (1974, 1977) (General RLT quantum expressions are presented in reviews by Dogonadze *et al.*, 1972; and Ulstrup, 1979). For example, the isotope-exchange reactions with the one-frequency (ω_c) ion-complex model are characterized by the free and activation energies:

$$F^{\ddagger} = \frac{E_c}{\beta'\omega_c} \tanh \frac{\beta'\omega_c}{4} + \frac{E_d}{4}, \qquad E_a = \frac{E_c}{4}\, ch^{-2} \frac{\beta'\omega_c}{4} + \frac{E_d}{4} \tag{104}$$

where $\beta' = \hbar/kT$. These expressions and a more general result for $\Delta F_0 \neq 0$ can be obtained from Eqs. (11), (99), (100) with use of the stationary-phase method for the integral in Eq. (99).

For complexes like $Fe^{3+}(H_2O)_6$ the characteristic frequencies of totally symmetric ligand vibrations are about $\hbar\omega_c \sim 400\ cm^{-1}$ and $\Delta R \sim 0.16$ Å. This gives the value $E_c \sim 30$ kcal/mol. The available data for a number of ions have been presented by Kestner *et al.* (1969). But the absolute value $E_c = 5.36$ kcal/mol given for $Fe^{2+}(H_2O)_6 + Fe^{3+}(H_2O)_6$ must be multiplied by a factor of 6 according to the coordination number of these complexes. At 300 K the ion-complex contribution to the activation energy is about 70% of its classical value $E_c/4$.

With taking into account the quantal character of the ion-complex vibrations, the dependence $F^{\ddagger}(\Delta J)$ loses its quadric form (89). It becomes strongly asymmetric and almost linear for $\Delta F_0 > E_R$, i.e., in the so-called abnormal regime (Dogonadze *et al.* 1972; Van Duyne and Fisher, 1974; Efrima and Bixon, 1974; Ulstrup and Jortner, 1975). The conveniently derived expressions for the reaction rate have been applied by Van Duyne and Fisher (1977) to the ET reactions, including aromatic anions. However, in reality, even with the inclusion of the quantum effects, the calculations do not explain the observed, almost diffusion-controlled rate values in the abnormal regime $\Delta F_0 > E_R$ and compel the assumption of the participation of an electronically excited product in a charge-transfer reaction.

For homogeneous oxidation–reduction reactions the first classical calculations of complete absolute rate have been carried out by Hush (1961). Hush has found good agreement between theoretical and experimental activation energies for some reactions, but he has used an incorrect expression for entropy (a value higher than the correct one by the factor $\epsilon_s \sim 80$). Correct calculations show that the adiabatic theory gives a much higher reaction rate than experiment.

The most systematic calculations of the homogeneous reaction parameters have been carried out by Bockris *et al.* (1974; see also Bockris and Khan, 1979). According to their conclusions, the ion-complex reorganization energy is from one-half to two-thirds of the total E_R. The calculated total free energy $F^{\ddagger} = (E_c + E_d + \Delta F_0)^2/4(E_c + E_d)$ actually coincides with the activation energy E_a (with an accuracy to quantum corrections of about $0.3E_c$). However, Bockris *et al.* compared this value with the free-energy reaction defined as $F^{\ddagger}_{exp} = kT \ln(W_{exp}(T)kT/\hbar) = H^{\ddagger} - TS^{\ddagger}$ rather than the enthalpy of reaction $H^{\ddagger}_{exp} = E_a - 0.6$ kcal/mol and found that agreement was good. But according to Bassolo and Pearson (1967), the characteristic values of free energy and enthalpy fall to essentially different regions ($F^{\ddagger}_{exp} = 12$–23 kcal/mol and $H^{\ddagger}_{exp} = 7$–14 kcal/mol). This means that complete consideration of ion-complex and dielectric reorganization gives too high an activation energy, and at the same time the adiabatic theory does not predict the observed large negative entropy $S^{\ddagger} = 10$–40 e.u.

Detailed calculations of certain ET reactions (Berdnikov, 1977;

Dogonadze and Berdnikov, 1977) show good agreement with experiment. It would be desirable to extend these calculations to a large number of systems with detailed analysis of their accuracy.

At the present stage the absolute reaction-rate predictions cannot yet be expected to be very accurate. The theory does not consider the liquid structure around the ions and the change in orientation of the inner shell molecules. In particular, the observed change of ion-complex radius in the transition might be accompanied by the rotation of inner shell molecules rather than their displacement relative to the ion. Then, because of the quantum character of ligand librations ($\omega \sim 800$ cm^{-1} for H_2O), their contribution to the activation energy might be small and that to the entropy, great. Therefore comparative calculations of the structure and vibrational spectra of ion complexes, together with information obtained by ESR and X-ray structural analysis would be very important.

As to the external molecule contribution, its quantitative description is impossible without calculation of the hydrogen bonds of molecules in the first and second coordination shells. Though the continuum dielectric approach is too crude, nevertheless, the very important conclusion about the large contribution of the second and third coordination-shell molecules to ET activation remains to be seen.

It would be expedient to discuss this question in connection with the fluctuation theory proposed by Brockris and Sen (1973). In this theory the probability of the electrostatic energy fluctuation of the continuum appears to be too small, contrary to the Marcus result. Some critical notes concerning this theory have been made by Schmickler (1976), but there also remains an important question about the applicability of the Gaussian expression to the fluctuation probability. In this relation a new derivation of the Marcus result for a simple dielectric model consisting of classical rigid molecular dipoles μ_0 with density $1/v_0$ (v_0 is a molecular volume) shall be given here (Ovchinnikov, 1981). This treatment is of interest because it permits simultaneous derivation of the Kirkwood result for a dielectric constant ϵ_s and reveals the limitation of the macroscopic continuum description for this model.

We divide the solvent into small macroscopic volumes containing large numbers $N_m = \Delta v_m / v_0$ of dipoles, but such that $\Delta v_m \ll l^3$, where l is the scale of the average electric field variation in solvent. Then the mean long-range polarization $P(r)$ may be introduced so that the vector

$$\mathbf{P}_m = \mathbf{P}(r_m)\,\Delta v_m = \sum_{k=1}^{N_m} \boldsymbol{\mu}_k \tag{105}$$

is the total dipole moment of the volume Δv_m. Owing to the thermal reorientation of molecular dipoles $\boldsymbol{\mu}_k$, the vector P_m fluctuates and is

governed by unknown short-range forces. However, since $N_m \gg 1$ one can assume the fluctuation distribution to be Gaussian,

$$f(\mathbf{P}_m) = (\sigma N_m/\pi)^{-3/2} \exp(-\mathbf{P}_m^2/\sigma N_m) \tag{106}$$

The constant σ can be obtained by comparing the dispersion $N_m\sigma = \langle(\mathbf{P}_m)_x^2\rangle$ found from Eq. (105) and that from Eq. (106). This gives

$$\sigma = N_m^{-1} \sum_{kk'=1}^{N_m} \overline{(\boldsymbol{\mu}_k)_x(\boldsymbol{\mu}_{k'})_x} = \mu_0^2(1 + n\,\overline{\cos\gamma})/3 \tag{107}$$

where n is the number of the adjacent molecules around the preset one and $\overline{\cos\gamma}$ is the average angle between adjacent dipoles, which is nonzero for structured liquids (Kirkwood, 1939). The correlation $\mu_k\mu_{k'}$ is assumed to be retained only for adjacent dipoles. Then the properties of long-range polarization fluctuations may be obtained using the distribution (106) and the total electrostatic interactions of charges with molecular dipoles and that between the dipoles:

$$U_{el} = -\int \mathbf{D}(\mathbf{r})\mathbf{P}(\mathbf{r})\,dv + 2\pi\iint \operatorname{div}\mathbf{P}(\mathbf{r}')\operatorname{div}\mathbf{P}(\mathbf{r})|\mathbf{r} - \mathbf{r}'|^{-1}\,dv'\,dv \tag{108}$$

Using Eqs. (106) and (108) and neglecting the boundary effects in Eq. (108), the total distribution function for the long-range fluctuations of polarization can be written as follows:

$$\varphi(\mathbf{P}) = f(\mathbf{P})Ae^{-\beta U_{el}} = A\,\exp\left\{-\beta\left[2\pi c\int \mathbf{P}^2(\mathbf{r})\,dv - \int \mathbf{D}(\mathbf{r})\mathbf{P}(\mathbf{r})\,dv\right]\right\} \tag{109}$$

$$c = 1 + kT/(2\pi\sigma v_0)$$

If one requires the mean polarization $\langle\mathbf{P}(\mathbf{r})\rangle = c\mathbf{D}(\mathbf{r})/4\pi$ found from (109) to be equal to its expression $\langle\mathbf{P}\rangle = \mathbf{D}(\epsilon_s - 1)/4\pi\epsilon_s$ following from macroscopic electrostatics, then the expression for the static dielectric constant ϵ_s will be

$$\epsilon_s = 1 + 4\pi\mu_0^2(1 + n\,\overline{\cos\gamma})/3kT \tag{110}$$

It coincides with the result derived by Kirkwood (1939) with an accuracy to the previously obtained factor $3\epsilon_s/(2\epsilon_s + 1)$ in the second term, which must be reinvestigated.

On the other hand, it can be readily verified that the distribution (109) of nonequilibrium states characterized by the long-range fluctuation $P(r)$ exactly coincides with the distribution

$$\varphi(\mathbf{P}(\mathbf{r})) \sim \exp[-F(\mathbf{P})/kT] \tag{111}$$

defined by the Marcus free-energy expression (86) for our model with $\epsilon_{op} = 1$ and ϵ_s defined by Eq. (110).

Now, using (109) one can derive the distribution functions $\varphi_1(U_1)$, $\varphi_2(U_2)$, and $\varphi_{12}(\Delta U)$ for electrostatic energies in each electronic state and for its difference $\Delta U = U_1 - U_2$. All these functions are different. The function $\varphi_{12}(\Delta U)$ is Gaussian for all values of ΔU, just as $\varphi_2(U_2)$ for $|U_2 - E_d| \ll E_d$:

$$\varphi(x) \sim \exp[-(x - \langle x \rangle)^2/\sigma_k], \qquad \sigma_{12} = 4E_d kT, \qquad \sigma_2 \sim 4E_d$$

But $\varphi_1(U_1)$ is non-Gaussian for all value U_1:

$$\varphi_1(U_1) \sim \exp\{-U_1/kT[1 + O(1/\epsilon_s)]\}$$

so that the probability $\varphi_1(U_1^*)$ of fluctuation of electrostatic energy U_1 up to the value U_1^* appears to be much greater than that predicted by Bockris and Sen using the Gaussian distribution with the same second moment. This removes the argument of Bockris and Sen against the Marcus treatment. [The different character of distribution functions $\varphi_1(U_1)$, $\varphi_2(U_2)$, and $\varphi_{12}(\Delta U)$ can be readily seen for a simple oscillator model.]

This treatment reveals that the continuum solvent model with the macroscopic dielectric constant is correct when the scale l of the average electric field variation exceeds the length of correlation of molecular dipoles in liquid (for water it is about two to three diameters of the molecule). At the same time for a typical ion-complex radius $R_i \sim 3$–4 Å, only the second- and third-coordination shells make significant contributions to outer solvent reorganization. The phenomenological approach to consider the solvent structure has been proposed by Dogonadze and Kornyshev (1972) in terms of the spatial dispersion of the dielectric constant with unknown empirical parameters. However, the interactions with ligands of a nonelectric nature (hydrogen bonds for example) may be significant for second and third coordination shells.

It can be expected that calculations of discrete structure models of ET transition state will soon become available since such hydration-energy calculations are now being carried out (see Richards, 1979). Note that due to the slowness of the orientational relaxation in liquids, the ET rate calculations will require knowledge of only the static distributions $\varphi(\Delta U, U_1)$ over all quasi-equilibrium structures of liquids, but not of their time correlations (the latter is important for vibrational but not for orientational motion).

An important special case of ET includes the electrochemical reactions in which the electron is transported through the boundary of two phases: from metal to liquid. For these reactions there is a specific possibility of large-scale change of the energetics of elementary reaction steps by changing the electrode potential. Theoretical treatment of these reactions has a long history which has been reviewed in detail by Marcus

(1964), Dogonadze and Kuznetsov (1978), and Bockris and Khan (1979), and therefore it is not discussed here. Only the reaction of electrochemical hydrogen evolution on metals with high overvoltage (Hg, Pb, Cd, etc.) is mentioned here. The rate-determining stage of the whole electrochemical process in this case is the hydrogen ion discharge

$$H_3O^+ + e^-_{Me} \rightarrow H_2O + H_{ads}$$

The measured electrochemical hydrogen evolution current (and therefore the rate of reaction) was found to depend on the electrode potential according to the known Tafel law $j \sim \exp[\varphi/(a + bT)]$, and this law is fulfilled at a very large range of current variation: over 10–12 orders of magnitude (Nurnburg, 1967; Conway *et al.* 1970; Babenko *et al.*, 1978; Ovchinnikov and Bendersky, 1979; Benderski *et al.*, 1980). This surprising fact contradicts the classic Marcus-type quadric dependence of $\ln j$ on the overpotential. This contradiction has been removed in a recent treatment by Benderski *et al.* (1980). For these reactions, besides the usual FC factor due to solvent reorganization, there is an additional FC factor for the reaction coordinate (the distance between H_2O and H^+) with a significantly repulsive final term (unstable H_3O radical). Besides, the ET probability must be averaged over the Fermi distribution of electrons in metal. Taking into account both these factors permits a description of the Tafel law with sufficient accuracy; a detailed treatment can be found in a review by Benderski and Ovchinnikov (1980).

More detailed discussion of the specific applications of the RLT theory is not possible here. However, even the present rather general review article demonstrates the necessity of using more realistic models for the description of PES and the dynamics of processes or more reliable distribution functions over reactant states. Quantum chemical calculations of molecular systems will be of great importance to progress in this field.

Appendix 1. Tunnel Trajectory in QTST

Making use of the semiclassical propagator, the quantity (58) is

$$N(t) = \int dx \int dy C \exp\{iS_1(x, y, t - i\beta/2) + iS_2(y, x, -t - i\beta/2)\} \quad \text{(A1.1)}$$

where x and y belong to the reactant and product regions, respectively; S_1 and S_2 are the actions along the trajectories $z_1(t')$, $z_2(t')$ with the boundary conditions (x, y) and (y, x) in the time intervals $(0, t - i\beta/2)$, $(t - i\beta/2, -i\beta)$. The stationary-phase condition with respect to variables x and y in Eq. (A1.1) requires an equality of momenta of two trajectories at points x and y. This means that these trajectories form a unique periodic trajectory $z(t)$ with the period $-i\beta$. For $t = 0$ and sufficiently low temperatures,

one-half of this sought-after tunnel trajectory $z_0(t)$ connects two turning points x_0 and y_0 in both channels. But at $t \neq 0$, the periodic trajectory is constructed from $z_0(t)$ by continuation of it into each channel with the real-time increment beginning at points x_0, y_0. The properties of the periodic trajectories and the possibility of displacement of time $t \to t + \Delta t$ result in $N(t) = Kt$, and K is given by Eq. (59), derived by Miller (1975b).

Appendix 2. Semiclassical Estimation of the Rotational Transition Matrix Elements

For the momentum $J \gg 1$ and $J\theta$, $J|\pi - \theta| \gg 1$, the semiclassical function of free rotation with $m = J_z = 0$ is (Landau and Lifshitz, 1974)

$$\varphi_J = (2/\pi J)^{1/2} \sin[(J + \tfrac{1}{2})\theta + \tfrac{1}{4}\pi]/(\sin\theta)^{1/2}$$

It may be divided into two components: $\varphi = \varphi^{(1)} + \varphi^{(2)}$ so that each of them exponentially decreases if they are analytically continued to the upper or lower parts of the θ complex plane, respectively. Then the integrals $I_{0J} = I_1 + I_2 = 2\,\mathrm{Re}\,I_1$ in Eq. (78) can be calculated along the deformed contour $(0, i\tau, i\tau + \pi, \pi)$ instead of the real interval $(0, \pi)$ for I_1. Moreover, the contributions from the vertical lines $(0, i\tau)$ and $(i\tau + \pi, \pi)$ are purely imaginary so that

$$I_{0J} = (2\pi J)^{-1/2}\,\mathrm{Re}\left\{\int_0^{\pi} d\alpha\, \exp[\eta\cosh(\tau - i\alpha) - J(\tau - i\alpha)]\right\}$$

The last integral can be readily estimated by the stationary-phase method if the contour is made to pass just through the stationary-phase point

$$i\tau_0 = i\,\mathrm{arcsinh}(J/\eta) \simeq i\ln(2J/\eta)$$

This gives

$$I_{0J} = (4\sqrt{J})^{-1}\exp[-J\ln(2J/\eta e)] \tag{A2.1}$$

In a similar way a more general integral $I_{JJ'}$ at $J, J', |\Delta J| \gg 1$ can be found $(\Delta J = J' - J)$,

$$I_{JJ'} = (2/\pi)^{1/2}[4(|\Delta J|)^{1/2}]^{-1}\exp[-|\Delta J|\ln(2|\Delta J|/\eta e)] \tag{A2.2}$$

The comparison of Eqs. (A2.1) and (A2.2) permits us to conclude that these expressions are accurate (to a factor of about 1.25) for all J and J' if $|\Delta J| \gg 1$.

ACKNOWLEDGMENT

The very helpful discussions with Prof. V. A. Benderski, Prof. J. O. M. Bockris, Prof. E. E. Nikitin, Dr. S. Ya. Umanski, and Dr. N. S. Erikhman are gratefully acknowledged.

References

Adelman, S. A. (1980). *Adv. Chem. Phys.* **44,** 143–253.

Adelman, S. A., and Doll, J. D. (1976). *J. Chem. Phys.* **64,** 2375–2388.

Albery, W. J. (1980). *Annu. Rev. Phys. Chem.* **31,** 227–264.

Albrecht, A. C. (1978). *In* "Advances in Laser Chemistry" (A. H. Zewail, ed.), pp. 235–248. Springer-Verlag, Berlin and New York.

Aleksandrov, V. I. (1980). *Teor. Exp. Khim.* **16,** 435–448.

Allen, R. T., and Feuer, P. (1964). *J. Chem. Phys.* **40,** 2810–2812.

Altkorn, R. I., and Schatz, G. C. (1980). *J. Chem. Phys.* **72,** 3337–3347.

Babenko, S. D., Benderski, V. A., Krivenko, A. G., and Ovchinnikov, A. A. (1978). *J. Electroanal. Chem.* **91,** 321–342.

Basolo, F., and Pearson, R. G. (1967). "Mechanisms of Inorganic Reactions." Wiley, New York.

Bell, R. P. (1933). *Proc. R. Soc. Ser. A* **139,** 466–478.

Bell, R. P. (1973). "The Proton in Chemistry." 2nd ed. Chapman and Hall, London.

Benderski, V. A., and Ovchinnikov, A. A. (1980). *In* "Fizicheskaya Khimiya" (Ya. M. Kolotyrkin, ed.), pp. 202–246. Khimiya, Moscow.

Benderski, V. A., Krivenko, A. G., and Ovchinnikov, A. A. (1980). *J. Electroanal. Chem.* **111,** 19–44.

Berdnikov, B. M. (1977). *Zh. Fiz. Khim.* **51,** 1396–1398.

Berkowitz, M., and Gerber, R. B. (1977). *Chem. Phys. Lett.* **49,** 261–268.

Berkowitz, M., and Gerber, R. B. (1979). *Chem. Phys.* **37,** 369–388.

Beswick, J. A., and Jortner, J. (1977). *Chem. Phys. Lett.* **49,** 13–18.

Birks, J. B. (1973). *Org. Mol. Photophys.* **1,** 1–56.

Birks, J. B. (1975). *Org. Mol. Photophys.* **2,** 409–629.

Bixon, M., and Jortner, J. (1968). *J. Chem. Phys.* **48,** 715–726.

Bockris, J. O'M., and Khan, S. U. M. (1979). "Quantum Electrochemistry." Plenum, New-York.

Bockris, J. O'M., and Sen, R. R. (1973). *J. Res. Inst. Catal. Hokkaido Univ.* **21,** 55–69.

Bockris, J. O'M., Khan, S. U. M., and Matthews, D. B. (1974). *J. Res. Inst. Catal. Hokkaido* **22,** 1.

Bondebey, V. E., and Brus, L. E. (1975). *J. Chem. Phys.* **63,** 954–958.

Bondebey, V. E., and English, J. M. (1980). *J. Chem. Phys.* **73,** 87–92.

Bray, R. G., and Berry, M. J. (1979). *J. Chem. Phys.* **71,** 4909–4922.

Brodsky, A. M., and Tsarevsky, A. V. (1980). *Adv. Chem. Phys.* **42,** 483–543.

Brus, L. E., and Bondebey, V. E. (1980). *In* "Radiationless Transitions" (S. H. Lin, ed.), pp. 259–268. Academic Press, New York.

Burberry, M. S., and Albrecht, A. C. (1979). *J. Chem. Phys.* **70,** 147–152.

Burland, D. M., and Robinson, G. W. (1969). *J. Chem. Phys.* **51,** 4548–4559.

Burland, D. M., Castro, G., and Robinson, G. W. (1970). *J. Chem. Phys.* **52,** 4100–4108.

Burshtein, A. I., and Kofman, A. G. (1979). *Chem. Phys.* **40,** 289–300.

Byakov, V. M., Klyachko, B. S., and Ovchinnikov, A. A. (1973). Preprint of Inst. of Theoretical and Experimental Physics, N27. Moscow.

Byakov, V. M., Klyachko, B. S., and Ovchinnikov, A. A. (1974). Preprint of Inst. of Theoretical and Experimental Physics, N25. Moscow.

Bykhovski, V. K., Nikitin, E. E., and Ovchinnikova, M. Ya. (1967). *Zh. Eksp. Teor. Fiz.* **47,** 750–759.

Candlin, J. P., Halpern, J., and Trimm, D. L. (1964). *J. Am. Chem. Soc.* **86,** 1019–1022.

Chateau, M., Delalande, C., Frey, R., Gale, G. M., and Pradére, F. (1979). *J. Chem. Phys.* **71,** 4799–4804.

Child, M. S. (1974). "Molecular Collision Theory." Academic Press, New York.
Child, M. S. (1976). *Faraday Discuss. Chem. Soc.* **62,** 307–308.
Christov, S. G. (1958). *Z. Electrochem.* **62,** 567.
Conway, B. E., Bockris, J. O'M., and Lipton, M. (1956). *J. Chem. Phys.* **24,** 834–850.
Conway, B. E., MacKinnon, D. I., and Tillak, B. V. (1970). *Trans. Faraday Soc.* **66,** 1203–1226.
Davis, P. K., and Oppenheim, I. (1972). *J. Chem. Phys.* **57,** 505–516.
Delalande, C., and Gale, G. M. (1979). *J. Chem. Phys.* **71,** 4804–4811.
Diestler, D. J. (1974). *J. Chem. Phys.* **60,** 2692–2699.
Diestler, D. J. (1976). *In* "Radiationless Processes in Molecule and Condensed Phase" (F. K. Fong, ed.), pp. 169–236.
Diestler, D. J. (1980). *Adv. Chem. Phys.* **42,** 305–352.
Diestler, D. J., Knapp, E. W., and Ladouceur, H. D. (1978). *J. Chem. Phys.* **68,** 4056–4065.
Dogonadze, R. R. (1971). *In* Reactions of Molecules on Electrodes" (N. S. Hush, ed.), p. 135. Wiley, New York.
Dogonadze, R. R., and Berdnikov, B. M. (1977). *Teor. Eksp. Khim.* **13,** 747–752.
Dogonadze, R. R., and Kornyshev, A. A. (1972). *Phys. Status Solidi* **53,** 439–450.
Dogonadze, R. R., and Kuznetsov, A. M. (1971). *Electrokhimiya* **7,** 763–770.
Dogonadze, R. R., and Kuznetsov, A. M. (1973). "Itogi Nauki i Tekhniki. Fizicheskaya Khimiya. Kinetika," Vol. 2. VINITI, Moscow.
Dogonadze, R. R., and Kuznetsov, A. M. (1975). *Prog. Surf. Sci.* **6,** 1–41.
Dogonadze, R. R., and Kuznetsov, A. M. (1978). "Itogi Nauki i Tekhniki. Kinetika i Katalis," Vol. 5. VINITI, Moscow.
Dogonadze, R. R., Kuznetsov, A. M., and Levich, V. G. (1969). *Dokl. Akad. Nauk SSSR* **188,** 383–386.
Dogonadze, R. R., Kuznetsov, A. M., and Vorotyntsev, M. A. (1972). *Phys. Status Solidi* **54,** 125–134.
Dolgikh, V. A., and Plotnikov, V. G. (1978). *Izv. Acad. Nauk SSSR* **42,** 409–413.
Dolgikh, V. A., and Plotnikov, V. G. (1979). *Opt. Spektrosk.* **47,** 231–238.
Dubost, H., and Charneau, R. (1978). *Chem. Phys.* **12,** 407–418.
Efrima, S., and Bixon, M. (1974). *Chem. Phys. Lett.* **25,** 34–37.
Endicott, J. F., and Taube, H. (1964). *J. Am. Chem. Soc.* **86,** 1686–1691.
Englman, R., and Jortner, J. (1970). *Mol. Phys.* **18,** 145–158.
Fang, H. L., and Swofford, R. L. (1980a). *J. Chem. Phys.* **72,** 6382–6381.
Fang, H. L., and Swofford, R. L. (1980b). *J. Chem. Phys.* **73,** 2607–2617.
Feynman, R. P., and Hibbs, A. R. (1965). "Quantum Mechanics and Path Integrals." McGraw-Hill, New York.
Fisher, S. F. (1970). *J. Chem. Phys.* **53,** 3195–3207.
Fisher, S. F. (1971a). *Chem. Phys. Lett.* **10,** 397–401.
Fisher, S. F. (1971b). *Chem. Phys. Lett.* **11,** 577–580.
Fisher, S. F., and Schneider, S. (1971). *Chem. Phys. Lett.* **10,** 392–395.
Fisher, S. F., Schlag, E. W., and Schneider, S. (1971). *Chem. Phys. Lett.* **11,** 583–587.
Fong, F. K., Naberhuis, S. L., and Miller, H. M. (1972). *J. Chem. Phys.* **56,** 4020–4026.
Ford-Smith, M. H., and Sutin, N. J. (1961). *J. Am. Chem. Soc.* **83,** 1830–1834.
Freed, K. F. (1976). *Top. Appl. Phys.* **15,** 23–164.
Freed, K. F. (1980). *Adv. Chem. Phys.* **42,** 207–271.
Freed, K. F., and Band, Y. B. (1977). *In* "Excited States" (E. C. Lim, ed.), Vol. III, pp. 110–203. Academic Press, New York.
Freed, K. F., and Metiu, H. (1977). *Chem. Phys. Lett.* **48,** 262–266.

Garrett, B. C., and Truhlar, D. G. (1979). *J. Phys. Chem.* **83,** 188–201, 1079–1089.
Gelbart, W. M., Freed, K. M., and Rice, S. H. (1970). *J. Chem. Phys.* **52,** 2460–2473.
Gelbart, W. M., Elert, M. L., and Heller, D. F. (1980). *Chem. Rev.* **80,** 403–416.
George, T. F., and Miller, W. H. (1972). *J. Chem. Phys.* **57,** 2458–2472.
Goldanski, V. I. (1959a). *Dokl. Akad. Nauk SSSR* **124,** 1261–1264.
Goldanski, V. I. (1959b). *Dokl. Akad. Nauk SSSR* **127,** 1037–1042.
Goldanski, V. I. (1977). *Annu. Rev. Phys. Chem.* **28,** 85–126.
Grebenshikov, D. M., and Personov, R. I. (1969). *Opt. Spectrosk.* **26,** 264–270.
de Groot, M. S., and van der Waals, H. (1963). *Mol. Cryst.* **6,** 545–552.
Guttman, G., and Rice, S. A. (1974). *J. Chem. Phys.* **61,** 651–660.
Halpern, J., and Orgel, L. E. (1960). *Discuss. Faraday Soc. Ser. N* **29,** 32–41.
Heller, A. (1969). *Mol. Photochem.* **1,** 257–269.
Heller, D. F., Freed, K. F., and Gelbart, W. M. (1972). *J. Chem. Phys.* **56,** 2309–2328.
Henry, B. R. (1974). *Acc. Chem. Res.* **7,** 225–235.
Henry, B. R. (1976). *J. Phys. Chem.* **80,** 2160–2163.
Henry, B. R., and Hung, I-Fu (1978). *Chem. Phys.* **29,** 465–475.
Henry, B. R., and Siebrand, W. (1968). *J. Chem. Phys.* **49,** 5369–5376.
Henry, B. R., and Siebrand, W. (1973). *Org. Mol. Photophys.* **1,** 153–238.
Henry, B. R., and Siebrand, W. (1975). *Org. Mol. Photophys.* **2,** 303–312.
Holstein, T. (1953). *Ann. Phys. (N.Y.)* **8,** 343–384.
Howard, W. E., and Schlag, E. W. (1980). *In* "Radiationless Transitions" (S. H. Lin, ed.), pp. 81–134. Academic Press, New York.
Huang, C. S., and Lim, E. C. (1975). *J. Chem. Phys.* **62,** 3826–3828.
Huang, K., and Rhys, A. (1950). *Proc. R. Soc.* **204,** 406–422.
Hunt, G. R., and McCoy, E. F. (1962). *Aust. J. Chem.* **17,** 591–608.
Hush, N. S. (1961). *Trans. Faraday Soc.* **57,** 557–580.
Ivanov, G. K., and Kozhyshner, M. A. (1978). *Fiz. Tverd. Tela* **20,** 9–15.
Johnston, H. S., and Rapp, P. J. (1961). *J. Am. Chem. Soc.* **83,** 1–9.
Jortner, J. (1959). *J. Chem. Phys.* **30,** 839–846.
Jortner, J., Rice, S. A., and Hochstrasser, R. W. (1969). *Adv. Photochem.* **7,** 149.
Kestner, N. R. (1976). *In* "Electron-Solvent and Anion Solvent Interaction" (L. Kevan and B. C. Webster, eds.), p. 1. Elsevier, Amsterdam.
Kestner, N. R., Logan, J., and Jortner, J. (1974). *J. Phys. Chem.* **78,** 2148–2165.
Kirkwood, J. G. (1939). *J. Chem. Phys.* **7,** 911–925.
Klochikhin, V. L., Pshezhetskii, S. Ya., and Trakhtenberg, L. I. (1979). *Zh. Fiz. Khim.* **54,** 1324–1328.
Konoplev, G. G., Ovchinnikov, A. A., and Plotnikov, V. G. (1974). *Zh. Eksp. Teor. Fiz.* **66,** 1956–1969.
Krivoglaz, M. A. (1953). *Zh. Eksp. Teor. Fiz.* **25,** 191–198.
Kubo, R. (1957). *J. Phys. Soc. Jpn.* **12,** 570–596.
Kubo, R., and Toyozawa, Y. (1955). *Prog. Theor. Phys.* **13,** 160–182.
Kühn, I. H., and Metz, F. (1979). *Chem. Phys.* **33,** 137–150.
Kühn, I. M., Heller, D. F., and Gelbart, W. H. (1977). *Chem. Phys.* **22,** 435–452.
Kuznetsov, A. M. (1971). *Elektrokhimiya* **7,** 1067–1069.
Kuznetsov, A. M. (1981). *Elektrokhimiya* **17,** 84–89.
Landau, L. D., and Lifshitz, E. M. (1974). "Quantum Mechanics." Nauka, Moscow.
Laubereau, A., and Kaiser, W. (1978). *Rev. Mod. Phys.* **50,** 607–666.
Laubereau, A., Fisher, S. F., Spanner, K., and Kaiser, W. (1978). *Chem. Phys.* **31,** 335–344.
Lawetz, V., Siebrand, W., and Orlandi, G. (1972). *Chem. Phys. Lett.* **16,** 448–451.

Lax, M. (1952). *J. Chem. Phys.* **20,** 1752–1764.
Legay, F. (1977). *In* "Chemical and Biochemical Application of Lasers" (C. B. Moore, ed.), Vol. II, pp. 43–86. Academic Press, New York.
Le Roy, R. J., and Scott-Carley, J. (1980). *Adv. Chem. Phys.* **42,** 353–421.
Le Roy, R. J., Murai, H., and Williams, F. (1980). *J. Am. Chem. Soc.* **102,** 2325–2334.
Levich, V. G. (1970). *In* "Physical Chemistry. An Advanced Treatise" (H. Eyring, D. Hendersen, and W. Jost, eds.), Vol. 9, p. 986. Academic Press, New York.
Levich, V. G., and Dogonadze, R. R. (1959). *Dokl. Akad. Nauk SSSR* **124,** 123–126.
Levich, V. G., and Dogonadze, R. R. (1960). *Dokl. Akad. Nauk SSSR* **133,** 158–161.
Libby, W. F. (1952). *J. Phys. Chem.* **56,** 833.
Lim, E. C. (1977). *In* "Excited States" (E. C. Lim, ed.), Vol. 3, pp. 305–360. Academic Press, New York.
Lin, S. H. (1966). *J. Chem. Phys.* **44,** 3759–3767.
Lin, S. H. (1974). *J. Chem. Phys.* **61,** 3810–3820.
Lin, S. H. (1976). *J. Chem. Phys.* **65,** 1053–1052.
Lin, S. H. (1980). *In* "Radiationless Transitions" (S. H. Lin, ed.), pp. 363–415. Academic Press, New York.
Lin, S. H., and Bersohn, R. (1968). *J. Chem. Phys.* **48,** 2732–2736.
Lin, S. H., Lin, H. P., and Eyring, H. (1979). *Proc. Natl. Acad. Sci. U.S.A.* **76,** 3571.
Madigosky, W. H., and Litovitz, T. A. (1961). *J. Chem. Phys.* **34,** 489–497.
Makshantsev, B. I. (1972). *Spectrosc. Lett.* **5,** 1–7, 7–12.
Makshantsev, B. I. (1980). *Chem. Phys.* **49,** 397–415.
Makshantsev, B. I., and Fleurov, V. N. (1980). *Chem. Phys.* **49,** 77–86.
Makshantsev, B. I., and Perstnev, I. P. (1971a). *Opt. Spektrosk.* **30,** 371–375.
Makshantsev, B. I., and Perstnev, I. P. (1971b). *Opt. Spektrosk.* **31,** 881–884.
Marcus, R. A. (1956). *J. Chem. Phys.* **24,** 966–972.
Marcus, R. A. (1957). *J. Chem. Phys.* **26,** 867–871; *26,* 872–877.
Marcus, R. A. (1964). *Annu. Rev. Phys. Chem.* **15,** 155–196.
Marcus, R. A., and Cottrin, M. E. (1977). *J. Chem. Phys.* **67,** 2609–2612.
Martin, T. E., and Kalantar, A. H. (1969). *J. Chim. Phys. Physicochim. Biol.* Special issue, pp. 101–104.
Medvedev, E. S. (1982). *Zh. Khim. Fiz. N2,* 188–194.
Medvedev, E. S., and Osherov, V. I. (1968). *Dokl. Acad. Nauk SSSR* **180,** 905–908.
Medvedev, E. S., Osherov, V. I., and Pshenichnikov, V. M. (1977). *Chem. Phys.* **23,** 397–410.
Metieu, H., Oxtoby, D. W., and Freed, K. F. (1977). *Phys. Rev. Ser. A* **15,** 361–366.
Metz, H. (1975). *Chem. Phys. Lett.* **22,** 186–191.
Metz, F. (1976). *Chem. Phys.* **18,** 385–399.
Miller, W. H. (1974). *Adv. Chem. Phys.* **25,** 69–177.
Miller, W. H. (1975a). *Adv. Chem. Phys.* **30,** 77–183.
Miller, W. H. (1975b). *J. Chem. Phys.* **62,** 1899–1907.
Murata, S., Iwanaga, C., Toda, T., and Kokubun, H. (1972a). *Chem. Phys. Lett.* **13,** 101–105.
Murata, S., Iwanaga, C., Toda, T., and Kokubun, H. (1972b). *Chem. Phys. Lett.* **15,** 152–157.
Nikitin, E. E. (1974). "Theory of Elementary Atomic and Molecular Processes." Oxford Univ. Press (Clarendon), London and New York.
Nikitin, E. E., and Umanski, S. Ya. (1979). "Nonadiabatic Transitions at Slow Atomic Collisions." Atomizdat, Moscow.
Nikitin, E. E., and Ovchinnikova, M. Ya. (1980). *Zh. Eksp. Teor. Fiz.* **78,** 1551–1567.

Nitzan, A., and Jortner, J. (1973). *Theor. Chim. Acta* **30,** 217–229.
Nitzan, A., Mukamel, S., and Jortner, J. (1974). *J. Chem. Phys.* **60,** 3929.
Nitzan, A., Mukamel, S., and Jortner, J. (1975). *J. Chem. Phys.* **63,** 200.
Novak, F. A., Rice, S. A., Morse, M. D., and Freed, K. F. (1980). *In* "Radiationless Transitions" (S. H. Lin, ed.), pp. 135–185. Academic Press. New York.
Nurmukhamedov, R. N. (1971). "Absorption and Luminescence of Aromatic Compounds." Khimiya, Moscow.
Nurnburg, H. W. (1967). *Fortschr. Chem. Forsch.* **8,** 242.
Ovchinnikov, A. A. (1972). *Teor. Matem. Fiz.* **11,** 366–376.
Ovchinnikov, A. A. (1981). *Dokl. Acad. Nauk SSSR* (in press).
Ovchinnikov, A. A., and Benderski, V. A. (1978). *Dokl. Acad. Nauk SSSR* **243,** 393–395.
Ovchinnikov, A. A., and Benderski, V. A. (1979). *J. Electroanal. Chem.* **100,** 363–572.
Ovchinnikov, A. A., and Erikhman, N. S. (1971). *Zh. Eksp. Teor. Fiz.* **61,** 2391–2400.
Ovchinnikov, A. A., and Erikhman, N. S. (1972a). *Opt. Spektrosk.* **33,** 68–73.
Ovchinnikov, A. A., and Erikhman, N. S. (1972b). *Opt. Spektrosk.* **14,** 2825–2833.
Ovchinnikov, A. A., and Erikhman, N. S. (1973a). *Opt. Spektrosk.* **34,** 690–695.
Ovchinnikov, A. A., and Erikhman, N. S. (1973b). *Opt. Spektrosk.* **34,** 887–891.
Ovchinnikov, A. A., and Erikhman, N. S. (1975). *Zh. Eksp. Teor. Fiz.* **69,** 267–273.
Ovchinnikov, A. A., and Erikhman, N. S. (1982). *Opt. Spektrosk.* (in press).
Ovchinnikov, A. A., and Ovchinnikova, M. Ya. (1969a). *Zh. Eksp. Teor. Fiz.* **56,** 1278–1279.
Ovchinnikov, A. A., and Ovchinnikova, M. Ya. (1969b). *Dokl. Akad. Nauk SSSR* **186,** 76–79.
Ovchinnikov, A. A., and Plotnikov, V. G. (1977). *Chem. Phys.* **21,** 349.
Ovchinnikov, A. A., Benderski, V. A., Babenko, S. D., and Krivenko, A. G. (1978). *J. Electroanal. Chem.* **91,** 321–337.
Ovchinnikova, M. Ya. (1965). *Dokl. Akad. Nauk SSSR* **161,** 641–643.
Ovchinnikova, M. Ya. (1968). *Theor. Eksp. Khim.* **4,** 575–582.
Ovchinnikova, M. Ya. (1977). *Chem. Phys.* **19,** 313–326.
Ovchinnikova, M. Ya. (1979). *Chem. Phys.* **36,** 85–96.
Ovchinnikova, M. Ya. (1981). *Theor. Eksp. Khim.* **17,** 651–654.
Ovchinnikova, M. Ya. (1982). *In* "Teoreticheskie Problemy Khimicheskoi Fiziki" (N. N. Semenov, N. D. Sokolov, and E. E. Nikitin, eds.), p. 89–101. Nauka, Moscow.
Ovchinnikova, M. Ya., and Ovchinnikov, A. A. (1970). *Opt. Spectrosk.* **26,** 964–970.
Oxtoby, D. W. (1977). *Mol. Phys.* **34,** 987–994.
Oxtoby, D. W. (1979). *Adv. Chem. Phys.* **40,** 1–48.
Oxtoby, D. W., and Rice, S. A. (1976). *Chem. Phys. Lett.* **42,** 1–7.
Pagitsas, M., and Freed, K. F. (1977). *Chem. Phys.* **23,** 387–396.
Pekar, S. I. (1954). "Untersuchungen ueber die Electronentheorie der Kristalle." Academicher Verlag, Berlin.
Plotnikov, V. C. (1979). *Int. J. Quantum Chem.* **16,** 527–541.
Plotnikov, V. G. (1980). *Usp. Khimii* **69,** 327–361.
Plotnikov, V. G., and Dolgikh, V. A. (1977), *Opt. Spektrosk.* **43,** 882–890.
Plotnikov, V. G., and Dolgikh, V. A. (1978). *Opt. Spektrosk.* **44,** 450–457.
Plotnikov, V. G., and Ovchinnikov, A. A. (1978). *Usp. Khimii* **47,** 444–476.
Plotnikov, V. G., Dolgikh, V. A., and Komarov, V. M. (1977). *Opt. Spektrosk.* **43,** 1072–1078.
Pogorelov, V. E., Lizengevich, A. I., Kondilenko, I. I., and Buyan, G. P. (1979). *Usp. Fiz. Nauk* **127,** 683–704.
Prais, M. G., Heller, D. F., and Freed, K. F. (1974). *Chem. Phys.* **6,** 331–352.

Pshenichnov, E. A., and Sokolov, N. D. (1967). *Int. J. Quantum Chem.* **1,** 885–893.
Reddy, K. V., Bray, R. G., and Berry, M. J. (1978). *In* "Advances in Laser Chemistry" (A. H. Zewail, ed.), p. 48. Springer-Verlag Berlin and New York.
Reynolds, W. L., and Lumry, R. W. (1966). "Mechanisms of Electron Transfer." Ronald, New York.
Rice, S. A. (1975). *In* "Excited States" (E. C. Lim, ed.), Vol. II, pp. 111–320. Academic Press, New York.
Richards, W. G. (1979). *In* "Water: A Comprehensive Treatise. Vol. 6. Recent Advances" (F. Franks, ed.), p. 123. Plenum, New York.
Robinson, G. W., and Frosh, R. P. (1963a). *J. Chem. Phys.* **37,** 1962–1968.
Robinson, G. W., and Frosch, R. P. (1963b). *J. Chem. Phys.* **38,** 1187–1203.
Robinson, G. W. (1974). *In* "Excited States" (E. C. Lin, ed.), Vol. 1, pp. 1–34. Academic Press, New York.
Rosetti, R., and Brus, L. E. (1979). *J. Chem. Phys.* **71,** 3663–3970.
Sacher, S., and Laidler, K. J. (1964). *In* "Modern Aspects of Electrochemistry" (J. O'M. Bockris and B. E. Conway, eds.), pp. 1–54. Butterworths, London.
Sage, M. L. (1979). *J. Phys. Chem.* **83,** 1455–1457.
Sakun, V. P. (1976). *Fiz. Iverd. Tela.* **18,** 2517–2524.
Saxton, R. (1952). *Proc. R. Soc. Ser. A* **213,** 473–492.
Scharf, B. (1979). *Chem. Phys. Lett.* **68,** 242–244.
Schlag, E. W., and von Weysenhoff, H. (1969). *J. Chem. Phys.* **51,** 2508–2514.
Schlag, E. W., Schneider, S., and Fisher, S. F. (1971). *Annu. Rev. Phys. Chem.* **22,** 405–526.
Schmidt, P. P. (1973). *J. Chem. Phys.* **57,** 3749–3762.
Schmidt, P. P. (1974). *J. Chem. Phys.* **58,** 4384–4388.
Schmickler, W. (1973). *Ber. Bunsenges. Phys. Chem.* **77,** 991–997.
Schmickler, W. (1976). *Ber. Bunsenges. Phys. Chem.* **80,** 835–840.
Shugard, M., Tully, J. C., and Nitzan, A. (1978). *J. Chem. Phys.* **6,** 336–345.
Siebrand, W. (1966). *J. Chem. Phys.* **44,** 4055–4057.
Siebrand, W. (1967a). *J. Chem. Phys.* **46,** 440–447; *47,* 2411–2422.
Siebrand, W. (1967b). *In* "The Triplet State" (A. B. Zahban, ed.), p. 31. Cambridge Univ. Press, London and New York.
Siebrand, W. (1971). *J. Chem. Phys.* **54,** 363–367.
Siebrand, W., and Zgierski, M. (1975). *Chem. Phys. Lett.* **68,** 242–244.
Siebrand, W., and Zgierski, M. Z. (1980). *J. Chem. Phys.* **72,** 1641–1646.
Suga, K., Mizota, J., Kanzaki, Y., and Aoyagni, S. (1973). *J. Electroanal. Chem.* **41,** 313.
Sun, H. Y., and Rice, S. A. (1965). *J. Chem. Phys.* **42,** 3826–3830.
Swofford, R. L., Burberry, M. S., Morrell, J. A., and Albrecht, A. C. (1977). *J. Chem. Phys.* **66,** 5245–
Trakhtenberg, L. I., Klochikhin, V. L., and Pshezhetski, S. Ya. (1981). *Chem. Phys.* **59,** 191–203.
Ulstrup, J. (1979). "Charge Transfer Process in Condensed Media." Springer-Verlag, Berlin and New York.
Ulstrup, J., and Jortner, J. (1975). *J. Chem. Phys.* **63,** 4358–4368.
Van Duyne, R. P., and Fisher, S. (1974). *Chem. Phys.* **5,** 183–197.
Van-Duyne, R. P., and Fisher, S. (1977). *Chem. Phys.* **26,** 9–16.
Velsko, S., and Oxtoby, D. W. (1980). *J. Chem. Phys.* **72,** 2260–2263; 4853–4856.
Wallace, R. (1975). *Chem. Phys.* **11,** 189–192.
Ware, W. R., Selinger, B. K., Parmeter, C. S., and Shyler, M. W. (1976). *Chem. Phys. Lett.* **6,** 342–346.

Wiesenfeld, J. M., and Moore, C. B. (1976). *Bull. Am. Chem. Soc.* **21,** 1289.
Wiesenfeld, J. M., and Moore, C. B. (1979). *J. Chem. Phys.* **70,** 930–946.
Yakobson, B. I., and Burshtein, A. I. (1980). *Chem. Phys.* **49,** 385–395.
Zwolinski, B. J., Marcus, R. J., and Eyring, M. (1955). *Chem. Rev.* **55,** 157–180.
Zusman, L. D. (1975). *Zh. Eksp. Teor. Fiz.* **69,** 1558–1560.
Zusman, L. D. (1980). *Chem. Phys.* **49,** 295–304.

Practical Valence-Bond Calculations

G. A. GALLUP, R. L. VANCE,* J. R. COLLINS, and J. M. NORBECK†

Department of Chemistry
University of Nebraska
Lincoln, Nebraska

I. Introduction

A. Why the Valence-Bond Method?

The valence-bond method for calculating molecular structures and energies has had an enduring popularity among chemists as a conceptual tool for interpreting chemical reactivities and processes at the qualitative level. It has not, however, enjoyed the same popularity as a method for obtaining quantitative results at an *ab initio* level, and a common thread

* Present Address: Dow Chemical Co., Midland, Michigan 48640.
† Present Address: Ford Motor Research Laboratory, Dearborn, Michigan 48121.

ADVANCES IN QUANTUM CHEMISTRY, VOLUME 16

ISBN 0-12-034816-0

running through much recent literature is the view that calculations at this level are impractically difficult. Inspite of this, many workers apparently wish to consider valence-bond wave functions for the insight they provide into chemical phenomena. This has produced efforts to transform molecular orbital treatments into valence-bond form (Hiberty, 1981; Hiberty and Leforestier, 1978), and for some small systems this may be done exactly. However, in most cases this transformation can be done only approximately, and no way is available at this time to test the accuracy of the approximation. The only alternative is to calculate the valence-bond wave functions directly at the desired level of accuracy. For a number of years we have used the procedures discussed in this article and have treated problems involving a number of systems to the level of accuracy expected with other computational methods and with no greater level of difficulty (Gallup, 1977a,b; Gallup and Macek, 1977; Gallup and Norbeck, 1973a,b,c, 1974, 1975; Sramek, 1980; Sramek *et al.*, 1980a,b; Vance and Gallup, 1978, 1980). We suggest that using these procedures, valence-bond calculations are not too difficult to be practical.

The term *valence bond* has been used to describe a number of different types of approaches, so for clarity we must define our usage. All practical methods of calculating electronic structure and energies as a function of geometry involve some configuration interaction (CI) at least implicitly, and the interacting configurations are constructed from selected sets of single-particle orbitals. In this article, a valence-bond treatment is defined as a CI which allows complete flexibility for the overlaps between single-particle orbitals and, in particular, one in which there are no constraints that all or selected pairs of orbitals must be orthogonal. In some cases the phrase multiconfiguration valence bond (MCVB) is useful because of the extra descriptiveness, but we use the shorter term "valence bond" in this article. The name "multistructure valence bond" has also been used (Balint-Kurti and Karplus, 1968).

Although early valence-bond discussions tended to emphasize π-electron systems, and these still occupy the attention of many workers using semiempirical techniques, the flexibility allowed in our definition means that there is a much wider range of application than this. Since there are no restrictions on the orbitals, we are free to use our ingenuity to its fullest in tailoring a wave function to treat the problem of interest, and at the same time remain securely within a linear variation framework. This characteristic is particularly useful in discussing associating or dissociating systems, but has many other applications.

B. The Traditional Approach

Traditionally, valence-bond calculations have been done with an electron pair bond basis which is a generalization of the Heitler–London calcu-

lation of the H_2 molecule (Heitler and London, 1927). We will call these Heitler–London–Slater–Pauling (HLSP) functions (Slater, 1931). Considerable effort has been expended over the years to analyze the algebraic properties of this formulation, and many rules are known for the evaluation of matrix elements (Pauling, 1933; Cooper and McWeeny, 1966; Shull, 1969). However, when the orbitals are not orthonormal many of these methods are exceedingly difficult to apply. Matrix elements of the Hamiltonian for an N-electron system may always be written as a sum over $N!$ permutations. The labor in using such a sum for numerical work grows at an alarming rate with increasing N and these formulas cannot be considered practical. Probably the most efficient formulation for HLSP functions consists of writing them as a sum of $2^{N/2-S}$ Slater determinants, where S is the total spin quantum number. These may then be dealt with using the cofactor methods of Löwdin (1955). But the labor here still grows at an exponential rate with N, and only relatively small systems can be treated. So far as we know this is the best that one can expect to do when dealing with the HLSP basis directly.

Simonetta *et al.* (1968) and Raimondi *et al.* (1972, 1973, 1975) have systematized this procedure, have applied it to a number of molecules, and have clearly provided a useable method for obtaining valence-bond results.

Balint-Kurti and Karplus (1968, 1974; see also Van Lenthe and Balint-Kurti, 1980) have implemented an alternative method using HLSP functions which gives a large-scale systematization of an early suggestion of Moffitt (1953). In this procedure, the Slater determinants, in terms of which the HLSP functions are written, are transformed to a new set over orthogonal orbitals. The new Slater determinants provide much simpler algorithms for the determination of the matrix elements. The wave functions and matrix elements in terms of the HLSP basis are then obtained by using the inverse of the original transformation.

More recently, Pyper and Gerratt (1977) and Wilson and Gerratt (1975) have developed a spin-coupled valence-bond procedure in which Slater determinants are used to reproduce the geneological spin functions. It requires $\binom{N}{N/2-S}$ Slater determinants to write all of these spin functions. Although this is larger than the $2^{N/2-S}$ for HLSP functions, the total labor tends toward the same value for large N and small S.

The approach we describe here uses a different basis of what we call *tableau functions*. The bases of tableau functions and HLSP functions, each generated from the same configurations, are always exactly equivalent, and a transformation between the two may always be made. A tableau function can be written as a sum of $\frac{1}{2}(N/2 - S + 1)$ [or $\frac{1}{2}(N/2 - S + 2)$, whichever is an integer] determinantal functions and provides a clear computational advantage over the HLSP basis. At the present stage of

development it appears that *tableau functions* provide the most efficient way to calculate matrix elements for the Hamiltonian between configurations of nonorthogonal orbitals. The transformation of the final wave function to an HLSP basis, if so desired, is a relatively trivial problem. In Section II we give an outline of the complete method for evaluating matrix elements.

The book on spin eigenfunctions by Pauncz (1979) provides a complete discussion of the relationships between various methods for dealing with spin. However, the reader will observe that in Section II we use arguments based upon symmetric group theory and spin-free quantum chemistry (Matsen, 1964; Goddard, 1967; Gallup, 1968, 1969) to discuss the tableau functions. At the moment this appears necessary since no one has arrived directly at these results from a more familiar starting point such as a spin-projected Slater determinant.

Another feature of our calculations which can provide enormous savings of time is a core–valence separation. This is discussed in Section III, along with the construction of independent configurations and transformations to HLSP functions.

Section IV consists of some reasonably brief comments about the nonorthogonal eigenvalue problem with emphasis on methods for dealing with large matrices. Section IV also contains a discussion of the *weights* of structures or components in a wave function.

Section V contains applications of the procedures described. Many specific calculations could be used to illustrate characteristics of the valence-bond approach, but we have chosen only two to give in this article. The first of these is a π-only (frozen σ core) calculation of planar butadiene. We describe the minimal basis calculation and show how a double-zeta treatment may be used to obtain better energies without relinquishing the easy interpretability of the simple wave function. The second system we treat consists of an ethylene molecule and a methylene radical. We consider some pathways for the insertion of methylene into C_2H_4 to form cyclopropane, with particular emphasis on the symmetries of the interacting states and the single–triplet crossing point(s) in the process.

II. The Evaluation of Matrix Elements

The majority of problems in chemistry which require the solution of Schrödinger's equation

$$\hat{H}\psi = E\psi \tag{1}$$

are based on a spin-free Born–Oppenheimer Hamiltonian

$$\hat{H} = \sum_{i=1}^{N} \left(-\frac{1}{2}\nabla_i^2 - \sum_{\alpha=1}^{N} \frac{Z_\alpha}{r_{\alpha i}} \right) + \sum_{i<j}^{N} \frac{1}{r_{ij}} + \sum_{\alpha<\beta} \frac{Z_\alpha Z_\beta}{R_{\alpha\beta}} \tag{2}$$

where $r_{\alpha i}$ is the distance between electron i and nucleus α; Z_α is the charge on nucleus α; and $R_{\alpha\beta}$ is the distance between α and β. Because of the absence of any terms which depend explicitly on spin, the Hamiltonian in Eq. (2) commutes with the total spin operator $\hat{S}^2$ and its z component $\hat{S}_z$. As a result, each state of the system can be an eigenfunction of the operators $\hat{H}$, $\hat{S}^2$, and $\hat{S}_z$ simultaneously. Therefore, in addition to requiring that ψ be antisymmetric (Pauli principle),

$$\pi\psi = (-1)^{\sigma_\pi}\psi \tag{3a}$$

where π is a permutation of electron coordinates and σ_π is the parity, we also require that ψ be an eigenfunction of the spin

$$\hat{S}^2\psi = S(S+1)\psi, \qquad \hat{S}_z\psi = M\psi \tag{3b}$$

Pauncz (1979) has reviewed the many methods developed for constructing wave functions which satisfy the above requirements. However, all the various approaches may be classified into two basic categories, depending upon which of the above conditions the wave function is required to satisfy first during the construction procedure.

Methods which are based upon Slater determinants can be viewed as first requiring that the wave function satisfy the antisymmetry condition (3a). Since, in general, Slater determinants are not eigenfunctions of $\hat{S}^2$, linear combinations must be formed in order to satisfy the spin eigenfunction requirement (Eyring *et al.*, 1944).

The other approach involves first imposing the spin requirement on the wavefunction followed by application of the antisymmetry principle. This point of view requires consideration of the effect of permutations on spin eigenfunctions and leads quite naturally to the theory of the symmetric group. This approach has not enjoyed the same level of popularity as that of the former. However, there have been numerous discussions and applications given by various workers (Van Vleck, 1934; Serber, 1934a,b; Yamanouchi, 1937; Pauncz, 1979).

A. Eigenfunctions of the Spin

We follow the second approach and show that the most general function which satisfies the spin eigenfunction and antisymmetry requirements is of the form

$$\psi = \sum_{k=1}^{f_S^N} \Theta_{SM;k}^N \Phi_{kS} \tag{4}$$

where the $\Theta^N_{SM;k}$ are eigenfunctions of $\hat{S}^2$ and $\hat{S}_z$ and the Φ_{kS} are functions of the spatial coordinates (Wigner, 1959; Messiah, 1967). Our symbol N is the number of electrons and k labels the various functions which span the "spin-degeneracy" space for N and S. In addition, we will show that for spin-free Hamiltonians such as Eq. (2) the expectation value of the energy is dependent only on the spatial function Φ_{1S}

$$E = \langle\psi|H|\psi\rangle / \langle\psi|\psi\rangle = \langle\Phi_{1S}|H|\Phi_{1S}\rangle / \langle\Phi_{1S}|\Phi_{1S}\rangle \tag{5}$$

We assume that we have a complete orthonormal set of spin eigenfunctions $\Theta^N_{SM;k}$ such that

$$\hat{S}^2\Theta^N_{SM;k} = S(S+1)\Theta^N_{SM;k}, \qquad k = 1, 2, \ldots, f^N_S \tag{6a}$$

$$\hat{S}_z\Theta^N_{SM;k} = M\Theta^N_{SM;k}, \qquad k = 1, 2, \ldots, f^N_S \tag{6b}$$

where

$$S = \tfrac{1}{2}N, \tfrac{1}{2}N - 1, \ldots, \begin{cases} 0 \\ 1/2 \end{cases}, \quad M = S, \quad S-1, \quad \ldots, \quad -S+1, \quad -S$$

$$f^N_S = (2S+1)N!(\tfrac{1}{2}N + S + 1)!(\tfrac{1}{2}N - S)!$$

(Pauncz, 1979) where N is the number of electrons and S is the spin state. Since $\hat{S}^2$ and $\hat{S}_z$ are observables and their spectra are discrete, we may form the resolution of the identity

$$\sum_{SMk} |\Theta^N_{SM;k}\rangle\langle\Theta^N_{SM;k}| = 1 \tag{7}$$

Considering the subspace $S'M'$, we form the projection operator

$$\hat{P}^N_{S'M'} = \sum_k |\Theta^N_{S'M';k}\rangle\langle\Theta^N_{S'M';k}| \tag{8}$$

which has the properties

$$\begin{aligned} &\text{(a)}\ \hat{S}^2\hat{P}^N_{S'M'} = S'(S'+1)\hat{P}^N_{S'M'}, \qquad &&\text{(c)}\ \hat{S}_z\hat{P}^N_{S'M'} = M\hat{P}^N_{S'M'} \\ &\text{(b)}\ \hat{S}^2\hat{P}^N_{S'M'} = \hat{P}^N_{S'M'}\hat{S}^2, &&\text{(d)}\ \hat{S}_z\hat{P}^N_{S'M'} = \hat{P}^N_{S'M'}\hat{S}_z \end{aligned} \tag{9}$$

Applying Eqs. (9b) and (9d) to ψ_{SM} gives

$$[\hat{S}^2\hat{P}^N_{S'M'} - \hat{P}^N_{S'M'}\hat{S}^2]\psi_{SM} = 0 \tag{10a}$$

$$[\hat{S}_z\hat{P}^N_{S'M'} - \hat{P}^N_{S'M'}\hat{S}_z]\psi_{SM} = 0 \tag{10b}$$

Operating on ψ_{SM} in Eqs. (10a) and (10b) by the terms in square brackets gives

$$[S'(S'+1) - S(S+1)]\hat{P}^N_{S'M'}\psi_{SM} = 0 \tag{11a}$$

$$[M' - M]\hat{P}^N_{S'M'}\psi_{SM} = 0 \tag{11b}$$

Therefore, from Eqs. (11a) and (11b) we have the result that for $S' \neq S$ and $M' \neq M$,

$$\hat{P}^N_{S'M'}\psi_{SM} = 0 \tag{12}$$

Since $\sum_{S'M'}\hat{P}^N_{S'M'} = I$ (resolution of the identity), we have $\psi_{SM} = \sum_{S'M'}\hat{P}^N_{S'M'}\psi_{SM}$, but from Eq. (12) all the terms in the above sum are zero except for the case $S' = S$ and $M' = M$, therefore

$$\psi_{SM} = \hat{P}^N_{SM}\psi_{SM} \tag{13}$$

Substituting Eqs. (8) into (13) gives

$$\psi_{SM} = \sum_k |\Theta^N_{SM;k}\rangle\langle\Theta^N_{SM;k}|\psi_{SM}\rangle \tag{14}$$

where $\langle\Theta^N_{SM;k}|\psi_{SM}\rangle$ is an integral over spin coordinates only and, therefore, a function of the spatial coordinates. Therefore, we have for the most general wave function

$$\psi_{SM} = \sum_k \Theta^N_{SM;k}\Phi_{kS} \tag{15}$$

where Φ_{kS} is the spatial wave function given by $\Phi_{kS}(\bar{r}_1, \bar{r}_2, \bar{r}_3, \ldots, \bar{r}_n) = \langle\Theta^N_{SM;k}|\psi_{SM}\rangle$.

It should be noted that as our notation implies Φ_{kS} does not depend on the quantum number M. This can be shown by considering the spin-raising and spin-lowering operators (Messiah, 1967) $\hat{S}^{\pm} = \hat{S}_x \pm \hat{S}_y$. Applying $\hat{S}^{\pm}$ to ψ_{SM} and $\Theta^N_{SM;k}$ gives

$$\hat{S}^{\pm}\psi_{SM} = [(S \mp M)(S \pm M + 1)]^{1/2}\psi_{SM\pm1}$$

$$\hat{S}^{\pm}\Theta^N_{SM;k} = [(S \mp M)(S \pm M + 1)^{1/2}\psi^N_{SM\pm1;k}$$

We now form the following matrix element, $\langle\Theta^N_{SM+1;k}|\psi_{SM+1}\rangle$, which can be rewritten by making use of the spin-raising operator

$$\left\langle \Theta^N_{SM+1;k} \middle| \frac{S^+\psi_{SM}}{[(S - M)(S + M + 1)]^{1/2}} \right\rangle \tag{16}$$

By making use of the turnover, rule (16) can be rewritten as

$$\left\langle \hat{S}^-\Theta^N_{SM+1;k} \middle| \frac{\psi_{SM}}{[(S - M)(S + M + 1)]^{1/2}} \right\rangle$$

or

$$\langle\Theta^N_{SM+1;k}|\psi_{SM+1}\rangle = \langle\Theta^N_{SM;k}|\psi_{SM}\rangle$$

Thus, Φ_{kS} is independent of the spin quantum number M.

Now that our function is an eigenfunction of $\hat{S}^2$ and $\hat{S}_z$, it must be made antisymmetric [Eq. (3a)],

$$\pi\psi_{SM} = \sum_k \pi^r \Phi_{kS} \pi^\sigma \Theta^N_{SM;k} = (-1)^{\sigma_\pi} \psi_{SM} \tag{17}$$

Here we have written the permutation π in terms of an operator acting on the spatial coordinates π^r and an operator acting on the spin coordinates π^σ. The functions $\Theta^N_{SM1;k}$ form a basis for the symmetric group of order N (Wigner, 1959), S_N, we have

$$\pi^\sigma \Theta^N_{SM;k} = \sum_{k'} \Theta^N_{SM;k'} D^{[\tilde{\lambda}]}(\pi)_{k'k} \tag{18}$$

where the $D^{[\tilde{\lambda}]}(\pi)$ form an irreducible representation of S_N and $[\tilde{\lambda}]$ refers to the partition $[N/2 + S,\ N/2 - S]$ (Rutherford, 1948). Recalling Eq. (15), Eq. (17) can be rewritten as

$$\sum_k \Theta^N_{SM;k} (-1)^{\sigma_\pi} \Phi_{kS} = \sum_{k'} \Theta^N_{SM;k'} \sum_k \pi^r \Phi_{kS} D^{[\tilde{\lambda}]}(\pi)_{k'k} \tag{19}$$

which after multiplication on both sides by $\Theta^N_{SM;k''}$ and integration over spin coordinates gives

$$(-1)^{\sigma_\pi} \Phi_{k''S} = \sum_k \pi^r \Phi_{kS} D^{[\tilde{\lambda}]}(\pi)_{k''k} \tag{20}$$

where we have made use of the orthonormality of the spin eigenfunctions. Multiplying both sides of Eq. (20) by $D^{[\tilde{\lambda}]}(\pi)_{k''k'}$ and summing over k'' gives

$$\sum_{k''} (-1)^{\sigma_\pi} \Phi_{k''S} D^{[\tilde{\lambda}]}(\pi)_{k''k'} = \sum_{k''} \sum_k \pi^r \Phi_{kS} D^{[\tilde{\lambda}]}(\pi)_{k''k'}$$

or

$$\pi^r \Phi_{kS} = \sum_{k'} (-1)^{\sigma_\pi} D^{[\tilde{\lambda}]}(\pi)_{k'k} \Phi_{k'S} \tag{21}$$

where the following relation has been used: $\Sigma_k D^{[r]}(\pi)_{kl} D^{[r]}(\pi)_{kn} = \delta_{ln}$. Noting that $(-1)^{\sigma_\pi} D^{[\tilde{\lambda}]}(\pi) = D^{[\lambda]}(\pi)$, we have

$$\pi^r \Phi_{kS} = \sum_{k'} D^{[\lambda]}(\pi)_{k'k} \Phi_{k'S} \tag{22}$$

Therefore, the Φ_{kS} form a representation of S_N with partition $[2^{N/2-S}, 1^{2S}]$ which is conjugate to the partition $[N/2 + S,\ N/2 - S]$. It should be mentioned that the above treatment depends upon the representation of S_N being *real* unitary.

Using the definition of the Frobenius operator (Littlewood, 1950), $e^{[\lambda]}_{k'k''} = (f^N_S/N!) \Sigma_\pi D^{[\lambda]}(\pi)_{k'k''} \pi$ and Eq. (22) gives

$$e^{[\lambda]}_{k'k''}\Phi_{kS} = \frac{f_S^N}{N!}\sum_{k'''}\sum_{\pi} D^{[\lambda]}(\pi)_{k'''k}D^{[\lambda]}(\pi)_{k'k''}\Phi_{k'''S} = \delta_{k''k}\Phi_{k'S}$$

Specifically, we have the symmetry requirement [which is equivalent to the two requirements embodied in Eqs. (3a and 3b)]

$$\Phi_{kS} = e^{[\lambda]}_{kk'}\Phi_{k'S} \tag{23}$$

and since Φ_{kS} is independent of k', we choose $k' = 1$, which gives for the total wave function

$$\psi_{SM} = \sum_k e^{[\lambda]}_{k1}\Phi_{1S}\Theta^N_{SM;k} \tag{24}$$

We are now in a position to consider the matrix element of the spin-free Hamiltonian given in Eq. (2)

$$\langle\psi_{SM}|\hat{H}|\psi_{SM}\rangle = \sum_j\sum_k \langle e^{[\lambda]}_{j1}|\Phi_{1S}|\hat{H}|e^{[\lambda]}_{k1}\Phi_{1S}\rangle\langle\Theta^N_{SM;j}|\Theta^N_{SM;k}\rangle$$

or (25)

$$\psi_{SM}|\hat{H}|\psi_{SM}\rangle = \sum_k \langle\Phi_{1S}|\hat{H}|\Phi_{1S}\rangle$$

where, in addition to Eq. (23), we have made use of the following properties

$$\langle\Theta^N_{SM;j}|\Theta^N_{SM;k}\rangle = \delta_{jk}, \qquad e^{[\lambda]}_{ij}e^{[\lambda]}_{k1} = \delta_{jk}e^{[\lambda]}_{i1}, \qquad (e^{[\lambda]}_{st})^\dagger = e^{[\lambda]}_{ts}$$

The sum in Eq. (25) contains f_S^N terms, therefore, the Hamiltonian matrix element is just

$$\langle\psi_{SM}|\hat{H}|\psi_{SM}\rangle = f_S^N\langle\Phi_{1S}|\hat{H}|\Phi_{1S}\rangle \tag{26}$$

Similarly, we have for the overlap matrix element

$$\langle\psi_{SM}|\psi_{SM}\rangle = f_S^N\langle\Phi_{1S}|\Phi_{1S}\rangle \tag{27}$$

The expectation value of the Hamiltonian can now be written as

$$E = \langle\Phi_{1S}|H|\Phi_{1S}\rangle/\langle\Phi_{1S}|\Phi_{1S}\rangle \tag{28}$$

with the requirement that $\Phi_{1S} = e^{[\lambda]}_{11}\Phi_{1S}$ which is equivalent for spin-free operators to the combined antisymmetry condition and the condition that ψ_{SM} be an eigenfunction of spin.

B. $\theta\hat{N}\hat{P}\hat{N}$ Tableau Functions

In the last section we arrived at the important formula (28) giving the energy of the spin-free Hamiltonian in terms of only one component of the spatial part of the wave function. The constraint which our spatial function must satisfy,

$$\Phi_{1S} = e_{11}^{[\lambda]}\Phi_{1S} \tag{29}$$

is, because of the idempotency of $e_{11}^{[\lambda]}$, most easily guaranteed by having

$$\Phi_{1S} = e_{11}^{[\lambda]}\Phi \tag{30}$$

where Φ is a function of more general symmetry. For our valence-bond method we are particularly interested in forms for Φ which are linear combinations of products of N orbitals. As a first step we consider the case when Φ is just one orbital product,

$$\Phi = u_1(1), \quad u_2(2), \quad \ldots, \quad u_N(N) \tag{31}$$

where we require only that the orbitals be normalized. In particular, they are neither orthogonal nor necessarily distinct.

In the foregoing we have emphasized the importance of using an idempotent $e_{11}^{[\lambda]}$, which allows efficient algorithms for the evaluation of matrix elements. An examination of this problem convinces one that antisymmetry in an operator can lead to rapid algorithms for dealing with it. Thus, since $e_{11}^{[\lambda]}$ is not a unique algebraic quantity and may be displayed in an infinity of forms depending upon unitary transformations of representations, we may choose the $e_{11}^{[\lambda]}$ by criteria based upon efficiency as well as any other property. We thus expect that an $e_{11}^{[\lambda]}$, which is as close as possible to a single antisymmetrizer, is likely to allow the most efficient algorithms for its evaluation.

Following this line of reasoning, one of us proposed (Gallup, 1968) that

$$e_{11}^{[\lambda]} = \theta\hat{N}\hat{P}\hat{N} \tag{32}$$

should provide the optimum form for calculational purposes. This form of the operator is based upon a Young tableau for the partition $[\lambda] = [2^{N/2-S}, 1^{2S}]$,

1 $\vdots$ $N/2 - S$	$N/2 + S + 1$ $\vdots$ N
$\vdots$ $N/2 + S$	

and $\hat{N}$ is the product of the separate *antisymmetrizers* for the numbers in the two columns of the tableau,

$$\hat{N} = \hat{a}(1, \ldots, N/2 + S)\hat{a}(N/2 + S + 1, \ldots, N) \tag{33}$$

This gives the form we want; $\hat{P}$ is the *symmetrizer* on numbers in the same row of the tableau,

$$\hat{P} = [I + (1, N/2 + S + 1)][I + (2, N/2 + S + 2)] \times \cdots [I + (N/2 - S, N)] \tag{34}$$

where the symbol (i, j) represents the binary interchange between i and j. The constant θ must have a value such that the coefficient of the identity I is $f_S^N/N!$ where f_S^N is given in Eq. (6).

Because of Eq. (33) we expect that the function Ψ,

$$\Psi = \theta \hat{N} \hat{P} \hat{N} \Phi \tag{35}$$

is likely to resemble a determinant and may be easily expressed as a sum of only a few determinants. We now indicate how these expectations are borne out.

We consider any $N \times N$ matrix $\mathbf{A}$ and partition it into four blocks:

$$\mathbf{A} = \begin{array}{c} \begin{array}{cc} N/2 + S & N/2 - S \end{array} \\ \left[\begin{array}{c|c} \mathbf{A}_{11} & \mathbf{A}_{12} \\ \hline \mathbf{A}_{21} & \mathbf{A}_{22} \end{array}\right] \end{array} \begin{array}{l} N/2 + S \\ N/2 - S \end{array} \tag{36}$$

where the numbers of rows and columns in each block are shown. We now define the new matrix $\mathbf{A}(q)$, a function of the real variable q, as

$$\mathbf{A}(q) = \begin{bmatrix} \mathbf{A}_{11} & \mathbf{A}_{12} \\ \mathbf{A}_{21} & q\mathbf{A}_{22} \end{bmatrix} \tag{37}$$

$$\mathbf{A} = \mathbf{A}(1) \tag{38}$$

We are interested in the determinant of $\mathbf{A}(q)$,

$$D_{\mathbf{A}}(q) = |\mathbf{A}(q)| \tag{39}$$

which is a polynomial in q of degree $\leq N/2 - S$.

We now specifically consider the matrix of functions which is associated with the product function Φ,

$$\mathbf{\Phi} = \begin{bmatrix} u_1(1) & u_2(1) & \cdots & u_N(1) \\ u_1(2) & u_2(2) & \cdots & u_N(2) \\ \vdots & \vdots & \vdots & \vdots \\ u_1(N) & u_2(N) & \cdots & u_N(N) \end{bmatrix} \tag{40}$$

and the corresponding $D_{\Phi}(q)$,

$$D_\Phi(q) = |\Phi(q)| \tag{41}$$

It is possible to show that the tableau function ψ is given by

$$\psi = \frac{f_S^N}{N!} \sum_{k=1}^{k_{\max}} C_k(N, S) |\Phi(q_k(N, S))| \tag{42}$$

where $C_k(N, S)$ and $q_k(N, S)$ are sets of numbers dependent upon N and S. The number of terms in Eq. (42) also depend upon N and S so that

$$k_{\max} = k_{\max}(N, S) = [N - 2S + (2 \text{ or } 4)]/4 \tag{43}$$

whichever is an integer. In order to determine C_k and q_k, we need the roots and derivatives of the Jacobi polynomials (Abramowitz and Stegun, 1965),

$$G_m(p, q, x) \equiv (-1)^m \frac{\Gamma(m + p)}{\Gamma(2m + p)} x^{1-q}(1 - x)^{q-p} \times \frac{d^m}{dx^m}[x^{q+m-1}(1 - x)^{p-q+m}] \tag{44}$$

We need the roots of the equation

$$G_{k_{\max}}(2S + 1, 2S + 1, t_k) = 0, \qquad k = 1, 2, \ldots, k_{\max} \tag{45}$$

from which we get

$$q_k(N, S) = -t_k/(1 - t_k) \tag{46}$$

$$C_k(N, S) = (-1)^{N/2-S}(N/2 + S + 1)[(1 - t_k)^{N/2-S-1}/t_k] \times \left[\binom{2k_{\max} + 2S}{k_{\max}} G'_{k_{\max}}(2S + 1, 2S + 1, t_k)\right]^{-2} \tag{47}$$

where the prime in $G'_{k_{\max}}$ represents the derivative, and $\binom{x}{y}$ indicates the ordinary binomial coefficient. These relations are most easily derived (Gallup, 1972) using a method which parallels the determination of optimal quadrature formulas (Krylov, 1962), although alternative paths are possible. Table I gives values of $C_k(N, S)$ and q_k for $2 \leq N \leq 10$ and $0 \leq S \leq 5/2$.

As we have pointed out some of the orbitals in Φ may be repeated (doubly occupied). Under these circumstances an important simplification of our expression for ψ is possible. Assume that we have p pairs of orbitals in Φ and that they are arranged in Φ so that columns $1, 2, \ldots, p$ are identical with columns $N/2 + S + 1, N/2 + S + 2, \ldots, N/2 + S + p$. We now partition $\Phi(q)$ even farther and write

TABLE I

VALUES OF q_k AND C_k DEFINED IN Eqs. (46) AND (47) FOR THE LINEAR COMBINATIONS THAT GIVE TABLEAU FUNCTIONS

N	S		$k = 1$	$k = 2$	$k = 3$
2	0	q_k	-1		
		C_k	-1		
	1	q_k	1		
		C_k	1		
3	1/2	q_k	-2		
		C_k	$-1/2$		
	3/2	q_k	1		
		C_k	1		
4	0	q_k	$-(2 - \sqrt{3})$	$-(2 + \sqrt{3})$	
		C_k	$(2 + \sqrt{3})/4$	$(2 - \sqrt{3})/4$	
	1	q_k	-3		
		C_k	$-1/3$		
	2	q_k	1		
		C_k	1		
5	1/2	q_k	$-(3 - \sqrt{6})$	$-(3 + \sqrt{6})$	
		C_k	$(3 + \sqrt{6})/18$	$(3 - \sqrt{6})/18$	
	3/2	q_k	-4		
		C_k	$-1/4$		
6	0	q_k	$-(2 - \sqrt{3})$	$-(2 + \sqrt{3})$	
		C_k	$-(9 + 5\sqrt{3})/18$	$-(9 - 5\sqrt{3})/18$	
	1	q_k	$-(4 - \sqrt{10})$	$-(4 + \sqrt{10})$	
		C_k	$(4 + \sqrt{10})/48$	$(4 - \sqrt{10})/48$	
	2	q_k	-5		
		C_k	$-1/5$		
7	1/2	q_k	$-(3 - \sqrt{6})$	$-(3 + \sqrt{6})$	
		C_k	$-(18 + 7\sqrt{6})/144$	$-(18 - 7\sqrt{6})/144$	
	3/2	q_k	$-(5 - \sqrt{15})$	$-(5 + \sqrt{15})$	
		C_k	$(5 + \sqrt{15})/100$	$(5 - \sqrt{15})/100$	
8	0	q_k	$-0.12701\ 66537\ 92583$	$-1.00000\ 00000\ 00000$	$-7.87298\ 33462\ 07418$
		C_k	$0.86088\ 70384\ 67491$	$0.13888\ 88888\ 88889$	$0.00022\ 40726\ 43620$
	1	q_k	$-(4 - \sqrt{10})$	$-(4 + \sqrt{10})$	
		C_k	$-(10 + 3\sqrt{10})/200$	$-(10 - 3\sqrt{10})/200$	
	2	q_k	$-(6 - \sqrt{21})$	$-(6 + \sqrt{21})$	
		C_k	$(6 + \sqrt{21})/180$	$(6 - \sqrt{21})/180$	
9	1/2	q_k	$-0.26958\ 41903\ 10437$	$-1.44220\ 00577\ 89383$	$-10.28821\ 57519\ 00192$
		C_k	$0.16126\ 06798\ 68883$	$0.03866\ 50697\ 02502$	$0.00007\ 42504\ 28615$
	3/2	q_k	$-(5 - \sqrt{15})$	$-(5 + \sqrt{15})$	
		C_k	$-(45 + 11\sqrt{15})/1800$	$-(45 - 11\sqrt{15})/1800$	
10	0	q_k	$-0.12701\ 66537\ 92583$	$-1.00000\ 00000\ 00000$	$-7.87298\ 33462\ 07418$
		C_k	$-0.91663\ 63626\ 34544$	$-0.08333\ 33333\ 33333$	$-0.00003\ 03040\ 32122$
	1	q_k	$-0.41843\ 52700\ 93916$	$-1.88181\ 31036\ 92589$	$-12.69975\ 16262\ 13472$
		C_k	$0.05179\ 25118\ 40754$	$0.01484\ 29282\ 79300$	$0.00003\ 12265\ 46595$
	2	q_k	$-(6 - \sqrt{21})$	$-(6 + \sqrt{21})$	
		C_k	$-(63 + 13\sqrt{21})/4410$	$-(63 - 13\sqrt{21})/4410$	

$$\Phi(q) = \begin{bmatrix} \Phi_{11} & \Phi_{12} & \Phi_{13} & \Phi_{14} \\ \Phi_{21} & \Phi_{22} & q\Phi_{23} & q\Phi_{24} \end{bmatrix} \tag{48}$$

where Φ_{11} is $(N/2 + S) \times p$, Φ_{12} is $(N/2 + S) \times (N/2 + S - p)$, and Φ_{23} is $(N/2 - S) \times p$. The remainder of the blocks have sizes to match the full $N \times N$ size of (q). Because of our assumption concerning paired orbitals, we have $\Phi_{11} = \Phi_{13}$ and $\Phi_{21} = \Phi_{23}$. When we form the determinant of $\Phi(q)$, the equalities allow subtractions of selected columns to get

$$|\Phi(q)| = \begin{bmatrix} \Phi_{11} & \Phi_{12} & 0 & \Phi_{14} \\ 0 & \Phi_{22} & \Phi_{23} & q\Phi_{14} \end{bmatrix} (q - 1)^p, \qquad q \neq 1 \tag{49}$$

the $(q - 1)^p$ may be combined with the C_k coefficients where now we get

$$\psi = \frac{f_S^N}{N!} \frac{(N/2 + S + 1)}{(N/2 + S - p + 1)} \sum_{k=1}^{k_{\max}} C_k(N - 2p, S) \times \begin{bmatrix} \Phi_{11} & \Phi_{12} & 0 & \Phi_{14} \\ 0 & \Phi_{22} & \Phi_{23} & q_k\Phi_{24} \end{bmatrix} \tag{50}$$

where $k_{\max} = k_{\max}(N - 2p, S)$ and $q_k = q_k(N - 2p, S)$. Thus, with the modified determinant the sum giving Ψ is shortened as if the electrons in doubly occupied orbitals were not there; Ψ is still an N-electron function, of course.

Equation (50) gives Ψ in the form we need, and in the following discussions we assume the reductions possible when $p > 0$ are always made. It will be observed that the form of Eq. (50) passes smoothly into that of Eq. (42) when $p = 0$.

The pattern of zeros and functions in the determinant in Eq. (50) is clearly very critical. We wish to make our notation more explicit and introduce the notion of a *masking* matrix w. This matrix has elements 1, 0, or q, in the pattern.

$$\begin{array}{c} \quad p \quad\quad N/2 + S - p \quad\quad p \quad\quad N/2 - S - p \\ \mathbf{w}(q) = \left[\begin{array}{c:c:c:c} \mathbf{w}_{11} & \mathbf{w}_{12} & 0 & \mathbf{w}_{14} \\ \hdashline 0 & \mathbf{w}_{22} & \mathbf{w}_{23} & \mathbf{w}_{24} \end{array}\right] \begin{array}{l} N/2 + S \\ N/2 - S \end{array} \end{array} \tag{51}$$

where the $\mathbf{w}_{ij}$ are rectangular matrices as shown by the numbers of rows and columns in the partitioned form. Each of the elements of $\mathbf{w}_{24}$ is the variable q, and each of the other $\mathbf{w}_{ij}$ is the constant matrix consisting of all 1's. Writing a single element of the entire $\mathbf{w}(q)$ matrix as w_{ij}, we may give a slightly different form for our functional determinant,

$$D_\Phi(q) = |w_{ij}u_j(i)| = \begin{bmatrix} \Phi_{11} & \Phi_{12} & 0 & \Phi_{11} \\ 0 & \Phi_{22} & \Phi_{23} & q\Phi_{24} \end{bmatrix} \tag{52}$$

and the simplifications possible because of orbital pairing are explicitly present in the masking matrix w. The determinant defined by Eq. (52) has a central role in our considerations. We name it a *masked-orbital determinant*. Rewriting Eq. (50) now gives

$$\psi = \frac{f_S^N}{N!} \frac{(N/2 + S + 1)}{(N/2 + S - p + 1)} \sum_{k=1}^{k_{\max}} C_k(n - 2p, S) D_\Phi(q) \tag{53}$$

and we are able to represent Ψ by a linear combination of masked orbital determinants.

Although there are few occasions when one wants the value for a particular set of coordinates of an N-electron function like Ψ, a little reflection shows that the labor of this evaluation is a good measure of the ease of using Ψ in general. It is well known that a determinant may be evaluated in "polynomial time"; specifically, the labor is proportional to N^3. Since for small p and S, the number of terms in $\Psi \sim N/4$, our algorithm for Ψ can be carried out in polynomial time, specifically $N^4/4$. This situation is to be contrasted with the standard procedure for writing HLSP valence-bond functions as a sum of $2^{N/2-S-p}$ Slater determinants, which thus have "exponential-time" algorithms, $\sim N^3 2^{N/2}$. For sufficiently large N, using tableau functions will certainly be faster.

C. Matrix Elements of Two Tableau Functions

The results of the last section are easily applied to the problem of calculating matrix elements between two tableau functions. We now assume that we have two-orbital product functions and their corresponding tableau function

$$\begin{aligned} \Phi_n &= u_1(1) \cdots u_N(N), & \Phi_v &= v_1(1) \cdots v_N(N) \\ \Psi_u &= \theta\hat{N}\hat{P}\hat{N}\Phi_u, & \Psi_v &= \theta\hat{N}\hat{P}\hat{N}\Phi_v \end{aligned} \tag{54}$$

where the set $\{u\}$ may or may not be different from the set $\{v\}$. We shall also assume that the number of paired orbitals in v is no less than the number in u. We interchange the roles of u and v if necessary to accomplish this. The matrix elements to be evaluated are

$$\begin{aligned} S_{uv} &= \langle \Psi_u | \Psi_v \rangle = \langle \Phi_u | \Psi_v \rangle \\ F_{uv} &= \langle \Psi_u | F | \Psi_u \rangle = \langle \Phi_u | F | \Psi_v \rangle \\ G_{uv} &= \langle \Psi_u | G | \Psi_u \rangle = \langle \Phi_u | G | \psi_v \rangle \end{aligned} \tag{55}$$

where the rightmost equality is possible because $\theta\hat{N}\hat{P}\hat{N}$ is idempotent, Hermitian, and commutes with the other operators. We also have

$$F = \sum_i f_i, \qquad G = \sum_{i<j} g_{ij}, \qquad H = F + G \tag{56}$$

as the standard one- and two-particle operator expressions used when dealing with the Hamiltonian.

The values of all three integrals (55) depend upon the matrix $\mathbf{Q}_{uv}$ defined by

$$(\mathbf{Q}_{uv})_{ij} = \langle u_i | v_j \rangle \tag{57}$$

which will occupy a central position in our considerations. This matrix contains overlaps between the two orbital sets and has equalities reflecting the pairing in u and v.

With these abbreviations we obtain, using Eqs. (52) and (53),

$$S_{uv} = \frac{f_S^N}{N!} \frac{(N/2 + S + 1)}{(N/2 + S - p + 1)} \sum_{k=1}^{k_{\max}} C_k(N - 2p, S) D_\Phi(q_k) \tag{58}$$

where $k_{\max}$, q_k, and p refer to the statistics of the v set of orbitals. This is the result of the form we use with $\theta\hat{N}\hat{P}\hat{N}$ applied to the ket function in the integral. It must be emphasized that the masking matrix $\mathbf{w}(q)$ is determined by the v set also. We have, therefore,

$$D_{\mathbf{Q}}(q) = |w_{ij}(q)\langle u_i | v_j \rangle| \tag{59}$$

to get the appropriate determinantal form of the $\mathbf{Q}$ matrix.

We see from Eq. (58) that S_{uv} is zero if the rank of the "masked" matrix in Eq. (57) [Eq. (59)] is $<N$ for all values of q_k. This will certainly be the case if one of the v orbitals is orthogonal to all of the u's or one of the u orbitals is orthogonal to all of the v's, but this is not a necessary condition.

Löwdin (1955) shows how matrix elements of the one- and two-particle operators depend on determinantal cofactors for Slater determinants. This treatment can be carried over to our masked-orbital determinant functions and we obtain

$$\langle \psi_u | F | \Phi_v \rangle = \sum_{ij} \langle u_i | f | v_j \rangle A_{ij} \tag{60}$$

$$\langle \psi_u | G | \psi_v \rangle = \sum_{\substack{i<k \\ j<l}} \{ \langle u_i u_k | g | v_j v_l \rangle B_{ik,jl} - \langle u_i u_k | g | v_l v_j \rangle C_{ik,jl} \} \tag{61}$$

where

$$A_{ij} = K \sum_m C_m(N - 2p, S) w_{ij}(q_m) D_{\mathbf{Q}}^{ij}(q_m) \tag{62}$$

$$B_{ik,jl} = K \sum_m C_m(N - 2p, S) w_{ij}(q_m) w_{kl}(q_m) D_Q^{ik,jl}(q_m) \tag{63}$$

$$C_{ik,jl} = K \sum_m C_m(N - 2p, S) w_{il}(q_m) w_{kj}(q_m) D_Q^{ik,jl}(q_m) \tag{64}$$

$$K = \frac{f_S^N}{N!} \frac{(N/2 + S + 1)}{(N/2 + S - p + 1)}$$

The quantities D_Q^{ij} and $D_Q^{ik,jl}$ are, respectively, first- and second-order cofactors (signed minors) of the D_Q determinant. We discuss algorithms for the calculation of these cofactors in Section II,D.

Equations (58)–(64) contain all of the results we need to solve the algebraic problem of converting overlap, one-electron, and two-electron integrals for nonorthogonal orbitals into matrix elements between tableau functions, and hence to generate matrices of the spin-free Hamiltonian having a given spin state and satisfying the Pauli principle.

D. Calculation of Cofactors

The expressions for matrix elements given in Section II,C are relatively useless unless efficient methods of evaluating cofactors are available. As Löwdin pointed out in his original treatment, the cofactors are easily obtained from the inverse for nonsingular matrices. However, we must frequently deal efficiently with singular matrices also. King *et al.* (1967) discussed the problem of obtaining cofactors of singular matrices by a method, one step of which involves matrix diagonalization. Voter and Goddard (1981) have criticized cofactor methods as tedious and recommended the diagonalization procedure followed by a transformation of the one- and two-electron integrals to a new basis to utilize the biorthogonalization of the overlaps. Prosser and Hagstrom (1968) have given a procedure depending upon a purely algebraic biorthogonalization of the matrix. The process of evaluating cofactors, although long and laborious if done directly, is nevertheless of a finite algebraic nature and does not involve any limiting processes. We therefore prefer a finite numerical scheme if possible such as that of Prosser and Hagstrom. We successfully use still another procedure, which is a finite algebraic algorithm, but which requires a simple limiting process in its derivation. This process does not require a four-index transformation of integrals as does the Voter–Goddard proposal.

The concept of the rank of a matrix plays a key role in the cofactor problem. If an $N \times N$ matrix is nonsingular, its rank is said to be N. This means the determinant of the full matrix is nonzero. In case the matrix is singular, then a smaller determinant may be nonzero. If the *largest* nonzero determinant which can be assembled by striking out rows and col-

umns of the matrix is $r \times r$, the number r is defined to be the rank of the matrix.

The first-order cofactors in Eq. (62) are, of course, $(N-1) \times (N-1)$ determinants which are necessarily zero if the rank of the masked $\mathbf{Q}(q)$ matrix is less than $(N-1)$ (for all the q's). The determinant, $D_{\mathbf{Q}}(q)$, is also necessarily zero under these circumstances. The second-order cofactors in Eqs. (63) and (64) are $(N-2) \times (N-2)$ determinants and are zero if the rank of $\mathbf{Q} < N-2$. We, therefore, have to consider only three cases, when the rank of $\mathbf{Q}$ is N, $(N-1)$, or $(N-2)$.

Case a. Rank of $\mathbf{Q}$ *is* N. This is the simplest case since the cofactors can be obtained easily from the inverse. We let $\mathbf{Q}$ be a general, nonsingular square matrix, $D_{\mathbf{Q}}$ is its determinant, and $\mathbf{Q}^{-1}$ is its inverse. The general expressions for the first- and second-order cofactors are

$$D_{\mathbf{Q}}^{ij} = D_{\mathbf{Q}}(\mathbf{Q}^{-1})_{ji} \tag{65}$$

$$D_{\mathbf{Q}}^{ik,jl} = D_{\mathbf{Q}}[(\mathbf{Q}^{-1})_{ji}(\mathbf{Q}^{-1})_{lk} - (\mathbf{Q}^{-1})_{li}(\mathbf{Q}^{-1})_{jk}] \tag{66}$$

and these give all the quantities we need for evaluating Eqs. (58) and (62)–(64) for this case.

We use a somewhat specialized method to obtain $\mathbf{Q}^{-1}$ for these formulas. It is designed to give $D_{\mathbf{Q}}$, $\mathbf{Q}^{-1}$ or test its rank so that this procedure can itself decide which of the cases we have.

A standard procedure for evaluation of $\mathbf{Q}^{-1}$ is Gaussian elimination. Among the various options which may be used in the algorithm is *full pivoting*. This consists of searching for the element of largest magnitude through all remaining unreduced rows and columns of the matrix, and then rearranging so that it is in the target position. In this way it is possible by Gaussian elimination to find a decomposition of $\mathbf{Q}$,

$$\bar{\mathbf{Q}} = \mathbf{RQP} \tag{67}$$

where $\mathbf{P}$ is a permutation matrix (one and only one "one" in each row or column), $\mathbf{R}$ is nonsingular, and $\bar{\mathbf{Q}}$ has a partitioned form

$$\bar{\mathbf{Q}} = \begin{bmatrix} \mathbf{I}_r & \mathbf{b} \\ \mathbf{0} & \mathbf{0}_{N-r} \end{bmatrix} \tag{68}$$

the structure of which depends upon the rank r of $\mathbf{Q}$; I_r is the $r \times r$ identity and $\mathbf{0}_{N-r}$ the $(N-r) \times (N-r)$ null matrix; $\mathbf{b}$ is, in general, not zero. If the rank of $\mathbf{Q}$ is N then $\bar{\mathbf{Q}} = \mathbf{I}$ and

$$\mathbf{Q}^{-1} = \mathbf{PR} \tag{69}$$

which is, of course, a very simple product since $\mathbf{P}$ is simply a permutation of the rows of $\mathbf{R}$.

When $r < N$ we define the matrix $\mathbf{Q}(z)$, a function of the variable z, such that

$$\bar{\mathbf{Q}}(z) = \mathbf{R}\mathbf{Q}(z)\mathbf{P}, \qquad \mathbf{Q}(0) = \mathbf{Q} \tag{70}$$

where

$$\bar{\mathbf{Q}}(z) = \begin{bmatrix} \mathbf{I}_r & \mathbf{b} \\ 0 & z\mathbf{I}_{N-r} \end{bmatrix} \tag{71}$$

We never actually need $\mathbf{Q}(z)$ explicitly and use only the indirect definition of Eq. (71). Clearly, $\mathbf{Q}(z)$ is nonsingular except at $z = 0$, and we have

$$\mathbf{Q}(z)^{-1} = \mathbf{P}\begin{bmatrix} \mathbf{I}_r & -z^{-1}\mathbf{b} \\ 0 & z^{-1}\mathbf{I}_{N-r} \end{bmatrix}\mathbf{R} \tag{72}$$

We may partition $\mathbf{R}$ to match the structure of $\bar{\mathbf{Q}}(z)^{-1}$, and we obtain

$$\begin{aligned} \mathbf{Q}(z)^{-1} &= \mathbf{P}\bar{\mathbf{Q}}(z)^{-1}\begin{bmatrix} \mathbf{R}_{11} & \mathbf{R}_{12} \\ \mathbf{R}_{21} & \mathbf{R}_{22} \end{bmatrix} \\ &= \mathbf{P}\begin{bmatrix} \mathbf{R}_{11} - z^{-1}\mathbf{b}\mathbf{R}_{21} & \mathbf{R}_{12} - z^{-1}\mathbf{b}\mathbf{R}_{22} \\ z^{-1}\mathbf{R}_{21} & z^{-1}\mathbf{R}_{22} \end{bmatrix} = \mathbf{u} + z^{-1}\mathbf{v} \end{aligned} \tag{73}$$

$$\mathbf{u} = \mathbf{P}\begin{bmatrix} \mathbf{R}_{11} & \mathbf{R}_{12} \\ 0 & 0 \end{bmatrix} \tag{74}$$

$$\mathbf{v} = \mathbf{P}\begin{bmatrix} -\mathbf{b}\mathbf{R}_{21} & -\mathbf{b}\mathbf{R}_{22} \\ \mathbf{R}_{21} & \mathbf{R}_{22} \end{bmatrix} \tag{75}$$

During the course of determining $\mathbf{P}$, $\bar{\mathbf{Q}}(z)$, and $\mathbf{R}$, the algorithm may be easily arranged to give the determinant $|\mathbf{Q}(z)|$, also. This is closely related to the determinants of $\mathbf{P}$ and $\mathbf{R}$, and we have

$$|\mathbf{Q}(z)| = z^{N-r}/|\mathbf{P}\mathbf{R}| \tag{76}$$

where we see the $|Q(0)|$ is zero when $r < N$. Using Eqs. (74)–(76), we may now give simple expressions for the cofactors of $\mathbf{Q}$.

Case b. Rank of $\mathbf{Q}$ *is* $N - 1$. As was emphasized for Case a, the cofactors for a nonsingular matrix are easily determined from the inverse. This situation certainly pertains for $\mathbf{Q}(z)$, $z \neq 0$, and we have, using Eqs. (73) and (76),

$$D^{ij}_{\mathbf{Q}(z)} = [z(\mathbf{u})_{ji} + (\mathbf{v})_{ji}]/|\mathbf{P}\mathbf{R}| \tag{77}$$

The cofactors we want are obtained for $z = 0$, and we obtain

$$D_{\mathbf{Q}}^{ij} = (\mathbf{v})_{\mu}/|\mathbf{PR}| \tag{78}$$

A similar treatment gives us the second-order cofactors for this case. First, writing the expression for $\mathbf{Q}(z)$, $z \neq 0$, we have

$$\begin{aligned} D_{\mathbf{Q}(z)}^{ik,jl} = \{ & z\,[(\mathbf{u})_{\mu}(\mathbf{u})_{\nu k} - (\mathbf{u})_{\nu i}(\mathbf{u})_{\mu k}] \\ & + [(\mathbf{u})_{\mu}(\mathbf{v})_{\nu k} + (\mathbf{v})_{\mu}(\mathbf{u})_{\nu k} - (\mathbf{u})_{\nu i}(\mathbf{v})_{\mu k} - (\mathbf{v})_{\nu i}(\mathbf{u})_{\mu k}] \\ & + z^{-1}[(\mathbf{v})_{\mu i}(\mathbf{v})_{\nu k} - (\mathbf{v})_{\nu i}(\mathbf{v})_{\mu k}]\}/|\mathbf{PR}| \end{aligned} \tag{79}$$

The appearance of the z^{-1} term in Eq. (79) need cause no alarm since it is actually identically zero, because when $r = N - 1$, the rank of $\mathbf{v}$ is 0 or 1. We may thus again obtain our result by letting $z = 0$, and we have

$$D_{\mathbf{Q}}^{ik,jl} = [(\mathbf{u})_{\mu}(\mathbf{v})_{\nu k} + (\mathbf{v})_{\mu}(\mathbf{u})_{\nu k} - (\mathbf{u})_{\nu i}(\mathbf{v})_{\mu k} - (\mathbf{v})_{\nu i}(\mathbf{u})_{\mu k}]/|\mathbf{PR}| \tag{80}$$

These expressions provide the cofactors we need for $r = N - 1$. Of course, $D_{\mathbf{Q}}$ itself is zero for this case.

Case c. Rank of $\mathbf{Q}$ *is* $N - 2$. When $r = N - 2$, $D_{\mathbf{Q}}$ and $D_{\mathbf{Q}}^{ij}$ are all zero and we need only the second-order cofactors. An analysis parallel to that we carried out for $r = N - 1$ may be done and the final result is

$$D_{\mathbf{Q}}^{ik,jl} = [(\mathbf{v})_{\mu}(\mathbf{v})_{\nu k} - (\mathbf{v})_{\nu i}(\mathbf{v})_{\mu k}]/|\mathbf{PR}| \tag{81}$$

The technique we have described here may be used to obtain cofactors of other orders, but since these are not needed for evaluation of our matrix elements, we shall not discuss such extensions here. The method described here is based on a considerably improved upon method originally given by Gallup and Norbeck (1973e).

E. Summary

In Section II, we have described the construction of tableau functions, which include the effects of the Pauli exclusion principle and specific total spin values, and we have given mathematical apparatus for evaluating matrix elements between two tableau functions for one- and two-particle operators and the Hamiltonian. Computer programs which implement these methods are relatively simple and do not require complicated logic decisions.

It is fairly simple to analyze these algorithms to see that each matrix element may be obtained in polynomial time. The matrices $\mathbf{P}$ and $\mathbf{R}$ or $\mathbf{u}$ and $\mathbf{v}$ are obtained in N^3 time, and, therefore, the assembly of the second-order cofactors of which there are $\sim N^4/4$ is overriding. Since the number of masked-orbital determinants in a tableau function $\sim N/2$, we see that each matrix element may be calculated in $(1/8)N^5$ time. This is actually a very conservative estimate since many opportunities to save

time are available in these algorithms when a zero is encountered. We discuss methods for further reducing this time in Section III.

III. Arrangement of Bases

A. Sets of Linearly Independent Tableau Functions

A practical calculation of molecular structure and energies requires a configuration interaction (CI) basis which will include tableau functions generated from a number of different orbital sets. In the normal situation the chemical problem under consideration will determine a set of "atomic" orbitals we must consider,

$$\{\mathbf{x}\} = \{x_1, x_2, \ldots, x_M\} \tag{82}$$

The configurations are obtained by selecting N orbitals from this set, no orbital chosen more than twice. We specify each configuration by an M-component vector

$$\overline{\alpha} = [\alpha_1, \alpha_2, \ldots, \alpha_M] \tag{83}$$

where each α_i is one of the three numbers 0, 1, or 2, and gives the number of times x_i is chosen in the configuration. Since we have N electrons, clearly,

$$\sum_i \alpha_i = N \tag{84}$$

The actual number of configurations which can be generated from the set $\{\mathbf{x}\}$ for a given N is a number of some importance in the theory. We denote this by $C(M, N)$. It is rather surprising, but it appears no very simple formula for $C(M, N)$ is available. A simple combinatorial argument gives a *generating polynomial* for $C(M, N)$,

$$(1 + t + t^2)^M = \sum_{N=0}^{2M} C(M, N)t^N \tag{85}$$

where the coefficient of t^N gives the number. An infinite series generating function is also available for the number of configurations,

$$\begin{aligned}\sum_{M=[N/2]}^{\infty} C(M, N)z^M = {} & \frac{z^{N/2}}{2^{(N+1)}(1 - z)^{N+1}(4 - 3z)^{1/2}} \\ & \times \{[(4 - 3z)^{1/2} + z^{N+1} \\ & + (-1)^N(4 - 3z)^{1/2} - z^{N+1}]\}\end{aligned} \tag{86}$$

where the series converges for $|z| < 1$, and the lowest value of M is $N/2$ or $(N + 1)/2$, whichever is an integer. For small values of M and N, $C(M, N)$ is most easily obtained from the recursion relation

$$C(M + 1, N) = C(M, N) + C(M, N - 1) + C(M, N - 2) \quad (87)$$

The set of atomic orbitals $\{\mathbf{x}\}$ must be linearly independent to serve our purposes, and we assume this is always true. Under these circumstances, any two product functions

$$\phi_u = u_1(1), \ldots, u_N(N) \quad (88)$$

$$\phi_v = v_1(1), \ldots, v_N(N) \quad (89)$$

are linearly independent if the u's are a selection from $\{\mathbf{x}\}$ specified by $\overline{\alpha}$ and the v's are specified by $\overline{\alpha}'$, with $\overline{\alpha} \neq \overline{\alpha}'$. Again, if $\overline{\alpha} \neq \overline{\alpha}'$, the corresponding tableau functions

$$\psi_u = \theta\hat{N}\hat{P}\hat{N}\phi_u \quad (90)$$

$$\psi_v = \theta\hat{N}\hat{P}\hat{N}\phi_v \quad (91)$$

are linearly independent. Therefore, in a full CI based upon the set $\{\mathbf{x}\}$ we must include functions corresponding to all of the possible $\overline{\alpha}$'s.

We now consider the number of linearly independent tableau functions which arise from a single $\overline{\alpha}$. We let p be the number of 2's among the components of $\overline{\alpha}$, i.e., p is the number of selected orbitals which are paired. There are, therefore, $N!/2^p$ different ways that the N electrons can be assigned to the orbitals in a product function. All $N!/2^p$ of these product functions are linearly independent, but in this case, *not* all of the corresponding tableau functions for a given spin, S, are linearly independent. There is no unique linearly independent set, but any such set spans the subspace, and *one way* of obtaining one uses the concept of standard tableau invented by Young (Rutherford, 1948).

In order to apply this idea we must order the orbital symbols selected by $\overline{\alpha}$. Since tableau functions belonging to different $\overline{\alpha}$'s are automatically independent, there is no necessary connection between the orderings for these, and each $\overline{\alpha}$ is considered independently.

For definiteness, we assume that $u_1, u_2, \ldots, u_p$ are the *paired* orbitals from $\overline{\alpha}$ and $u_{p+1}, u_{p+2}, \ldots, u_{N-p}$ are the singly occupied ones. (We emphasize that these orbitals may have different subscripts in the ordering for different α's.) We may place the numbers $1, 1, 2, 2, \ldots, p, p, p + 1, p + 2, \ldots, N - p$ into a Young tableau shape [defined in Section IIB] $N!/2^p$ ways. We use the two-column tableaux corresponding to the $\theta\hat{N}\hat{P}\hat{N}$ and S under consideration.

Among all the tableaux the standard tableaux are a subset which satisfy the two conditions: (1) The numbers are nondecreasing from left to right in the rows, and (2) The numbers are definitely increasing downward in each column. For the case $N = 9$, $S = 1/2$, $p = 2$, we have

1	1	1	1	1	1	1	1	1	1
2	2	2	2	2	2	2	2	2	2
3	4	3	4	3	5	3	5	3	6
5	6	5	7	4	6	4	7	5	7
7		6		7		6		5	

and no more satisfying the two conditions. These five standard tableaux tell us that there are five linearly independent tableau functions in this case, and they are

$$\psi_1 = \theta\hat{N}\hat{P}\hat{N}(u_1u_2u_3u_5u_7u_1u_2u_4u_6), \qquad \psi_4 = \theta\hat{N}\hat{P}\hat{N}(u_1u_2u_3u_4u_6u_1u_2u_5u_7)$$

$$\psi_2 = \theta\hat{N}\hat{P}\hat{N}(u_1u_2u_3u_5u_6u_1u_2u_4u_7), \qquad \psi_5 = \theta\hat{N}\hat{P}\hat{N}(u_1u_2u_3u_4u_5u_1u_2u_6u_7)$$

$$\psi_3 = \theta\hat{N}\hat{P}\hat{N}(u_1u_2u_3u_4u_7u_1u_2u_5u_6) \tag{92}$$

where the electrons are numbered in order, i.e., down the first column and then down the second. There are $N!/2^p = 90{,}720$ different ways of associating two paired and five unpaired orbitals with the numbers $1, 2, \ldots, 9$, and hence 90,720 different product functions. Young's result tells that when $\theta\hat{N}\hat{P}\hat{N}$ is applied to these product functions, only five are linearly independent (in the doublet spin state) and the standard tableaux give *a way* of choosing them (Littlewood, 1950).

It is interesting that the total number $D(M, N, S)$ of linearly independent tableau functions which can be constructed from all $\overline{\alpha}$'s for M orbitals, N electrons, and spin S is given by the fairly simple Weyl dimension formula (Weyl, 1956).

$$D(M, N, S) = \frac{2S+1}{M+1}\binom{M+1}{N/2+S+1}\binom{M+1}{N/2-S} \tag{93}$$

where we have used the standard symbol for binomial coefficients. This, then, is the size of a full CI based upon these orbitals, when no account is taken of possible spatial symmetry.

B. "Core–Valence" Separation

Many chemical problems can be well described by CI wave functions in which one particular subset of the orbitals is doubly occupied in all configurations. Typical examples include inner shells of atoms and orbitals describing σ electrons in π-only calculations of planar conjugated organic systems. For convenience we designate the orbitals doubly occupied in all configurations as the *core orbitals* and the remainder the *valence orbitals*. We use this terminology regardless of the actual physical or chemical situation, and in some cases we may conveniently have valence-like behavior represented by the core orbitals or vice versa.

The presence of a set of core orbitals of this type allows a frequently significant decrease in the labor of doing a CI calculation. This process was first described by McWeeny (1954; see also McWeeny and Ohno, 1960) in connection with an orthogonalized valence-bond approach. The separation is actually of great generality and we give a derivation here using tableau functions.

For the purposes of the discussion in this section we change our orbital notation slightly and use $c_1, c_2, \ldots, c_p$ for the core-orbitals and $v_1, v_2, \ldots, v_{N-2p}$ for the valence orbitals. There may be more paired orbitals in a configuration than those represented by the core, but there is no loss of generality if we ignore the simplifications allowed by these. Under these restrictions all of the masked orbital determinants have the form

$$D_\Phi(q) = \begin{bmatrix} \Phi_{11} & \Phi_{12} & 0 & \Phi_{14} \\ 0 & \Phi_{22} & \Phi_{23} & q\Phi_{24} \end{bmatrix} \tag{94}$$

where Φ_{11} and Φ_{23} have p columns of the core orbitals. Because of the properties of determinants, we may subtract multiples of one column from any other, and this allows a transformation of all of the valence orbitals from their original form—without changing the value of $D_\Phi(q)$.

The transformation we use is generated by the operator which projects onto the *orthogonal complement* of the subspace spanned by $c_1 \cdots c_p$. In other terms we wish to orthogonalize all of the v's to the c's. Letting

$$\begin{aligned} \mathbf{Q}^c &= \begin{bmatrix} \langle c_1|c_1\rangle & \langle c_1|c_2\rangle & \cdots & \langle c_1|c_p\rangle \\ \langle c_p|c_1\rangle & \cdots & \cdots & \langle c_p|c_p\rangle \end{bmatrix} \\ \hat{P}_{cc} &= \sum_{i,j} |c_i\rangle(\mathbf{Q}^{c-1})_{ij}\langle c_j| \end{aligned} \tag{95}$$

the orthogonal complement operator is $1 - P_{cc}$ and the transformed orbitals are

$$|v_i'\rangle = (1 - \hat{P}_{cc})|v_i\rangle = |v_i\rangle - \sum_{jk} |c_j\rangle(\mathbf{Q}^{c-1})_{jk}\langle c_k|v_i\rangle \tag{96}$$

The core orbitals must be linearly independent, so that $\mathbf{Q}^{c-1}$ always exists and we may always accomplish this transformation. We recall that we have always assumed that our orbitals are normalized. Therefore, these transformed orbitals v_i' are not normalized. In fact, it is important that we do not renormalize the valence orbitals after their orthogonalization. To do so would change the value of $D_\Phi(q)$, an outcome we wish to avoid. We may now write

$$D_\Phi(q) = \begin{bmatrix} \Phi_{11} & \Phi_{12}' & 0 & \Phi_{14}' \\ 0 & \Phi_{22}' & \Phi_{23} & q\Phi_{24}' \end{bmatrix} \tag{97}$$

where the primes indicate we use valence orbitals orthogonalized to the core.

When we consider the masked **Q** matrix, we now find it has the form

$$[w_{ij}(\mathbf{Q})_{ij}] = \begin{bmatrix} \mathbf{Q}^c & 0 & 0 & 0 \\ 0 & \mathbf{Q}^v_{11} & 0 & \mathbf{Q}^v_{12} \\ 0 & 0 & \mathbf{Q}^c & 0 \\ 0 & \mathbf{Q}^v_{21} & 0 & q\,\mathbf{Q}^v_{22} \end{bmatrix} \tag{98}$$

$$D_{\mathbf{Q}}(q) = |\mathbf{Q}^c|^2 \begin{bmatrix} \mathbf{Q}^v_{11} & \mathbf{Q}^v_{12} \\ \mathbf{Q}^v_{21} & q\mathbf{Q}^v_{22} \end{bmatrix} \tag{99}$$

Thus, every $D_{\mathbf{Q}}$ term factors in the same way with $|\mathbf{Q}^c|^2$ common to all matrix elements between any two functions in the CI.

When we consider the matrix elements we obtain

$$S_{VW} = |\mathbf{Q}^c|^2 K \sum_k C_k(N - 2p, S) D_{\mathbf{Q}_v}(q_k), \quad K = \frac{N/2 + S + 1}{N/2 + S - 2p + 1} \tag{100}$$

where we have to deal only with the determinant $D_{\mathbf{Q}_v}(q_k)$ in the sum. We have written the overlap matrix element S_{VW} and emphasize that only the valence orbitals may differ between the bra and ket functions.

The expression for the one-particle operator assumes a simplified form also:

$$F_{VW} = S_{VW} F^c + \sum_{ij} \langle v_i' | f | w_j' \rangle A^v_{ij} \tag{101}$$

where v_i' is one of the V set of orthogonalized valence orbitals and w_j' is one of the W set. In Eq. (101) we also have

$$F^c = 2 \sum_{ij} \langle c_i | f | c_j \rangle (\mathbf{Q}^{c-1})_{ji} \tag{102}$$

$$A^v_{ij} = |\mathbf{Q}^c|^2 K \sum_k C_k(N - 2p, S) w_{ij}(q_k) D^{ij}_{\mathbf{Q}_v}(q_k) \tag{103}$$

where we see that we need to determine the cofactors of only the $\mathbf{Q}^v$ part of the determinant.

The two-particle operator splits into core–core, core–valence, and valence–valence terms, and we have

$$G_{VW} = S_{VW} G^{cc} + \sum_{ij} \langle v_i' | g^c | w_j' \rangle A^v_{ij} + \sum_{\substack{i<k \\ j>l}} [\langle v_i' v_k' | g | w_j' w_l' \rangle B^v_{ik,jl} - \langle v_i' v_k' | g | w_l' w_j' \rangle C^v_{ik,jl}] \tag{104}$$

where

$$G^{cc} = 2 \sum_{\substack{i<k \\ j>l}} [2\langle c_i c_k|g|c_j c_l\rangle - \langle c_i c_k|g|c_l c_j\rangle](\mathbf{Q}^{c-1})_{ij}(\mathbf{Q}^{c-1})_{kl}$$

$$\langle v_i'|g^c|w_j'\rangle = 2 \sum_{kl} [\langle c_k v_i'|g|c_l w_j'\rangle - \langle c_k v_i'|g|w_j' c_l\rangle](\mathbf{Q}^{c-1})_{kl}$$

and $B^v_{ik,jl}$ and $C^v_{ik,jl}$ are given by expressions such as Eqs. (63) and (64) with the factor $|\mathbf{Q}^c|^2$ and only the $D_{\mathbf{Q}^v}(q)^{ik,jl}$ cofactors needed.

A careful examination of these results shows that we may make a transformation of the valence orbitals, modify the one-particle integrals and thereafter treat the core orbitals and the 2p electrons in them *as if they were not present at all* in determining matrix elements. The transformation of the orbitals is given by Eq. (96), the transformed valence–valence overlaps are

$$(\mathbf{Q}^v)_{ij} = \langle v_i'|w_i'\rangle \tag{105}$$

the new "one-particle" integrals are

$$\langle v_i'|f'|w_j'\rangle = \langle v_i'|f + g^c|w_j'\rangle \tag{106}$$

and we must transform all

$$\langle v_i v_j|g|v_k v_l\rangle \rightarrow \langle v_i' v_j'|g|v_k' v_l'\rangle \tag{107}$$

We obtain our final result by calculating the matrix elements of the valence part of the configuration with transformed orbitals and integrals as if the core electrons and orbitals were absent, adding $S_{VW}(F^c + G^{cc})$, and multiplying the whole result by $|\mathbf{Q}^c|^2$.

It cannot be emphasized too strongly that this core–valence separation is an artifice to aid in the evaluation of matrix elements. The orthogonalization of the valence orbitals to the core is allowed simply as a consequence of the Pauli principle and does not in any way represent a "contamination" of any valence orbitals by core orbitals. The overlap and Hamiltonian matrix elements, and hence the coefficients in CI eigenfunctions, are the same as we would obtain if the entire product function for the configuration were used directly with *untransformed* orbitals and orbital matrix elements. Thus the relatations given by Eqs. (96) and (105)–(107) can all be internal to the calculation and need not be visible "on the outside."

Nevertheless, the savings of time can be enormous. We have seen in Section II,C that the calculation of a matrix element is done in a time $\sim(1/8)N^5$, where N is the number of electrons. Thus if one-half of the electrons in a system may be described adequately as being in a "core," the matrix will be calculated in only 1/32 the time required for a direct

"all-electron" procedure. One admittedly extreme case we have calculated involves Ba_2^{2+}, where all but two electrons were in a core which consisted of the Ba atoms inner shells. In this case the core–valence separation yields a rate of matrix element calculation $\sim 8 \times 10^6$ times that involving all electrons. The transformations in the core–valence separation involved 54 core and 18 valence atomic orbitals and were not at all prohibitive.

C. Transformation to HLSP Functions

The procedures we have been discussing will, of course, give the energies and wave functions according to the valence-bond prescription, but not in terms of the traditional HLSP basis. If we establish a convention for the arrangement of orbitals in tableau and HLSP functions, then the coefficients of the transformations need to be determined only once. The transformation is a purely symmetric group theoretic problem and can always be done exactly as long as every standard tableau of the configurations used are included.

Klein *et al.* (1971; see also Roel, 1976) have shown that if, instead of the operator $\theta\hat{N}\hat{P}\hat{N}$, we use the operator $(f_S^N/N!)NP$, we obtain sets of functions equivalent to the HLSP basis. Our problem, then, is to determine the transformation between the two sets of functions. This may be stated precisely as

$$\frac{f_S^N}{N!}\hat{N}\hat{P}\hat{\rho}_i\phi_u = \theta\hat{N}\hat{P}\hat{N}\sum_j a_{ij}\hat{\tau}_j\phi_u \tag{108}$$

where $\hat{\rho}_i(\hat{\rho}_1 = I)$ is the permutation giving the ith Rumer diagram from the first; $\hat{\tau}_j(\hat{\tau}_1 = I)$ is the permutation giving the ith standard tableau from the first; ϕ_u is a product function arranged so that the functions in the same *row* of the *first* standard tableau are *bonded together* in the *first* Rumer diagram. As an example, consider the five orbitals, a, b, c, d, e. In order to satisfy this condition, we must have

$$\phi_u = a(1)\ c(2)\ e(3)\ b(4)\ d(5) \tag{109}$$

if the first standard tableau is

$$\begin{array}{ll} a & b \\ c & d \\ e & \end{array}$$

and the first Rumer diagram is

$$\begin{array}{ll} a\text{–}b & c \\ & \vert \\ *\text{–}e & d \end{array}$$

Once this convention is established we may determine the elements of the transformation matrix A given in Eq. (108). This has been done for $n = 3$, 4, 5, 6, 7, 8, and nontrivial cases of $0 \leq S \leq 3/2$. We give the values of A and $\mathbf{A}^{-1}$ between Rumer and tableau functions for these cases in the Appendix. Cantu (1970) has given the relationship between a single spin-projected Slater determinantal function and HLSP functions in singlet and doublet cases up to $N = 8$.

One cautionary statement about these considerations should be emphasized. Our prescription, in terms of the spatial part of the wave function (30), will not include any ± 1 phase factors for the spin eigenfunctions. This phase factor will need to be accounted for when making comparisons between wave functions computed this way and methods using Slater determinants. In practice this means that the signs of the coefficients in the final wave function may differ between treatments, although energies and actual wave functions are the same. The difference is in the basis.

D. Summary

In Section III we have outlined the methods of arranging the basis so that a full CI may be done. In addition, we have outlined a core–valence separation technique which can provide enormous savings of labor in cases where a less than full CI is appropriate with some always doubly occupied orbitals.

We may effect savings of labor under some circumstances by making suitable modifications of the orbital basis. However, most of these vary considerably with specific physical situations and are difficult to describe in general terms. We shall illustrate two useful orbital modifications in the applications given in Section V.

IV. Eigenvalues and Eigenvectors

A. Nonorthogonal Eigenvalue Problem

Once the Hamiltonian and overlap matrices are determined, we must obtain the eigenvalues and eigenvectors of the system,

$$(\mathbf{H} - E_k\mathbf{S}')\mathbf{C}_k = 0, \qquad \mathbf{C}_k^{\dagger}\mathbf{S}\mathbf{C}_k = 1 \tag{110}$$

For relatively small calculations, this is most easily accomplished by a Gram–Schmidt orthogonalization followed by a diagonalization of the transformed Hamiltonian. In matrix language, we find an upper triangular N such that

$$\mathbf{N}^{+}\mathbf{S}\mathbf{N} = \mathbf{I} \tag{111}$$

$$\overline{\mathbf{H}} = \mathbf{N}^{+}\mathbf{H}\mathbf{N} \tag{112}$$

and then find $\mathbf{x}_k$,

$$\overline{\mathbf{H}}\mathbf{x}_k = E_k\mathbf{x}_k \tag{113}$$

$$\mathbf{C}_k = \mathbf{N}\mathbf{x}_k \tag{114}$$

With the help of the Givens–Householder method for eigenvalues and eigenvectors, this sequence of procedures is easily used to obtain a few eigenvalues for matrices up to about 200 rows and columns.

For larger matrix systems, a scheme similar to the method of optimal relaxation (Shavitt *et al.*, 1973) has been found to be very useful. These procedures are based upon a method for taking an approximate eigenvector of the matrix system with its approximate eigenvalue

$$(\mathbf{H} - \lambda\mathbf{S})\mathbf{C}' \simeq 0 \tag{115}$$

and calculating a correction vector $\boldsymbol{\delta}$ such that $\mathbf{C}' + \alpha\boldsymbol{\delta}$ is an improved eigenvector. This process may then be continued iteratively until a suitable convergence criterion is satisfied. For valence-bond matrices, we have found the expression,

$$\boldsymbol{\delta} = (\mathbf{S}^{-1}\mathbf{H} - \lambda)\mathbf{C}' \tag{116}$$

to provide a usefully rapid convergence rate. We have tested a number of possibilities, and among these Eq. (116) is the only one to do so. It will be observed that the matrix product $\mathbf{S}^{-1}\mathbf{H}$ need not be formed, but that calculating $\mathbf{HC}'$ and then $\mathbf{S}^{-1}\mathbf{HC}'$ gives a much faster scheme. In practice, the new eigenvector $\mathbf{C}''$

$$\mathbf{C}'' = \alpha\mathbf{C}' + \beta\boldsymbol{\delta} \tag{117}$$

is obtained by solving a small eigenvalue problem in the subspace of the previous approximation and correction vectors. This is done using the scheme outlined in Eqs. (111)–(114). The size of the subspace is allowed to grow to 10–15 as successive $\boldsymbol{\delta}$ vectors are obtained and then collapsed back to a small number. This whole procedure may be implemented to obtain the lowest few eigenvalues of the large system sequentially by choosing the first, second, etc., eigenvalues from the small problem. These procedures are well known in the literature (Davidson, 1975), and are independent of the fact that in our case $\mathbf{S} \neq \mathbf{I}$.

Equation (116) requires that we know $\mathbf{S}^{-1}$. This fact provides the principal drawback to this procedure, but routines for inverting large, symmetric matrices are fairly simple (Gallup, 1982). Once the inversion is done, obtaining a few eigenvalues and eigenvectors is reasonably easy. We have used this procedure successfully on a few 922 × 922 matrix systems, and see no reason larger problems could not be handled should the occasion arise.

B. Inverse Overlap Weights

Chemists have always wanted to exploit the superposition principle of quantum mechanics by interpreting the structure of a molecular system as a composite of simple structures in the way that the actual wave function is a sum of the simpler basis functions. The appeal of the valence-bond approach arises from the closeness of the simple-structure interpretation of the basis functions to traditional chemical thinking. Quantum mechanics also allows a quantitative solution to the problem, since in a CI wave function,

$$\Psi_A = \sum_k C_{kA}\psi_k \tag{118}$$

for the state A, the magnitude of the coefficient C_{kA} in some sense measures the weight in the composite of the simple structure represented by ψ_k.

If the basis used is orthonormal then numerical weights assigned as $|C_{kA}|^2$ constitute a useful and rational solution. If, however, the ψ_k are not orthonormal, this choice is inappropriate. We may describe the difficulty in vectorial language.

The tableau function ψ_k,

$$\langle\psi_k|\psi_k\rangle = 1 \tag{119}$$

has only a portion which is unique to it, since, in general, it is overlapped by other functions used (Gallup and Norbeck, 1973d). The "length" of ψ_k is 1 by Eq. (119), but we may show that the "length" of the unique portion of ψ_k is only $[(\mathbf{S}^{-1})_{kk}]^{-1/2}$, which depends upon the diagonal element of the $\mathbf{S}^{-1}$ matrix. This provides a way of modifying the $|C_{kA}|^2$ in an appropriate way to give useful weights in the nonorthogonal case. Letting ω_k denote the desired weight, we set

$$\omega_k = K|C_{kA}|^2/(\mathbf{S}^{-1})_{kk} \tag{120}$$

where K is adjusted to make the weights add to 1. This result reduces to the simpler one when the basis is orthonormal.

The inverse overlap weights are easily calculated, since the $(\mathbf{S}^{-1})_{kk}$ are readily available from either of the eigenvalue schemes given in Section IV,A. We either obtain $\mathbf{S}^{-1}$ directly or we can obtain it from Eq. (111)

$$\mathbf{S}^{-1} = \mathbf{N}\mathbf{N}^{\dagger}, \qquad (\mathbf{S}^{-1})_{kk} = \sum_j |(\mathbf{N})_{kj}|^2 \tag{121}$$

and then ω_k is easily determined.

We illustrate the use of the inverse overlap weights in Section V.

V. Applications

The procedures we have described provide a flexible approach to investigating chemical problems connected with electronic structure of atoms and molecules. Many systems could illustrate the kinds of information we can obtain, but we give just two examples emphasizing the methods of applying these algorithms and the times required to carry out various operations.

A. Butadiene

The spectrum of butadiene has been the subject of many experimental (Hudson and Kohler, 1974; Doering, 1979; McDiarmid and Doering, 1980) and theoretical studies (Buenker and Whitten, 1968; Hau *et al.*, 1972). This interest is motivated to a considerable extent because butadiene occupies a unique position in being the first member of the polyene homologous series. A principal question concerns the relative positions of the lowest ^1B_u and first-excited ^1A_g (framework constrained to be C_{2h}) energy states. The valence-bond method in this case provides no new answers concerning the *energies* of these states, but we do obtain new quantitative information about the wave functions for the first three states of butadiene and we show how extended bases are easily used in π-only calculations in the valence-bond method.

For our calculation we used a 3G-STO basis with the standard (Hehre *et al.*, 1969) ζ values for carbon and hydrogen to obtain the conventional, closed-shell SCF orbitals and wave functions for the molecule. For the 26 σ electrons this provides 13 σ orbitals which we use as a "core" in our core–valence separation, and the four p_z orbitals on the carbons then become the valence set. As we pointed out above, this procedure is exactly equivalent to one including all 30 electrons explicitly, but keeping the 13 σ orbitals doubly occupied in all configurations. With the separation, we have only a four-electron problem, and it is particularly simple in this case since these p_z orbitals are all already exactly orthogonal to the σ core in planar geometries.

We have done several sets of calculations. The simplest consists of a full valence-bond CI consisting of the 20 possible structures consistent with four electrons in four orbitals. For this minimal full calculation we optimized the ζ value of the four p_z orbitals (with respect to a minimum in the ground state) and found a value 0.91 of the standard value. (This was done without changing the ζ values for the carbon p orbitals in the σ core.)

Previous calculations have shown (Buenker and Whitten, 1968; Hau *et al.*, 1972) that diffuse orbitals are necessary to treat the butadiene π system correctly. We have therefore performed two sets of calculations in

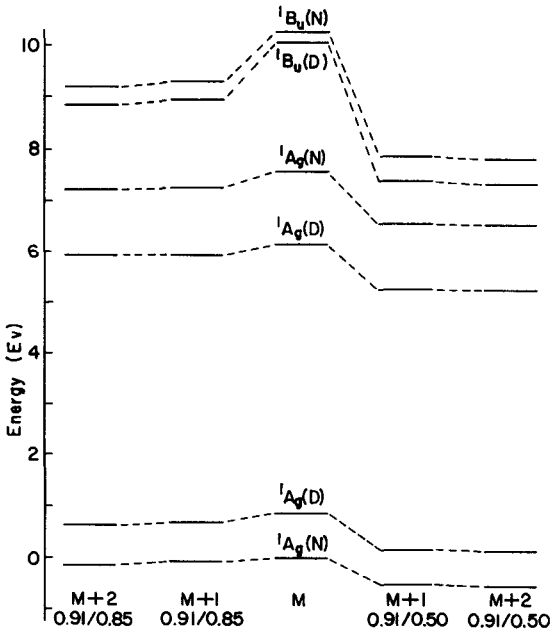

Fig. 1. Energies for the π-only calculation of the first two ^1A_g states and the first ^1B_u state of 1,3-butadiene. The variation of the energy with different numbers of basis functions is shown.

which a double-ζ set of p_z orbitals were used. In the first set $\zeta = 0.85$ times the standard was used and in the second, $\zeta = 0.5$ times the standard. In all cases the more diffuse p_z orbital was orthogonalized to the more concentrated one at the same center, so that we have essentially a $2p_z$ and a $3p_z$ (with an extra radial mode) at each center. We have obtained the energies and wave functions for the system in a basis consisting of the 20 minimal configurations plus those with all possible occupations involving three $2p_z$ and one $3p_z$ orbitals ($M + 1$), and in a basis consisting of all these configurations plus those with all possible occupations involving two $2p_z$ and two $3p_z$ orbitals ($M + 1 + 2$). We performed this same series of calculations for both ζ values of the diffuse orbital and for both the experimental geometry and a hypothetical distorted geometry with a double-bond length in the center and single-bond lengths at the ends of the molecule. The σ-core SCF orbitals were determined for the distorted geometry so that total energies were more reliable. Shih *et al.* have compared these geometries also. We show the results for our energy calculations in Fig. 1, and the times for significant parts of the calculation in Table II.

TABLE II

TIMES FOR CALCULATING CORE–VALENCE SEPARATIONS AND VALENCE-BOND MATRICES OF VARIOUS CASES FOR BUTADIENE[a]

				Minimal basis (sec)	Double-ζ basis (sec)
Core–valence separation				86	246
Valence-bond matrices	(M)	^1A_g	12[b]	3	
		^1B_u	8	2	
	(M + 1)	^1A_g	52		33
		^1B_u	48		31
	(M + 2)	^1A_g	122		164
		^1B_u	110		145

[a] IBM 370/158.

[b] This column contains the dimensions of the Hamiltonian and overlap matrices for the basis and symmetry.

The most notable point about these results is the great preference for the more diffuse $3p_z$ orbital and the fact that the (M + 1) energies are lowered very little by the addition of the double-substitution configurations.

We also see that the ground state prefers the normal (N) geometry, while the two excited states prefer the distorted (D). We note, however, that the $2\,^1A_g$ state prefers (D) overwhelmingly while the ^1B_u state shows a relatively smaller effect. This behavior has been noted before, but we can illuminate it in a different way if we examine the wave functions for these states.

Let p_1, p_2, p_3, and p_4 denote the carbon p_z orbitals in the system. We symbolize by t_1 and t_2 the two tableau functions

$$t_1 = \begin{array}{|c|c|}\hline p_1 & p_2 \\ \hline p_3 & p_4 \\ \hline \end{array}, \qquad t_2 = \begin{array}{|c|c|}\hline p_1 & p_2 \\ \hline p_2 & p_4 \\ \hline \end{array} \tag{122}$$

and by h_1 and h_2 the two HLSP functions

$$h_1 = \begin{matrix} p_1 - p_2 \\ p_4 - p_3 \end{matrix}, \qquad h_2 = \begin{matrix} p_1 & p_2 \\ | & | \\ p_4 & p_3 \end{matrix} \tag{123}$$

The transformation between these two sets of functions is given in Table II. The functions t_1 and t_2 constitute the principal configurations in the first two ^1A_g states, and the relative amounts of each determine the nature of

the spin couplings in the state. In the ground state the ratio of the coefficients $c_1t_1 + c_2t_2$ are $c_1/c_2 = -2.72$. We note from Table II that if $c_1/c_2 = -2$ exactly, the ground ^1A_g state would contain the h_1 HLSP function, which corresponds to the standard chemical covalent structure of butadiene:

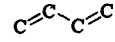

The discrepancy is a measure of the amount the other covalent structure contributes:

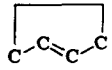

For the first-excited ^1A_g state the ratio $c_1/c_2 = -0.153$. This ratio does not correspond closely to a single HLSP function but rather corresponds approximately to the tableau function t_2 alone. The function t_2 represents an excited triplet system at each end of the molecule, coupled together to form the overall singlet. This type of structure was considered by Nascimento and Goddard (1979), and following them, we draw this:

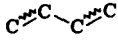

with wavy lines to indicate the triplet couplings. We now see that the behavior of the energy of these two states as the molecule is distorted follows very logically from the nature of the wave functions: The ground state definitely wants a double bond at each end of the molecule, and the first-excited ^1A_g wants the end bonds lengthened to relax the less desirable triplet couplings. The two center carbons in the triplet–triplet function are not singlet coupled in an exact sense, but attract each other to some extent.

The situation with the ^1B_u state is quire different. The covalent functions t_1 and t_2 (or h_1 and h_2) are of pure ^1A_g symmetry and do not contribute at all in this case. Ionic states of the type

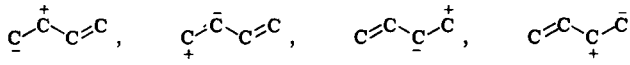

are the principal configurations and linear combinations of these are best described as antiresonance between the two chemical structures

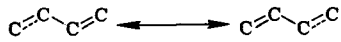

where the dotted line indicates an *excited* singlet coupling. In molecular orbital (MO) terms, the dotted line means a singlet bonding–antibonding

electron pair associated with the two carbons. On the average we still have approximately 1/2 a π bond at each end, but there is some tendency for the structures

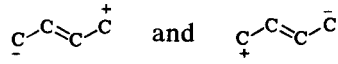

to enter, which contributes to shortening the central bond.

These descriptions of the first three states of butadiene have been based upon the minimal calculation, but the weights of the $2p_z$ configurations are not changed significantly by the addition of the diffuse functions. We thus come to the same qualitative conclusions concerning the nature of these states when we analyze the more extended calculations.

This short description of our butadiene results adequately shows the ability of the valence-bond method in handling π-only calculations at the *ab initio* level. In addition, our *ab initio* core–valence separation, unlike a π-only semiempirical method, allows us to test the effects on energy of geometry distortions since the core energy is included completely. There are many other interesting points in these results, but we leave their description to a more detailed article on butadiene alone.

B. Methylene and Ethylene

Carbene chemistry has been the subject of intense interest by organic chemists because of the many useful synthetic techniques it provides (Moss and Jones, 1978). Many properties of methylene, the simplest of the carbenes, have attracted theoretical interest, and a problem of enduring interest concerns the details of the mechanism whereby singlet or triplet CH_2 inserts into a bond.

We have used the valence-bond procedures described earlier to calculate portions of the lower singlet and triplet energy surfaces of $CH_2 + C_2H_4$ to investigate the formation of cyclopropane or the triplet trimethylene radical. This study uses an arrangement of the orbital basis we called *targeted correlation* (Vance and Gallup, 1981), which allows us to treat the C—H bonds in the methylenes more approximately than the C—C bonds. With this orbital basis, cyclopropane effectively becomes a triatomic system.

An SCF calculation of $^3B_2$ CH_2 yields three doubly occupied MOs, a σ nonbonding orbital, and a π orbital, each singly occupied. We may assemble wave functions for three methylenes in which the three doubly occupied MOs of each are included in a nine-orbital "core" and the two singly occupied MOs of each give the six-orbital "valence" set. We may

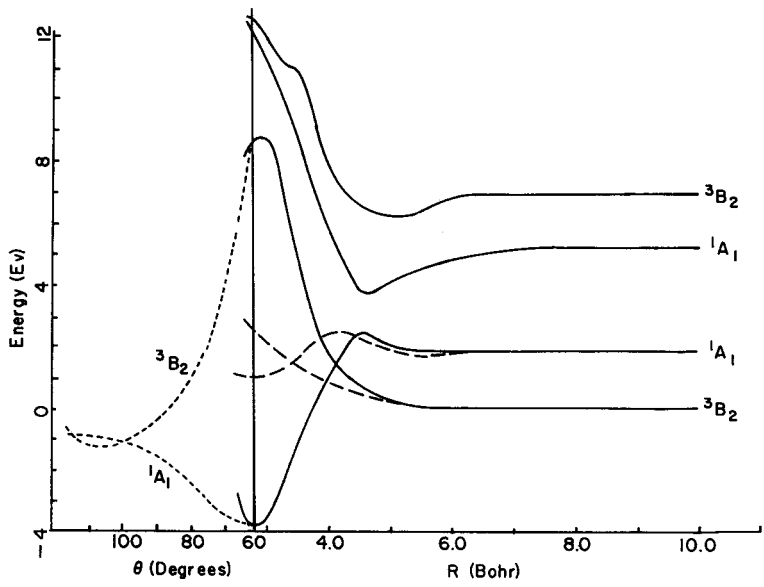

Fig. 2. Several slices through the energy surfaces for the interaction of an ethylene molecule with methylene. To the right of the solid vertical line the energies are presented as a function of the distance between the ethylene and the methylene: (—) curves for the C_{2v} (isoceles triangle) arrangement; (– – –) curves showing the energies for the C_s (right-angled) arrangement. To the left of solid vertical line the energies are given as a function of the central angle in an isoceles triangle, ring-opened arrangement. These are in a C_{2v} configuration also, and are represented by the (---) curve.

then distribute six electrons throughout the valence set to construct the valence-bond CI, and we reproduce a *full* CI for the C—C bonds, while we use what is effectively a single configuration for the C—H bonds.

We have made a number of calculations of this system using 3G-STO orbitals in C_{2v} and C_s geometries, with the hydrogen atoms always held symmetrically above and below the plane of symmetry. When using an IBM 370/158 this arrangements requires 65 sec for the core–valence separation and 460 sec to generate the matrices for 159 configurations. These times are typical for geometries in which the three methylenes are all interacting strongly. When distances within the system are large ($\sim$1000 a.u.), the times can be reduced by factors of 2 or 3 because of the increased sparcity of the basic orbital-overlap matrix.

Figure 2 shows the energy of the lowest triplet and lowest singlet states of C_2H_4 and CH_2 for three different sections through the surfaces. The first of these corresponds to a C_{2v} interaction of C_2H_4 + CH_2

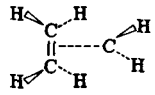

which is plotted as a function of the distance between the carbon and the center of the C=C double bond. The second section shows a similar energy curve for a distorted case where the C=C—C angle is held to be 90°.

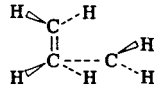

The energy is again plotted as a function of the ethylene–methylene distance. In both of these cases, the C=C distance has been relaxed to give an energy minimum. The third section shows the opening of cyclopropane to trimethylene in both the singlet and triplet cases as a function of an internal C—C—C angle.

Our results predict that the insertion of singlet methylene into the double bond of ethylene is an exoergic process with a small barrier of ~0.8 V. This calculation does not yield the singlet–triplet separation of methylene correctly since the 3G-STOs we used have no diffuse orbitals. If they were added, we would expect the asymptotic $^1A_1$–$^3B_2$ separation to be considerably smaller. We also expect the diffuse orbitals to be less important in molecular geometries, and their introduction should increase the barrier somewhat. The barrier is still present in the C_s geometries and appears not to be an artifact of the restriction to C_{2v} geometries. In C_{2v} the $^3B_2$ state is repulsive at all distances, but the repulsion is decreased considerably in the C_s arrangements we show. For the C_{2v} case the singlet and triplet states cross at approximately 4 Bohr.

When we examine the opening of the cyclopropane ring we see that there is no barrier in the singlet curve, but there is a very small barrier when there is a change in multiplicity. These results predict that if triplet trimethylene were formed in the course of a reaction, a rapid internal conversion to the singlet manifold should be possible since any crossings of various vibrational states should occur. In our calculations we have not considered the rotation of CH_2 planes and do not know the effect on triplet versus singlet energies.

We feel that this calculation shows the great flexibility which the valence-bond method allows one to use in devising orbitals sets and wave functions which are particularly designed to address specific chemical questions. We leave other details of the C_3H_6 system to a future publication.

Appendix. Transformation Matrices between Tableau Functions and HLSP Function for a Few Cases[1]

$N = 4$, $S = 0$: CD[2] for A = 3; CD for $A^{-1} = 2$

A	$\begin{matrix} a & b \\ c & d \end{matrix}$	$\begin{matrix} a & c \\ b & d \end{matrix}$	A^{-1}	HLSP	
$a-b$ $d-c$	4	−2	Tableaux	1 −1	−1 −2
$\begin{matrix} a & b \\ \vert & \vert \\ d & c \end{matrix}$	−2	−2			

$N = 4$, $S = 1$: CD for A = 4; CD for $A^{-1} = 3$

A	$\begin{matrix} a & b & a & c & a & d \\ c & & b & & b & \\ d & & d & & c & \end{matrix}$	A^{-1}	HLSP		
$\begin{matrix} a-b & c \\ & \diagdown \\ * & *-d \end{matrix}$	6 −3 3	Tableaux	1 −1 1	−2 −2 2	−1 1 3
$\begin{matrix} a & b-c \\ \vert & \\ * & *-d \end{matrix}$	−3 −3 0				
$\begin{matrix} a & b & c \\ \vert & \vert & \vert \\ * & * & d \end{matrix}$	0 3 3				

[1] Rather than repeat the tableaux and the Rumer diagrams of the A matrices for the A^{-1} matrices, we indicate the correct set for the row or column labels and assume that the functions are in the order indicated for the A matrix.

[2] CD, common denominator for each of the elements of each matrix.

$N = 5$, $S = 3/2$: CD for $\mathbf{A} = 5$; CD for $\mathbf{A}^{-1} = 4$

A	$a\,b$ $c\,d$ e	$a\,c$ $b\,d$ e	$a\,d$ $b\,c$ e	$a\,e$ $b\,c$ d
a–b c d / * * *–e	8	−4	4	−4
a b–c d / * * *–e	−4	−4	0	0
a b c–d / * * *–e	0	4	4	0
a b c d / * * * e	0	0	−4	−4

$\mathbf{A}^{-1}$	HLSP			
Tableaux	1	−3	−2	−1
	−1	−2	2	1
	1	2	3	−1
	−1	−2	−3	−4

$N = 6$, $S = 0$: CD for $\mathbf{A} = 2$; CD for $\mathbf{A}^{-1} = 3$
($N = 5$, $S = 1/2$: For this case, eliminate the last letter of the $N = 6$ case)

A	$a\,b$ $c\,d$ $e\,f$	$a\,b$ $c\,e$ $d\,f$	$a\,c$ $b\,d$ $e\,f$	$a\,c$ $b\,e$ $d\,f$	$a\,d$ $b\,e$ $c\,f$
a–b c / f–e d	4	−2	−2	1	−3
a b–c / f–e d	−2	1	4	−2	3
a–b c / f e–d	−2	4	1	−2	3
a b–c / f e–d	1	−2	−2	1	0
a b c / f e d	1	1	1	1	0

$\mathbf{A}^{-1}$	HLSP				
Tableaux	2	1	1	1	1
	0	−1	1	−1	1
	0	1	−1	−1	1
	−2	−1	−1	1	3
	0	1	1	3	1

$N = 6$, $S = 1$: CD for $\mathbf{A} = 5$; CD for $\mathbf{A}^{-1} = 12$

A	*a b* *c d* *e* *f*	*a b* *c e* *d* *f*	*a b* *c f* *d* *e*	*a c* *b d* *e* *f*	*a c* *b e* *d* *f*	*a c* *b f* *d* *e*	*a d* *b e* *c* *f*	*a d* *b f* *c* *e*	*a e* *b f* *c* *d*
a–*b* *c*–*d* *f*–* *–*e*	12	−6	6	−6	3	−3	−9	9	−6
a *b* *c* *d* | | | | *f* * * *e*	−6	−6	0	3	3	0	0	−3	−3
a–*b* *c* *d* \ \ \ *f* * *–*e*	0	6	6	0	−3	−3	3	3	0
a *b* *c*–*d* \ \ \ *f*–* *–*e*	−6	3	−3	−6	3	−3	0	0	0
a *b*–*c* *d* | \ *f* * *–*e*	3	3	0	3	3	0	0	0	0
a *b*–*c* *d* \ \ | *f*–* * *e*	0	−3	−3	0	−3	−3	0	0	0
a–*b* *c* *d* | | *f*–* * *e*	0	0	0	−3	−3	0	0	−3	−3
a *b*–*c* *d* \ / \ *f*–* *–*e*	0	0	0	0	3	3	3	3	0
a *b* *c*–*d* | | *f* * *–*e*	−6	3	−3	3	−6	3	0	−3	3

$\mathbf{A}^{-1}$	HLSP								
Tableaux	−1	−4	−2	−3	2	1	2	−1	−4
	1	−1	2	3	8	1	3	1	4
	−1	1	3	−3	−8	−9	−3	−6	−4
	1	4	2	−2	8	4	−2	1	4
	−1	1	−2	2	2	−4	−3	−1	−4
	1	−1	−3	−2	−2	−6	3	6	4
	−4	−1	2	−2	−2	4	3	6	−6
	4	1	3	2	2	6	−3	9	6
	−4	−6	−3	−2	−12	−6	−12	−9	−6

$N = 8$, $S = 0$: CD for $\mathbf{A} = 5$; CD for $\mathbf{A}^{-1} = 12$
($N = 7$, $S = 1/2$: For this case, eliminate the last letter of the $N = 8$ case)

A	*a b* *c d* *e f* *g h*	*a b* *c d* *e g* *f h*	*a b* *c e* *d f* *g h*	*a b* *c e* *d g* *f h*	*a* *c* *d* *e*	*b* *f* *g* *h*	*a c* *b d* *e f* *g h*	*a c* *b d* *e g* *f h*	*a c* *b e* *d f* *g h*	*a c* *b e* *d g* *f h*	*a c* *b f* *d g* *e h*	*a* *b* *c* *g*	*d* *e* *f* *h*	*a d* *b e* *c g* *f h*	*a* *b* *c* *e*	*d* *f* *g* *h*	*a e* *b f* *c g* *d h*
a–b c–d *h–g f–e*	16	−8	−8	4	−12	−8	4	4	−2	6	−12	6	−18	12			
a–b c–d *h–g–f–e*	−8	−8	4	4	0	4	4	−2	−2	0	6	6	0	0			
a–b–c–d *h–g–f–e*	4	4	−2	−2	0	4	4	−2	−2	0	0	0	0	0			
a–b c d *h–g f e*	−8	4	−8	4	0	4	−2	4	−2	0	0	0	0	0			
a b c d *h g f e*	4	−2	4	−2	0	−2	4	−2	4	0	0	0	0	0			
a–b–c–d *h–g–f–e*	−8	4	4	−2	6	−8	4	4	−2	6	0	0	0	0			
a b c–d *h g f–e*	−8	4	4	−2	6	4	−2	−2	−2	−6	6	−6	6	−6			
a b–c d *h g–f e*	−2	−2	−2	−2	0	−2	−2	−2	−2	0	0	0	0	0			
a b–c d *h g f–e*	4	−2	−2	4	0	4	−2	−2	4	0	0	0	0	0			
a–b c d *h g f–e*	−8	4	4	−8	0	4	−2	−2	4	0	6	−6	6	−6			
a b–c d *h–g f e*	4	−2	4	−2	0	4	−2	4	−2	0	0	0	0	0			
a b c–d *h–g f e*	8	4	4	−2	6	4	−2	−8	4	−6	0	0	6	−6			
a–b c d *h g–f e*	4	4	4	4	0	−2	−2	4	4	0	0	0	0	0			
a b c–d *h g–f e*	4	4	−2	−2	0	−2	−2	4	4	0	0	0	0	0			

(*Continued*)

(*Continued from p. 269*)

A^{-1}	HLSP													
Tableaux	−2	−1	2	−1	2	−1	−1	2	1	−2	1	−2	1	1
	2	1	3	1	−2	1	1	−2	−1	2	−1	2	4	4
	2	1	−2	1	3	1	1	−2	−1	2	4	2	4	−1
	−2	−1	−3	−1	−3	−1	−1	−8	−1	−2	−4	−2	1	−4
	2	1	3	1	3	6	6	8	9	−3	4	2	−1	4
	2	1	3	1	−2	1	1	−2	4	2	4	2	−1	−1
	−2	−1	2	−1	2	−1	1	−8	−4	−2	−4	−2	−4	−4
	−2	−1	−3	−1	−3	−1	−1	−8	−4	−2	1	−2	−4	1
	2	1	−2	1	3	1	1	−2	4	2	−1	2	−1	4
	−2	−1	2	−1	−3	4	−6	2	6	3	1	−2	1	−4
	2	6	3	1	3	1	6	8	4	2	−1	−3	4	9
	−2	4	2	−1	−3	−1	−6	2	−4	−2	1	3	1	6
	−8	−4	−2	1	3	−4	−9	−2	−6	−3	−1	−3	−1	−6
	8	4	2	9	12	4	9	12	6	3	6	3	6	6

References

Abramowitz, M., and Stegun, I. (1965). "Handbook of Mathematical Functions." Dover, New York.

Balint-Kurti, G. G., and Karplus, M. (1968). *J. Chem. Phys.* **50,** 478.

Balint-Kurti, G. G., and Karplus, M. (1974). *In* "Orbital Theories of Molecules and Solids" (N. H. March, ed.). Oxford Univ. Press, London and New York.

Buenker, R. J., and Whitten, J. L. (1968). *J. Chem. Phys.* **49,** 5381.

Cantu, A. A. (1970). *Mol. Phys.* **19,** 1.

Cooper, I. L., and McWeeny, R. (1966). *J. Chem. Phys.* **45,** 226.

Davidson, E. R. (1975). *J. Comp. Phys.* **17,** 87.

Doering, J. P. (1979). *J. Chem. Phys.* **70,** 3902.

Eyring, H., Walter, J., and Kimball, G. E. (1944). "Quantum Chemistry." Wiley, New York.

Gallup, G. A. (1968). *J. Chem. Phys.* **48,** 1752.

Gallup, G. A. (1969). *J. Chem. Phys.* **50,** 1206.

Gallup, G. A. (1972). *Int. J. Quantum Chem.* **6,** 899.

Gallup, G. A. (1977a). *J. Chem. Phys.* **66,** 2252.

Gallup, G. A. (1977b). *Mol. Phys.* **33,** 9453.
Gallup, G. A. (1982). *J. Comp. Chem.* (In press.)
Gallup, G. A., and Macek, J. H. (1977). *J. Phys. B* **10,** 160.
Gallup, G. A., and Norbeck, J. M. (1973a). *Chem. Phys.* **2,** 20.
Gallup, G. A., and Norbeck, J. M. (1973b). *J. Am. Chem. Soc.* **95,** 4469.
Gallup, G. A., and Norbeck, J. M. (1973c). *Int. J. Quantum Chem.* **57,** 161.
Gallup, G. A., and Norbeck, J. M. (1973d). *Chem. Phys. Lett.* **21,** 495.
Gallup, G. A., and Norbeck, J. M. (1973e). *Chem. Phys. Lett.* **22,** 161.
Gallup, G. A., and Norbeck, J. M. (1974). *J. Am. Chem. Soc.* **96,** 11.
Gallup, G. A., and Norbeck, J. M. (1975). *J. Am. Chem. Soc.* **97,** 970.
Goddard, W. A. (1967). *Phys. Rev.* **157,** 73, 81, 93.
Hau, K., Buenker, R. J., and Peyerimhoff, S. D. (1972). *J. Am. Chem. Soc.* **94,** 5639.
Hehre, W. J., Stewart, R. F., and Pople, J. A. (1969). *J. Chem. Phys.* **51,** 2657.
Heitler, W., and London, F. (1927). *Z. Phys.* **44,** 455.
Hiberty, P. C. (1981). *Int. J. Quantum Chem.* **19,** 259.
Hiberty, P. C., and Leforestier, C. (1978). *J. Am. Chem. Soc.* **100,** 2012.
Hudson, B., and Kohler, B. (1974). *Annu. Rev. Phys. Chem.* **25,** 437.
King, H. F., Stanton, R. E., Kim, H., Wyatt, R. E., and Parr, R. G. (1967). *J. Chem. Phys.* **47,** 1936.
Klein, D. J., Poshusta, R. D., Junker, B. R., and Matsen, F. A. (1971). *Int. J. Quantum Chem.* **45,** 141.
Krylov, V. I. (1962). "Numerical Approximation of Integrals." Macmillan, New York.
Littlewood, D. E. (1950). "The Theory of Group Characters." Oxford Univ. Press, London and New York.
Löwdin, P.-O. (1955). *Phys. Rev.* **97,** 1474.
McDiarmid, R., and Doering, J. P. (1980). *J. Chem. Phys.* **73,** 4192.
McWeeny, R. (1954). *Proc. R. Soc. (London) Ser. A* **223,** 306.
McWeeny, R., and Ohno, K. A. (1960). *Proc. R. Soc. (London) Ser. A* **255,** 367.
Matsen, F. A. (1964). *Adv. Quantum Chem.* **1,** 59.
Messiah, A. (1967). "Quantum Mechanics," Vols. 1 and 2. Saunders, New York.
Moffitt, W. (1953). *Proc. R. Soc. (London) Ser. A* **218,** 486.
Moss, R. A., and Jones-Carbenes, M. (1978). *In* "Reactive Intermediates" (R. A. Moss and M. Jones, eds.), Vol. 1. Wiley, New York.
Nascimento, M. A. C., and Goddard, W. A. (1979). *Chem. Phys.* **36,** 147.
Pauling, L. (1933). *J. Chem. Phys.* **1,** 280.
Pauncz, R. (1979). "Spin Eigenfunctions." Plenum, New York.
Prosser, F., and Hagstrom, S. (1968). *Int. J. Quantum Chem.* **2,** 89.
Pyper, N. C., and Gerratt, J. (1977). *Proc. R. Soc. (London) Ser. A* **355,** 407.
Raimondi, M., Simonetta, M., and Tantardini, G. F. (1972). *J. Chem. Phys.* **56,** 5091.
Raimondi, M., Simonetta, M., and Tantardini, G. F. (1973). *Int. J. Quantum Chem.* **7,** 893.
Raimondi, M., Simonetta, M., and Tantardini, G. F. (1975). *Mol. Phys.* **30,** 703, 797.
Roel, R. W. J. (1976). *In* "Group Theoretic Methods in Physics" (A. Janner *et al.*, eds.). Springer-Verlag, Berlin and New York.
Rutherford, D. E. (1948). "Substitutional Analysis." Edinburgh Univ. Press; reprinted by Hafner New York, 1968.
Serber, R. (1934a). *Phys. Rev.* **45,** 461.
Serber, R. (1934b). *J. Chem. Phys.* **2,** 697.
Shavitt, I., Bender, C. F., Pipano, A., and Hosteny, R. P. (1973). *J. Comp. Phys.* **11,** 90.
Shih, S., Buenker, R. J., and Peyerimhoff, S. D. (1972). *Chem. Phys. Lett.* **16,** 244.

Shull, H. (1969). *Int. J. Quantum Chem.* **3,** 523.
Simonetta, M., Gianinetta, E., and Vandoni, I. (1968). *J. Chem. Phys.* **48,** 1579.
Slater, J. C. (1931). *Phys. Rev.* **38,** 1109.
Sramek, S. J. (1980). *Phys. Rev.* **22,** 2630.
Sramek, S. J., Macek, J. H., and Gallup, G. A. (1980). *Phys. Rev. A* **21,** 1361.
Sramek, S. J., Macek, J. H., and Gallup, G. A. (1980b). *Phys. Rev. A* **22,** 1467.
Vance, R. L., and Gallup, G. A. (1978). *J. Chem. Phys.* **69,** 736.
Vance, R. L., and Gallup, G. A. (1980). *J. Chem. Phys.* **73,** 894.
Vance, R. L., and Gallup, G. A. (1981). *Chem. Phys. Lett.* **81,** 99.
Van Lenthe, J. H., and Balint-Kurti, G. G. (1980). *Chem. Phys. Lett.* **76,** 138.
Van Vleck, J. H. (1934). *Phys. Rev.* **45,** 405.
Voter, A. F., and Goddard, W. A. (1981). *Chem. Phys.* **57,** 253.
Weyl, H. (1956). "The Theory of Groups and Quantum Mechanics." Dover, New York.
Wigner, E. P. (1959). "Gruppentheorie." Academic Press, New York (publ. in German in 1931).
Wilson, S., and Gerratt, J. (1975). *Mol. Phys.* **30,** 777, 789.
Yamanouchi, T. (1937). *Proc. Phys.-Math. Soc. Jpn.* **19,** 436.

Index

D

E

F

G

H

I

K

L

M

N

O

P

Q

T

U

V

W

X

Z